Multi-Pultrusion Fibre Composite Truss Systems for Deployable Shelters

By

Tarek Omar

Supervised by

Prof. Gerard Van Erp

Assoc. Prof. Thiru Aravinthan

Dr. Tim Heldt

A dissertation submitted for the award of

DOCTOR OF PHILOSOPHY

Centre of Excellence in Engineered Fibre Composites
Faculty of Engineering & Surveying
University of Southern Queensland
Queensland, Australia

March 2008

Abstract

Deployable shelters of various forms have been utilized since ancient civilization. The need for these systems has not diminished over time and development continues for military forces, civilian humanitarian aid, and natural disaster scenarios. Recent developments have focused mainly on tent-type structures, air-beam technology and steel frames supporting soft fabric; yet none of these have fully satisfied the deployability requirements. The Military Modular Shelter System (M^2S^2) initiative is a research project with the University of Southern Queensland that aims to develop a fibre composite re-deployable arched shelter system with rigid PVC or fabric cladding. The main frames are formed from modular fibre composite truss panels that are connected and stressed into position by prestressing cables. Flexibility in defining the geometry of frames constructed by using this system is achieved by changing the number of panels per frame and the packer sizes between panels.

The current study is the first to investigate a suitable truss system for the M^2S^2 concept. Accordingly, it was necessary to validate the M^2S^2 concept by searching the literature for previously developed deployable shelter concepts and locate the currently used fibre composite truss systems. Then try to establish a suitable truss system that fulfils the deployability needs with sound structural performance.

An innovative all-composite truss concept, named Multi-Pultrusion Truss-System (MPTS), was developed as a result of this study. It overcame the classical difficulty of joining composite members by loading each component of the truss in its strength direction. In addition, the system had inherent redundancy that provided alternate load paths after reaching ultimate capacity. The basic idea of this system was to have chord and vertical members formed from a few pultrusions of the same size. The traditional usage of gussets was eliminated by using laminates for the bracing system which directly connected between the pultrusions. This system allowed direct

transfer of the bracing forces to the connected members (pultrusions). This layout led to reducing the concentration of stresses in the adhesive layers (due to its continuous nature), while providing symmetric joints with two double-lap joints. All these factors contributed to having failure away from the joint area. The confinement of the bracing system, due to its finite dimensions, was one of the characteristics of this construction technology.

Two MPTS alternatives were developed, tested and investigated. The first alternative used a Discrete-Diagonal (DD) bracing system made of sandwich diagonal. Two panels DI-MPTS panels were tested using this configuration, one with the diagonals under tension and the other with the diagonals under compression.

The second alternative used a Diaphragm (DI) bracing system. Three different DI-MPTS panels were investigated. The first panel had an empty diaphragm (no core); the second panel had a partially-filled sandwich diaphragm while the third panel had a completely-filled sandwich diaphragm.

To achieve understanding of the basic behaviour of each of these panels, finite element (FE) analyses were conducted at micro level. The different components of the panel were included in each model, with idealisations to achieve an efficient analysis process. The FE analysis results were used to investigate the distribution of forces in each of the panel components.

Due to the associated costs of micro-model analyses, macro-analysis models are important tools for engineers interested in modelling this system, conduct pre-micro-analysis parametric studies and in modelling the overall frame structure. This study ended with presenting simplified analysis procedures for the different panel types.

The work conducted in this study has revealed that this new fibre composite truss system suits the characteristics of fibre composites and accordingly provides an efficient solution for general truss applications. It combines simplicity, easiness of manufacturing, high-load carrying capacity and structural redundancy. In addition, its behaviour and failure modes can be accurately predicted by using the currently available finite element software packages.

Certification of Dissertation

I certify that the ideas, experimental work, results, analysis and conclusions reported in this dissertation are entirely my own effort, except where otherwise acknowledged. I also certify that the work is original and has not been previously submitted for any other award, except where otherwise acknowledged.

- / /

Signature of Candidate Date

Endorsed:

- / /

Signature of Supervisor/s Date

- / /

Signature of Supervisor/s Date

Acknowledgement

Putting my name, solely, as the author of this thesis is not quite fair. I was one of a team and, without the contribution of each member, this work would not be in this form. Many people in the Centre of Excellence in Engineered Fibre Composites (CEEFC) and the Faculty of Engineering and Surveying (FOES) made a direct and indirect contribution in helping me to complete my research work successfully. I sincerely appreciate the efforts of my supervisors - Prof. Gerard Van Erp, who introduced me to the world of composite materials in civil engineering, Assoc. Prof. Thiru Aravinthan for help in testing procedures and prestressing technologies, and Dr. Tim Heldt for starting the research work in this project. It would have been difficult to finish this thesis without their continual patience, advice, support and understanding.

I thank Strarch Australia and Kencana Composites for sponsoring this project and more specifically Dr. Peter Key who convinced me to join the CEEFC and supporting my shift to Australia. I thank especially Assoc. Prof. David Buttsworth, Associate Dean for Research, for his continuous support that facilitated my work through the different departments. Also, I would like to thank all the technical and administration staff who worked behind the scenes to support the research work, Darren Browne, John Ashby, Wayne Crowell, Henk Van Kerkwyk, and all the others for their valuable advice, innovation and co-operation. The library staff must have a special appreciation for their efforts to locate references from different destinations. Ian Mitchell, Ruth Hilton and Jean Althoff were of a great help in editing the text of the thesis and kept questioning me about the logistics of its contents. And it would be remiss not to mention the friendly environment we found from the wider community that made our settlement in Toowoomba quite enjoyable.

I wish to thank my parents for raising me to love my work, my wife who was very patient for the long time spent alone looking after the family while I was preparing this thesis and for my kids who missed my company for some time. At the end I like to thank You, the readers, who spend time in reading this thesis. I trust that the outcome of the effort of the team who worked in this project will be of a good value to you.

Associated Publications

Omar, T., Aravinthan, T., and Van Erp, G. (2007). "Behaviour of sandwich columns under edgewise compression loading." *Asia-Pacific Conference on FRP in Structures (APFIS 2007)*, Hong Kong, China.

Omar, T., Heldt, T., Key, P. W., and Van Erp, G. (2005). "Development of modular deployable composite shelters." *Australian Structural Engineering Conference - ASEC2005*, Newcastle City Hall, Newcastle, NSW, Australia.

Omar, T., Van Erp, G., Aravinthan, T., and Key, P. W. (2007). "Innovative all-composite multi-pultrusion truss system for stressed-arch deployable shelters." *Sixth Alexandria International Conference on Structural & Geotechnical Engineering (AICSCE 6)*, Alexandria, Egypt.

Omar, T., Heldt, T., Key, P. W., and Van Erp, G. (2006). "M^2S^2 Modular deployable composite shelters - concept and loading criteria." *Australian Journal of Structural Engineering*, 6(3), 217-226.

Omar, T., Van Erp, G., Aravinthan, T., and Key, P. W. (2007). "M^2S^2 modular deployable shelter system - concept and analysis technique." *Structural Engineering & Construction Conference (ISEC-4)*, Melbourne, Australia.

Omar, T., Van Erp, G., and Key, P. W. (2007). "Modular deployable composite shelters - truss system." *Proceedings of ACIC 07, Advanced Composites in Construction*, University of Bath, Bath, UK.

Omar, T., Van Erp, G., and Key, P. W. (2006). "Stressed-arch modular deployable composite shelters, concept and development." *Third International Conference on FRP Composites in Civil Engineering (CICE 2006)*, Miami, Florida, USA.

Table of Contents

List of Figures

CHAPTER 1 Introduction

CHAPTER 2 Deployable Shelters & Fibre Composite Trusses - State of the Art

CHAPTER 3 Behaviour of Discrete-Diagonal, Multi-Pultrusion Truss Systems

CHAPTER 4 Behaviour of Sandwich Members under Axial Loads – Application for Discrete-Diagonal, Multi-Pultrusion Truss System

CHAPTER 5 Behaviour of Diaphragm, Multi-Pultrusion Truss Systems (DI-MPTS)

CHAPTER 6 Simplified Analysis Models for the Multi-Pultrusion Truss Systems (MPTS)

Appendix B M^2S^2 Analysis Procedures

Appendix C Sandwich Columns with Mixed-Cores - Test Results

Appendix D Double-Bay DD-MPTS - Test Results

List of Tables

CHAPTER 1 Introduction

CHAPTER 3 Behaviour of Discrete-Diagonal, Multi -Pultrusion Truss Systems

CHAPTER 4 Behaviour of Sandwich Members under Axial Loads – Application for Discrete-Diagonal, Multi-Pultrusion Truss System

CHAPTER 5 Behaviour of Diaphragm, Multi-Pultrusion Truss Systems (DI-MPTS)

CHAPTER 6 Simplified Analysis Models for the Multi-Pultrusion Truss Systems (MPTS)

Appendix A Assessing Loads on Deployable Shelters

Appendix B M^2S^2 Analysis Procedures

Appendix C Sandwich Columns with Mixed-Cores - Test Results

1. Introduction

1.1. INTRODUCTION

In the 1980's, Lew Harding developed an innovative structural form capable of fast erection and achieving large spans, Strarch (1999). The system was named Strarch[1]. Strarch systems rely structurally on frame elements of truss form that function as relatively flat arches, Strarch (1999). Frames are assembled on the ground, complete with services and cladding, and the pre-assembled system is then "stress-erected" (Figure 1.1). The top chord is continuous, while the bottom chord is segmented (initially assembled with gaps). Stress-erection, by prestressing cables threaded through the bottom chord, causes the bottom chord gaps to close, thus causing the arch to rise into its final shape. The change in shape from straight to arch requires the continuous top chord to deform plastically during the erection process and remain in the plastically-deformed shape (Clarke and Hancock, 1994). The continuous nature of the top chord, the plastic deformation during stress-erection, and the strength-to-weight ratio associated with the steel trusses all provide challenges to the deployable functionality of conventional Strarch frame systems.

Figure 1.1 Strarch conventional shelters during erection
(www.strarch.com)

[1] The name STRARCH is a derivative of STRessed ARCH. This name was later adopted by an Australian company established to manufacture this type of structure.

In 2003, Strarch proposed the utilisation of fibre composites, as a construction material, with the stressed-arch structural system for deployable shelters to combine the advantages of being both fully deployable and light weight. This initiated a concept named M^2S^2 - Military Modular Shelter System (Key, 2004).

The current study was the first to investigate the concept of M^2S^2. Accordingly, a number of important aspects had to be addressed starting from validating the M^2S^2 concept to investigating different truss alternatives that suit the concept of M^2S^2 and developing an understanding of the main behavioural issues of these alternatives.

This chapter provides a brief background on deployable structures – and, more specifically, shelters - followed by a presentation of the concept of the M^2S^2 deployable shelter system, along with its potential components. The objectives of this study are then presented, followed by an outline of the thesis. The chapter ends with a summary of its contents and related references section.

1.2. BACKGROUND

Throughout history there has been a need for deployable structures. For example, since ancient times tent structures (Figure 1.2) have been used in different places around the world. Their design and capacity were limited typically by available materials, methods of construction, and transportation capacity.

Figure 1.2 Tent in Northern Africa, a deployable shelter system (www.google.com, keyword: Shelter)

In medieval times, several designers created new concepts for moveable and rapidly erectable structures. Escrig (1996) cites that Francesco de Giorgio proposed

machines that could change the geometry of the structures by pulling and pushing, using diagonal ties. Palladio, Verantius and Primaticio proposed temporary bridge systems. Leonard da Vinci developed umbrella and pantographic weight-lifting cranes (Escrig, 1996). In the twentieth century changes in styles of living, technology, transportation, communication and materials availability have changed significantly the nature of, and the need for, deployable structures. Modern deployable structures differ from their predecessors in the fabrication and erection processes, materials used, and transportation capacity.

Due to their broad scope of applications, different classifications are used for modern deployable structures. One classification is the environment of application, where two broad categories are used: earth or space application[2] (Chapter 1, p10, Gantes, 2001). In his review of deployable structures Gantes (2001) summarised the potential applications of deployable structures on earth as follows:

- emergency shelters or bridges that can be used after earthquakes or other natural disasters;
- temporary buildings in remote construction sites;
- shelters for temporary outdoor activities such as road construction, surveying measurements, or cold weather concreting;
- sports facilities;
- relocatable warehouses, hangers and maintenance facilities;
- lightweight camping and recreational structures and exhibition structures.

A recurring theme in this list is the provision of shelter systems. The need for these systems continues to grow for military forces, civilian humanitarian aid, and natural disaster scenarios.

Light-weight components, wherever possible, are a requirement in deployable shelters. This is to facilitate deployment and assembly, and to minimise costs associated with transportation. The assembled elements must be of manageable size to allow easy manoeuvring and further assembly, without using heavy equipment. Composite materials have the advantage of higher specific strength and stiffness compared to other construction materials. In addition, with composite materials, it is

[2] By earth we mean structures constructed on our planet, while by space we mean structures placed in orbits in space, for example, foldable telescopes.

possible to engineer the material properties such as strength, chemical attack resistance, environmental performance and fire resistance, to suite specific applications. This flexibility provides opportunities as well as challenges to researchers and engineers who use composites.

1.3. THE CONCEPT OF M^2S^2

The M^2S^2 concept is based on the stressed-arch system. However, to improve its deployability, the M^2S^2 frames are formed from manageable light-weight elements that do not require plastic deformation. The top chord deformation is concentrated at discrete joints designed to facilitate rotation during stress-erection. The M^2S^2 concept can be summarised as follows:

- Frames are manufactured, mostly, from identical standard panels with the dimension of the top chord larger than the bottom chord.
- Standard panels are aligned to form each frame on the ground. Panels are then connected by the top 'hinged' joints. The difference in dimension between the top chord and the bottom chord allows having initial gaps at the bottom chord.
- The prestressing cables are threaded through the bottom chord with one side of the frames fixed to the foundation, while the other is free to move horizontally.
- Roof sheeting and other services are assembled while the frames are still on the ground, prior to carrying out any prestressing (Assembly stage, Figure 1.3).
- Upon completion of the installation of services, frames are stressed by the prestressing cables. The stressing process forces the movable supports to move inwards. The bottom chord gaps allow for the changing of the frame geometry to the arch shape (Erection stage, Figure 1.4).

- Finalising the stressing process[3], the cables are blocked and the moveable frame support is fixed. The shelter is complete and ready to use (Deployed stage, Figure 1.5).

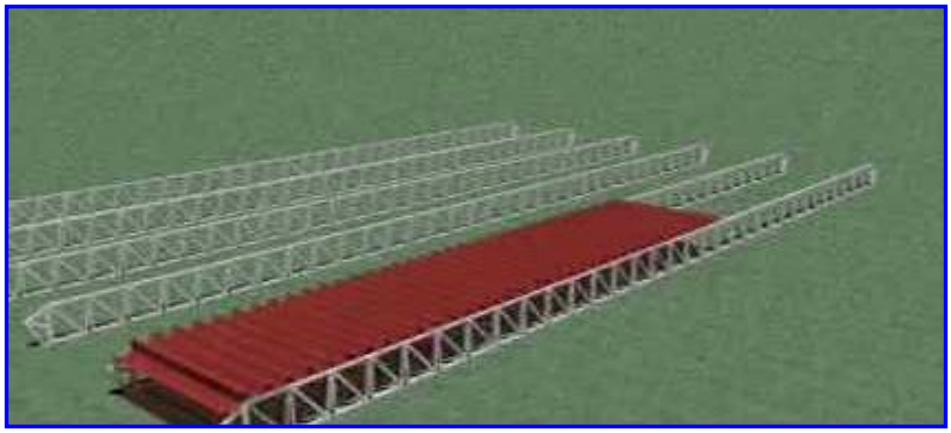

Figure 1.3 Fixing roof sheeting during assembly stage

Figure 1.4 Stressing the frames during erection stage

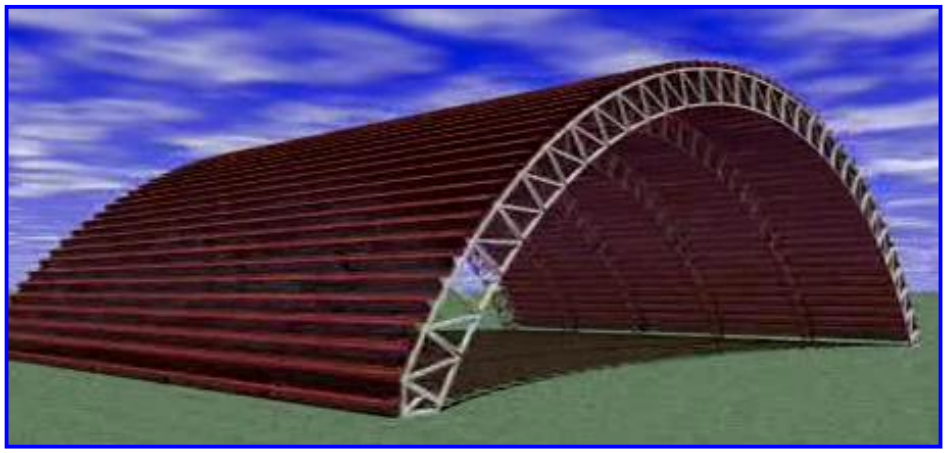

Figure 1.5 Deployed shelter system

[3] The level of prestressing in the cables should accommodate any losses and/or relaxation in addition to ensuring that the bottom chord will be in compression under any serviceability load combination.

1.4. M^2S^2 - MAIN COMPONENTS

Based on the concept presented in Sec.1.3, the main components of the M^2S^2 shelter frames are (i) the standard panel[4], (ii) the joints at the top and bottom chords, (iii) the prestressing cables and (iv) the packers at the bottom chord, with size to suite the frame geometry (Figure 1.6). The panel should be of manageable size with the top chord longer than the bottom chord. Differential rotations between adjacent panels are concentrated at the top and bottom chord joints.

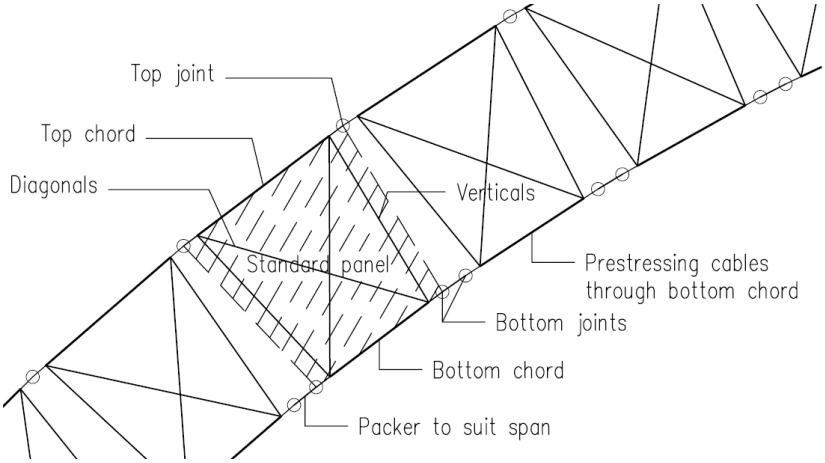

Figure 1.6 M²S² main components

The main functions of the different frame components can be summarised as follows:

- The modular panel is the essential component of the frame system. It should safely carry internal actions and transfer them to the inter-panel joint connectors to allow the flow of forces to the foundations.
- Due to the deployability requirements, top joint connectors should safely transmit forces during the different stages of erection, dismantling, and while the structure is in service. The joint transfers combined shear and axial (compression or tension) forces, while allowing differential rotations between adjacent panels.
- The bottom joints should have gaps that are open in the assembly position (Figure 1.3) and closed during the erection process (Figure 1.4). They should be kept closed while in the deployed status (Figure 1.5). While in service, the joint should be capable of transferring compressive forces and shear forces

[4] Standard panel consists of top chord, bottom chord, verticals and diagonals.

through the joint. In addition, they should accommodate any differential rotation between connecting panels and packers.

- The prestressing cables have a dual function. They are used as a deploying mechanism to change the status of the structure from the assembly position (Figure 1.3) to the deployed position (Figure 1.5) and vice versa. In addition, they provide the bottom chord with its stiffness, by keeping the bottom chord in compression under any serviceability limit state.

The modular nature of the M^2S^2 concept provides significant flexibility in defining the frame geometry. The number of panels per frame and the packer sizes are the two parameters that define the frame geometry in the deployed status. For example, increasing the packer sizes from 200mm to 220mm changes the arch[5] rise/span ratio from 0.33 to 0.25. It increases the frame span from 36.7m to 40.0m and reduces the frame height from 12.1m to 10.1m (Table 1.1).

Table 1.1 Effect of packer size on the frame geometry

Frame Alternative	**A1**	**A2**	**A3**
Packer Size(mm)	200	210	220
Rise/Span – Radius(m)	12.1/36.7– 19.9	11.1/38.4- 22.1	10.1/40.0- 24.8
Rise/Span Ratio	0.33	0.29	0.25
Subtended Angle (Degree)	133.3	120.3	107.2

1.5. OBJECTIVES OF THE STUDY

The current study is the first to investigate the concept of M^2S^2. Accordingly, a number of important aspects had to be addressed prior to conducting the main objective of this study. These include validating the M^2S^2 concept by reviewing available deployable shelter systems, investigating the deployability requirements, assessing the loading criteria and the magnitude of the member forces and exploring existing fibre composite truss system. The main objectives of this study are develop and investigate different fibre composite truss alternatives that can suit the concept of M^2S^2 and, with the aid of FE analysis, developing an understanding of the main behavioural issues of these alternatives. In summary, the major objectives of this study are:

- to assess the loading scenarios for this type of shelter structures;

[5] Frames are based on 32 standard panels of 1400mm Ht, top chord dimension 1400mm & bottom chord dimension 1150mm.

- to develop and explore innovative truss systems for the modular panel that mobilises the strengths of composites;
- to develop credible finite element (FE) models;
- to use the tested panels records and the FE analyses results to develop an understanding of the mechanics of force transfers and distributions, potential failure modes and panel capacity;
- to investigate the effect of material distribution and architecture on the panel behaviour;
- to develop a simplified modelling procedure to be used in conducting macro-level analysis for the frame.

It is important to mention that this study is focused on the structural behaviour of the panel system. Accordingly, no significant material development investigations are conducted. Existing materials and fibre architectures are used in an efficient form that suits the structural system. Composites usually face the challenge of being cost-competitive with other construction materials. No investigations are undertaken in this study regarding the economical feasibility of the truss system. However, consideration is given to the complexity of the developed system with the intent of facilitating efficient manufacturing.

The macro-level FE model is made as simple as possible to represent the behaviour of the tested panels. The model does not reach the level of detail to model the constituents of the composite. However, composites are modelled as laminae with orthotropic material properties with short-term properties.

1.6. OUTLINE OF THE THESIS

Each chapter starts with an overview and ends with a summary of the main conclusions. Notations used in each chapter are presented at the beginning of the chapter. Chapter-related references are shown at the end of the chapter. This is in addition to the **Bibliography** section at the end of the thesis. Data of detailed nature are located in appendices at the end of the thesis. As a few prototypes are presented, a naming convention is used to simplify referencing to these prototypes. A three digit code is used, proceeded with P, for example P719 is the 7^{th} prototype, revision 1 with the 9 indicating for reporting.

Over time, the performance requirements of modern deployable shelters have become more demanding. This has driven the development of more sophisticated structural forms and solutions. In **Chapter 2**, the literature is surveyed for deployability requirements and different deployable shelter systems developed over the last forty years. As the truss panel system is the main focus of this investigation, Chapter 2 also presents a review of the currently available fibre composite truss systems. The chapter ends with a discussion of the limitations of these systems.

The current investigations started with manufacturing and testing a number of panel alternatives. Based on these investigations, a range of different panel concepts were established. These concepts were based on using multi-pultrusion sections for the chords and verticals, subsequently referred to as the Multi-Pultrusion Truss System (MPTS). **Chapter 3** presents the research work conducted to establish the first MPTS which had a discrete-diagonal (DD) made of sandwich construction. The FE method of analysis was used to explore the main behavioural issues including mechanisms of force transfer, governing failure modes, and panel capacities.

As several of the truss concepts used sandwich structures for the diagonals, the behaviour of sandwich members under compressive loads was investigated. **Chapter 4** starts by surveying the literature for sandwich structure applications and methods of predicting their capacity. A number of prototype column sets were tested with different core material layouts. This was to investigate their effect on the column capacities and failure modes. With the understanding of the behaviour of sandwich columns, a full-scale truss panel was manufactured and tested with the diagonals in compression. The chapter concludes with recommendations for sandwich columns, their capacity predictions, and behavioural discussion of the DD-MPTS with diagonals subject to compressive forces.

Another alternative of MPTS was achieved by replacing the traditional diagonal truss member with a complete diaphragm (DI). In **Chapter 5**, the DI-MPTS alternative is investigated with three different types of diaphragms. The chapter concludes with a discussion of the basic behaviour of this new technology.

When developing new innovative composite truss systems, it is important to provide a simplified modelling approach to predict their behaviour. This can be a

valuable tool for researchers who are interested in conducting further parametric studies, without the need to use high-end FE software packages. It is also good for practising engineers who are interested in using these truss systems to model the overall behaviour of the truss, as part of the whole structure. **Chapter 6** focuses on these simplified procedures. The developed models are compared with the micro-analysis model results for the different MPTS. The chapter concludes with general recommendations for the simplified models.

The main body of the thesis ends with **Chapter 7** which contains the main conclusions and suggestions for future research work. More detailed information is provided in the attached appendices.

Assessing the loading criteria for deployable structures is a challenging process that requires engineering judgment, as these structures can be utilised in different places around the world where different local loading criteria and requirements apply, as per local national loading codes. A flexible assessment concept for global loading criteria is presented and discussed in **Appendix 'A'**.

The deploying mechanism and the erection stage are integral parts of the structural behaviour when in service. Two different types of analysis were used to assess the structural behaviour. **Appendix 'B'** presents and discusses the results of these different types of analysis.

In **Appendix 'C'**, the test results and observations for four different sets of sandwich columns are presented and briefly discussed.

The concept of DD-MPTS was extended by using double-bay panels. The usage of these panels can reduce the manufacturing costs due to having fewer panels to cover the same area. In **Appendix 'D'** both dynamic and static test results of this panel are presented and discussed.

1.7. SUMMARY

Deployable shelters are a sub-set of deployable structures that can be used for military and/or civil applications. The M^2S^2 deployable shelter system is a further development of the stressed-arch concept implemented by Strarch using steel frames. The M^2S^2 research programme aims to extend the existing Strarch concept into a system with dramatically improved deployment characteristics. This chapter presented an overview of the concept and components of the M^2S^2 shelter system and outlined the structure of this thesis.

1.8. REFERENCES

Clarke, M. J., and Hancock, G. J. (1994).Behaviour and design of stressed-arch (Strarch) frames. *IASS-ASCE International Symposium 1994 on spatial, lattice and tension structures*, Atlanta, 200-209.

Escrig, F. (1996). General survey of deployability in architecture. *Proceedings of MARAS'96, the second International Conference on Mobile and Rapidly Assembled Structures*, Seville, Spain, 3-22.

Gantes, C. J. (2001). *Deployable structures: Analysis and design*, WIT Press, Southampton, United Kingdom.

Google. Homepage, http://www.google.com.

Key, P. W. (2004). The Starch modular military shelter system - Load specification. Strarch, Sydney.

Strarch. Homepage, http://www.strarch.com.

Strarch. (1999). The Strarch building system - Technical discussion. Strarch, Sydney.

2. Deployable Shelters and Fibre Composite Trusses - State of the Art

2.1. GENERAL

The literature review presented in this chapter covers three main areas: (i) performance criteria for deployable shelters, (ii) available deployable shelter systems and (iii) structural systems of composite trusses.

Other literature reviews, related to specific topics such as FE modelling procedures, material characteristics, and buckling behaviour of sandwich members, are presented in Chapter 3 and Chapter 4 where they are directly related to the topics discussed in these chapters.

2.2. DEPLOYABLE SHELTERS PERFORMANCE CRITERIA

In searching the literature it was found that military documents, published on aircraft maintenance hangars, were one of the few sources that provided some guidance on performance criteria for deployable shelters. Originally, the Required Operational Capability (ROC), issued by the US Marines Corps (Strarch, 1991), specified the following criteria:

- no special tools or material handling equipment;
- repairs should be limited to structural and fabrics within the field capability with no special tools or machines;
- minimum internal dimensions of 27.45mW x 36.6mL x 7.0mH[1];

[1] W: Width or span, L: Length, H: Height.

- have an unused service life of 20 years;
- have in-use service life of 15 years with two cycles of assemble and dismantle per year;
- resistance to deleterious effects of sun, weather, salt and moisture;
- materials used should not support combustion nor produce high levels of hazardous fumes when exposed to fire;
- designed to withstand service wind speed of 29m/s that gusts to 40m/s;
- able to be erected in wind speed of 9m/s that gusts to 11m/s;
- designed to carry snow loads of 1.0kPa;
- operational temperature of -25c to +55c.

More recently, the Unified Facilities Criteria (UFC) system was introduced with the purpose of issuing related documents to provide planning, design, construction, sustainment, restoration, and modernization criteria for the different military construction projects (Department of Defence, 2005). Due to the light-weight of deployable shelters, wind loads usually govern the design of these structures. No specific requirements for deployable shelters are contained in the UFC documents. Although, they identify important design parameters for aircraft hangars by specifying the wind load data for different locations in the United States and worldwide along with specifying the borderline between “open-door” and “closed-door” shelters, UFC 4-211-01N (Department of Defence, 2004). More detailed discussion of assessing wind loading on deployable shelters is found in Appendix ‘A’.

2.3. MODERN DEPLOYABLE SHELTERS - REVIEW

The basic components of deployable shelters are the structural system (primary load transfer) and the cladding system. The cladding system can have different functions depending on its inherent properties and those of the structural system used. For example, cladding systems can be used to stabilize the structural system, assist in carrying primary loads, or can be integrated with the overall load-carrying system. Consequently the two systems are generally dependent on each other.

Recent developments of deployable shelter technology can be categorised as:

- Pantograph type structures;
- Air-inflated shelters;
- Rigid frames supporting soft fabric shelters;

This section explains the main characteristics of the different systems.

2.3.1. PANTOGRAPH TYPE STRUCTURES

Various deployable structural forms were explored in the second half of the twentieth century. Emilio Perez Pinero developed the concept of a travelling theatre (Peniro, 1961a, 1961b & 1962). His approach was based on the principle of a pantograph (Figure 2.1). In this system the frame members have three connections, with the end ones hinged while the middle one is pivotally connected to the crossing member. The basic structural system includes rigid bars and wire cables. The stability of the structure in its erected position is achieved by using locking devices such as cables. In spite of being a simple concept, using it in a large structure is problematic as securing and releasing the locking devices require skilled labour and a temporary supporting system (Chapter 2, Gantes, 2001).

Further development of the pantograph-type deployable structures was carried out by Zeigler (1976). Zeigler made use of the geometry of a partial spherical dome that is self-supported in the erected form, without any additional members or cables. To satisfy the geometrical requirements in Zeigler's system, each rod must radiate from the same apical point. This constraint has limited its application. In addition, the bent nature of the rods in the erected position significantly decreases the load-carrying capacity of such members (Gantes, 2001). Further investigation of the behaviour of pantograph systems was carried out by Raskin and Roorda (1996). They investigated the stiffness and stability of pantographs that utilised additional boundary conditions in the deployed configuration.

As can be observed, the currently developed pantograph systems have limited applications associated with the constraints in using them. With fibre composites, these systems are not favourable due to the nature of stress concentrations at the

joints which will significantly reduce the load carrying capacity and increase the costs associated with having many joints in the structure.

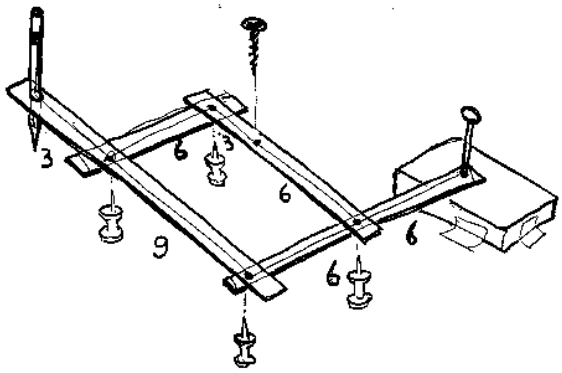

Figure 2.1 Principal of pantograph (Gantes, 2001)

2.3.2. AIR-INFLATED SHELTERS

2.3.2.1. M-51 Air-Supported Shelter

Air-inflated shelters use air-pressurised closed elements to support a fabric cladding (Gantes, 2001). The M-51 was the first air-inflated shelter system developed for the US military in the 1960s. It was a mobile air-supported shelter, manufactured from Tedlar/Neoprene-coated Dacron laminated fabric (http://dupont.com) , mounted on a 1.5 ton standard military trailer (Figure 2.2). In spite of being a state-of-the-art fabric at its time, it lacked flame retardant properties and was heavy and stiff to handle (Verge). In addition, the M-51 provided limited floor space (18.5m^2), and needed continuous blower operation.

Figure 2.2 M-51 - First deployable shelter system (Verge)

2.3.2.2. Battalion Aid Station Air-Supported Shelter

Based on further developmental work, Teflon-coated Kevlar (http://dupont.com) was selected to replace the Tedlar/Neoprene-coated Dacron in an air-inflated Battalion Aid Station (BAS). The more advanced materials and the use of a urethane

film laminated nylon bladder with an uncoated polyester sleeve, which served as the structural member of the beam, eliminated the requirement for a constant blower operation and allowed a larger span structure. The structural framework of vertical or leaning air beams with a diameter of 350mm, pressured to 10kPa, was successfully used for a 5.48mW x 7.5mL x 3mH shelter. This form was capable of carrying snow loads of 0.48kPa and wind loads due to a wind speed of 13.4m/s (Fowler and Sinofsky, 1986).

2.3.2.3. High-Pressure Air-Supported Shelter

As traditional woven air beams were of limited span, unreliable and unsafe at high pressure (Verge), Vertigo Inc developed a high-pressure braided air beam using Vectran[2] around a urethane bladder (Figure 2.3). The urethane is used for its ability to contain the air while the Vectran is used for its flexibility and high strength as reinforcement for the urethane bladder. Since 1986, Vertigo Inc and the Natick Soldier Centre (NSC) have worked to advance the technology of high pressure braided air beams. The largest shelter manufactured and utilised using this technique is the Aviation Inflatable Maintenance Shelter (AIMS). The shelter dimensions are 25.3mW x 52mL x 10.7mH. It consists of nine 750mm air beams inflated to 550kPa and takes two days to erect (Verge).

Figure 2.3 Braided air beam by Vertigo Inc (Verge)

[2] Vectran is a manufactured fiber, spun from a liquid crystal polymer. These fibers are noted for thermal stability at high temperatures, high strength and modulus, low creep, and good chemical stability. They are moisture resistant and are generally stable in hostile environments. They have gold color. They are often used in combination with some polyester as a coating around Vectran core; polyurethane coating can improve abrasion resistance and resistance to ultraviolet radiation and act as a water barrier. Vectran has a melting point of 330°C, with progressive strength loss from 220°C (http://en.wikipedia.org, keyword Vectran).

The air-inflated shelters seem to be purely a military technology. It requires the usage of high-tech materials, with associated high costs. They are purpose-built with no flexibility. In addition, currently, they seem to be of limited spans.

2.3.3. RIGID FRAMES SUPPORTING SOFT FABRIC SHELTERS

2.3.3.1. Battalion Aid Station Frame-Supported Shelter

Rigid frames supporting soft fabric shelters are the most common form of deployable shelters used in recent times. These systems use cables and membranes which provide tensile stiffness and can be folded. In the late 1960s, the US military developed the soft-fabric-frame-supported Battalion Aid Station (BAS). This BAS has the same geometric profile as the air-supported version. Five supporting frames, comprising of fibreglass rods with prestressed cables, are used to support the Teflon-coated Kevlar fabric (Figure 2.4). The fibreglass rods are bowed and prestressed via connection to a cable by means of a fabric web. Separating the tension and compression members of the frame simulates the relatively high section modulus of an I-beam (Verge).

Figure 2.4 Frame supported BAS (Verge)

2.3.3.2. Expeditionary Aircraft Maintenance Hanger

In the 1980s, the Frame Supported Tensioned Structure (FSTS) hanger concept was developed by the Naval Civil Engineering Laboratory in California (NCEL) for the Navy P-3 aircraft. The hanger system used metal arches with high-strength stressed composite fabrics for the roof covers (Figure 2.5). The Expeditionary Aircraft Maintenance Hanger (EAMH) was based on the FSTS concept. The EAMH design accommodate basic wind speeds of 17.9m/s (doors open) and 44.7m/s (doors closed). The EAMH can be transported in a standard 20ft container (NCEL).

Figure 2.5 Expeditionary Aircraft Maintenance Hangar (NCEL)

2.3.3.3. WideSpan Frame-Supported Shelter

A more recent development in frame supported hangers was undertaken by Weatherhaven Resources Ltd. Their WideSpan range is a modular rapid-erection shelter that does not need heavy equipment (cranes) or skilled labour (Figure 2.6). All assembly is on the ground. A 465m^2 shelter can be transported by a standard 20ft container. The maximum component size is 3.66m and weights 68kg (www.weatherhaven.com).

Figure 2.6 Weatherhaven WideSpan shelter system (www.weatherhaven.com)

2.3.3.4. Extra Large Deployable Aircraft Hangar

The Extra Large Deployable Aircraft Hangar System (XLDAHS), to maintain the B2 stealth aircraft, is the largest deployable shelter commercially built for the US military. The first two shelters of this kind, each 76.2mW x 18.30mH and with a weight of 80 tons, were assembled in December 2002. The assembly required 20 persons for more than 70 days. Two temporary erection towers were used to place the trusses. Once in place, each truss was anchored down with cables, and attached to the previous one. The shelter's covering consists of huge sheets of fabric with eyelets

through which rope is run, Figure 2.7, (www.globalsecurity.org/military/systems/aircraft/systems/xldahs-pics.htm).

Figure 2.7 XLDAHS Shelter during erection (www.globalsecurity.org)

2.3.4. TENT SHELTERS

Tent structures are another form of rigid frames supporting soft fabric shelters. In the late 1990s, Bea Maurer Inc (www.base-x.com) and World Shelters (www.worldshelters.org) produced the Base-X Shelter System (Figure 2.8). The Base-X system is manufactured as a series of soft walled tents supported on a one-piece expanding metal frame that spans 2.90, 4.25 or 5.50m. In spite of developing Base-X for general purpose applications, it has been adopted by many military divisions of the US forces because of its light weight, compact size and minimal set up time[3].

Figure 2.8 Base X Shelter System by Bea Maurer (www.base-x.com)

[3] A 41.8m^2 shelter weighs 1.98kN and folds into a package of 1.05m^3. It can be assembled by 3 personnel in 19 minutes.

2.4. FIBRE COMPOSITE TRUSS SYSTEMS

As the modular truss panel system is the main focus of this study, a review of currently available composite truss systems was undertaken. Structurally, trusses are one of the most successful forms that have been used since the nineteen century. The stiffness and strength of a truss is derived from its geometry (especially its depth) and the axial stiffness of its members. The fibre-composite truss systems found in the literature are presented in this section.

2.4.1. TRUSSES MADE OF PULTRUSIONS

Most composite truss systems found in the literature use pultrusions for the truss members with bolted and/or adhesively joined connections. In these types of structures, the connections usually determine the strength of the structure (Turvey, 2000). These types of composite trusses have been used for both pedestrian bridges and roof structures. A typical bridge of this type is the Pontresina Bridge that crosses the Flanz River in Switzerland (Figure 2.9). The bridge was constructed in 1997 as a temporary bridge, and is installed each year in autumn and removed each spring. It consists of two truss girders that span 2x12.5m. The truss joints are adhesively bonded on one span and bolted in the other span. A cross-diagonal bracing system is used to reduce the joint forces and to provide redundancy in the glued span (Keller, 2001). A similar composite truss system was used for the roof of a water storage reservoir at Darvel (Gilby, 1998). The 19m span truss members are connected with bolts and stainless steel gussets (Figure 2.10).

Figure 2.9 Pontresina bridge, Switzerland (Keller, 2001)

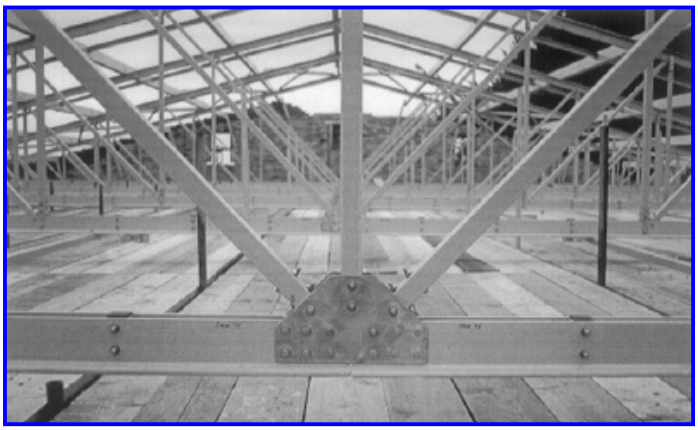

Figure 2.10 Composite trusses for storage reservoir roof at Darvel (Gilby, 1998)

2.4.2. BRIDGE DECKS WITH TRUSS FORM

In the past decade, many composite bridge decks have been constructed using pultrusion assemblies that are bonded together as a truss-like configuration. The increased strength and stiffness per unit weight, compared to reinforced concrete decks, allow for an increased live load rating for most bridges (Bakis et al, 2002).

EZSpan is a typical application of a bridge deck that uses a truss configuration. The EZSpan system was developed by the Atlantic Research Corp (ARC). The deck spans 3.05m and weighs 98kg/m^2 (Brown and Zureick, 2001). The triangular elements are fabricated using a single, thick ply of 3D braided fibreglass textile which is drawn through the pultrusion die (Figure 2.11). The triangular pultrusions are bonded together by the facing sheets.

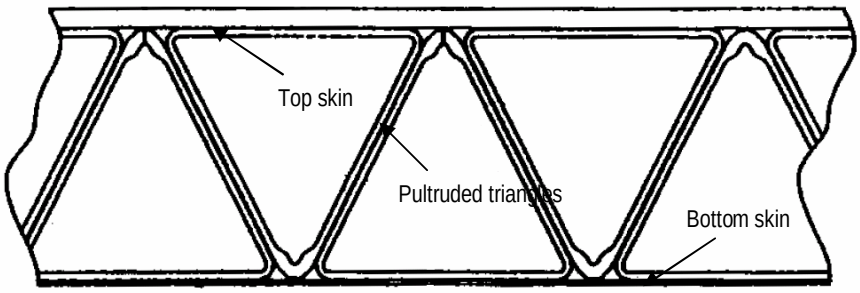

Figure 2.11 EZSpan system (Brown & Zureick, 2001)

2.4.3. MONOCOQUE FIBRE COMPOSITE TRUSS

Another non-conventional composite truss system was proposed by Humphreys et al (1999). The Monocoque Fibre Composite (MFC) truss concept is based on using double skins that contain the fibre structure of the truss members. The skins are

separated by a core material (Figure 2.12). The truss derives its strength from the reinforcing skins while the core material separates the skins to provide lateral stiffness for the members. Due to the difficulty in lapping the joints, Humphreys et al (1999) introduced the concept of strength and fill layers. The Strength layer is the layer where fibres are extended through the joint while the fill layers stop at the member intersections. In using a different sequence of strength and fill layers, each of the truss members can be connected to the joint (Figure 2.13).

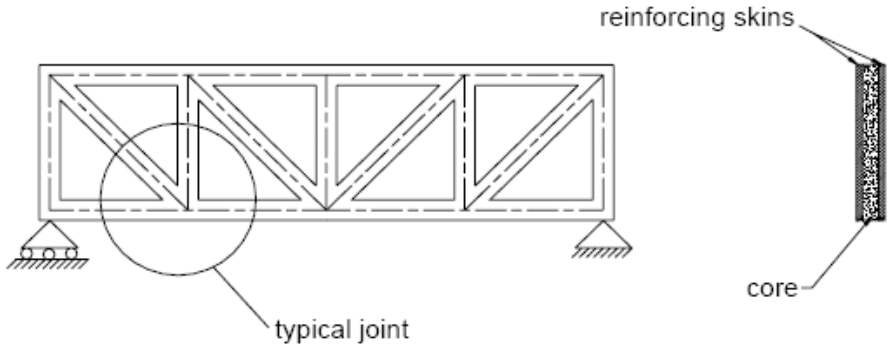

Figure 2.12 Monocoque Fibre Composite truss concept (Humphrey et al, 1999)

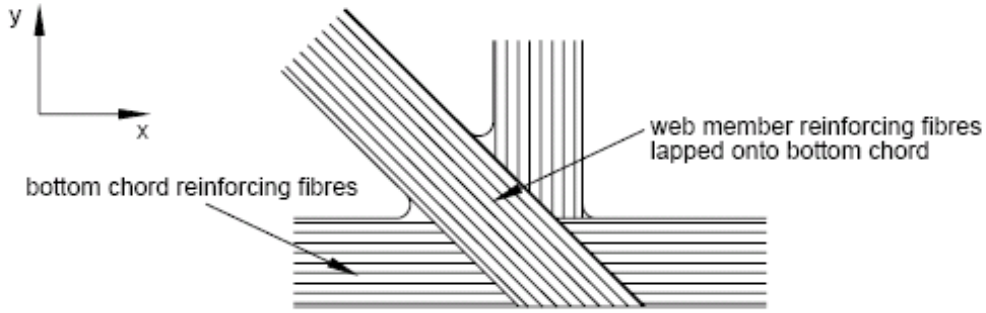

Figure 2.13 MFC concept of strength and fill layers (Humphrey et al, 1999)

2.4.4. FIBRE COMPOSITE TRUSS WITH SNAP-JOINT

Goldsworthy and Hiel (1998) developed an all-composite truss system for overhead transmission lines. They introduced the award-winning snap-joint concept (Figure 2.14) which is similar to that used for connecting wooden parts. Despite being limited to transmitting axial loads only, the jointing technique is quite simple and robust. The joint design is capable of distributing the stresses over a wide area and accordingly is quite suitable for connecting composites. The joint was used successfully in the construction of the Strongwell Ebert overhead line transmission tower (Figure 2.15, www.strongwell-ebert.com).

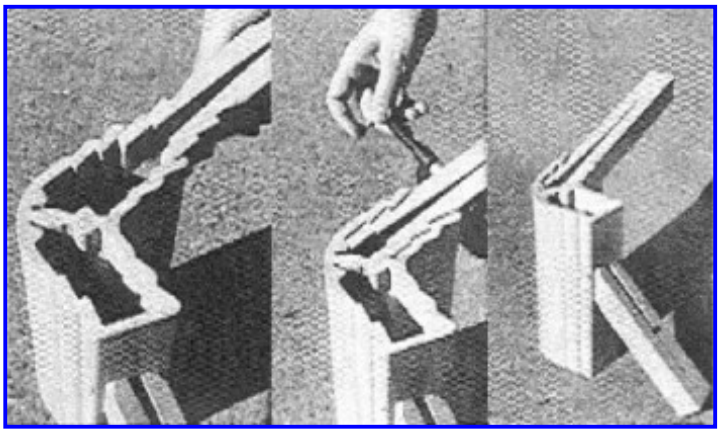

Figure 2.14 Assembly of snap-joint (Goldsworthy & Hiel, 1998)

Figure 2.15 Overhead transmission tower using snap-joint (www.strongwell-ebert.com)

2.4.5. MODULAR COMPOSITE TRUSS PANELS

Bradford et al (2001) have developed a modular composite panel concept that can be used for emergency shelters and bridge decks. The modular panel was optimised by integrating the connection within the panel. The selected trapezoidal shape allows two panels to slide and interlock (Figure 2.16). This set-up avoids the concentration of forces at the panel joints, as forces are dispersed evenly along the member. A trapezoidal profile also prevents the development of a weak hinge joint which can occur when using a triangular profile

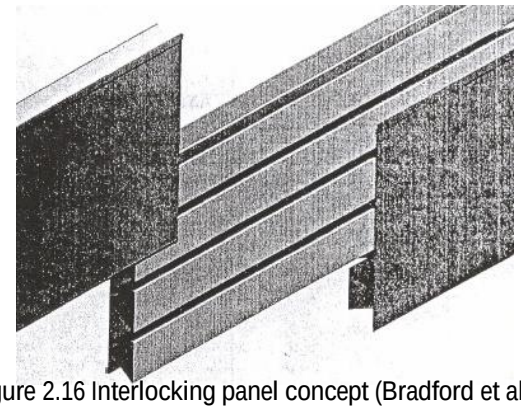

Figure 2.16 Interlocking panel concept (Bradford et al, 2001)

2.5. CONCLUSIONS

Based on the literature review presented in this chapter, the design of deployable shelters needs further research in a number of areas. The design criteria should be defined more clearly. They should be flexible enough to comply with the different national loading codes yet reflect the nature of the structure. Other than the frame-supported systems, most systems seem to have limited application for deployable shelters. Many of the developed frame-supported systems are not modular and accordingly lack flexibility in defining the geometry of the shelter. The availability of many systems without the predominant application of any one suggests that none has fully satisfied the shelter deployability requirements. None of the above systems used the concept of prestressed arch technology. This indicated the originality of the M^2S^2 concept.

The presented truss systems seem unsuitable for the modular panel for M^2S^2 trusses due to two main reasons. The first is strength requirements and the second is functional requirements. With the level of forces expected in a 30m trusses, Appendix B, none of the presented systems is capable to carry these forces, especially at joints. Functionally, the bottom chord should allow threading prestressing cables with sufficient seating for the bottom joints. In addition, the top chord should allow having the top joints. This necessitates developing an innovative truss system that suits the M^2S^2 concept and capitalises upon the characteristic strengths of composite materials. Clearly one of the key areas of investigation associated with this innovative development is the structural behaviour of this new truss system.

In Chapter 3, the development of an innovative truss system for the main frames is presented.

2.6. REFERENCES

Bakis, C. E., Brown, V. L., Cosenza, E., Davalos, J. F., Lesko, J. J., Machida, A., Rizkalla, S. H., and Triantafillou, T. C. (2002). Fibre-reinforced polymer composites for construction, State-of-the-art review. *J for Composites for Construction*, 6(2), 73-87.

Base-X. Base-X Home page, http://www.base-x.com/.

Bradford, N., Sen, R., and Mosallam, A. (2001). Development of a new modular composite panel system. *46th International SAMPE Symposium and Exhibition 2001 a Materials and Processes Odyssey*, Long Beach, CA, USA, 931-942.

Brown, R. T., and Zureick, A. (2001). Lightweight composite truss section decking. *Marine Structures*, 14, 115-132.

Department of Defence. (2004). Design: aircraft maintenance hangers: type I and type II. *UFC 4-211-01N*, USA.

Department of Defence. (2005). General building requirements. *UFC 1-200-01*, USA.

Du Pont Homepage. http://dupont.com.

Fowler, W., and Sinofsky, M. (1986). Development of an improved air-supported battalion aid station. *TR-88/029L*, US Army Natick Soldier Centre, Buffalo, New York.

Gantes, C. J. (2001). *Deployable structures: Analysis and design*, WIT Press, Southampton, United Kingdom.

Gilby, J. (1998). Pultrusion provides roof solution. *Reinforces Plastics*, 42(6), 48-52.

Globalsecurities. Homepage, http://www.globalsecurity.org/military/systems/aircraft/systems/xldahs-pics.htm.

Goldsworthy, W. B., and Hiel, C. (1998). Composite structures. *SAMPE Journal*, 34, 24-30.

Humphreys, M. F., Van Erp, G. M., and Tranberg, C. (1999). The structural behaviour of monocoque fibre composite truss joints. *Advanced Composite Letters*, 8(4), 173-180.

Keller, T. (2001). Recent all-composite and hybrid fibre-reinforced polymer bridges and buildings. *Prog. Structural Engineering Materials*, 3, 132-140.

Naval Civil Engineering Laboratory (NCEL). Frame supported tensioned structure (FSTS) hanger concept. Department of Navy - US, California.

Pinero, E. P. (1961a). A reticular movable theatre. *The Architects' Journal*, 134, 299.

Pinero, E. P. (1961b). Project for a mobile theatre. *Architectural Design*, 12, 570.

Pinero, E. P. (1962). Expandable space framing. *Progressive Architecture*, 12, 154.

Raskin, I., and Roorda, J. (1996). Buckling force for deployable pantographic columns. *Proceedings of MARAS'96, the second International Conference on Mobile and Rapidly Assembled Structures*, Seville, Spain, 305-314.

Strarch. (1991). An analysis of US military requirements for large deployable shelters. Strarch, Sydney.

Strongwell. Strongwell Ebert LLC Home page, http://strongwell-ebert.com/.

Turvey, G. J. (2000). Bolted connections in PFRP structures. *Prog. Structural Engineering Materials*, 2, 146-156.

Verge, A. S. Rapidly deployable structures in collective protection systems. U.S. Army Natick Soldier Center (www.natick.army.mil), Massachusetts, USA.

Weatherhaven. Homepage, http://www.weatherhaven.com/.

Wikipedia home page. http://en.wikipedia.org.

World Shelters. Homepage, http://www.worldshelters.com.

Zeigler, T. R. (1976). Collapsible self-supporting structures. US Pat 3 968 808, USA.

Chapter 3 Notations

b	Pultrusion flange flat clear width
$\mathbf{D_{jj}}$	Shell section jj stiffness matrix parameter
$\mathbf{E_1}$	Tensile modulus in the 1-1 (fibre) direction
$\mathbf{E_2}$	Tensile modulus in the 2-2 (normal to fibre) direction
$\mathbf{E_3}$	Tensile modulus in the 3-3 (normal to laminate plane) direction
$\mathbf{G_{12}}$	Shear modulus in the 1-2 plane
$\mathbf{G_{kl}}$	Shear modulus in the k-l plane
$\mathbf{K_{ii}}$	Thick shell transverse shear stiffness in the i-i direction
l	Plate characteristic length
t	Pultrusion flange thickness
l	Plate slenderness
n_{mn}	Poisson's ratio of the m-n plane

3. Behaviour of Discrete-Diagonal, Multi-Pultrusion Truss Systems

3.1. GENERAL

The concept of modularity in M^2S^2 is based on using standard panels. Frame modularity provides flexibility and ease of assembly, in addition to cost reductions associated with producing few components in quantities. As discussed in Chapter 2, an innovative truss system is needed to satisfy the modularity requirements of M^2S^2. The current chapter focuses on establishing such truss system.

Early, investigations conducted for the truss panels were of an exploratory nature. Panel alternatives were manufactured, tested or partially tested then considered for further investigations. This was accompanied by building experience in using composites and developing systems that suit its characteristics. The parameters considered in these investigations included the structural system, fabrication techniques, the structural performance (such as capacity, ductility, stability, durability and fire resistance) and operational considerations (such as handling, assembly, dismantling and storage). The merits of each panel system were initially assessed based on its functionality (as a structural system) and deployability. Other factors such as (i) manufacturability, (ii) possibility of integration and control of materials and components, and (iii) cost effectiveness were also considered, but with no detailed assessment.

The first panel investigated consisted of single pultrusion members that were adhesively bonded then coated with a particulate-filled-resin (PFR) system. The difficulties faced during its manufacture provided valuable experience highlighting the important factors to consider in developing further panels. This experience led to the development of the concept of a multi-pultrusion truss system (MPTS). Prior to

manufacturing a MPTS prototype panel, its joint system was investigated. These investigations revealed unsatisfactory structural performance of the joint, the concept was revised by eliminating the traditional use of gussets to connect truss members. This was achieved by using a sandwich construction for the diagonal members with skins directly joining the chord and vertical members.

Structural response is commonly predicted by physical testing on a scale model or a prototype. The first prototype Discrete-Diagonal (DD) MPTS was tested with diagonals subjected to tensile forces. The structural performance of DD-MPTS was excellent with failure occurring in the diagonal skins, outside of the joint area. FE modelling was used to simulate the test experiment. After verifying the model with the test records, the test observations and the FE model results were used to explain the behaviour of the DD-MPTS.

3.2. ADHESIVELY BONDED PULTRUSION / PFR TRUSS SYSTEM (PANEL: P109)

The first truss-shape panel (P109) had single pultrusion members that were adhesively joined and then coated with particulate-filled resin (PFR), using a casting technique. P109 proved to have shortcomings that precluded further development of this approach. However, the exercise provided valuable experience in the development of the panel concept. In this section, the P109 panel concept and the manufacturing process are briefly presented, highlighting the experience gained.

3.2.1. P109 - CONCEPT

P109 had cross-bracing and single chord and vertical members (Figure 3.1). Circular hollow sections (CHS) were used for the chords and rectangular hollow sections (RHS) were used for the verticals. The diagonals were formed from flat pultrusions with polyurethane (PUT) foam core. A double laminated joint system was used at each corner of the panel. Members and joints were encased in PFR. This was to protect the joint areas, provide suitable seating for the panel during erection and increase the panel fire rating by protecting both members and joints (Figure 3.1).

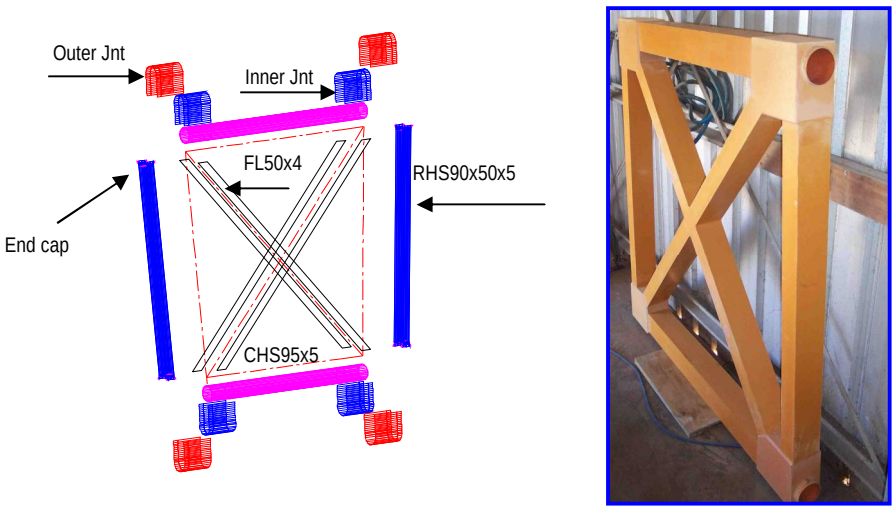

a) b)

Figure 3.1 P109 - Panel a) Components and b) Layout

3.2.2. P109 - PANEL MANUFACTURING

The P109 was manufactured in four stages. The first stage was the manufacture of individual members. The second stage was casting PFR around the members, except at the joint area (Figure 3.2). After casting the PFR, each member was post-cured at 150°C for four hours with one hour ramp[1]. This was to obtain PFR strength to avoid damage during the remaining manufacturing stages. The third stage was assembling members using adhesively-bonded joints. The fourth stage was casting the PFR at the joint areas.

Figure 3.2 P109 – Casting PFR on the chord members

[1] All the post-curing conducted for this panel was for four hours at 150˚c with one hour ramp.

3.2.3. P109 - PANEL EVALUATION

P109 was the first structure, in composites, to be built by the author. This exercise provided good experience in dealing with different and difficult materials at different stages of their forms (fibres, resins, adhesive and PFR), in curing and post-curing, and in manufacturing techniques. However, the P109 panel system suffered from serious shortcomings, summarised below, that prompted reassessment of its development.

- The manufacturing and assembling procedures were complex and labour intensive. This was due to using components of non-standard sizes, having many components, using curved-shaped surfaces and the multi-procedure process.
- Using CHSs for the chords resulted in continuous joints in double layers. This can be good in transferring forces from the diagonal flats to the joint layers. However, using curved surfaces complicated the assembly with other components.
- The quality of the joint gluing was very difficult to monitor and therefore ensure. This raised a concern about the level of quality control required in a normal manufacturing environment.
- The curing sequence and the use of PFR with variable thicknesses resulted in cracks forming in many locations in the PFR. These cracks were not of structural significance but were expected to affect the functionality of the PFR.
- Despite using light-weight fillers for the PFR, the PFR contributed about 60% of the panel weight with minor contribution to the panel strength.

3.2.4. IMPORTANT PARAMETERS FOR THE PANEL SYSTEM

The experience gained from manufacturing P109 contributed to the identification of a number of important factors that need to be considered in the next version of the panel system. These are:

- *Flat sided components*. This is important in the manufacturing and assembly processes. Flat side components, generally, do not require special tooling to

assemble. They can be assembled on flat surfaces, easily located, clamped and secured in position.

- *Minimal number and variety of components*. Minimising the number of components facilitates the assembly process and reduces the number of procedures required. Using standard components, as much as possible, eliminates the costs associated with the manufacturing and assembling of non-standard items.
- *Eliminate the use of PFR*. As discussed, using PFR complicates the manufacturing process and adds significant weight to the panel.
- *Reduce the number of post-curing cycles*. As the post-curing process is a time and energy consuming process, the panel should be constructed completely prior to conducting post-curing. The panel components should be strong enough to resist applied loads during assembly and transportation prior to conducting the post-curing.
- *Extend the joint area*. The development of P109 highlighted the importance of the joint. Preference is for a system that is not sensitive to construction imperfections and can be easily controlled and assessed.
- *Structural redundancy*. This characteristic is desirable in structural systems. Key elements in a structure should not fail resulting in sudden and complete structure failure.

3.3. DISCRETE-DIAGONAL, MULTI-PULTRUSION TRUSS SYSTEM (DD-MPTS) - CONCEPT DEVELOPMENT

The concept of a multi-pultrusion truss system (MPTS) was introduced to overcome the above-mentioned challenges. In this section, the development of the MPTS concept is presented. As the traditional use of gussets to join truss members was unsatisfactory, the concept was refined by eliminating the use of gussets and utilising instead diagonal skins (in sandwich construction) to join the connecting members.

3.3.1. DD-MPTS - CONCEPT

The MPTS was based on the use of three (or more) hollow square or rectangular pultrusions for the panel chords and the vertical members (Figure 3.3 & Figure 3.4). Diagonals were to be the same width as that of the middle pultrusion and be connected to the chord and verticals through gussets. The advantages of this approach are:

- Pultrusions are among the most efficient and economical forms in composite sections.
- Using multi-sections significantly improves the lateral stability of the members in compression.
- Local buckling resistance of the members is good due to the use of multiple sections rather than single section;
- Compared to the chord members, the diagonals carry lesser force. MPTS allows the use of smaller diagonals to match the middle pultrusion section.
- The joint area is naturally protected by the outer pultrusions.
- The proposed panel is simple to manufacture. It allows using more than one cable to conduct the prestressing process. It also provides much more area to join the adjacent panels.

.

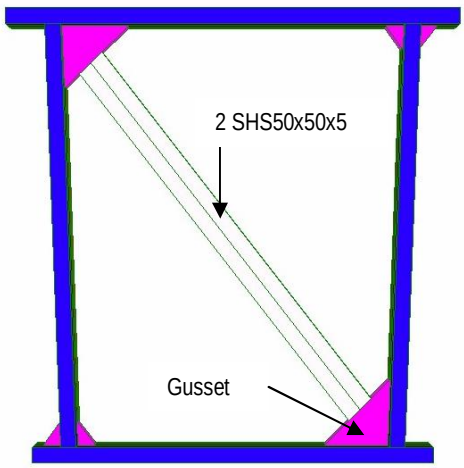

Figure 3.3 DD-MPTS - Initial concept

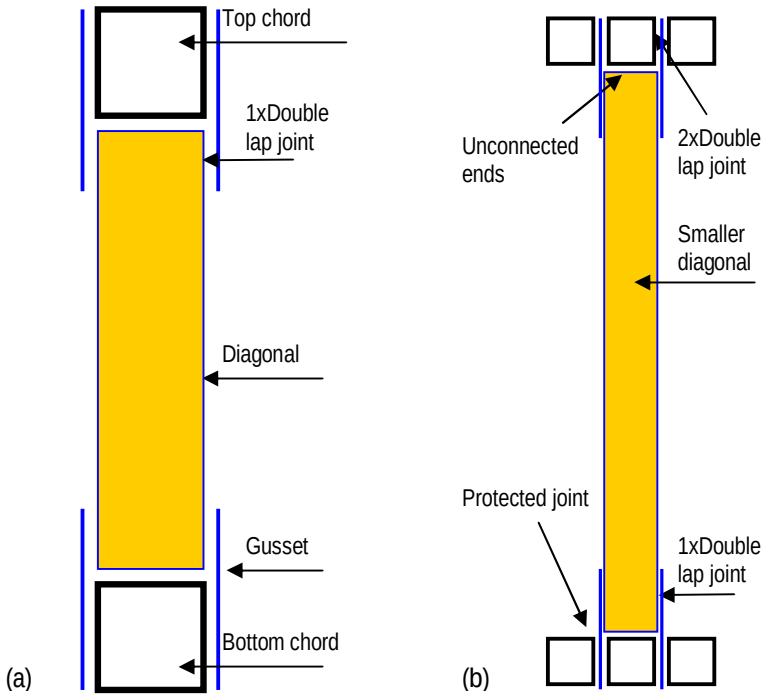

Figure 3.4 Developing the concept of DD-MPTS from (a) Traditional truss to (b) MPTS

3.3.2. DD-MPTS BRACKET (P209) MANUFACTURING AND MATERIALS USED

Prior to commencing with the costly panel prototyping, a few prototype joints were tested to investigate the behaviour of the proposed panel joint. Two parameters were considered in this investigation: the effect of the gusset structure and the type of the connecting member. The joint layout is shown in Figure 3.5a.

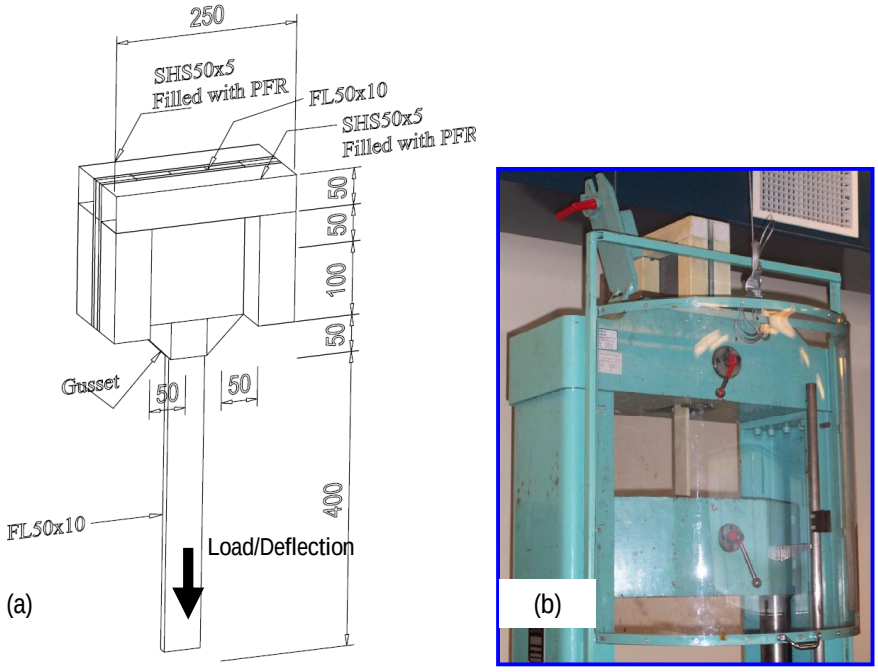

Figure 3.5 P209 - Bracket (a) dimensions, and (b) test layout

Brackets were manufactured from standard SHS50x50x5 pultrusions with gussets laminated, cut to dimension, then adhesively bonded. Due to the limitation of the testing machine clamping jaws, the diagonal box member was replaced by a 50x10mm flat.

Four prototype joints were tested, using two types of connecting members and three structures of gusset plates (Table 3.1). FL50x10-Pult was formed by cutting two faces of the pultrusion (polyester/glass) SHS50x50x5 (from Pacific Composites, www.pacomp.com.au), and gluing them together. FL50x10-Lam was laminated by gluing two laminates of 4 plies of 450gsm uni-glass (MU4500 from Colan, www.colan.com.au). Hyrez 201 epoxy (Rogers 2004), based on Bisphenol A and F with an amine-based hardener, was used for the laminate matrix. The mixing ratio, by weight, of the epoxy and hardener was 100:20.

Table 3.1 Description of the 209 joint brackets

Bracket	Description	
	Gusset	Member
01	10 plies of glass DB	FL50x10-Pult
02	6 plies of glass DB	FL50x10-Pult
03	4 plies of carbon DB	FL50x10-Pult
04	4 plies of carbon DB	FL50x10-Lam

The parameters considered for the gussets were stiffness and strength. In all cases, double bias (DB) fibre architecture was used with the fibre direction forming ±45deg of the loading axis. Hyrez 201 epoxy was used to laminate MX6000 glass (600gsm) from Colan (www.colan.com.au) and CF410BX/1270 carbon (410gsm) from Lavender (www.lavender-ce.com) with the number of plies shown in Table 3.1. Mid-plane symmetric construction was used for the gussets, with a maximum of 4 layers of laminates at once. HPR26 thixotropic toughened epoxy adhesive with HPR26 hardener (from ATL Composites, www.atlcomposites.com.au) was used with mixing ratio of 100:50, by weight, of adhesive and hardener.

The characteristics of the SHS50x50x5 polyester/glass pultrusions are shown in Table 3.2. Epoxy/glass uni-directional properties are shown in Table 3.3 while properties of the epoxy/double-bias are shown in Table 3.4. The typical properties of the adhesive, after post-curing at 80˚C for 8 hours, are shown in Table 3.5.

Table 3.2 Characteristics of pultrusions

Test	Testing Standard	Property	Testing values Average	Std Dev
Textile-glass content	ISO 1172 (1996)	Fibre fraction	71.42%	0.10%
Tensile	ISO 527-4/2/2(1993)	0 deg peak stress(MPa)	449.92	32.04
		0 deg tensile modulus (MPa)	33171	619
Shear	ASTM D537M-93	Peak stress(MPa)	62.93	5.05
		Shear modulus (MPa)	5167	249
Compression	ISO 14126(1999)	0 deg peak stress(MPa)	481.7	74.82
		0 deg compression modulus (MPa)	33890	3573
		90 deg peak stress(MPa)	116.02	7.38
		90 deg compression modulus (MPa)	15775	2031

Table 3.3 Characteristics of uni-glass laminates

Test	Testing Standard	Property	Testing values Average	Std Dev
Tensile neat resin	ISO 527-2/1B/1(1993)	Peak stress(MPa)	74.32	0.38
		Tensile modulus (MPa)	2762	85
Flexure neat resin	ISO 178(1997)	Peak stress(MPa)	112.6	1.43
		Flexure modulus (MPa)	2705	49
Textile-glass content	ISO 1172 (1996)	Fibre fraction	41.40%*	0.86%
Tensile	ISO 527-4/2/2(1993)	0 deg peak stress(MPa)	363.24	15.06
		0 deg tensile modulus (MPa)	18607	569
		90 deg peak stress(MPa)	24.31	2.33
		90 deg tensile modulus (MPa)	5707	277
Compression	ISO 14126(1999)	0 deg peak stress(MPa)	360.66	25.05
		0 deg compression modulus (MPa)	24519	1133
		90 deg peak stress(MPa)	96.65	2.77
		90 deg compression modulus (MPa)	7939	1317

* In the tested components it was noticed that the fibre fraction was 51.8%. In the FE models, the 0 deg properties were factored by the fibre volume fraction ratio. This was confirmed by conducting an indicative characterisation testing.

Table 3.4 Characteristics of double-bias laminates

Test	Testing Standard	Property	Testing values Average	Std Dev
Interlaminar shear	ISO 14130 (1997)	Interlaminar shear stress (MPa)	36.07	1.27
Shear	ISO 14129(1997)	Peak stress(MPa)	41.6	0.4
		Shear modulus (MPa)	2123	61
Tensile - glass	ISO 527-4/2/2(1993)	45 deg peak stress(MPa)	296.9	12.9
		45 deg tensile modulus (MPa)	16231	724
Tensile - carbon	ISO 527-4/2/2(1993)	45 deg peak stress(MPa)	612.4	51.2
		45 deg tensile modulus (MPa)	38213	1477

Table 3.5 HPR26 adhesive properties

Test	Testing Standard	Property	Value
Shear	ASTM D3163	Lap shear strength (MPa)	11.9
Tensile	ISO 527-4/2/2(1993)	Peak stress(MPa)	34.1
		Tensile modulus (MPa)	2410

After assembly, the brackets were post-cured at 60˚C for four hours followed by 100˚C for four hours with one hour ramp. After conditioning the brackets at 24˚C with relative humidity of 50% for 24 hours, they were tested in tension using Avery testing machine (model 7110-DCJ, capacity 530kN) with a loading rate of 1mm/min (Figure 3.5b). Both load and displacement were recorded at the movable machine jaw.

3.3.3. DD-MPTS BRACKET (P209) BEHAVIOUR

All brackets failed in a sudden brittle mode with complete loss of strength. Failure occurred at the interface between the gusset and the diagonal member by interlaminar shear (Figure 3.6). The main behaviour of the brackets can be summarised as follows:

- The bracket stiffness is directly related to the stiffness of the loading member (Figure 3.7). In all tests, slippage at the jaws was observed until achieving full gripping at a load of ~3kN. Brackets 01, 02 and 03 had exactly the same stiffness. Bracket 04 diagonal had less fibre fraction (compared to the pultrusion section, Appendix ‘E’) and accordingly 04 was less stiff. However, no direct relationship between the stiffness of the diagonal member and the joint capacity. For example, the 04 bracket failed at higher loads than other brackets.
- Increasing the stiffness of the gussets increased the joint capacity. In increasing the number of plies (01) or using carbon fibres (03) the bracket capacity increased from 71.6kN (02) to 77.5kN (108%) and 82.7kN (115%) respectively.

- The adherent matrix affects the capacity of the joint. As epoxies have higher inter-laminar shear strength compared to polyesters, 04 (99.2kN) recorded higher load carrying capacity compared to 03 (83.2kN).

It can be seen that both the adherent resin system of the member and the stiffness gusset were the main factors that affected the ultimate capacity of the brackets. The average failure strength was low (maximum of 6.6MPa[2] for 04) with joint efficiency of 42% (Clarke, 1996). The sudden failure of the brackets was another problem of this system. It was concluded that conventional use of gussets in the panel system will always govern the design leading to brittle failure mode. Accordingly, the DD-MPTS concept should be modified to avoid this shortcoming.

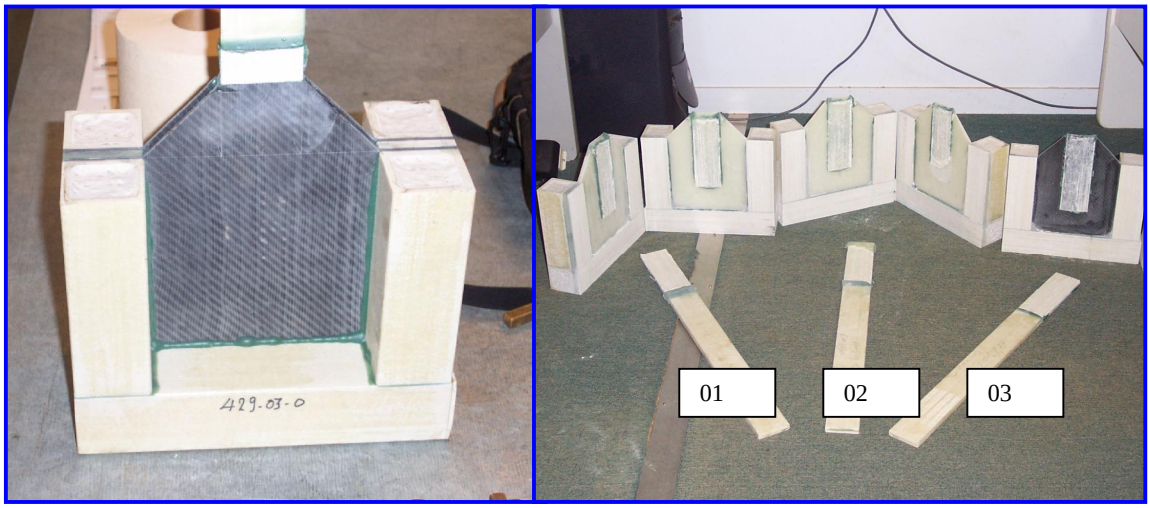

Figure 3.6 P209 - Failure modes

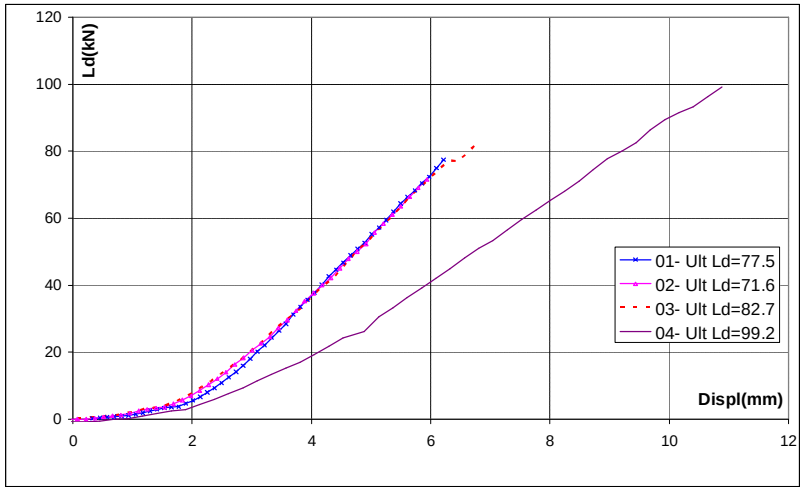

Figure 3.7 P209 - Load-displacement curves

[2] Ultimate strength was calculated by dividing the ultimate load by the adhesive shearing area.

3.3.4. DD-MPTS – THE UPDATED CONCEPT

As discussed in Sec.3.3.3, it became obvious that the joint system was a major problem. In the conventional approach of using gussets investigated in Sec. 3.3.1, the diagonal member stops short of the chord and vertical member. Hences, forces have to be transferred through the gussets (Figure 3.8a). To achieve direct transfer of forces, gussets should be eliminated.

Oneway to eliminate the indirect force transfer is to replace the pultrusion diagonal with sandwich diagonal (Figure 3.8b). Sandwich structures are a form of construction that offers high performance and low-weight. The basic components of the sandwich structure are two face sheets that can be manufactured from strong-high modulus materials, separated by a thick mid-layer core material. The face-sheets are the main carrier of bending and in-plane loads, while the core carries transverse shear. This alternative had many advantages that include:

- economical compared to using pultrusions with special section size;
- flexible in defining the diagonal geometry and structure;
- the diagonal member forces are carried by its skins which were in direct contact with the chord and the vertical members.

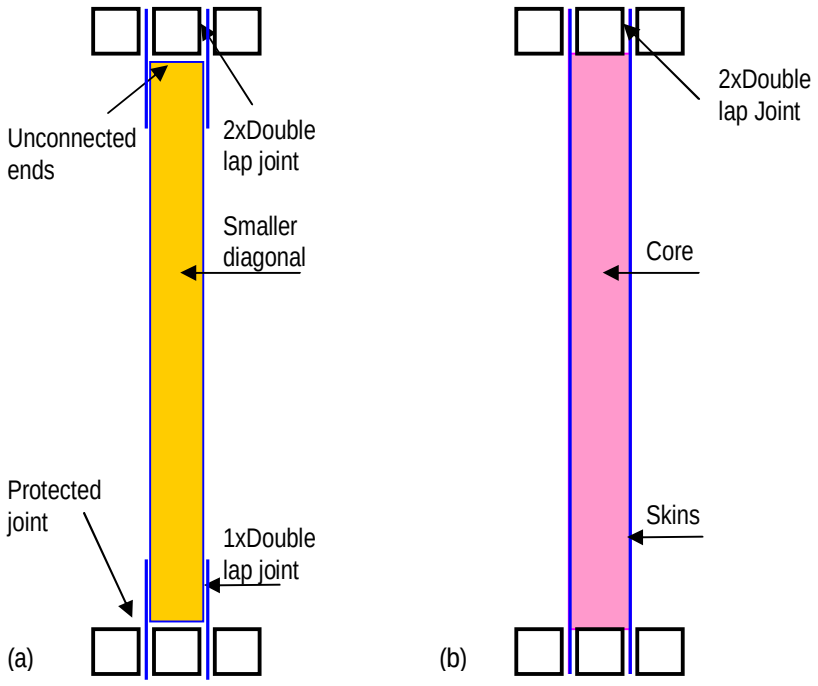

Figure 3.8 DD-MPTS (a) Original and (b) Updated concepts

3.4. DEVELOPMENT OF THE UPDATED DISCRETE-DIAGONAL, MULTI-PULTRUSION TRUSS SYSTEM (PANEL: P309)

The updated DD-MPTS panel (P309) was the first prototype to be tested (Figure 3.9). The test layout provided an insight of the joint capacity of the panel, achieving applying compressive forces to the top chord, and tensile forces to the bottom chord in a simple form where the panel is under equilibrium due to symmetry.

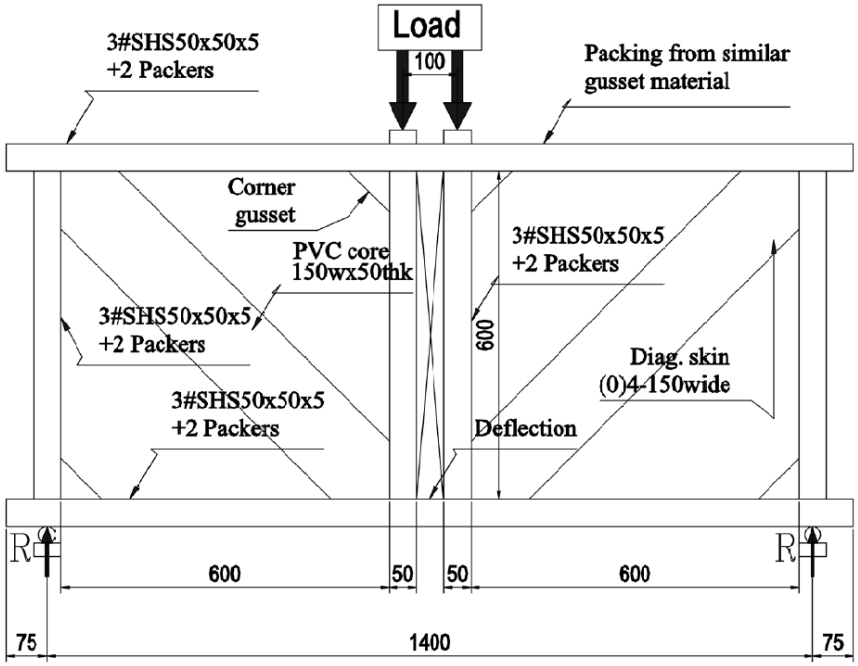

Figure 3.9 P309 - Dimensions and test layout

3.4.1. P309 - MATERIALS USED

The P309 concept was simple. Four components formed the panel constituents: SHS50x50x5 (polyester/glass) pultrusions (www.pacomp.com.au) for the chord and vertical members, Hyrez 201 epoxy/glass for the diagonal skins, Barakoda closed-cell PVC high density foam (www.diabgroup.com) for the diagonal's core and thixotropic toughened epoxy adhesive HPR26 (www.atlcomposites.com.au). As the main intent was to investigate the behaviour of the panel, the first prototype was constructed to be as simple as possible. Accordingly, the diagonal skins were formed from four layers of 450gsm uni-glass MU4500 (www.colan.com.au). The fibre direction was aligned with the member centreline. At locations other than corners, gaps between each pultrusion were filled with packers of the same architecture as the corner gussets (Figure 3.10). The gussets and the packers were laminated from 450gsm uni-glass (MU4500) and 600gsm DB-glass (MX6000) from Colan [+45/-45/0/0/-45/+45]. This architecture was to match the thickness of the diagonal skins

and have suitable 45 deg reinforcement for the gussets. Properties of the materials used are shown in Table 3.2 to Table 3.5 (Sec.3.3.2, p37-38) with properties of the Barakoda foam shown in Table 3.6.

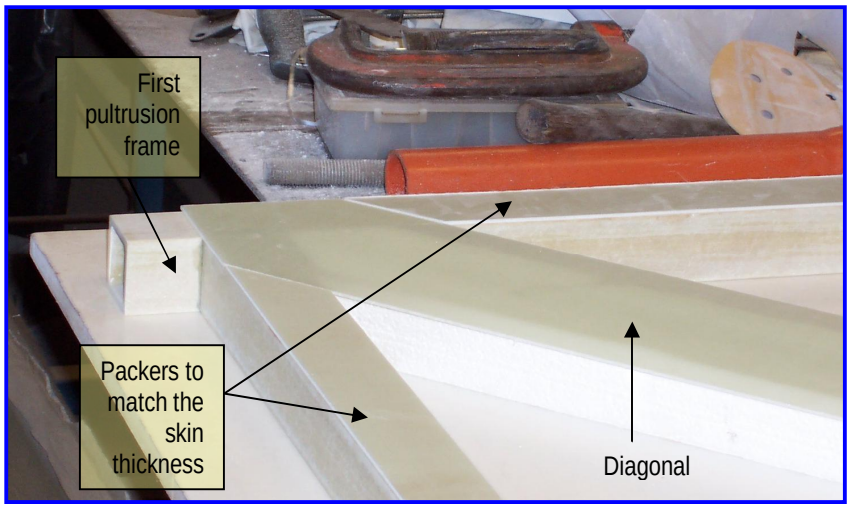

Figure 3.10 P309 – Diagonal skins and packers

Table 3.6 Characteristics of Barakoda foam

Test	Testing Standard	Property	Testing values	
			Average	Std Dev
Compression	ASTM D1621-94	Strength (MPa)	3.54	0.15
		Modulus (MPa)	131.00	5.00

3.4.2. P309 - PANEL MANUFACTURING

The P309 was relatively simple to manufacture. The manufacturing and assembly procedures are detailed below:

- Pultrusions were cut to length, sanded and cleaned with acetone.
- Each frame (a set of chord and verticals in one plane of the panel) was assembled by gluing the chord and vertical members then leaving it to cure for 24 hours.
- Excess glue was removed by sanding.
- Skin, gusset and packer laminates were completed with peel plies on each surface. Then they were cut to the required dimensions by using a diamond-coated bench saw.

- The first frame was fixed to the jig and an adhesive layer was applied to the frame side. The gussets, first diagonal skin and packers were placed on top (Figure 3.10).
- The second adhesive layer between the laminates and the second frame was then spread on the frame side. The second frame was placed and clamped ensuring the alignment of the frames and the in-between laminates. Excess glue was removed. The panel was left to cure for 24 hours at ambient temperature (Figure 3.11).
- The 150mm wide diagonals were assembled by applying adhesive layers to the inner sides of the bottom diagonal skins. Core foam was put in place. Glue was applied to the second skins. Skins and cores were then clamped and left to cure for 24 hours at ambient temperature (Figure 3.12).
- Remaining gussets and packers were placed with adhesive layers on both sides. The last frame was then assembled on top. The frame was then clamped and left to cure for 24 hours at ambient temperature (Figure 3.13).
- At the support and load locations, PFR hard points of 150mm in length, were fitted inside the pultrusions, then glued.
- The panel was post-cured for six hours at 80˚C with one hour ramp.

With few assembly procedures and a single post-curing cycle, the panel was easy to manufacture, which is a major advantage for civil engineering applications.

Figure 3.11 P309 - Assembling the first two frames

Figure 3.12 P309 - Assembling of diagonals

Figure 3.13 P309 - Assembling the last frame

3.5. P309 - FE MODELLING

The main objective of the FE analysis was to develop an understanding of the mechanics of force transfers in the panel until reaching ultimate capacity with the possibility of predicting this capacity. Accordingly, geometric-nonlinear/ material-linear analysis was conducted simulating the panel testing. The FE model was built in parts that were interconnected using tie (kinematic) constraints. A surface-based tie constraint was used in the FE model. This concept is useful for mesh refinement purposes. It allows rapid transitions in mesh density within the model (Hibbitt et al, 2004a, 2004b). Figure 3.14 shows the general concept used to model P309. At each end of the vertical member, a 1mm strip was used to represent the glue line between the chords and the vertical (Glue End, Figure 3.14).

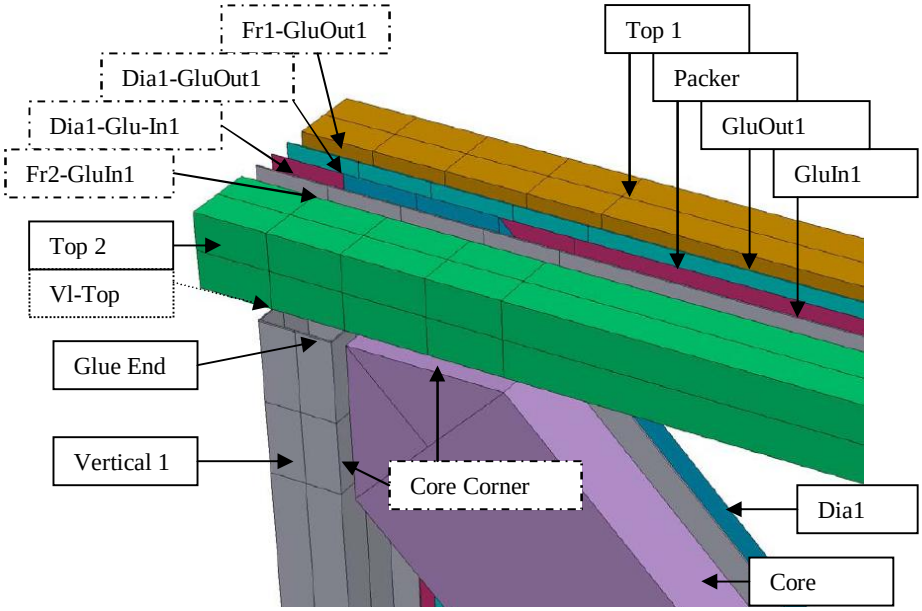

Figure 3.14 P309 - Modelling concept and interactions
Dash-dot boxes indicate surface-to-surface interactions
Dot boxes indicate node-to-surface interactions
Fr: Frame, Dia: Diagonal, GluIn: Inner glue layer, GluOut: Outer glue layer

Surface-based constraints were specified to connect different parts of the panel. Node-to-surface was used to constrain the glue end of the verticals (slave nodes) to the bottom of the top chord and the top of the bottom chord (master surface). Due to the mismatch of meshes used for frames and adhesive layers, surface-to-surface constraint was used with slave surfaces defined on the adhesive layers. The mesh definition ensured that the mesh density of the slave surfaces was similar or finer than that of the master surface. The more accurate stress on both surfaces was the other factor that led to using surface-to-surface constraint.

3.5.1. MODELLING PULTRUSIONS

Pultrusions can be modelled using either shell or continuum solid elements. The main issues to be considered in modelling pultrusions are:

- When using shell elements for closed-sections, ignoring the corner radii and the overlapping effects, Figure 3.15, can lead to stiffer models, (Omar, 2000).

- The low ratio of the clear width to thickness (b/t^3=8) can violate the inherent assumption, in the shell formulation, that plane sections must remain plane leading to inaccurate predictions.

- The use of continuum solid elements can lead to increasing the computational time.

A shell section slenderness check was conducted to ensure the suitability of using shell theory for the pultrusion. The material properties used are shown in Table 3.7, assuming that the section is transversely isotropic with shell thickness of 5mm and characteristic length (*l*) of 40mm. The minimum slenderness was 130, which indicated that pultrusions can be modelled accurately by using shell elements[4].

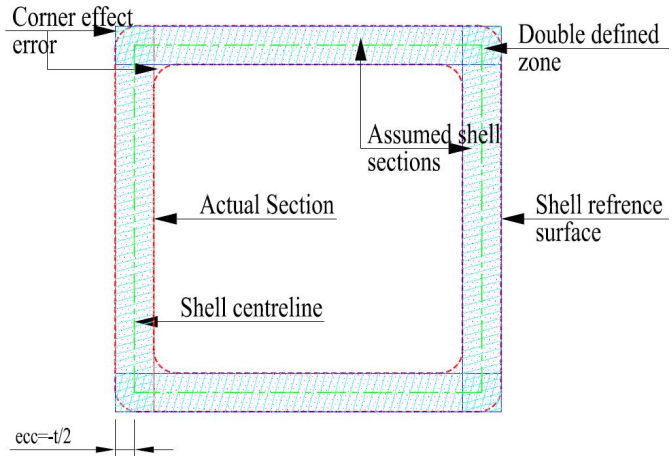

Figure 3.15 Expected errors in representing pultrusions using shell elements

Table 3.7 Material properties of pultrusions

E_1 (MPa)	E_2 (MPa)	E_3 (MPa)	G_{12} (MPa)	G_{13} (MPa)	G_{23} (MPa)	ν_{12}	ν_{13}	ν_{23}
32000	10000*	10000*	6700	6700	4545	0.30	0.30	0.10*

* Estimated values

To ensure both the accuracy of the FE model at its economy, , four models were built to address the above mentioned issues. The first model (21-07) used full-integration conventional shell element (S4[5]) with 4.50mm thickness[6]. The second model (21-08) used reduced-integration conventional shell elements (S4R) with 4.50mm thickness. The third model (21-09) used S4R with 5.0mm thickness. The last model (22-02) used continuum solid elements (C3D20R).

[3] Ignoring the internal radius.
[4] The minimum shell slenderness should exceed 100 (Hibbitt et al, 2004a).
[5] For the element names, reference should be made to Hibbitt et al (2004a).
[6] The 4.50mm thickness made the total section area 900mm^2 (equal to the cross sectional area of pultrusions)

A trade-off between the mesh density and the model performance is usually required. A few alternatives were investigated to assess the required mesh density. It was found that using four elements per each section side provided reasonable representation of the section, when compared to finer meshes. The aspect ratio of the element was about 1 at corners but did not exceed 2 in other locations[7].

3.5.2. MODELLING DIAGONALS

The sandwich diagonal was more complicated than other model parts. FE numerical solutions have been implemented to assess the stress and strain distributions in sandwich structures.

Vannucci et al (1998) conducted a comparison between the performance of some theories and FE models of sandwich plates and shells. Compared with Pagano (1970) for square and rectangular plates, they concluded that using discrete-shear quadrilateral elements, based on the theory of Mindlin-Reissner for the analysis of thick plates, provided the best response with results within 20% of the exact solution.

Akfert (1994) used the commercial FE package (Abaqus) with a foam material model based on a volumetric hardening model as described by Gibson et al (1982) Maiti et al (1984), and Gibson et al (1997), with skins, adhesive layers and core materials modelled as plain strain two-dimensional continuum elements.

Muc and Zuchara (2000) investigated the buckling and failure analysis of thin-walled composite sandwich plates. Their 2-D geometrical nonlinear formulation was found to correlate well with the 3-D FE analysis. Shell elements were used for the sandwich skins while 3-D solid (20 nodes brick) elements were used to model the core. This approach was found to be quite effective for static and impact problems (Haug and Jamjian, 1996).

Bazant and Beghini (2004), in using variational analysis and comparing them with standard FE model predictions, concluded that it is correct to simulate soft-core sandwich structures with the standard FE programs using Lagrangian updating

[7] At corners finer mesh was used due to high stress gradients.

algorithm, based on Green's Lagrangian strain tensor of m=2 which agree with Engesser-type formula[8].

Accordingly, Solid-Shell elements were used to model the sandwich diagonal. S4R and S3 shell elements were used to model the laminate. S3 elements were used to model the corners of the diagonal (Figure 3.16). Shell-Only elements are used to model sandwich columns (Chapter 4) and to simplify the macro-level model (Chapter 6).

The composite shell section was defined with elastic properties and failure limits as obtained from the standard characterisation tests (Appendix 'E'). The laminate definition assumed that the 1-1 local axis was aligned with the diagonal centreline. For each ply, Simpson's rule was used with three integration points through each ply thickness.

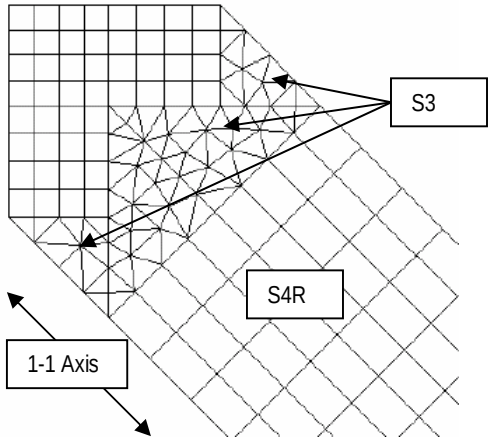

Figure 3.16 Shell elements definition for the diagonal skins

Solid continuum elements were used to model the diagonal core. The mesh was defined to match the skin (Figure 3.17). The PVC foam was modelled as an isotropic material with Poisson's ratio of 0.30. This simplification can be reasonable with stresses not exceeding the proportional stress level.

[8] Refer to chapter 4 for more detailed discussion about different formulations.

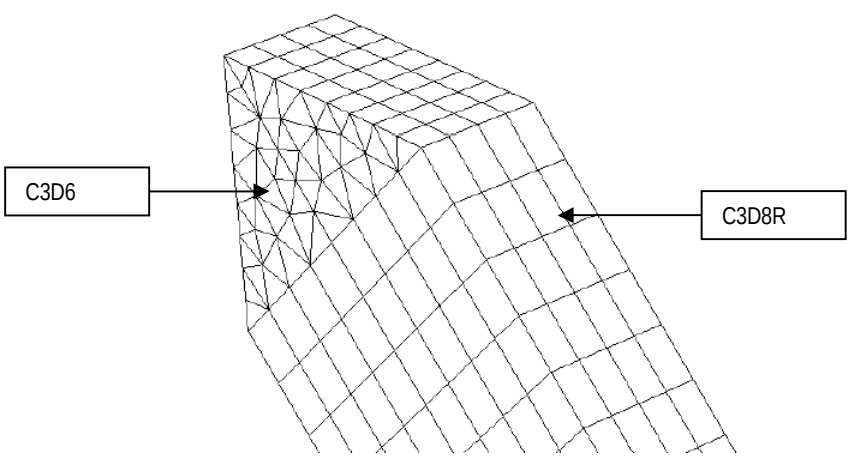

Figure 3.17 Assigning solid continuum elements to the diagonal core

3.5.3. MODELLING ADHESIVE LAYERS

Abaqus offers a library of cohesive elements to model the behaviour of adhesive joints allowing for the effect of material damage and failure, Hibbitt (2004a). As no adhesive failure was observed during the panel testing, adhesive layers were modelled as solid continuum elements (C3D20R) with isotropic material of Young's modulus (2430MPa, www.atlcomposites.com.au) and Poisson's ratio 0.30. This assumption was reasonable as the objective of including the adhesive layers in the model was to provide prediction of the stress level in these layers at ultimate capacity and provide transfer media for stresses between the connected members.

3.5.4. P309 - MODELLING OPTIONS

Half the panel was modelled due to symmetry along 1-axis (**Error! Reference source not found.**). No symmetry was assumed along the 3-axis so as to pick the local buckling of the diagonal, when in compression.

To assess the required mesh density, a few indicative runs were conducted for the panel. Based on these runs, it was found that having an average element size of 12.5mm, with aspect ratio within the 0.5-2.0 limits, provided very comparable results to finer meshes.

Displacement-controlled loads were applied to the top surface of the pultrusion to simulate applying the loads through the loading plates (Figure 3.18). A 20mm displacement was applied in a single loading step with automatic incrementation starting with initial load factor of 2%.

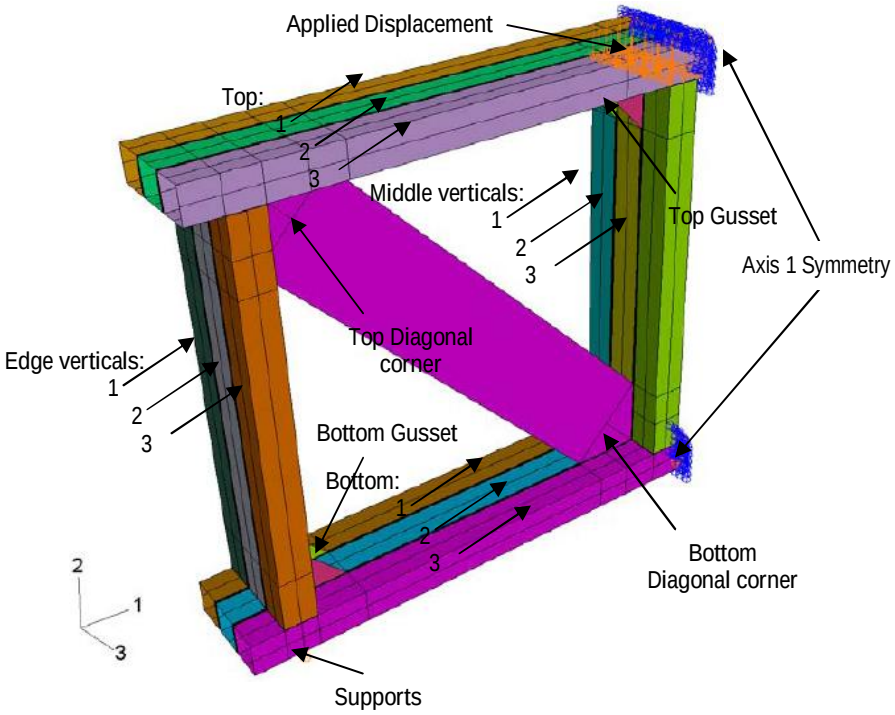

Figure 3.18 P309 – FE model layout

3.6. P309 - TEST AND FE RESULTS

The servo-controlled testing machine with Instron loading ram of 600kN capacity (type: A1340-1006ASP) was used with the displacement-controlled loads applied at a rate of 0.75mm/min with data collected to a standard PC through System-5000 data acquisition system. Strain gauge (SG) locations are shown in Figure 3.19.

The test and FE model results are presented in this section. Mid-span load-displacement curves are shown in Figure 3.20. Strain-displacement curves are shown in Figure 3.21 to Figure 3.25. Graph legends show the FE model number. Load and deflection are abbreviated as **Ld** and **Displ** respectively. After finishing the analysis, Abaqus calculates the CPU time required to complete the solution, as an indication of the computational costs. The time consumed to analyse the different models are shown in Table 3.8.

Table 3.8 P309 FE analyses performance

Element Type	FE Model	Analysis parameters			
		Thk(mm)	Element	# Elements	CPU Time(s)
Shell	21-07	4.5	S4	17140	4302
	21-08	4.5	S4R	17140	3573
	21-09	5.0	S4R	17140	4202
Solid	22-02	5.0	C3D20R	26420	17760

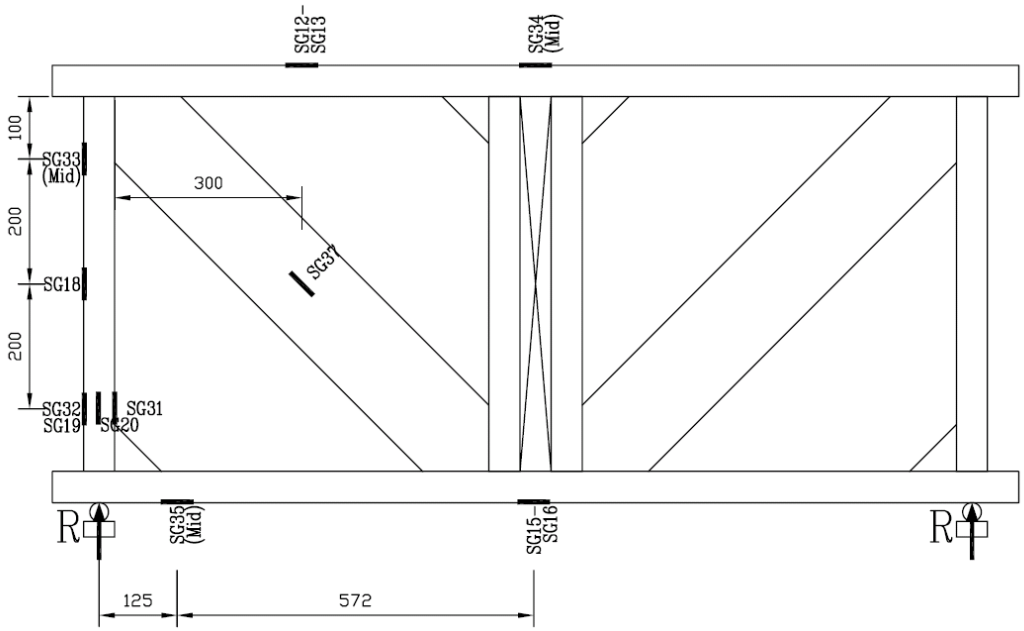

Figure 3.19 P309 - Strain gauge locations

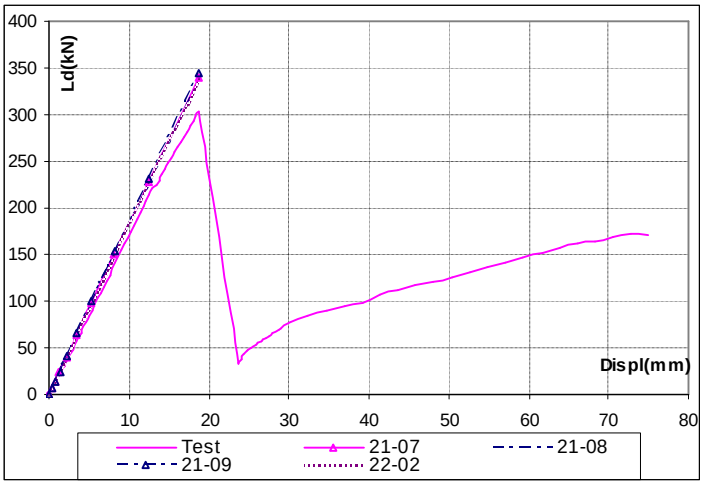

Figure 3.20 P309 - Load-displacement curves

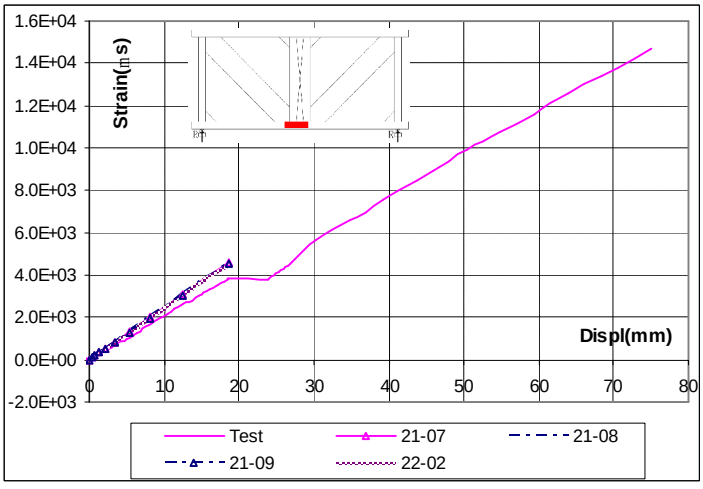

Figure 3.21 P309 - SG15 Strain-displacement curves

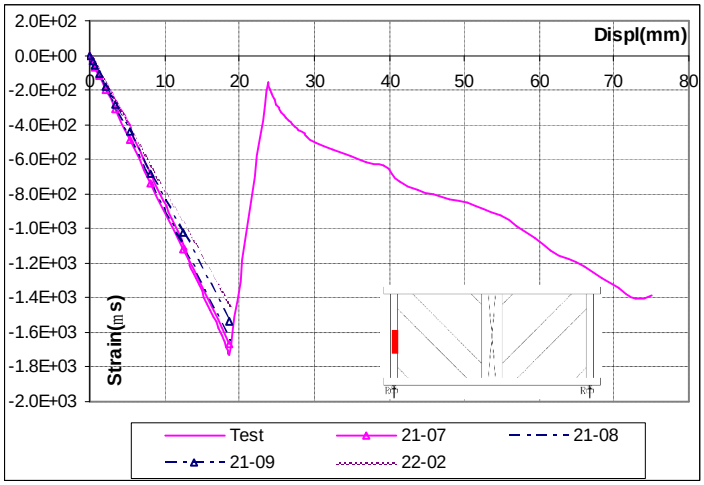

Figure 3.22 P309 – SG18 Strain-displacement curves

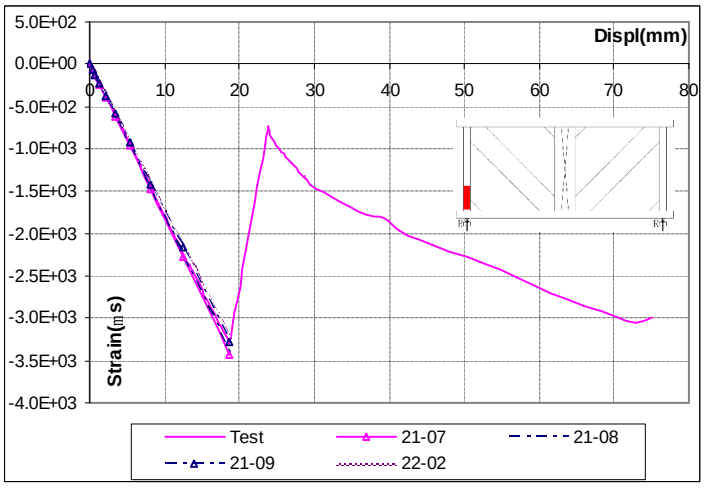

Figure 3.23 P309 – SG32 Strain-displacement curves

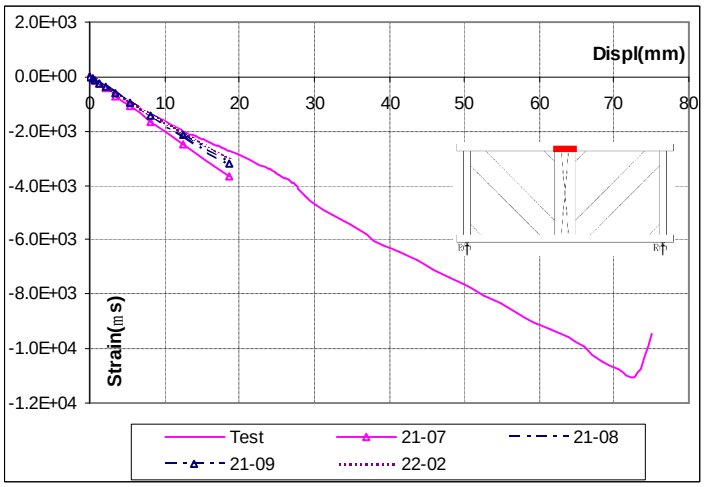

Figure 3.24 P309 – SG34 Strain-displacement curves

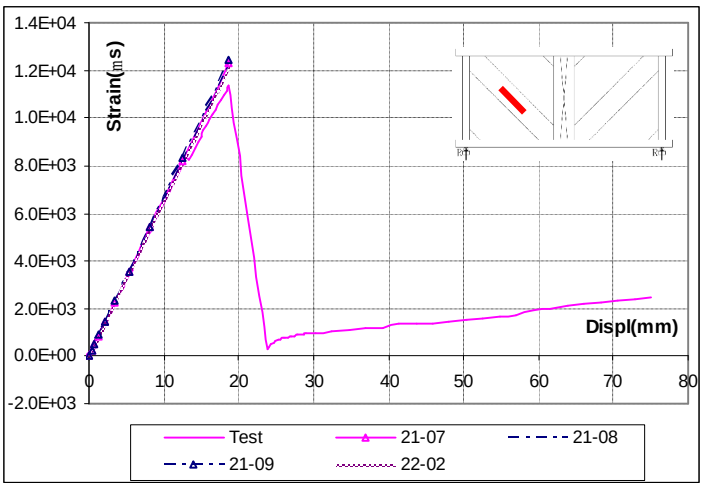

Figure 3.25 P309 – SG37 Strain-displacement curves

3.6.1. P309 - EXPERIMENTAL OBSERVATIONS AND FE MODEL VERIFICATIONS

In this section the test observations and the performance of the FE models are presented and used to explain the panel behaviour.

3.6.1.1. Test Observations

The first impression obtained during the test was that the performance of the panel was quite good as it reached an ultimate load of 303kN. On reaching the ultimate (maximum) capacity, failure originated in the skins (Figure 3.26). The panel lost most of its stiffness at this point. However, in increasing the applied displacement, the panel was able to carry increasing loads until reaching final failure at a load of 173kN. The maximum deflection at final failure was 81mm (span/17.2). In releasing the applied load, the panel recovered most of its deflections. The panel stiffness was linear until reaching its ultimate capacity. The panel lost part of its stiffness due to partial failure of the diagonal skins (Figure 3.26).

Failure began with the rupturing of the skins of the right diagonal. Losing one half of the diagonal led to stiffness reduction of one side of the panel and accordingly, the panel swayed towards the left side (Figure 3.27). At this point, the loading plates moved towards the right. In reaching the ultimate capacity, longitudinal cracks propagated along the diagonal centreline. These were more extended in the left diagonal. With further application of load, the panel's distortion increased - leading to final failure at the upper left corner (Figure 3.28).

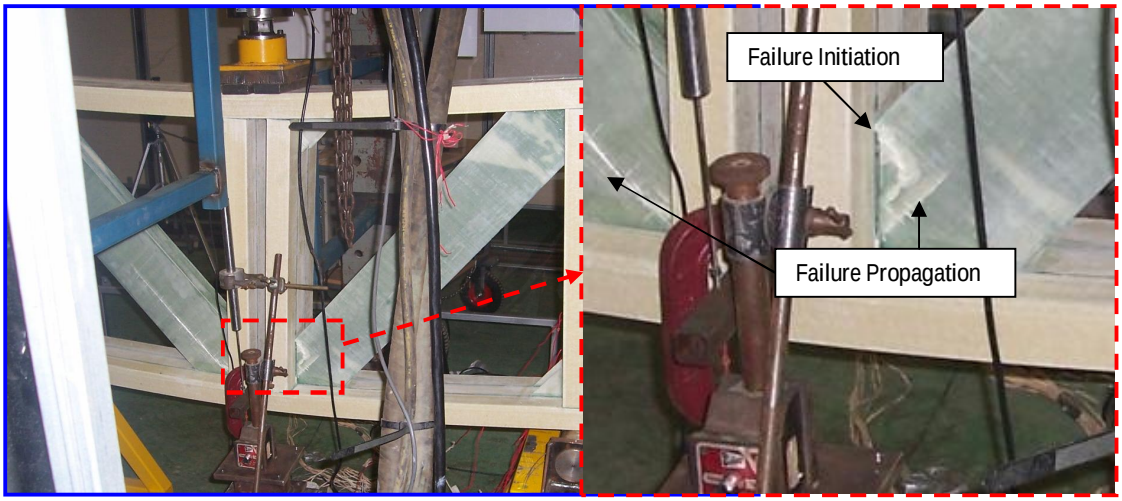

Figure 3.26 P309 - Failure at ultimate load

Figure 3.27 P309 - Sway after reaching ultimate capacity

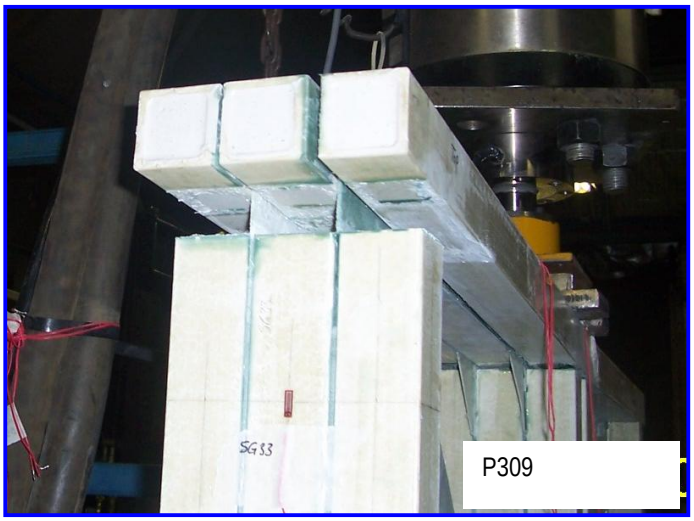

Figure 3.28 P309 final failure

In comparing the strain curves of Figure 3.20 to Figure 3.24 the following can be observed:

- The recorded strains can be categorised into two groups. The first showed linear relationship with the displacement. The second showed linear relationship with the applied loads. Chord pultrusions strains (SG15, SG16 and SG34) fall into the first category while the vertical pultrusions strains and the diagonal strains (SG18, SG32 and SG37) fall into the second category.
- Strain gauges at the same elevation location, but at different pultrusion, e.g., SG15 and SG16, SG32 and SG19, had very similar strain curves.
- The diagonals were the most stressed members of the panel with strain of 1.139% at ultimate load (for SG37).
- After reaching the ultimate load, load-proportional strains increased with the increase in applied loads. However, the ratio of strains at final failure to the ultimate load strains were 22% in the damaged diagonal (SG37) and 82%-92% in the verticals (SG18 & SG32).
- Strains in the vertical pultrusions changed along and across the member in a linear manner. This suggested the development of bending moments at the corners of the panel.
- The continuous increase in strains in the chord pultrusions can be attributed to the developed bending stresses in the chord due to the increase in the members' curvature.

3.6.1.2. Performance of the FE Models

It was noticed that conventional shell element models (21-07, 21-08 and 21-09) were very economical compared to solid elements model (22-02) - their analysis time ranged from 20-25% of the time for 22-02 (Table 3.8, p50). All analyses reached the specified load factor in 9 increments with no warnings. This is an indication for the soundness of the chosen modelling procedures. In comparing the data, the following can be noted:

- The FE models closely predicted the load-deflection curve of the tested panel, with slightly higher stiffness. The shell element with pultrusion thickness of 5.0mm (21-09) formed the upper bound. Other runs were very similar.
- The solid continuum element model (22-02) analysis had good correlation with the test results - however at much higher computational cost compared to the shell element models.
- For the different strain locations, the best analyses that matched the test records were 21-07 and 21-08 models. Both the full and reduced-integration models acted in exactly the same way.
- The only advantage in using the reduced-integration element model (21-08) was its reduced computational costs, when compared to the full-integration model (21-07). However, there was nearly no difference between the accuracy of both models.

It can be concluded that the FE models captured the main panel characteristics. As the shell element model with reduced-integration elements (21-08) provided accurate and economical results, this model was used for the remaining research into the panel behaviour.

3.6.2. P309 - BEHAVIOUR

Based on the test results, P309 showed quite important and excellent structural performance. The panel had high capacity. Its behaviour was semi-ductile, with no sudden complete failure. The adhesive layer failed finally due to severe distortion of the panel at that stage.

The current section focuses on developing a basic understanding of the panel behaviour based on the test observations and the FE analysis results. Each component of the panel is discussed in a separate sub-section. The last subsection discusses the general behaviour of the panel.

3.6.2.1. P309 – Behaviour of the Diagonals

In testing the panel, failure originated and propagated in the diagonal skins. To understand the onset and propagation of failure, force distributions were investigated along defined paths (Figure 3.29)[9]. Paths were divided into (i) along the member (1 to 3), (ii) across the member (4 and 5), and (iii) parallel to the frame pultrusions (6 to 9).

Maximum skin moments occurred at the corners (6b, 7b, 8b and 9b) with a maximum value of 3Nmm/mm. From here on as the moment effects are quite negligible, the discussion will focus on section forces. The two normal section forces (SF1 and SF2) and the shear force (SF3) along the specified section paths are shown in Figure 3.30 to Figure 3.32. In investigating the section forces the following was noted:

- Axial forces (SF1) were nearly equal along and across the diagonal[10].
- Except near the ends of the diagonal, there was no transverse axial (SF2) or shear (SF3) forces.
- Axial forces (SF1) quickly dissipated once the laminate gets in between the pultrusions.
- Transverse compressive forces (SF2) were developed near the diagonal corners. The level of forces varies across the diagonal width (ranged from 100N/mm to 300N/mm).
- The deformed shape for the corners is shown in Figure 3.33. When the diagonal was under tension, their corners tended to close due to the difference of stiffness along the connected members (member ends near the corners have higher stiffness compared to the rest of the member). This generated transverse confining compressive forces. Consequently, the skins are mainly under uni-axial stresses, except at corners where they are subjected to bi-axial stresses. The lateral stresses (2-2) were of opposite sign to the longitudinal stresses (1-1).

[9] Each section path started from 'a' point and ends at 'b' point.
[10] The reduction in forces at both ends of paths P4 and P5 is attributed to the averaging of the element forces with the less-stressed elements between the pultrusions which are joined at these nodes.

- The Tsai-Wu failure index factor (FIF[11]) was calculated for the six corners of the diagonal[12], at the failure load of 303kN, by linear interpolation of the last two increments of the analysis (Table 3.9). It was found that the FIF is linear with the level of stressing.
- In an attempt to investigate the effect of modifying the diagonal to improve its capacity, analysis 11-01 was performed. It was similar to 21-08 but with diagonal skins slotted. This modification showed significant reduction in the developed lateral stresses compared to 21-08 (Figure 3.34 and Figure 3.35).
- Due to the diagonal geometry, the axial strengths and stiffness in both 1-1 and 2-2 directions were the main factors that affect the failure mode. Using transverse reinforcements will provide more strength and stiffness, which will attract more loads.
- With the diagonals subjected to tensile forces, the core material in the sandwich construction did not carry any loads, axial or shear.

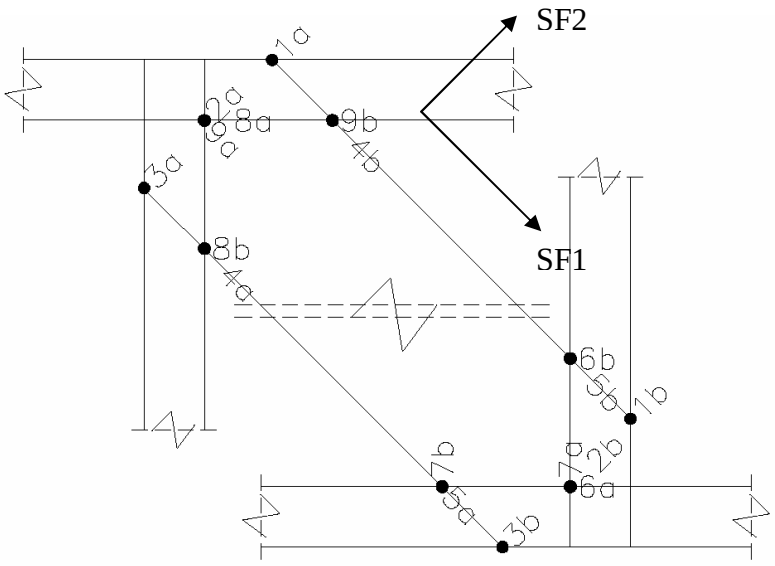

Figure 3.29 Section definitions for the diagonal member

[11] The stresses scaling factor required to locate the stress level on the failure surface. When FIF exceeds unity, it indicates failure.
[12] Assuming interaction term of -0.50, as recommended by Tsai (1991).

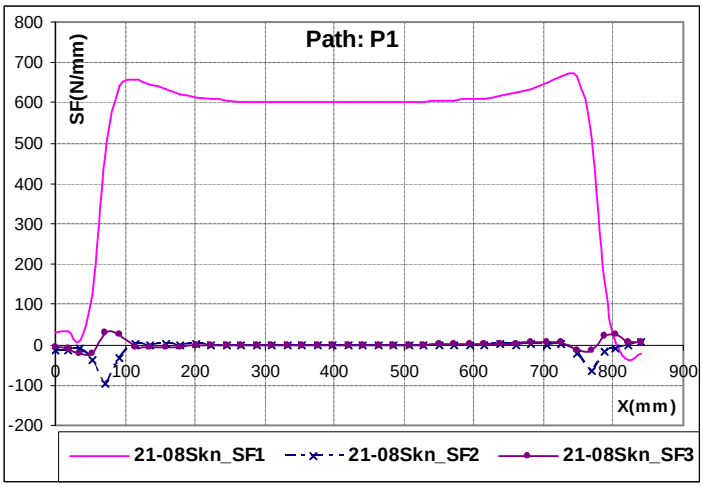

Figure 3.30 21-08 - Section forces along section P1

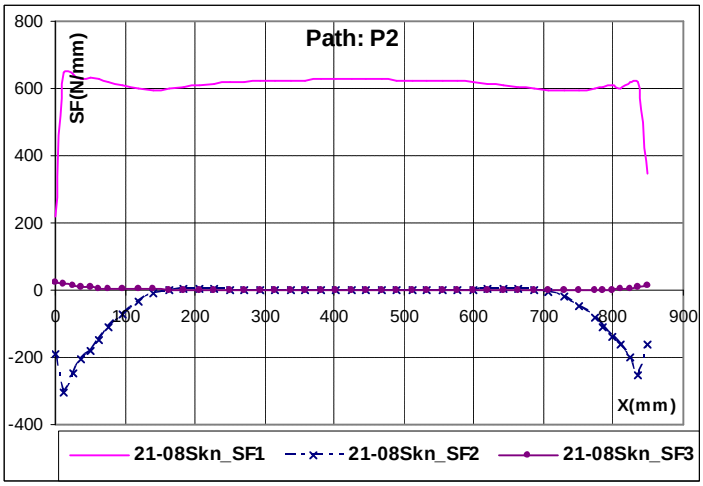

Figure 3.31 21-08 - Section forces along section P2

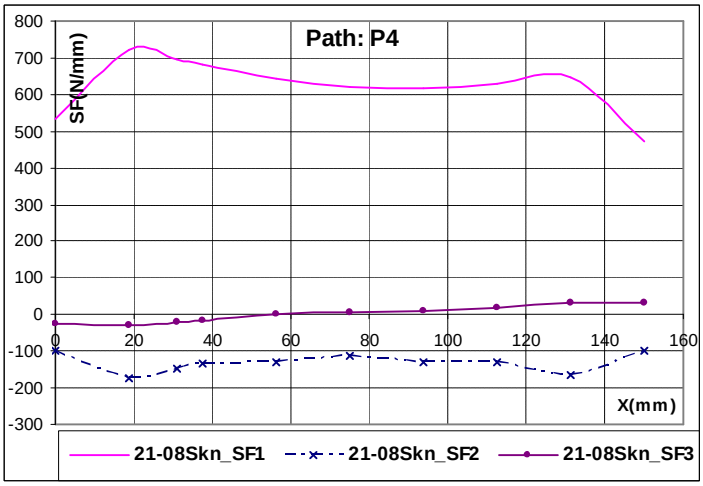

Figure 3.32 21-08 - Section forces along section P4

Table 3.9 Tsai-Wu failure index factors

	Upper left corner			Lower right corner		
Analysis	**8b**	**9a**	**9b**	**6b**	**7a**	**7b**
21-08	1.44	1.54	1.38	1.10	1.30	1.12
11-01	1.01	0.82	0.79	0.70	0.72	0.79

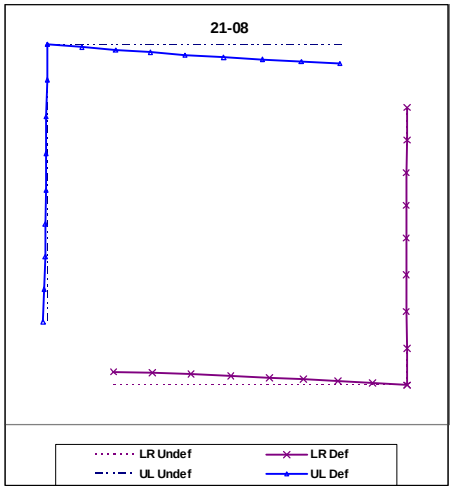

Figure 3.33 21-08 - Deformed shape at corners
LR: Lower right corner, UL: Upper left corner, Undef: Undeformed edges, Def: Deformed edges

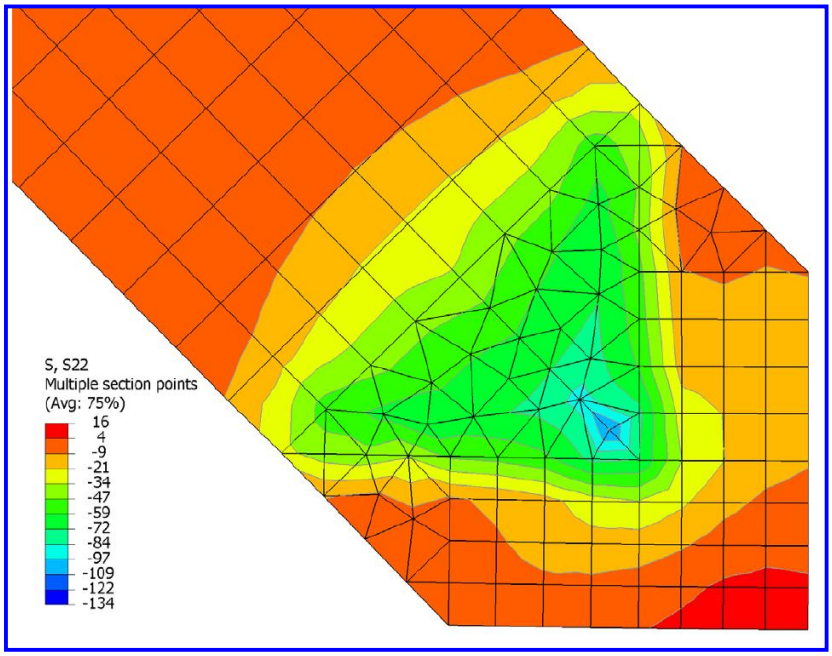

Figure 3.34 21-08 - Lateral stresses (S22)

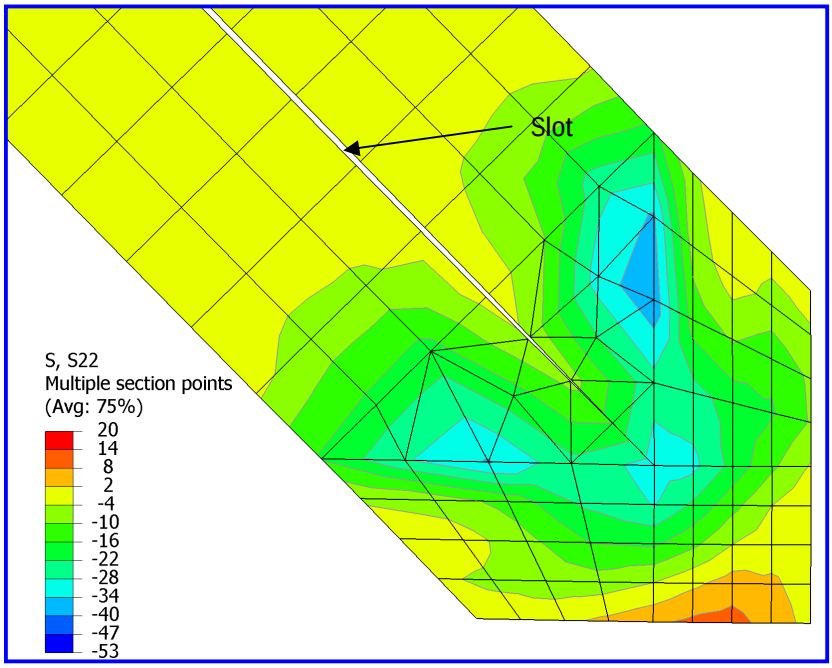

Figure 3.35 11-01 - Lateral stresses (S22)

The loading conditions for the diagonals were quite favourable. In general, forces were aligned with the fibre directions. Due to the confinement between the vertical and the chord member, transverse forces were generated at both ends of the member. Maximum FIF was at the 9a corner. However, failure was initiated at the 6b corner (FIF was slightly less than 9b). With this small margin, many parameters can affect the failure location. These include manufacturing accuracy, initial defects in the laminates, loading eccentricity in addition to the limitation in the criteria[13]. In general, the model predicted the potential failure location well. It predicted the first failure at 6b to occur at 254kN load.

The confinement effect could not be avoided. However, the failure of the diagonal can be controlled by reducing this confinement and/or changing the fibre architecture of the diagonal skins. For example, making a slot through the diagonal (Figure 3.35) can reduce the lateral stresses and accordingly improve the diagonal capacity.

3.6.2.2. P309 – Behaviour of the Pultrusions

The DD-MPTS system uses multi-pultrusion sections for the chord and vertical members. Analysis results are presented along the length of the member (Figure 3.36). Top (P_T), bottom (P_B), edge vertical (P_VL) and middle vertical (P_VM)

[13] Refer to chapter 4 for further discussion about failure predictions.

symbols are used. For P_T and P_B members, section paths were defined from the end towards the panel centreline. While for the vertical members, they were defined from top to bottom. Each graph legend indicates the member location followed by the section force components, separated by an underscore sign '_'[14].

The tested panel and the FE model did not show any lateral buckling. Accordingly, the data presented in Figure 3.37 to Figure 3.44 were based on Pultrusions 1 and Pultrusions 2 (assuming Pultrusions 3 is a mirrored image of Pultrusions 1).

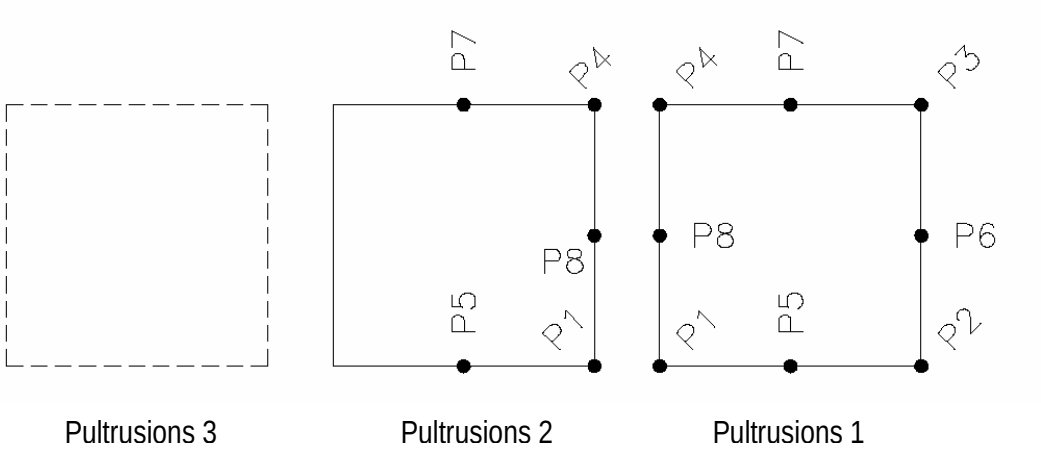

Figure 3.36 Section paths along the pultruded members

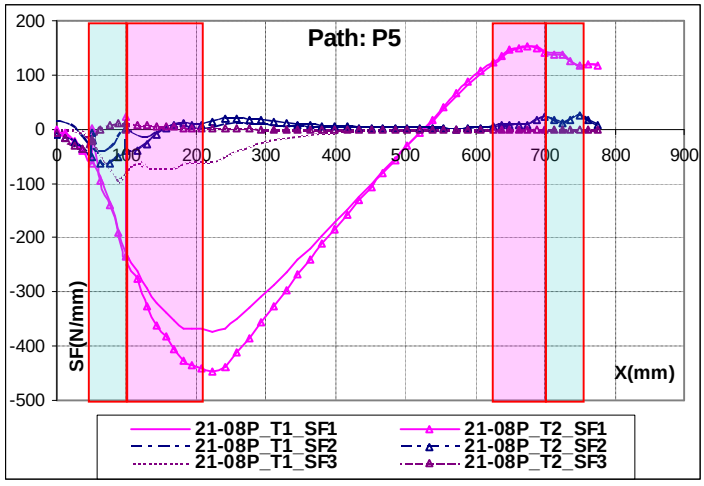

Figure 3.37 21-08 - Section forces along top chord – P5

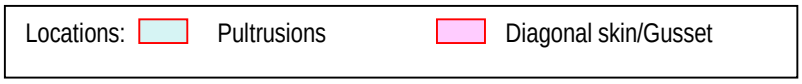

[14] For example, P_VL1_SF3 = edge vertical member (P_VL), frame 1 – section forces 3 (in-plane shear force).

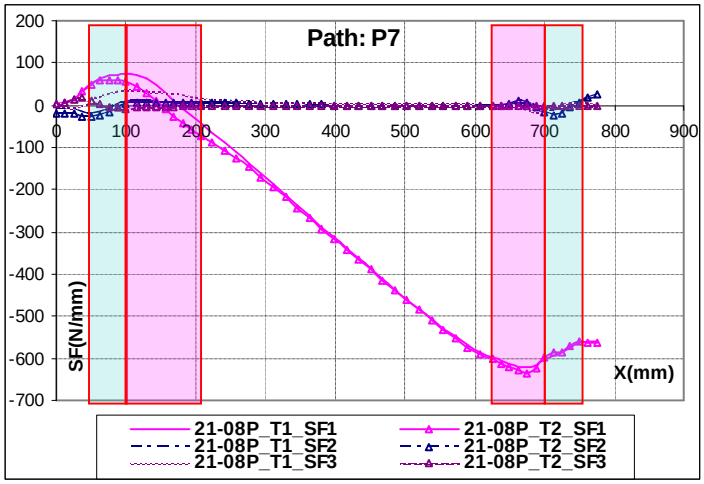

Figure 3.38 21-08 - Section forces along top chord – P7

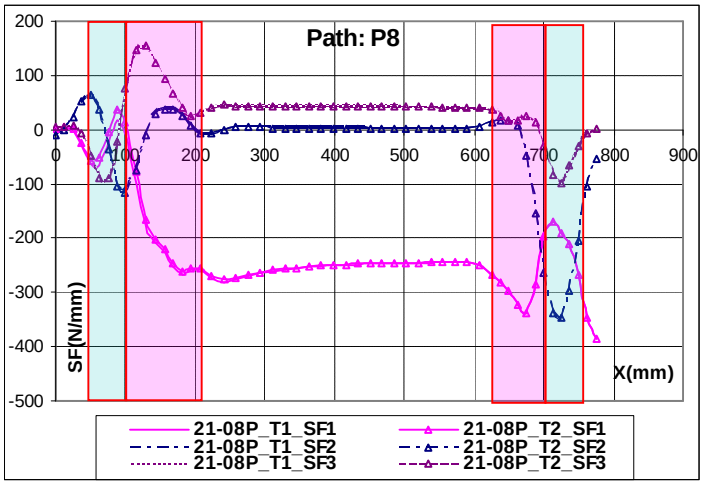

Figure 3.39 21-08 - Section forces along top chord – P8

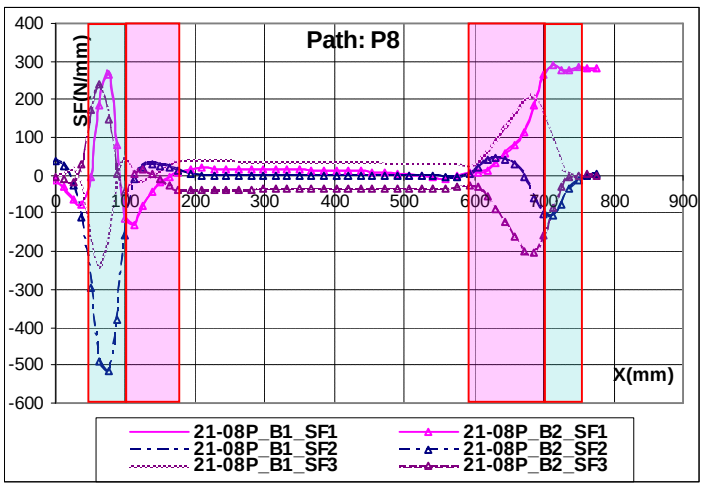

Figure 3.40 21-08 - Section forces along bottom chord – P8

Locations: Pultrusions Diagonal skin/Gusset

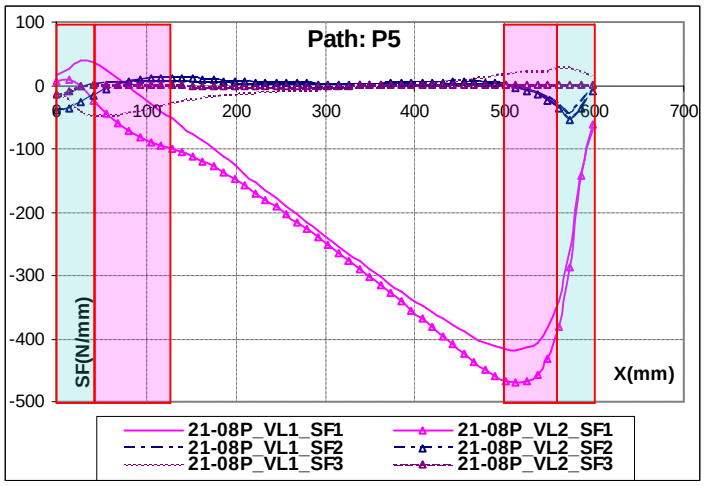

Figure 3.41 21-08 - Section forces along edge vertical – P5

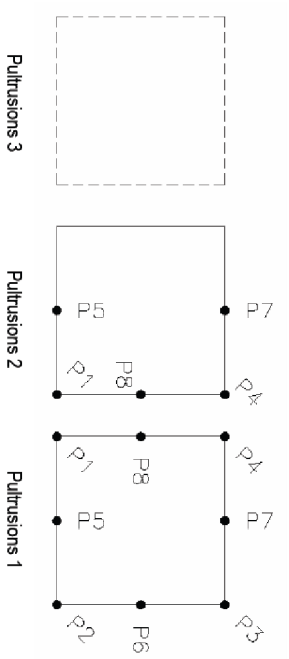

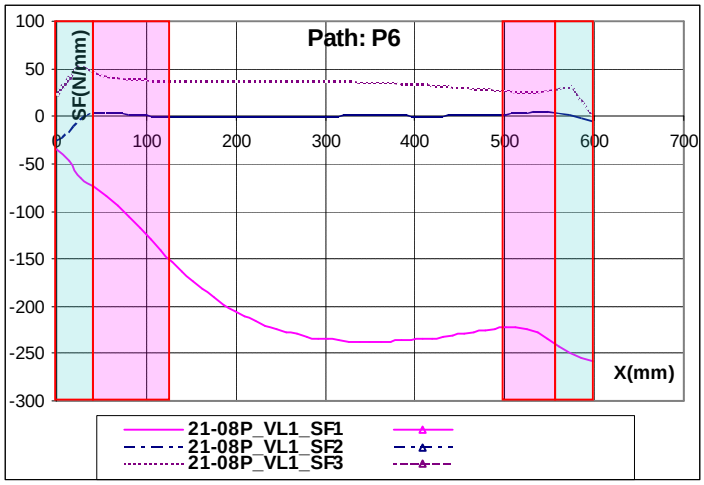

Figure 3.42 21-08 - Section forces along edge vertical – P6

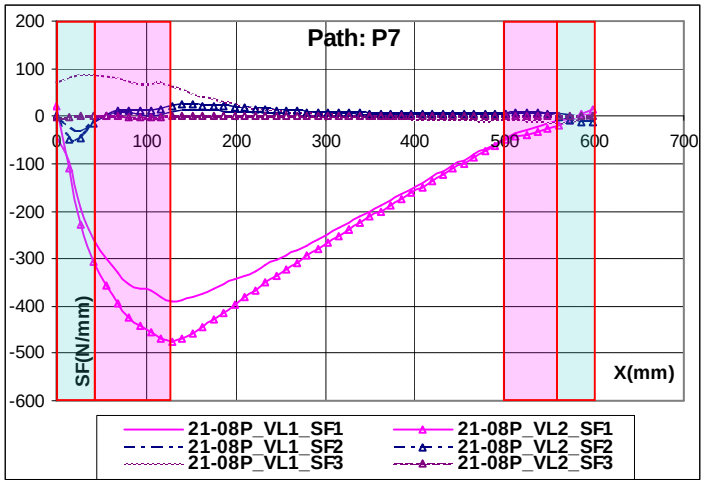

Figure 3.43 21-08 - Section forces along edge vertical – P7

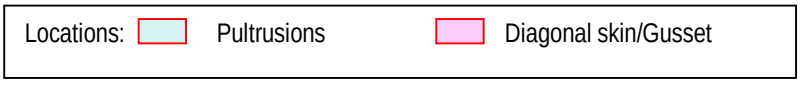

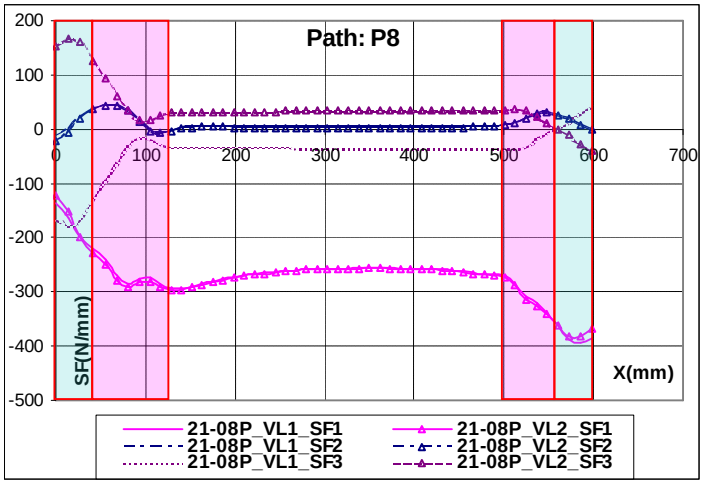

Figure 3.44 21-08 - Section forces along edge vertical – P8

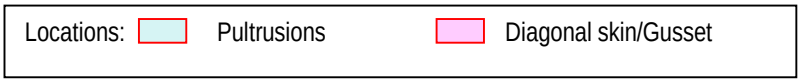

Based on the section force distributions shown in Figure 3.37 to Figure 3.44, the general behaviour of the pultrusions is described below:

- Similar forces were predicted in parallel pultrusions at the same location of the panel, except at the diagonal corners. This indicates that the connections in the corners are able to distribute the forces between the chord and vertical pultrusions.
- At the top chord (Figure 3.39) a nearly uniform SF1 force of 263N/mm was predicted. Integrating this over the cross section produced an equivalent member force of 157.8kN. Bottom chord P8 (Figure 3.40) showed approximately zero member forces. These force levels are in agreement with those calculated using simple hand calculations.
- At the diagonal corners (P8, Figure 3.39), axial forces SF1 were reduced with the increase in shear stresses.
- Edge vertical pultrusions had similar axial force SF1 as that of the top chord pultrusions (Figure 3.44).
- Stress concentrations were noticed at the support and load locations (Figure 3.40).
- At the diagonal corners, SF1 forces at Pultrusion 1 & Pultrusion 3 (P5 of the top chord, Figure 3.37) were less than that of Pultrusion 2 by about 15%. At

these locations, shear forces were developed in Pultrusion1 and Pultrusion 3.

- For the chord members, maximum shear forces were found in the vertical walls at the face of the vertical members. Almost all the shear forces were carried by the vertical walls of pultrusions adjacent to the glue lines (Table 3.10).
- The pultrusions are mainly subjected to forces along the 1-1 direction, which aligned with their fibre directions. No significant lateral forces (SF2) were found.

Table 3.10 21-08 - Shear force distribution between pultrusion webs

Member	Pultrusion #	Vertical wall (Figure 3.36)	Equivalent force(kN)	Total Forces (kN)
Top Corner*	1&3	P2-P3	1.44	
	1&3	P1-P4	6.25	
	2	P1-P4	6.21	27.80
Bottom Corner*	1&3	P2-P3	2.63	
-at mid-span	1&3	P1-P4	9.13	
	2	P1-P4	8.91	41.33
Edge Vertical**	1&	P2-P3	0.56	
	1&3	P1-P4	7.44	
	2	P1-P4	6.26	28.52
Middle Vertical***	1&3	P2-P3	0.48	
	1&3	P1-P4	6.33	
	2	P1-P4	6.54	26.70

*** at face of verticals, ** at top end, *** at bottom end**

From the above, the FE model showed important and positive characteristics about the panel pultrusions. At diagonal corners, forces transferred from the diagonal needed a distance to redistribute between the pultrusions (Figure 3.45). This explains why lower axial stresses in the Pultrusion 1 & Pultrusion 3 were observed. This redistribution generated shear forces in the horizontal walls of the pultrusions at these locations. Axial forces in the diagonal were transferred directly to both the chord and the vertical members through axial and shear components. The results show that the packers carry part of the shear forces. This is why the pultrusions shear forces, recorded by the model, were much less than the diagonal force component. Pultrusions are mainly subjected to axial and bending stresses which are favourable with almost all fibres in the 1-1 direction resisting these actions (strong direction).

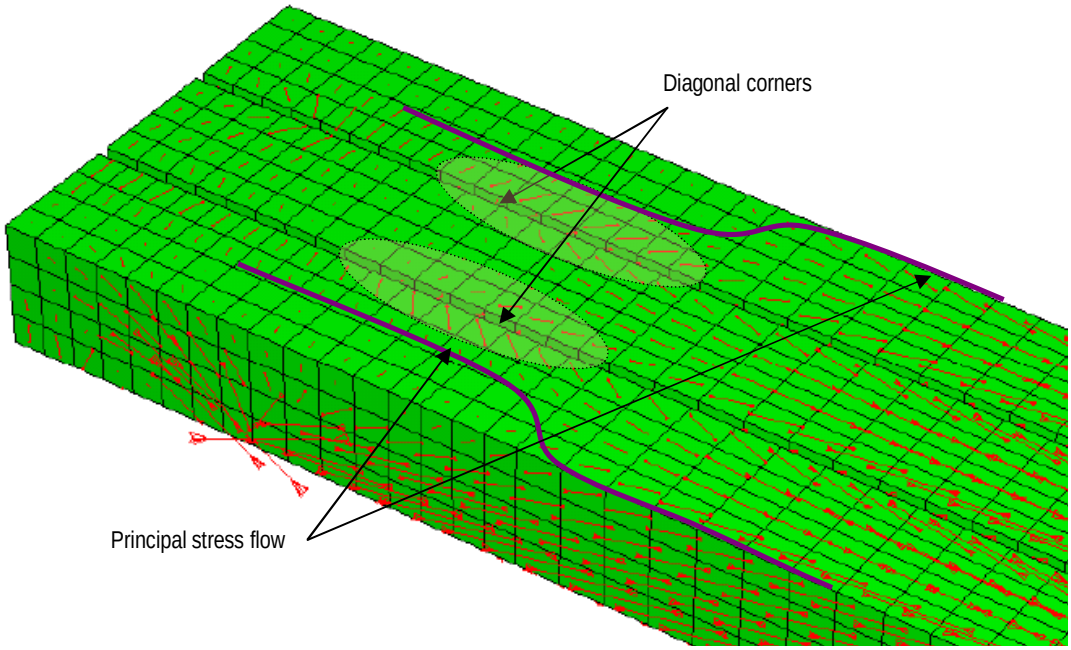

Figure 3.45 Principal stress vectors in the top chord

3.6.2.3. P309 – Behaviour of the Adhesive Layers

The three main stress components, which are usually of concern regarding glue behaviour, are the 'tensile' stress normal to the glue surface (S33) and the shear stresses in the glue plane (S13 and S23). Adhesive layer stresses are presented along six horizontal paths (P1 to P6) and two vertical paths (P7 and P8, Figure 3.46). They are shown in Figure 3.47 to Figure 3.51. These graphs were for analysis increment 9 of 333kN load. Accordingly, presented stresses are 10% more than that in the tested panel at ultimate load. The stresses along P1, P2 and P3 were found similar to that along P4, P5 and P6 respectively.

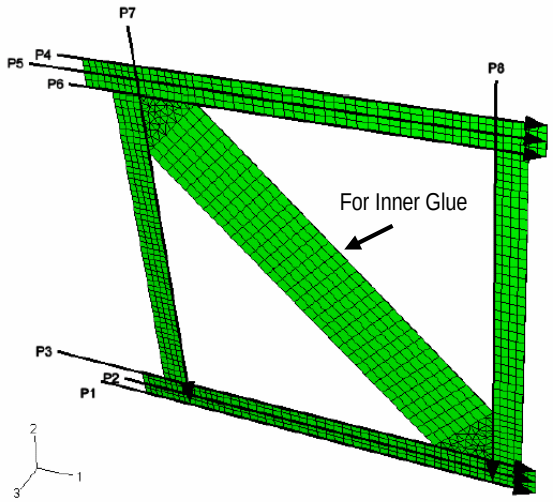

Figure 3.46 21-08 - Glue section paths layout

In the figures legends, the ‘In’ abbreviation was used for the inner glue line between Pultrusion 2 and the laminated skin while the ‘Out’ abbreviation was used for the outer glue line between Pultrusion 1 and the laminated skin. The shear stresses were represented by the resultant shear stress (S3).

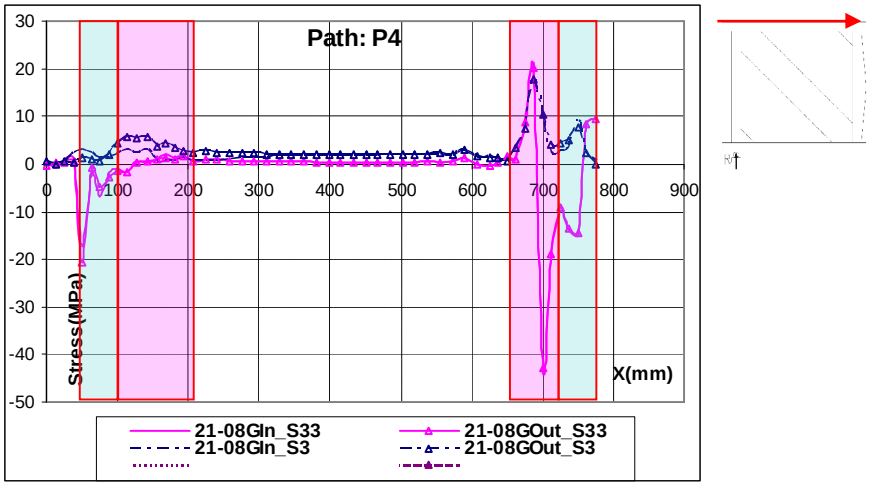

Figure 3.47 21-08 - Glue stresses along path P4

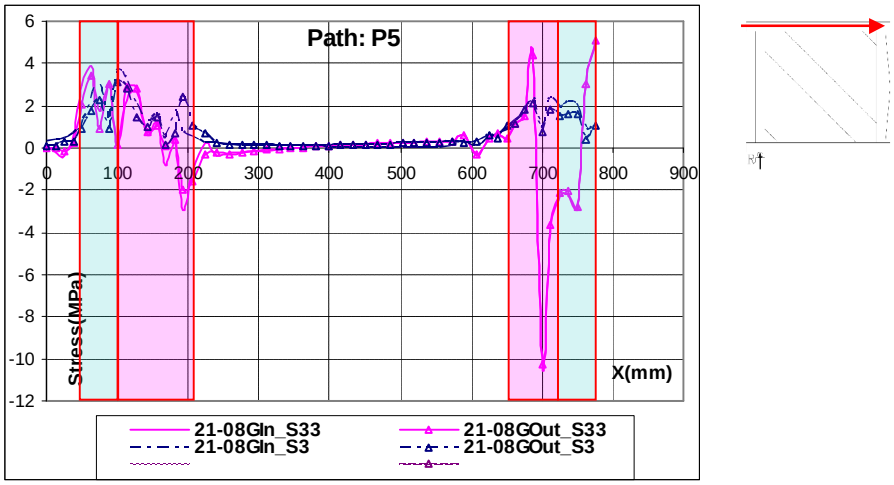

Figure 3.48 21-08 - Glue stresses along path P5

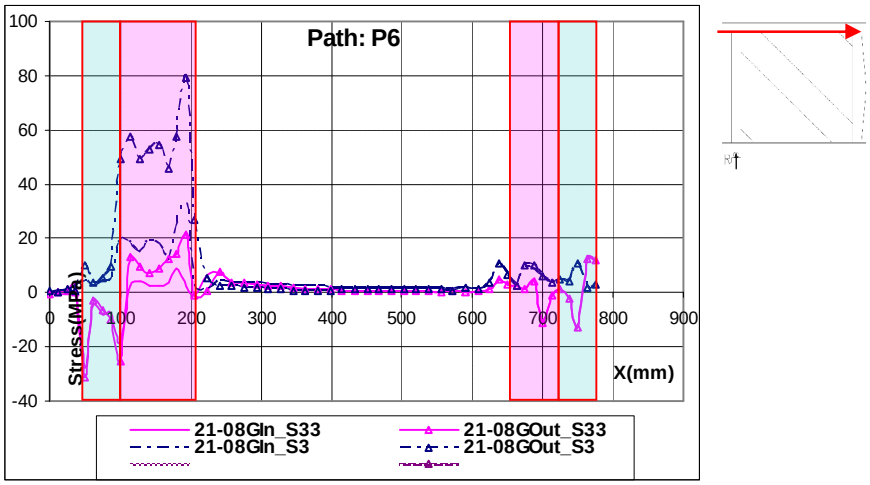

Figure 3.49 21-08 - Glue stresses along path P6

Locations: Pultrusions Diag. skin/Gusset

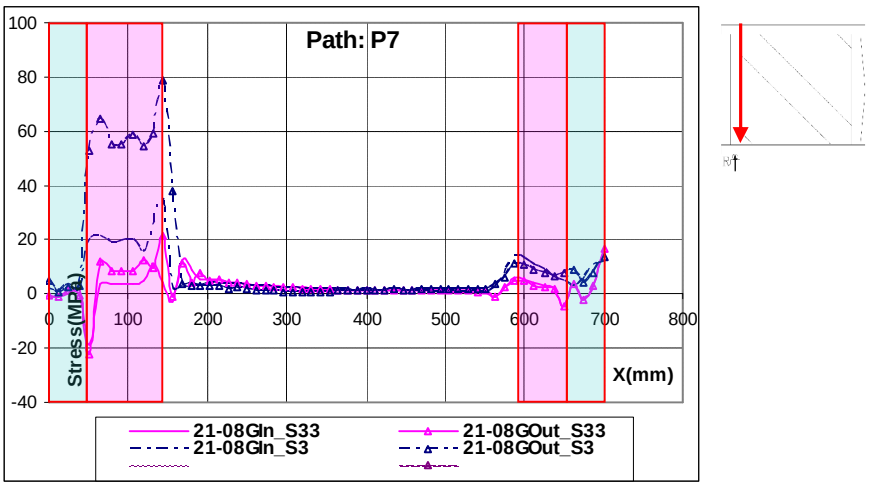

Figure 3.50 21-08 - Glue stresses along path P7

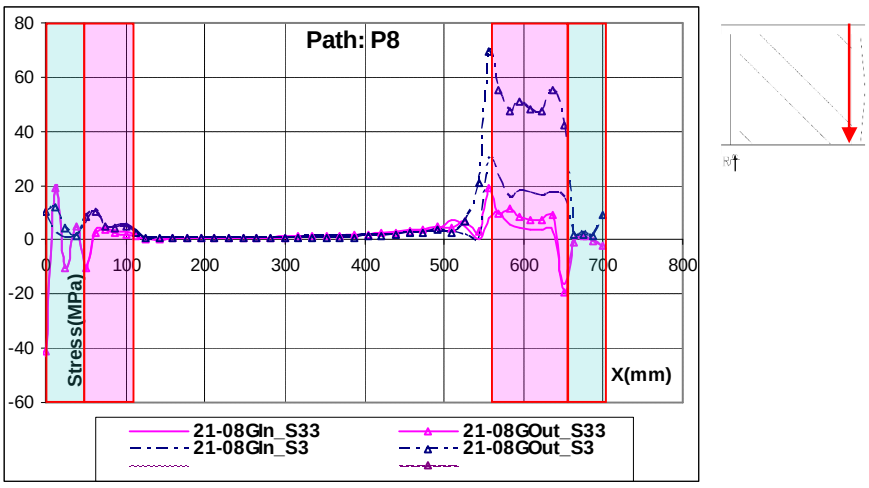

Figure 3.51 21-08 - Glue stresses along path P8

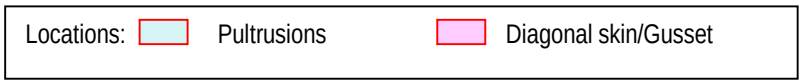

Based on the glue stress distributions along the different paths, the following was observed:

- Very small stresses (less than 2MPa) were observed along the different members, away from the corner locations.
- Shear and axial stresses at section paths (P3, P6, P7 and P8) increased at the diagonal corners and, to a lesser extent, at the gusset corners.
- The predicted stress levels in the inner glue line (at the diagonal corners) were lower than those at the outer glue line. This can be attributed to the continuation of the inner glue line between the diagonal skin and core (Figure 3.46), which reduced the stress concentrations at to the diagonal intersection with the pultrusions.

- At diagonal corners, the average inner glue tensile stress was 20MPa, with a maximum of 30MPa. While for the outer glue line, it was 40MPa and 70MPa respectively, with a maximum shear stress of 20MPa.
- P2 and P5 show that the stresses normal to the glue line were less than 5MPa at all locations. The only exception was at the support and the load locations where shear stresses of 17MPa and 12MPa were predicted. This indicates that almost all the forces are nearly transferred within the first 25mm of the joint.
- For P7 and P8 stresses were symmetric.
- The most critical location for the glue lines was the top left corner of the outer glue line, where the diagonal meet the top chord with a combination of maximum shear and tensile stresses (Figure 3.47). This was where final failure occurred in the tested panel.

The results show the importance of having continuous adhesive layers. The concept of multi-pultrusions, with embedded diagonal skins, provides an excellent joining technique. The FE model ignored the adhesive layer fillets (Figure 3.52). Accordingly, it is expected that it conservatively predicted the stress levels in the glue lines.

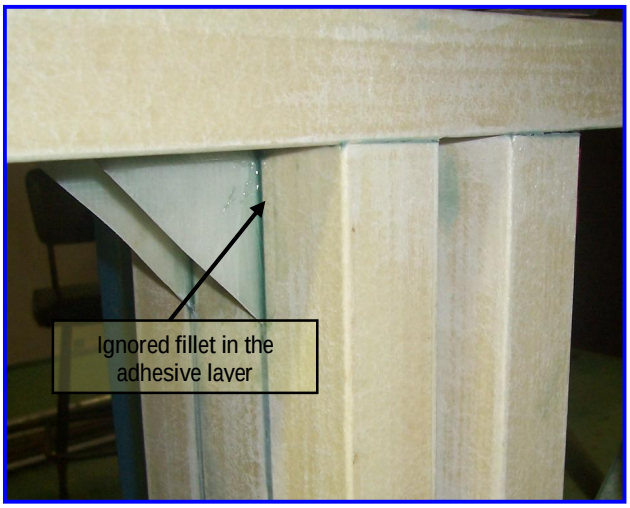

Figure 3.52 P309 - Glue fillet

3.6.2.4. P309 – Behaviour of the Gussets

The main observations of the gusset forces and stresses (Figure 3.53 to Figure 3.56) can be summarised as follows:

- At load locations, the gusset transferred part of the applied loads to the vertical member, with the other part transferred by direct bearing. Accordingly, vertical forces (SF1) were found to be constant until reaching the middle vertical pultrusions where they reduced gradually towards the gusset edge (Figure 3.53).
- Maximum tensile forces occurred at the exposed edge of the gusset with maximum values at the top chord corner (Figure 3.53). This was due to the confinement effect, with the tendency of the corner to open.
- The horizontal forces (SF2), at the top chord, changed from tension to compression, showing the development of the moment at the gusset connection (Figure 3.54).
- Maximum shear forces were observed at the exposed part of the gusset. Maximum principal stresses also occurred at this location (Figure 3.56);
- Forces in the exposed part can be attributed to the confinement effect and the relative rotation of the chord and vertical pultrusions. This generated stresses (tensile when the diagonal is under tension and vice versa). With one free edge, this zone will be susceptible to buckling when in compression.

As shown in the different graphs, the force levels were much lower than those of the diagonal skins. Accordingly, it can be a common practice to finalise the diagonal skin architecture then check the gusset architecture to match the thickness of the skins.

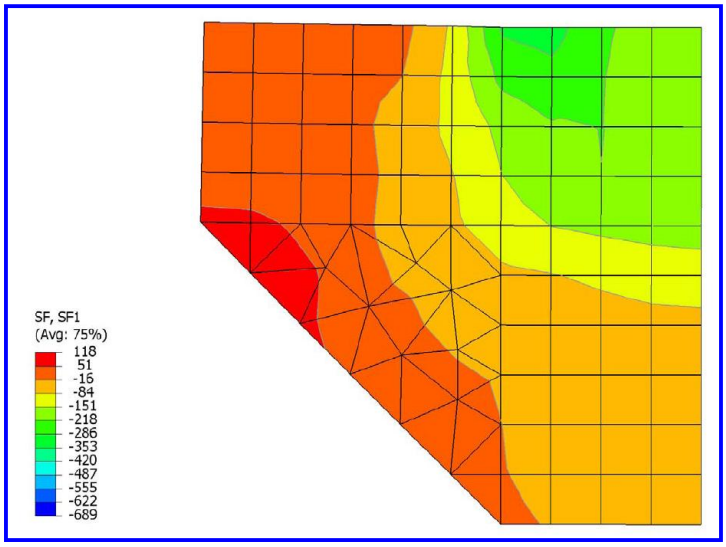

Figure 3.53 21-08 - Gusset section forces SF1 (vertical)

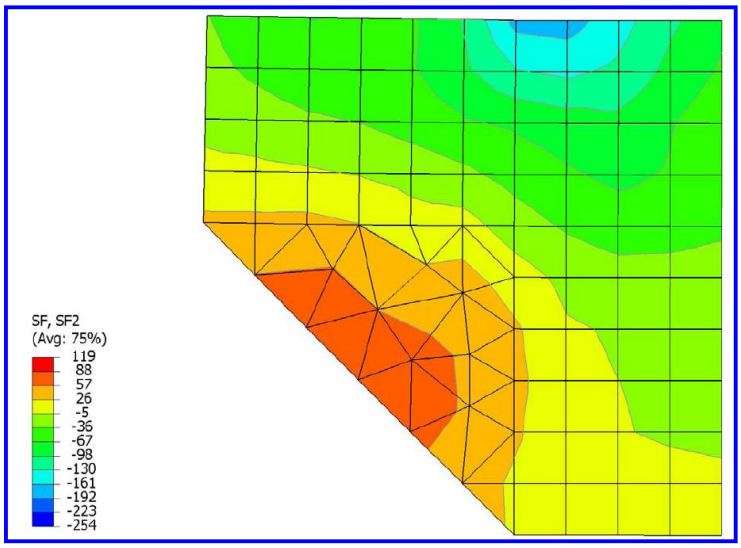

Figure 3.54 21-08 - Gusset axial section forces SF2 (horizontal)

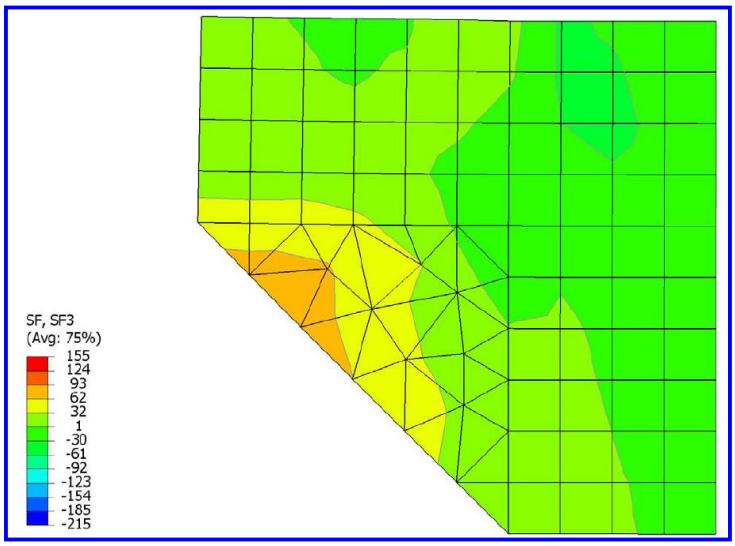

Figure 3.55 21-08 - Gusset shear section forces SF3

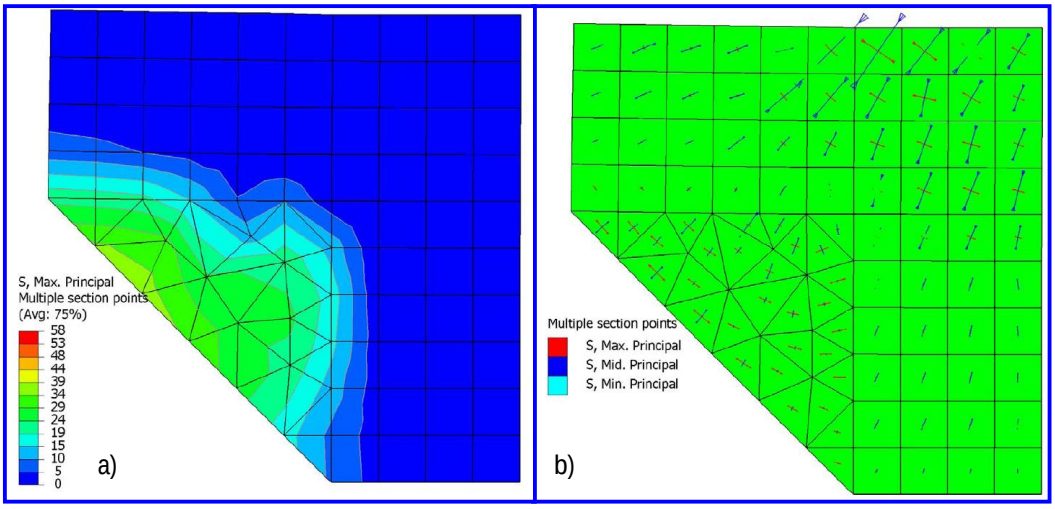

Figure 3.56 21-08 - Gusset (a) Principal stresses and (b) Vectors

3.6.2.5. P309 – General Behaviour

The test results and the FE model predictions presented in this section show the important behavioural characteristics of the DD-MPTS with diagonals under tension.

- The panel showed good distribution of stresses which is attributed to the continuous nature of the adhesive layer and the availability of packers that allow sharing of forces between the pultrusions.
- Stress concentrations at the joints were small with elements loaded in their strength directions.
- Diagonals were loaded in the axial direction, the major fibre direction, with the development of transverse stresses at their ends.
- Pultrusions were loaded in the direction of the fibres with a combination of axial and bending stresses. Some shear stresses were developed at the diagonal corners; however, their values were much less than the shear strength of the pultrusions.
- The adhesive layers were loaded in tension and shear. Using multi-pultrusions allowed for a stiff connection and improved the peel strength of the joint. This combined with the continuity of the adhesive layer, led to a reduced concentration of stresses in the adhesive layers.
- When tested with diagonals under tension, the panel showed linear behaviour.

- Other behavioural issues of buckling of the diagonals and any effects of imperfection in setting the panel need to be assessed. These issues are discussed in Chapter 4.
- The packers played important role by redistributing the forces between the three pultrusions ensuring their composite actions and carrying part of the shear forces at the diagonal joint location.
- Compared to the joint efficiency of the bracket P209, Sec. 3.3.3 p38, the failure occurred in the diagonal member not at the joint, 100% joint efficiency. However, due to the confinement of the diagonal at its ends, the member capacity was reduced when compared to the uni-directional stressed member. Comparing the force in the diagonals at ultimate load (210kN) to the equivalent of the uni-axially loaded skins (239kN) reveals that the overall member efficiency is 87% which is much higher than the joint capacity of P209 (42%).
- In correlating the load capacity of the panel to the strain level in the diagonal, as a measure of the level of stress at ultimate load, P309 in tension reached 26.6N/microstrain.

3.7. CONCLUSIONS

This chapter presented the investigations conducted for the discrete diagonal truss systems. The first panel to be manufactured was adhesively bonded composite sections cast in PFR. The panel was not tested due to many shortcomings which include a complicated manufacturing process, lack of any redundancy in the system, and the increased weight due to the PFR.

Based on the exercise of constructing the first panel, the main considerations for future panel developments were established. Subsequently, the discrete-diagonal, multi-pultrusion truss-system (DD-MPTS) was developed. The concept was refined by eliminating the use of gussets by using diagonals of sandwich construction with skins embedded between the chord and vertical pultrusions. This allowed direct transfer of forces, and, accordingly, achieved high load carrying capacity.

The first DD-MPTS prototype panel to be tested has diagonals under tension - the most critical loading condition for the joints. The panel structural performance was outstanding with failure occurring in the diagonal skins. The good characteristics of this system include (i) its high load carrying capacity, (ii) desirable failure modes with no sudden complete failure, (iii) alternate load paths, (iv) predictable failure mode, and (iv) ease of manufacturing.

The FE results developed to simulate the panel test showed an excellent correlation with the test results. The FE results were used to derive an understanding of the main characteristics of the panel system. The good performance of the test panel was attributed to its structural system which allowed each of its components to be loaded in its strength direction.

A characteristic of this system was the confinement effect due to the finite dimension of the diagonal at corners and the tendency of other members to rotate relative to each other. As failure originated and propagated in the diagonals, the behaviour of the panel with diagonals under compression will be more complicated.

In Chapter 4, the DD-MPTS concept will be investigated further by researching the behaviour of DD-MPTS panel with sandwich diagonals subjected to compressive forces.

3.8. REFERENCES

Akfert, A. (1994). Finite element analysis of composite sandwich beams and plates, MSc, University of Manchester, Manchester.

ATL Composites Homepage. http://www.atlcomposites.com.au.

Bazant, Z. P., and Beghini, A. (2004). Sandwich buckling formulas and applicability of standard computational algorithm for finite strain. *Composites Pt B*, 35, 573-581.

Clarke, J. L. (1996). Structural design of polymer composites - Eurocomp. E & FN Spon, London.

Colan Homepage. http://www.colan.com.au.

Diab Homepage. http://www.diabgroup.com.

Gibson, L. J., Ashby, M. F., Schajer, G. S., and Robertson, C. I. (1982). The mechanics of two-dimensional cellular materials. *Proceedings of the Royal Society*, London, 25–42.

Gibson, L. J., and Ashby, M. F. (1997). *Cellular solids: structure & properties*, Cambridge University Press, Cambridge.

Haug, A., and Jamjian, M. (1996). Numerical simulation of the impact resistance of composite structures. Numerical analysis and modelling of composite materials, J. W. Bull, ed., Blackie Academic, London, 185-244.

Hibbitt, Karlsson & Sorensen Inc. (2004a). *ABAQUS Analysis user's manual*, Pawtucket, USA.

Hibbitt, Karlsson & Sorensen Inc. (2004b). *ABAQUS Theory manual*, Pawtucket, USA.

Lavender Composites Homepage. www.lavender-ce.com.

Maiti, S. K., Gibson, L. J., and Ashby, M. F. (1984). Deformation and energy absorption diagrams for cellular solids. *Acta Metallurgica*, 32(11), 1963–1975.

Muc, A., and Zuchara, P. (2000). Buckling and failure analysis of FRP faced sandwich plates. *Composite Structures*, 48, 145-150.

Omar, T. (2000). Behaviour of concrete-filled-steel-tube members in flexure, ME, University of Auckland, Auckland, New Zealand.

Pacific Composites Homepage. http://www.pacomp.com.au/.

Pagano, N. J. (1970). Exact solutions for rectangular bidirectional composites and sandwich plates. *J of Composite Materials*, 4, 20-34.

Rogers, D. (2004). Characterisation of Hyrez 201 laminating resin. Polymer Testing Laboratory, University of Southern Queensland, Toowoomba, Queensland.

Tsai, S. W. (1991). *Composite Design*, Think Composites, Dayton, Ohio.

Vannucci, P., Aivazzadeh, S., and Verchery, G. (1998). A comparative analysis of some theories and finite elements for sandwich plates and shells. Mechanics of sandwich structures, A. Vautrin, ed., Kluwer Academic Publishers, Saint-Etienne, 45-52.

Chapter 4 Notations

A	Column cross-sectional area
A_s	Sandwich column skins cross-sectional area
b	Sandwich column width
E_c	Sandwich column modulus of elasticity of the core material in the loading direction
EI	Effective bending stiffness of the cross-section
E_s	Sandwich column modulus of elasticity of the skins in the loading direction
GA	Effective shear stiffness of the cross-section
G_{ij}	Shear modulus in the i-j plane
G_{kl}	Shear modulus in the k-l plane
I	Equivalent moment of inertia of the cross section
h	Sandwich column core thickness
l	Effective column height
L	Actual column height
P_E	Euler buckling load
P_{Eng}	Column buckling load based on Engresser formulation
P_{Har}	Column buckling load based on Haringx formulation
P_{mb}	Axial load for micro-buckling failure in sandwich columns
P_u	Ultimate capacity of the element
SD	Standard deviation
t	Sandwich column skin thickness
λ	Column slenderness
ν_{ij}	Poisson's ratio of the skins in the i-j plane
ν_{mn}	Poisson's ratio of the m-n plane
σ_{cr}	Critical stress in the skins due to core shear instability
σ_{mb}	Plastic micro-buckling strength of the skins

4. Behaviour of Sandwich Members under Axial Loads – Application for Discrete-Diagonal Multi-Pultrusion Truss Systems

4.1. GENERAL

The multi-pultrusion truss system (DD-MPTS) panel, with diagonals under tension, showed excellent structural behaviour as detailed in Chapter 3. In real life situations, diagonals will be subjected to both tension and compression, due to load fluctuation or their location in the structure. Accordingly, it was necessary to investigate the DD-MPTS with diagonals under compression. Using sandwich construction for the diagonals provided many advantages to the concept of DD-MPTS (Sec.3.3, p33). However, with sandwich diagonal under compression, other factors such as transverse shear modulus of the core material, skin architecture and end restraints can significantly affect its ultimate capacity and failure mode. The other important specific issue regarding DD-MPTS is the bi-axial stress status at the diagonal ends, transverse tensile stresses combined with longitudinal compressive stresses. All these issues need to be addressed in investigating the DD-MPTS with diagonals under compression.

In this chapter, the behaviour of sandwich columns, under edge-wise compression, is investigated to form the bases for investigating the behaviour of DD-MPTS with diagonals under compression. With the understanding of the behaviour of the prototype sandwich columns, informed decisions can be made for the DD-MPTS. Preliminary investigations were conducted for a limited number of column specimens with different core materials. These investigations showed the significance of the core material on the column capacity and failure mode.

The literature review relevant to this chapter provides an overview of the different applications of sandwich structure, confirming that their use in civil engineering applications has been limited. In addition, the literature review enabled identification of the behavioural issues relevant to sandwich columns and mathematical expressions to predict their capacities. Single-core columns are commonly used in sandwich columns. No reference was located that referred to mixed-core column behaviour.

A total of six sets of columns were tested under compression. They had similar skin fibre architecture with three different arrangements of core materials: low-density closed-cell PVC foam, high-density balsa[1] and a combination of the low-density foam and balsa (mixed-core).

To keep the panel simple so effort could be directed towards developing a basic understanding of its behaviour, single-core sandwich diagonals were used in the DD-MPTS panel. Detailed analysis of the test results for the single-core columns is presented in this chapter. However, mixed-cores were included in the column tests as material availability, weight optimisation, cost, failure and post-failure structural behaviour are good reasons for considering their use. The test results for the mixed-core sandwich columns are presented in Appendix C for interested researchers who may wish to pursue the concept.

The FE model, presented in Chapter 3, successfully predicted the DD-MPTS behaviour with diagonals under tension. FE modelling procedures similar to those used with DD-MPTS diagonals were followed to model the sandwich columns, with slight modification to predict their buckling behaviour. In verifying the FE model with the test results, simplified FE modelling procedures are presented and compared to the more detailed model. This provided the base to develop simplified models at the macro-level analysis as detailed in Chapter 6. Sandwich column design equations found in the literature were verified using the FE models.

With knowledge gained in investigating sandwich columns, a full-height DD-MPTS panel was tested with diagonals under compression. The test results

[1] Originally, it was planned to use high-density closed-cell PVC foam. However, being unavailable for a few months, end-grain balsa was used as a high shear modulus alternative.

confirmed the predictions of the panel FE model. This proved that the modelling procedures used are reliable in predicting the general DD-MPTS panel behaviour. This chapter concludes with recommendations on predicting the capacity of DD-MPTS with diagonals under compression.

4.2. PRE-INVESTIGATIONS OF SANDWICH PROTOTYPE COLUMNS

Prior to doing the literature review presented in Sec.4.3 and Sec.4.4, preliminary test investigations were conducted to highlight the effect of the core material on the column compression capacity. In this section, the sample preparations, testing procedures and results are presented and discussed.

4.2.1. SAMPLE PREPARATIONS AND TESTING PROCEDURES

The first decision to be made was to determine the dimensions of the prototype columns, with the testing limitation of 600mm in height. Initial thought was to have columns with a slenderness ratio close to that of the future full-scale panels. In sandwich construction, the cross-section stiffness is derived from the skins that are separated by the core. To calculate the column slenderness, the laminate modulus along the loading axis was derived using the laminae properties, Appendix 'E', and applying the theory of composite plates. The effective length of the diagonal was assumed 0.50 of the clear height (clamped at both ends) while it was assumed to be 0.70 of the clear height (clamped-hinged ends). The slenderness was calculated based on Equation 4-1. The predicted slenderness of the prototype columns and the diagonal are shown in Table 4.1.

$$l = \sqrt{\frac{l^2 A_s}{I}} \qquad \text{Equation 4-1}$$

Table 4.1 Slenderness of prototype columns

	Laminate			h(mm)	Equiv uniform section			
Column	**Arch.**	**t(mm)**	**E_s(GPa)**		**A_s(mm^2)**	**I(mm^4)**	***l*(mm)**	l
Diagonal	$[0/90/0]_s$	3.30	18.10	50	990	7.04E+05	0.5x1500	28.12
Prototype	$[0]_s$	1.10	23.60	20	264	2.94E+04	0.7x460	30.51

Prototype columns of 460mm, clear height, and 120mm wide were manufactured using Hyrez 202 glass/epoxy (450gsm uni-glass by Huntsman, www.huntsman.ivt.com.au) skins with a 20mm thick core. Loading blocks were manufactured using pultrusions SHS50x50x5 (by Pacific Composites, www.pacomp.com.au), 250mm in length, that were filled with 45% loading epoxy-based PFR. Their section was slotted from one side to allow gluing the column ends inside the block. After gluing the skins to the core, columns were cut to dimension (560mmx120mm) then glued to the loading blocks. The glue was left to cure for 24 hours. End blocks were filled with 45% loading Hyrez 202 epoxy-based PFR. After curing the end blocks for 24 hours, specimens were post-cured for 8 hours at 70˚C[2].

Four columns, with different core materials, were tested. T01-01 used Klegecell-R45 low-density (48kg/m^3) PVC closed-cell foam from Diab (www.diabgroup.com), pink foam. T01-02 used Barracuda high-density (200kg/m^3) PVC closed-cell foam from Diab (www.diabgroup.com), white foam. T01-03 had glue-stiffened pink foam. Triangular patterns of the pink foam with 141mm chord length were glued to form the core material (Figure 4.1). The HPR26 thixotropic-toughened epoxy glue system was used (www.atlcomposites.com.au). T01-04 had end-grain balsa wood, SB100 from ATL composites (www.atlcomposites.com.au).

The prototype columns were tested in fixed-hinged configuration on the Shimadzu machine model CSP-300 of 100kN capacity (Figure 4.2). Loads were applied as displacement controlled with a loading rate of 2mm/min. Applied loads were recorded by a 222kN loading cell connected to a System-5000 data acquisition system.

[2] Curing schemes changed from one element to another depending on the resin system, the core material used and the structure of the element. Thick elements need more time to allow heat to reach the inner parts. Dynamic mechanical analysis (DMA) was used to investigate the post-curing effects on the different resin glass transition temperature (T_g) and the level of curing (by detecting any remaining active cells within the resin). Generally, post-curing at 80˚C for 6 hours was found sufficient for epoxy-based elements.

Figure 4.1 Patterned pink foam for T01-03 column

Figure 4.2 Prototype test layout of T01 columns

4.2.2. TEST RESULTS

Two failure modes were observed. The white foam (T01-02) and the balsa-core (T01-04) columns had skin failure at the column-fixed end, on the maximum compression side. After failure, the white foam column retained its shape, as the foam accommodated the excessive strains at the failure region (Figure 4.3). The balsa column split into two parts (Figure 4.4). The pink foam columns (T01-01 and T01-03) failed by overall buckling due to shearing of the core (Figure 4.5). Column capacities and failure modes are summarised in Table 4.2.

Figure 4.3 T01-02 - Failure mode

Figure 4.4 T01-04 - Failure mode

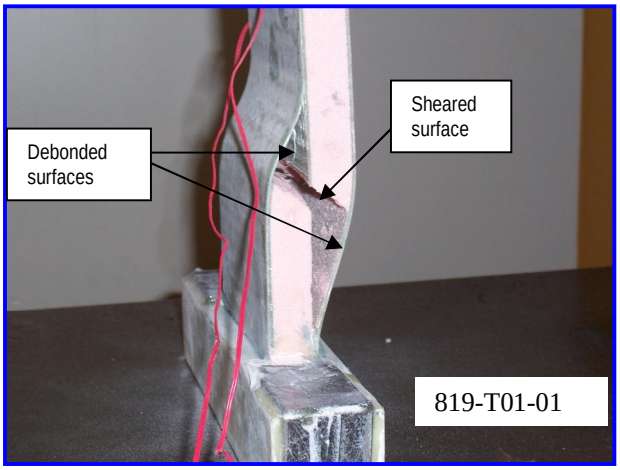

Figure 4.5 T01-01 - Failure mode

Table 4.2 T01 column capacities

Column	Core	Ult Capacity (kN)	Std Dev* (kN)	Failure Mode
T01-01	Pink	23.24	0.64	Core shear macro buckling (CS)
T01-02	White	50.17	1.63	Skins Micro buckling (SM)
T01-03	Pat Pink	35.93		CS
T01-04	Balsa	51.09		SM
T01-01a	Repaired Pink	36.77	6.94	Edge caps at fixed end of column

* Available for samples of two specimens.

The test results showed that the core material significantly affected the column capacity and failure mode. Reinforcing the pink core (T01-03), by glue patterns, significantly increased their capacities. This indicated that, for this column configuration, the column capacity was sensitive to the shear modulus of the core material. Increasing the core modulus, by using denser foam or balsa, shifted the failure from the core to the skins. This is why both T01-02 and T01-04 had a similar failure load. In all cases, there was no load redundancy and columns failed in a sudden brittle mode.

4.3. DEVELOPMENT OF SANDWICH STRUCTURES

Although, some records refer the use of sandwich panels by Fairbairn (1849) and even as early as Leonardo da Vinci (Allen, 1969), the Second World War "Mosquito" aircraft is generally accepted as the first major structure that incorporated sandwich panels. Sandwich structures started to gain popularity during the middle of the 20th century when different metallic faces and core materials were used for the construction of aircrafts and marine vessels. This can be attributed to their high specific[3] shear and compression strengths compared to other core materials. The percentage of sandwich components in aircrafts has increased significantly with time. For example, the percentage usage of sandwich panels for the wetted surface[4] in Boeing aircrafts increased from 8% in the B707 to 46% in the B757 (Bitzer, 1992). In addition, sandwich components are used in fuselage shells, floors, side panels, ceiling and engines. Beech Starship (Figure 4.6) was the first all-sandwich aircraft with Nomix honeycomb core with carbon and Kelvar faces. The first Starship flew in late 1988 with development costs in excess of $300 million (http://en.wikipedia.org, keyword: Starship).

Figure 4.6 Beech Starship, the first all-composite sandwich aircraft (Robert Scherer, www.bobscherer.com)

The development of high-strength, high-modulus, light-weight fibres and new forms of core materials opened a new era for sandwich structures. With the use of composites, structural properties can be fully adapted to meet design requirements, such as light weight and thermal stability. In addition, the orthotropic nature of composite materials, along with the flexibility in selecting the fibre types and

[3] Related to their density.
[4] The airplane's surface that would be wet if the aircraft was submerged in water, Vinson (1999).

architecture, can significantly increase the buckling capacity of the sandwich structure (Librescu and Hause, 2000).

The US Navy and other ship manufacturers are using honeycomb-sandwich bulkheads to reduce a ship's weight above the waterline (Vinson, 1999). Other transport applications include boats, racing cars, and sports goods such as kayaks, water skis and platform tennis paddles. Due to its excellent absorption of mechanical and sound energy, honeycomb sandwich construction is used in insulative barriers and crash barriers in high speed trains (Mamalis et al, 2005).

In civil applications, sandwich construction is used in wall and roof cladding where metallic face-sheets are commonly used with light-weight insulating cores (Davies, 1997). One of the important structural applications of sandwich construction in civil engineering is sandwich bridge decks. The short design life and the heavy weight of conventional concrete decks are among the factors that have driven the development of innovative composite sandwich forms for bridge decks. The use of sandwich decks also provides the opportunity to upgrade the load-carrying capacity of a bridge. An overview of innovative sandwich systems used for bridge decks can be found in Karbhari (1997).

Another form of sandwich application has been used in trusses. The Monocoque Fibre Composite (MFC) truss, proposed by Humphreys et al (1999) and presented in Chapter 2, used sandwich construction for building trusses. However, this truss system has limited application due to its complexity and low load-carrying capacity.

No other applications were found in the literature for sandwich structures in civil engineering. This clearly shows the originality of the MPTS concept that combined pultrusions and sandwich diagonal members to obtain high load-carrying capacity composite truss systems.

Using mixed-core sandwich panels (glass/polyester skins with honeycomb and balsa wood cores) were used during World War II by Wright Patterson Air Force Base in manufacturing the Vultee BT-15 fuselage (Rheinfrank and Norman, 1944). However, no other reference was located that investigated this subject.

4.4. BEHAVIOUR OF SANDWICH PANELS - REVIEW

The research in sandwich structures is recent, compared to other structural systems. The first published paper, which dealt with in-plane compression loads, was by Marguerre (1944). As metallic skins and cores were the original materials used for sandwich structures, early investigations focused on the behaviour of this form of sandwich structure. During the 1950s, the US Forest Products Laboratory (USFPL) was the primary group involved in developing analysis and design methods for sandwich structures. Their effort led to the publication of the military design handbook MIL-HDBK-23 (Anon, 1955) that was continuously updated until being cancelled in 1988. For many years, Allen (1969) and Plantema (1966) were the most popular references that provided simplified and practical approaches to the analysis and design of sandwich structures.

The review in this section focuses on predicting the capacities of sandwich columns and their associated failure modes. The FE models and mathematical formulae presented will be verified with the test records to confirm their credibility in predicting the column behaviour.

4.4.1. SANDWICH COLUMNS FAILURE MODES

Four failure modes for sandwich columns, two global and two local, are presented in the MIL-HDBK-23 (Anon, 1955) and found in many references such as Vinson (1999), and Fleck and Sridhar (2002). In addition to the overall buckling of the column (Figure 4.7A), shear crimping failure (Figure 4.7B) is another form of general overall buckling in which the wavelength of the buckles is very small, because of the low core-shear modulus. The crimping of the sandwich occurs suddenly and usually causes the core to fail in shear at the crimp; it may also cause shear failure in the bond between the facing and the core. It is important to note that the critical skin stress, where core shear instability can occur, is independent of the column dimensions. However, it is related to the core and skin properties and the boundary conditions (Vinson, 1999). If the core is of cellular structure, honeycomb, it is possible for the facings to buckle or dimple into the spaces between core walls or corrugations as shown in Figure 4.7C. Wrinkling is the fourth form of failure (Figure 4.7D). It can occur if the skin buckles inward or outward, depending on the flat-wise compressive strength of the core relative to the flat-wise tensile strength of the bond

between the facing and the core. If the bond between the facing and the core is strong, facings can wrinkle and cause tension failure in the core. This simulates plate-on-elastic foundation. The wrinkling load depends upon the elasticity and strength of the foundation system, namely, the core and the bond between the facing and the core. Since the facing is never perfectly flat, the wrinkling load will also depend upon the initial eccentricity of the facing or original waviness (Allen, 1969).

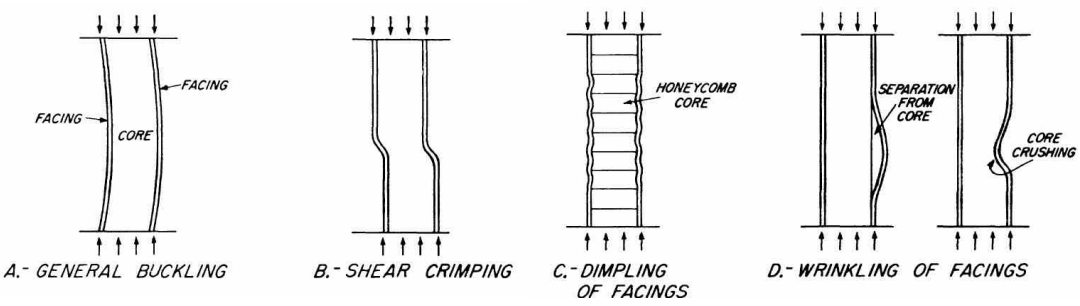

Figure 4.7 Modes of failure in sandwich panels under edge load - MIL-HDBK-23 (Anon, 1955)

Progressive end-crushing is another failure mode, Mamalis et al (2005), (Figure 4.8). This mode of failure can occur in short columns with high-density core material of non-brittle behaviour (typically used in crushing application).

Fleck and Sridhar (2002) investigated eight combinations of flat panels with different core and skin materials under edge-wise compression. Based on their study, they developed collapse mechanism maps to illustrate the dependence of failure mode upon the geometry and relative density of the core. They also used these maps to determine minimum weight designs as a function of the appropriate structural load index.

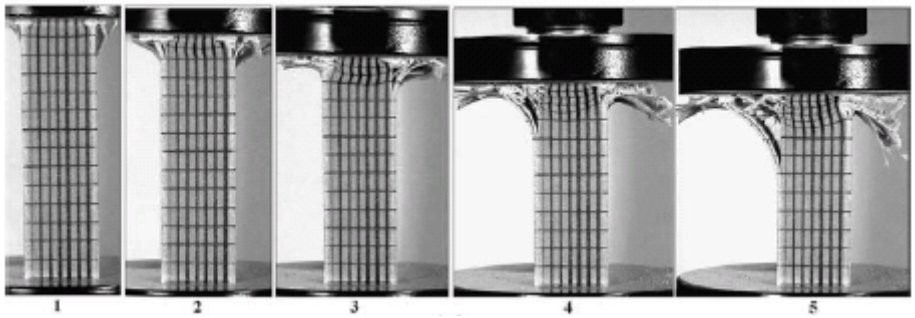

Figure 4.8 Progressive end-crushing failure mode for sandwich columns (Mamalis et al, 2005)

4.4.2. PREDICTING THE CAPACITY OF SANDWICH COLUMNS

Sandwich column capacity depends on the related failure mode that has the least critical load. In this section the literature is surveyed for methods of predicting the column capacity for the different failure modes, excluding crushing failure as it is only applicable to very short columns.

4.4.2.1. Overall Buckling Capacity (due to bending and shear)

Euler (1744) buckling formulation (Equation 4-2) is not suitable for predicting the buckling capacity of sandwich columns. This is attributed to the fact that its formulation was based on assuming plane sections remain plane after bending, meaning no transverse shear deformation is considered. Composite materials have an important distinguishing feature, namely, an extensional-to-transverse shear modulus ratio higher than metallic materials, with this ratio being more in sandwich construction due to the low shear-modulus of the core (Kardomateas and Simitses, 2004). This makes it essential to include the effect of transverse shear in the formulation of the buckling capacity. Transverse shear corrections for Euler capacity are based on two theories, Engesser (1891) and Haringx (1948). During the 1960s, there was polemics among proponents of different three-dimensional stability formulations associated with different strain measures. This was until Bazant (1971) concluded that all these formulations are equivalent, because the tangential elastic moduli of the material can not be taken as the same, but must have different values in each formulation. For buckling of columns, with significant shear deformations, the discrepancy between Engesser (Equation 4-3) and Haringx (Equation 4-4) formulae is attributed to the dependence of the tangential shear modulus (G) on the axial stress (Bazant, 1971). In addition, these differences will only matter when initial stresses at the critical state of buckling are not negligible compared to the elastic moduli (Bazant and Cedolin, 1991).

Applying this concept to sandwich columns resulted in some difficulties. Initial stress in the skins of the column is negligible to the elastic modulus of the skins and the initial axial stress in the core is zero. Accordingly, there should be no differences between the critical buckling load formulations associated with different finite strain measures. For short columns, the Engresser-type formulation (Doyale-Ericksen finite strain tensor of order m=2) gave lesser critical loads when compared with Haringx-

type formulation (Doyale-Ericksen finite strain tensor of order m=-2), Kardomateas & Simitses (2004). Bazant (2003) investigated this paradox and concluded that **shear modulus of the core depends on the axial stress in the skins**. Bazant and Beghini (2004) conducted an up-dated analysis and compared it with the experimental records. They concluded that to use non-dependent shear modulus for the core material, obtained by the small strain pure shear test or torsion test on a hollow thin-walled tube, the Engesser-type theory (m=2) must be used. In using Haringx-type formula, the shear modulus should be corrected according to Equation 4-5.

$$P_E = \frac{p^2 EI}{l^2},\ l = k\,L \qquad \text{Equation 4-2}$$

$$P_{Eng} = \frac{P_E}{1 + bP_E / GA} \qquad \text{Equation 4-3}$$

$$P_{Har} = \frac{\sqrt{1 + 4bP_E / GA} - 1}{2b / GA} \qquad \text{Equation 4-4}$$

$$G_{Eng} = G_{Har} + P / A \qquad \text{Equation 4-5}$$

Where,

β is the shear correction factor that depends on the cross-section. For sandwich column this is close to unity (Gere and Timoshenko, 1990).

k is the effective length factor: = 2 for cantilever, 1 for hinged ends and 0.50 for clamped ends.

For more accuracy in predicting the effective bending stiffness (EI) and shear stiffness (GA), Huang and Kadomateas (2002) included the effect of shear stiffness of the skins, as shown in Equation 4-6 and Equation 4-7 with the notations shown in Figure 4.9. These expressions can be simplified to the last term of the equations.

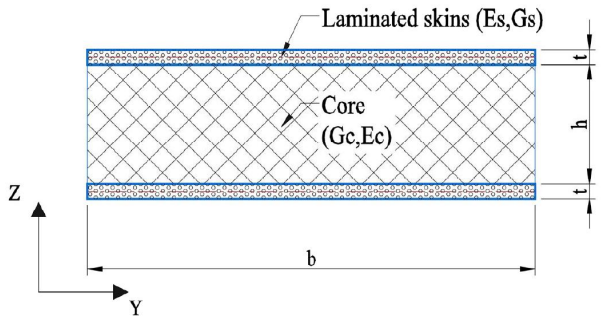

Figure 4.9 Sandwich column cross-section

Few sandwich column buckling formulae have been developed and reported, Bazant and Cedolin (1991), Huang and Kardomateas (2002), and Fleck and Sridhar (2002). Allen (1969) proposed two formulae, one for thin skins and the other for thick skins sandwich columns. Allen's formulae were based on Engesser theory. For thick skins, the formula uses the advanced sandwich theory, where faces bend locally in order to follow the shear deformation of the core. Thus the additional shear deflections of the core are reduced by the local bending stiffness of the skins (Allen and Feng, 1997). In this method, the Euler critical load is divided by the correction factor (r, Equation 4-8[5]) to obtain the critical load with shear correction. Vinson (1999) proposed a simpler factor for Euler critical load and natural frequency (Equation 4-9, assuming mid-plane symmetry and no bending-stretching coupling[6]). For skin stresses above the stress-strain proportional limit, many investigations have used the elastic equations where E has been multiplied by the plasticity reduction factor (η) - with considerable differences in opinions over its correct form (Vinson, 1999).

$$EI = b\left[E_s\frac{t^3}{6}+\frac{1}{2}E_s t(t+h)^2+E_c\frac{h^3}{12}\right]\approx\frac{1}{2}E_s bt(t+h)^2 \qquad \text{Equation 4-6}$$

$$GA=\frac{1}{2b}\left[\frac{E_s^{\,2}}{4(EI)^2G_s}\left(a^4t-\frac{2}{3}a^2(a^3-d^3)+\frac{1}{5}(a^5-d^5)\right)+\right.$$

$$\left.\frac{E_s^{\,2}}{(EI)^2G_c}\left(t^2c^2d+\frac{2E_c^{\,2}}{15E_s^{\,2}}d^5+\frac{2E_c}{3E_s}tcd^3\right)\right]^{-1}\approx G_c bh \qquad \text{Equation 4-7}$$

$$r=\frac{1+\left(1-\frac{EI_s}{EI}\right)\left(\frac{t^2EI}{l^2D_Q}\right)}{1+\left(1-\frac{EI_s}{EI}\right)\left(\frac{t^2EI}{l^2D_Q}\right)\left(\frac{EI_s}{EI}\right)} \qquad \text{Equation 4-8}$$

$$r=\sqrt{\left(1+\frac{p^2}{l^2}\frac{E_s th}{2G_c}\right)} \qquad \text{Equation 4-9}$$

[5] Thick skins equation can be used for both thin and thick skins.

[6] Introducing bending-stretching coupling will cause overstressing before reaching the buckling load in addition to reducing the buckling load (Vinson, 1999).

Where,

$a=t+(h/2)$, $c=(t+h)/2$ & $d=h/2$

$EI_s=E_s bt^3/6$ & $D_Q=4bc^2G_c/h$

Core shear instability can occur by increasing the section bending stiffness or reducing the core shear stiffness. The critical skin stress for shear instability can be predicted by Equation 4-10 (Mamalis et al., 2005).

$$s_{cr} = \frac{(t+h)^2}{2ht} G_c \qquad \text{Equation 4-10}$$

4.4.2.2. Face Plastic Micro-Buckling Capacity

Compressive failure of composites can result from a number of competing failure modes with large scatter with nominally identical specimens. Face plastic micro-buckling failure is a shear buckling instability of the face fibres due to large shear strains in the face matrix (Figure 4.10), Fleck (1997). The shear yield strength of the composite and the initial fibre misalignment angle are the main factors controlling the micro-buckling compressive strength, Argon (1972) and Budiansky (1983). The compression strength is sensitive to the degree of imperfection (fibre waviness) and the fibre mis-alignment with the loading direction. For sandwich columns, plastic micro-buckling of the skins is the most probable failure mode (Fleck and Sridhar, 2002). It occurs when the axial compressive stresses in the skins attains the plastic micro-buckling strength (σ_{mb}). Assuming uniform stress distributions, the micro-buckling capacity of the sandwich column is given by Equation 4-11.

$$s_{mb} = \frac{P_{mb}}{2bt} \qquad \text{Equation 4-11}$$

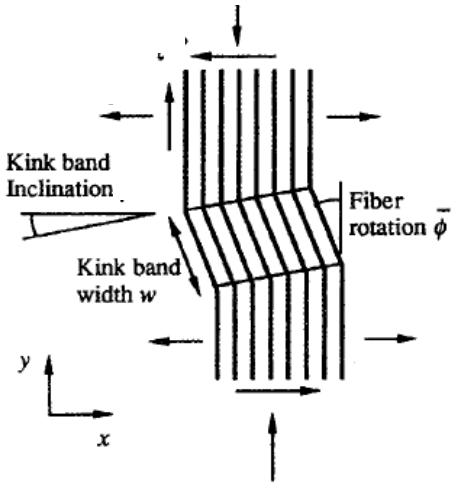

Figure 4.10 Plastic micro-buckling of composites under compression (Fleck, 1997)

Piggott and Harries (1980) and Piggott (1981) conducted an important study to investigate the effect of the matrix modulus on the compression capacity of the composite. The modulus was varied by partial post-curing. Based on their investigations, Fleck (1997) summarised their findings in Figure 4.11, for glass and Kevlar fibres with fibre volume fraction of 31% and $\gamma_y \sim 0.024$ (1.4˚). Piggott and Harries (1980) and Piggott (1981) data show that compression failure changed from plastic micro-buckling (where the strength increased with the increase of the matrix shear modulus) to fibre crushing (arrow location in Figure 4.11).

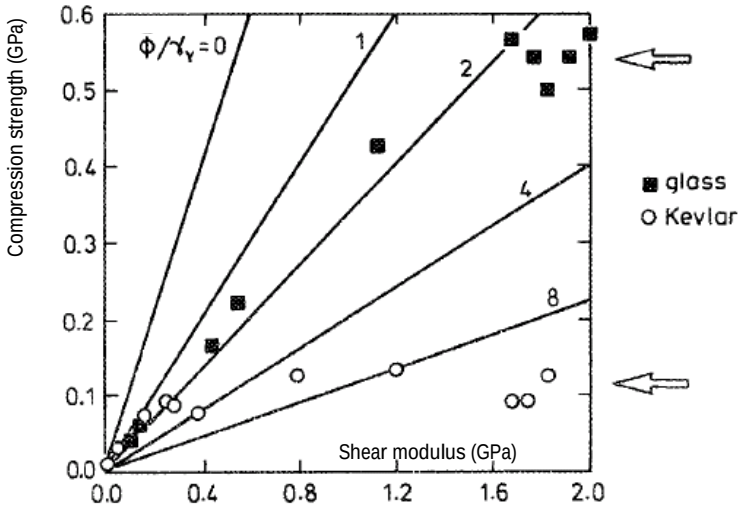

Figure 4.11 Measured compressive strength of glass and Kevlar fibre composites (Fleck, 1997)
Where,
ϕ: Initial fibre misalignment angle & γ_y: yield strain in longitudinal shear

4.4.2.3. Face Wrinkling Capacity

Face dimpling failure is not applicable to solid core sandwich columns. Accordingly, the face wrinkling is the last failure mode to present. The critical skin stress where faces start to wrinkle can be described by Equation 4-12 (Vinson, 1999). The other formula that is still in use is the Hoff and Mautner (1945) (Equation 4-13). There is disagreement between different researchers about the value of the constant C, in Equation 4-13. Few values were proposed, for example, 0.50, 0.60 and 0.65. Plantema (1966) used C=0.76. Dreher (1992) confirmed this value, based on his experimental data. For practical design purposes and based on the available test results, Plantema (1966) recommended using C=0.50.

$$s_{cr} = \left[\frac{2t}{3h} \frac{E_c \sqrt{E_{sx} E_{sy}}}{(1 - n_{xy} n_{yx})} \right]^{1/2}$$ Equation 4-12

$$s_{cr} = C\left[E_s \; E_c G_c \; \right]^{1/3}$$ Equation 4-13

The above equations refer to isotropic face and core materials. For orthotropic cores, Vonach and Rammerstorfer (2000) suggested Equation 4-14, with C=0.85.

$$s_{cr} = C\left[E_s \; (k^{thick})^2 \right]^{1/3}$$ Equation 4-14

Where,

$$k^{thick} = \left[\left(\frac{X_4}{m_2} - \frac{X_3}{m_1} \right) + n_{czx} \left((X_4 m_2 - X_3 m_1) \sqrt{\frac{E_{cx}}{E_{cz}}} \right) \right]^{-1} E_{cz} \sqrt[4]{\frac{E_{cx}}{E_{cz}}} ;$$

$$X_3 = \frac{m_2^2 + n_{cxz} \sqrt{D_{c3} / D_{c1}}}{m_1^2 - m_2^2} ;$$

$$X_4 = \frac{m_1^2 + n_{cxz} \sqrt{D_{c3} / D_{c1}}}{m_1^2 - m_2^2} ;$$

$$m_1 = \sqrt{x + \sqrt{x^2 - 1}} ; \; m_2 = \sqrt{x - \sqrt{x^2 - 1}} ; \; x = \frac{\sqrt{D_{c1} D_{c3}}}{D_{c13}} ;$$

$$D_{c1} = E_{cx} ; \; D_{c13} = \frac{2 E_{cx} G_{cxz}}{E_{cx} - 2 n_{cxz} G_{cxz}} ; \text{ and } \; D_{c3} = E_{cz} .$$

Gdoutos et al (2003) stated that the difference in the predicted critical stress, between using Equation 4-13 (assuming isotropic core material) and Equation 4-14, is less than 5% for the E_{cx}/E_{cz} ratio of 10-100%. However, for highly orthotropic core properties, the critical stress will be reduced significantly.

4.4.2.4. Failure Predictions in Composite Materials

From the review presented above, it is clear that there are differences in opinion in predicting the capacity of some of the failure modes of sandwich columns. Using laminates for the column skins adds more complexity in predicting their capacities. This is due to the lack of understanding of the mechanisms that lead to failure in composite materials. This is especially true for matrix or fibres under compression (Davila et al, 2005). This explains the generally poor predictions by most of the participants in the World-Wide Failure Exercise (WWFE). The current design practices place little or no reliance on the ability to predict the ultimate strength of the composite structure with any great accuracy. Failure theories are often used in the initial calculations to size the structure. Then experimental tests on coupons or structural elements are used to determine the global design allowables, which are usually less than 30% of the ultimate load (Soden et al, 1998). The issue addressed was the definition of failure. A designer would define failure as the point at which the structure ceases to fulfil its function. This definition is accordingly application-specific. It was concluded that the connection between events at the lamina level and the definitions of structural failure required by designers need to be established (Hinton and Soden, 1998).

The comparison, conducted by the organisers of the WWFE, between theoretical and experimental results, showed that failure theories of Puck (Puck and Schurmann, 1998 & 2002), Zinoviev (Zinoviev et al., 1998 & 2002), Tsai (Liu and Tsai, 1998 & Kuraishi, et al., 2002) and Sun (Sun and Tao, 1998, and Sun et al., 2002) are the top ranking theories, based on the available experimental data (Hinton et al, 2002a and 2002b). The assessment was based on five major areas that are summarised as follows:

- *Biaxial strength of unidirectional laminae*. Most theories achieved at least 50% of the experimental data with the closest by Tsai, Wolfe (Wolfe and Butalia, 1998 & Butalia and Wolfe, 2002), Puck and Chamis (Gotsis et al., 1998 & 2002). It was noticed that Tsai and Wolfe predict markedly higher strength levels than other theories, in the compression-compression (C-C) or tension-tension (T-T) quadrants for certain stress ratios. The lack of

experimental data in these quadrants avoided justifying their performance under these loading conditions.

- *Predicting initial strengths of multi-directional laminates*. Most of the theories failed to capture the laminate initial strength. The overall conclusion was that, to estimate the stress levels at which initial failure might occur in a multi-directional laminate, the current theories can predict this by an accuracy of $\pm$50% at best. This is partly due to residual stresses and in-situ lamina properties.
- *Predicting final strengths of multi-directional laminates*. Puck, Tsai, and Zinoviev outperformed other theories. This was attributed to their ability to model post-initial failure. At best, using these theories would estimate the ultimate failure within $\pm$10% in 40% of the cases.
- *Ability to predict a selection of general features*: Puck and Tsai showed the best performance of this category. They predicted the increase in shear strength when transverse compression stresses were applied to the lamina.

Based on the above overview, it is clear that laminate failure is difficult to assess theoretically and, accordingly, numerically. Tsai's theory is one of the best available theories in predicting the failure of the laminate. It employs the interactive Tsai-Wu failure criterion which is one of the best-known and mathematically satisfying theories (Hinton et al, 2002b). However, like many of the other theories, this theory is linear-elastic and it can not predict the large non-linear strains observed in tests with high lamina shear.

4.5. SINGLE-CORE PROTOTYPE COLUMNS TESTING PROGRAM

After conducting the preliminary column testing, it became clear that the core material properties dominated the compression capacity of the columns with two modes of failures - shear buckling and micro-buckling skin failure. The prototype column test program was divided into two parts: the first used single core material, the second used mixed core (pink foam-balsa[7] combination). This section details the specimen preparations, test observations and FE modelling for the single-core columns. Details of the mixed-core columns are presented in Appendix C.

[7] Balsa was used due its availability as a high-shear modulus alternative

4.5.1. SPECIMEN PREPARATIONS

Ten prototype columns of 550mmL[8]x120mmWx24mmThk were manufactured. Pink foam was used in five columns (T02-01) and end-grain balsa was used in five columns (T02-06). Columns were manufactured as follows:

- Skins were laminated from 3 plies of uni-glass 450gsm from Huntsman (www.huntsman.ivt.com.au) using Hyrez 202 epoxy-resin with peel plies at each face.
- After curing for 24 hours at room temperature, the laminated sheets were cut to 140mm wide by 600mm length, using a bench saw with diamond-coated cutting wheel.
- Core material was cut to 140mm width by 600mm length with a thickness of 20mm, using a band saw.
- Cores were vacuumed, using a normal vacuum cleaner, to remove dust.
- Cores were primed, by spraying Hyrez 202 epoxy. This process needed about three coats, to achieve a permanent glossy surface. This was to control the amount of adhesive absorbed through the core gaps and to achieve good bonding between the core and the skins.
- The core of each column was weighed before and after spraying to assess the amount of resin used.
- The primed core was allowed to cure for 24 hours at room temperature. After removing the peel plies, skins[9] were glued to the core material using the HPR26 thixotropic-toughened epoxy glue system from ATL Composites (www.atlcomposites.com.au).
- The columns were clamped in bundles of three to maximise the exclusion of excess glue and left to cure for 24 hours at room temperature (Figure 4.12).
- Columns were cut to dimension (120mmW x 550mmL) on a bench saw with diamond-coated blade.

[8] 460mm clear height.
[9] After removing the peel plies.

- Loading blocks were manufactured by filling pultruded sections SHS50x50x5, from Pacific Composites (www.pacomp.com.au), with 45% loading PFR with Hyrez 202 and cenospheres.
- Loading blocks were slotted using a bench saw to allow the embedding of column ends.
- After preparing the surfaces, column ends were glued to the loading blocks then clamped and left to cure for 24 hours at room temperature.
- End blocks were filled with PFR and left to cure for another 24 hours at room temperature.
- Test specimens were post-cured for eight hours at 70˚C with one hour ramp. This was the maximum curing temperature for the pink foam without having any dimensional instabilities in its structure (www.diabgroup.com).
- Standard 120Ohm strain gauges were then glued centrally, mid-height on both sides.

Figure 4.12 Gluing skins to the core for single core columns

4.5.2. CHARACTERISATION OF THE CORE MATERIALS

The shear modulus of the core material is the most important core property that affects the behaviour and failure mode of sandwich columns. A few attempts have been conducted to predict the shear modulus of the core materials. Generally, it was found that the usage of standard testing methods (for example ASTM C393-00 or ASTM C273-94) were suitable for low shear modulus materials. However, for relatively high core modulus, these procedures can provide inaccurate results.

The rocket testing procedure was developed and used in this study to assess the properties of both low-density and high-density core materials. This was especially for SB100. As shown in Table 4.3, the rocket test provided reasonable estimate of the material shear modulus when compared with the data provided by their manufacturers. The rocket test, was developed to test two plans of core material in a symmetric set-up (Figure 4.13) with loads applied with a displacement rate of 0.10mm/min. loads were recorded by the MTS machine, while displacement was recorded by using laser-extensometer with a measuring range of 50mm. the core material shear modulus was calculated by calculating the slope of the load/displacement curve and applying Equation 4-15.

$$G_c = \frac{St_{av}}{l_1 b_1 + l_2 b_2} \qquad \text{Equation 4-15}$$

Where,

S: Slope of load-displacement curve
t_{av}: Average thickness of core specimen on both sides
l_1,l_2: Core specimen length on both sides
b_1,b_2: Core specimen width on both sides

Table 4.3 Characteristics of core materials

Test	Testing Standard	Property	Testing values		Data sheet values
			Average	Std Dev	
Shear Modulus	Rocket	SB100	159.13	40.60	159.00
		C70.200	87.38	21.12	75.00
		C70.55	20.76		22.00
		R45	14.99		14.00
Shear Modulus	ASTM C393	R45	16.58	0.77	14.00
		SB100	33.73	2.89	159.00

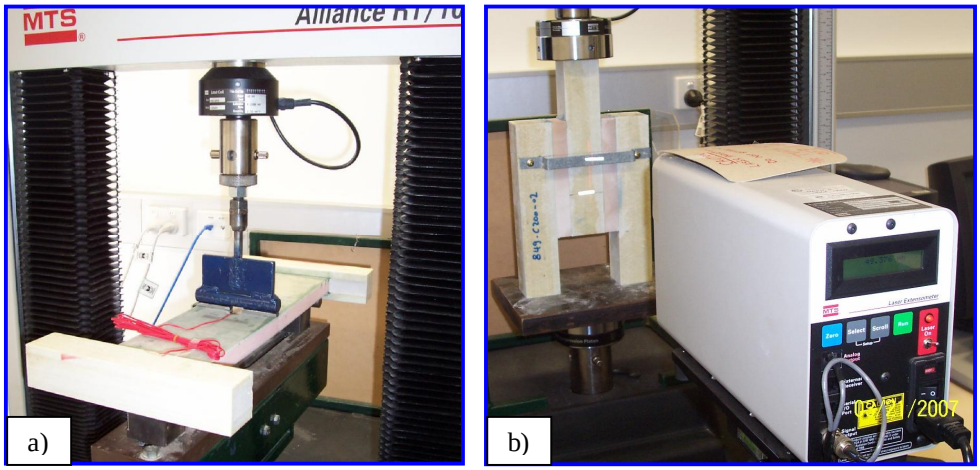

Figure 4.13 Characterising core materials a) ASTM C393-00 3-point test, b) Rocket test

4.5.3. TEST SET-UP AND OBSERVATIONS

As with the preliminary tests, column tests were conducted on the Shimadzu CSP-300 machine. Clamped-end restraints were implemented using a special fixture attached to the machine ram (Figure 4.14). Applied loads were recorded by a 222kN loading cell, vertical displacement was recorded using a string pot and horizontal displacement was recorded using a LVDT while strain gauges were attached at the mid-height of the column at both faces (Figure 4.14). All data were collected by the System-5000 data-acquisition system and recorded on a standard PC at time increments of 0.10s.

The test results confirmed that of the preliminary tests (Table 4.4). Changing the core material from the pink foam (T02-01) to balsa (T02-06) increased the average column capacity from 36kN to 99.5kN. In addition, different failure modes were observed. Generally, in each column set, all measurements were consistent across the different specimens.

Figure 4.14 T02 - Columns test setup

The pink foam columns (T02-01) failed in global buckling mode in a manner similar to that observed in T01-01 (Figure 4.5, p84 & Figure 4.15). The top-end fixity and the use of three plies of uni-glass increased the column capacity to 36kN (compared to 23kN for T01-01, Table 4.2, p84). The observed failure occurred at distances that ranged from 50mm to 130mm from the specimen bottom. The failure angle with the normal to the cross-section ranged from 27º to 39º. The failure planes were nearly flat across the cross-section.

The balsa column specimens (T02-06) failed in two modes (Figure 4.16). Two of the column specimens failed in the global shear crimping mode while the other three specimens failed in the local skin micro-buckling mode. Skin micro-buckling failure occurred directly adjacent to the bottom loading block. However, the shear crimp occurred at distances that ranged from 40mm to 260mm from the bottom.

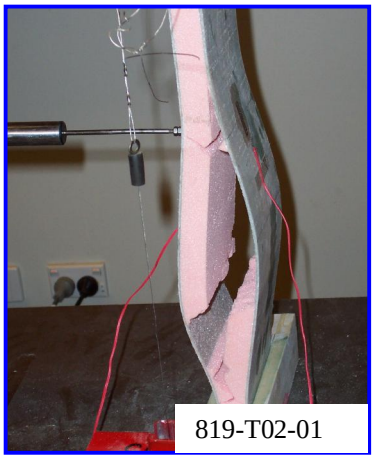

Figure 4.15 T02-01 – Failure mode

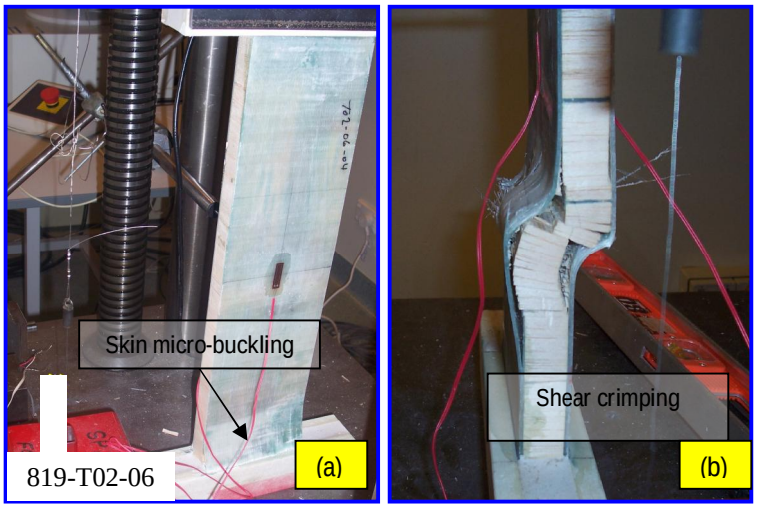

Figure 4.16 T02-06 - Failure modes (a) skin micro-buckling, (b) shear crimping

Table 4.4 T02 - Single-core columns strength & stiffness

	Ult Strength (kN)		Stiffness (kN/mm)		Weight	Sp. strength
Column	**Avg**	**Std Dev**	**Avg**	**Std Dev**	**(gr)**	**(kN/gr)**
T02-01	36.15	2.21	16.20	1.52	493	0.073
T02-06	99.47	4.47	20.00	1.40	595	0.167

Comparing the weight of both columns, T02-06 was 20% heavier than T02-01. The associated increase in strength was 128%. The column stiffness was measured by calculating the slope of the load deflection curves, at the straight portion. The column stiffness of T02-06 was slightly higher when compared with that of the T02-01 column. This indicated that the core material had limited effect on the column stiffness but had major effect on its strength.

4.5.4. FE MODELLING

As discussed in Sec.3.5 (p44), Solid-Shell FE model predictions have good correlation with the sandwich columns' experimental records. Abaqus is a Lagrangian code (Hibbitt et al, 2004b). Accordingly, its formulation is similar to an Engesser-type formula, with the core properties obtained from the direct shear tests with **independent values of the axial stress in the skins**. Accordingly, standard modelling procedures were used without the need to develop special sub-routines to change the material stiffness matrix during execution.

In modelling the T02 columns, a Solid-Shell model (CSO) was used, similar to the diagonal model presented in Chapter 3. Thick shell elements were used for the skins with composite properties for each ply, and solid elements were used for the glue and the core. The core material was modelled as an elastic material[10]. An average glue thickness of 0.5mm was used[11]. Surface-to-surface tie constraints were used to join each part of the model. For a more detailed description of the model, reference should be made to Sec.3.5.2 (p47).

Abaqus computes the shell transverse-shear stiffness by matching the shear response for the case of the shell bending about one axis, using a parabolic variation of transverse-shear stress in each layer. Generally, this approach provides a reasonable estimate of the shear flexibility of the shell. It also provides estimates of inter-laminar shear stresses in composite shells (Hibbitt et al, 2004b). In calculating the transverse-shear stiffness, Abaqus assumes that the shell section directions are the principal bending directions (bending about one principal direction does not

[10] The foam-crushed model was not required, as the core was not subjected to crushing strain under any load condition (unlike beam testing, where crush could occur at the load application and support locations). Using the foam-crushing material model complicated the analysis. In addition, it needed the conduct of additional tests for the core material, like assessing the hydrostatic tensile and compressive strengths to define the yield surface (Hibbitt, 2004a).

[11] The average glue thicknesses ranged from 0.40-0.50mm.

require a restraining moment about the other direction). These assumptions were satisfied in the tested columns. Accordingly, to simplify the column model, the composite Shell-Only FE model (CSH) was used. CSH model predictions were verified with the CSO model predictions and the test records to ensure its capability in predicting the column behaviour.

The FE analysis procedures were conducted in three steps, to capture the column buckling and to control the level of loads. The first was to obtain the imperfect modal shape by conducting Eigen-Value (EV) analysis (Figure 4.17). The second step was a non-linear Riks (arc-length) analysis with initial imperfection, based on the EV analysis mode shape. As both the displacement and load are unknowns in Riks analysis, to achieve control of the loading level Riks analysis was terminated prior to reaching the column buckling load. Analysis was then restarted, the third step, with non-linear fixed-step analysis until reaching the buckling capacity. An initial imperfection of 1mm was assumed. This assumption can be considered reasonable as composites have less construction tolerances when compared to other construction materials.

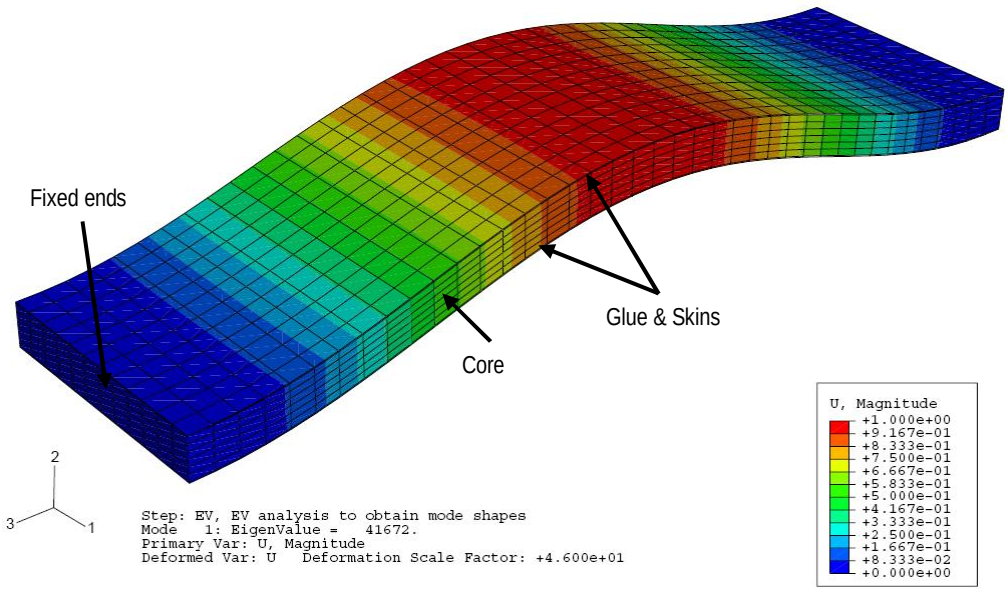

Figure 4.17 T02-01 - Solid-shell model layout and EV mode shape

4.5.5. VERIFICATION OF THE FE MODEL AND BEHAVIOUR OF T02-01 COLUMN

The T02-01 column failed in the global buckling mode. The first step in verifying the FE models was to investigate their ability to predict the buckling capacity of the column. This section covers this verification, comparing the model predictions for T02-01 with the test records and accordingly, investigates the main behavioural issues of this column.

EV factor was used as an indication of the overall buckling capacity. Summary of the predicted strains, stresses, failure loads, based on the equations presented in Sec. 4.4.2, and the test and FE analysis results are presented in Table 4.5.

Table 4.5 T02-01 - Summary of predicted failure capacities

Failure	**Parameters**	**e %**	**s (MPa)**	**Ld(kN)**
Overall buckling (Eqn. 4-8)		0.41%	93.2	36.9
Overall buckling (Eqn. 4-9)		0.85%	192.9	76.4
Shear crimping (Eqn. 4-10)		0.49%	111.0	44.0
Micro buckling (Eqn. 4-11)	Gc=1061.5MPa	1.58%	360.0	142.6
Wrinkling (Eqn. 4-13)	C=0.5	0.49%	111.0	44.0
FE model (buckling)	Eigen Value: 39.6kN	0.47%	107.0	34.7
Experimental (buckling)		0.43%	98.0	36.2

In verifying the graphs shown in Figure 4.18 to Figure 4.21, the important points to note are:

- In the different graphs, both the FE models (CSO & CSH) showed excellent correlation with the test records.
- Predictions of the FE model were accurate.
- EV analysis predicted the buckling capacity to a reasonable level. It over-estimated the capacity by 9.0%.
- Allen's prediction (Equation 4-8) provided an excellent match, while Vinson's prediction (Equation 4-9) over-estimated the column capacity.
- The strain-load curve was approximately linear until failure, where a large increase of strains was noticed.

- The effect of buckling was clearly shown in having higher strains on one skin, (Figure 4.20) than on the other (Figure 4.21).
- The maximum skin stress predicted by the strain gauge records was 98MPa, which exceeded the assumption of having equal stress distribution on both skins by 8%.
- Based on the predicted capacities of the different modes of failure, Table 4.5, it is clearly shown that the global buckling mode is the critical mode. This aligned well with the test results.
- Both the CSO and the CSH models had excellent correlation with the test results in predicting this column behaviour.

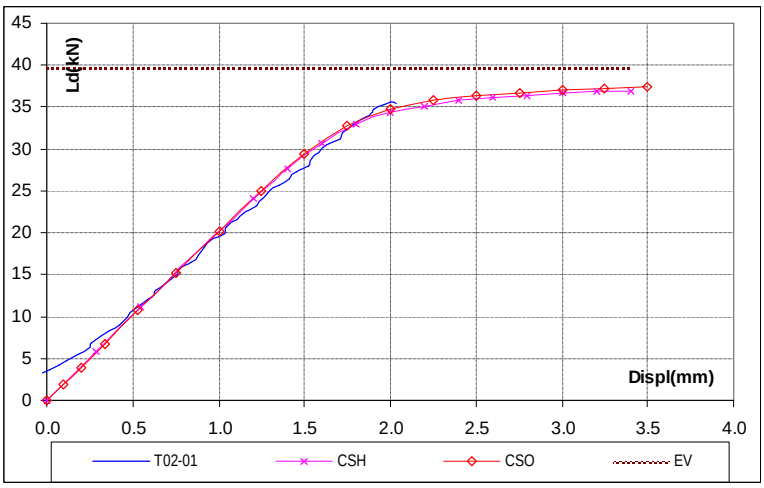

Figure 4.18 T02-01 - Load-Axial displacement

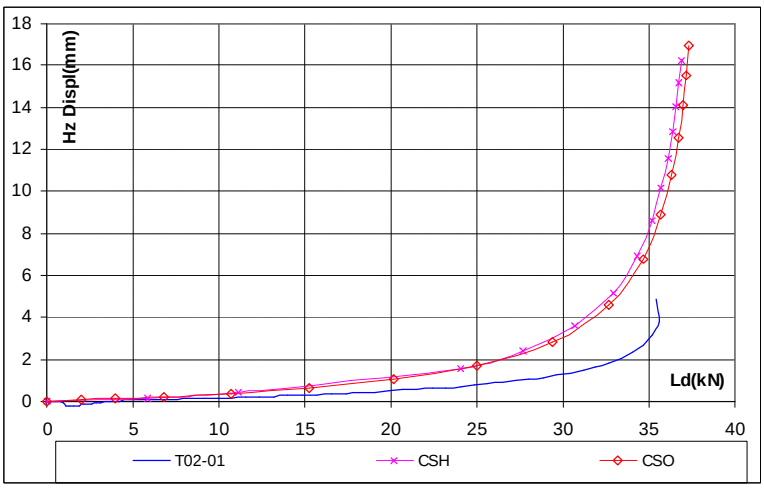

Figure 4.19 T02-01 – Horizontal displacement-Load

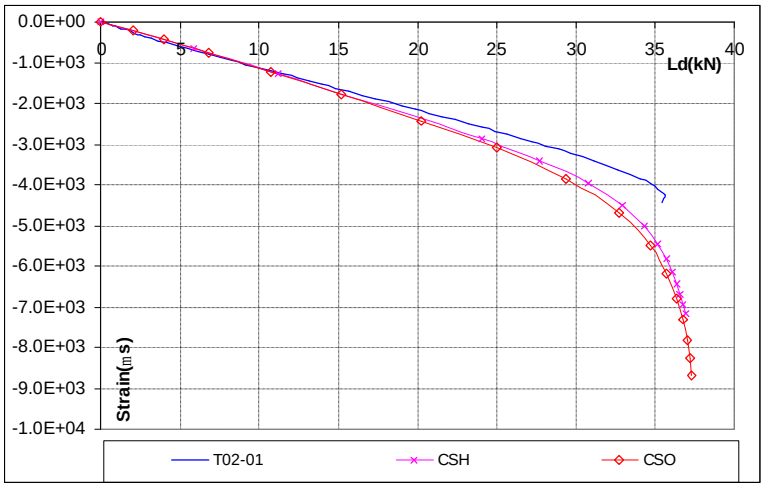

Figure 4.20 T02-01 – Maximum strain-Load (on concave face)

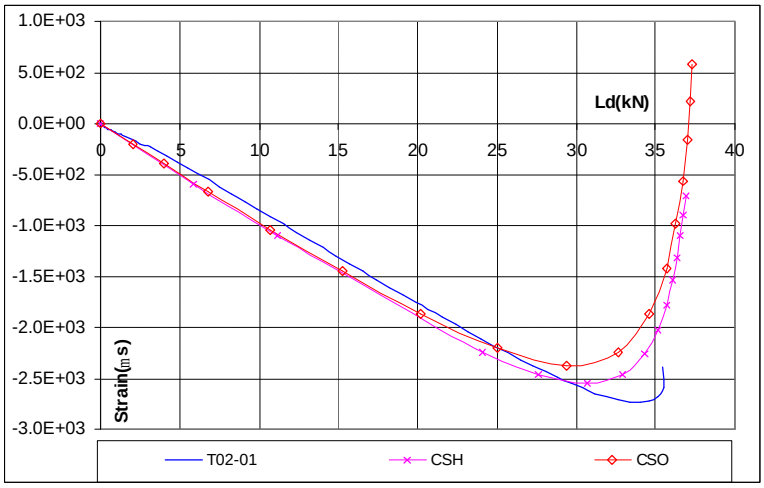

Figure 4.21 T02-01 – Minimum strain-Load (on convex face)

4.5.6. VERIFICATION OF THE FE MODEL AND BEHAVIOUR OF T02-06 COLUMN

The behaviour of the T02-06 column was more complex compared to the T02-01 column. This was attributed to the nature of the balsa core, as a natural product. Balsa sheets are formed from gluing tree chunks that have natural variations. This is in addition to the directional variation of properties related to tangential and radial directions, of each tree trunk (Figure 4.22). These complexities can lead to having different modes of failure, as observed in T02-06.

The inclusion of these variations in the FE model was very difficult to assess and implement. Simplified material properties were used ensuring the material stability in the stress space.

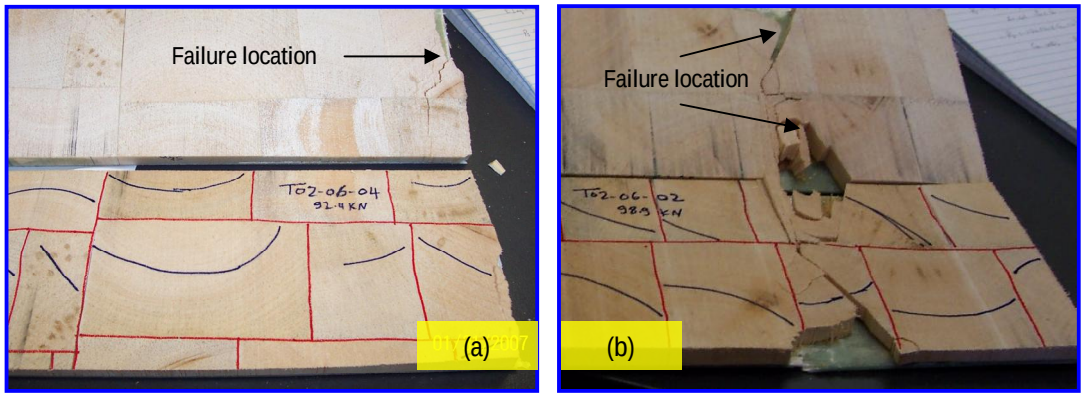

Figure 4.22 T02-06 - Core patterns for the two failure modes (a) at skins, and (b) at core
Red: glue lines between the balsa chunks
Blue: tangential directions of each chunk

Test records of two column specimens (T02-06Spc2 with shear crimp failure and T02-06Spc4 with skin micro-buckling failure), are presented and compared with the FE analysis predictions in Figure 4.23 to Figure 4.26. The presented FE analysis results were based on the Solid-Shell element models with the analysis options shown in Table 4.6. Summary of the predicted strains, stresses, failure loads, based on the equations presented in Sec. 4.4.2, and the test and FE analysis results are presented in Table 4.7. Section forces along the paths of the bottom skin-edge (B) and the top skin-edge (T) are shown in Figure 4.27 to Figure 4.30, with typical distribution as shown in Figure 4.31. These graphs were based on a load increment of 4.70mm (99.8kN).

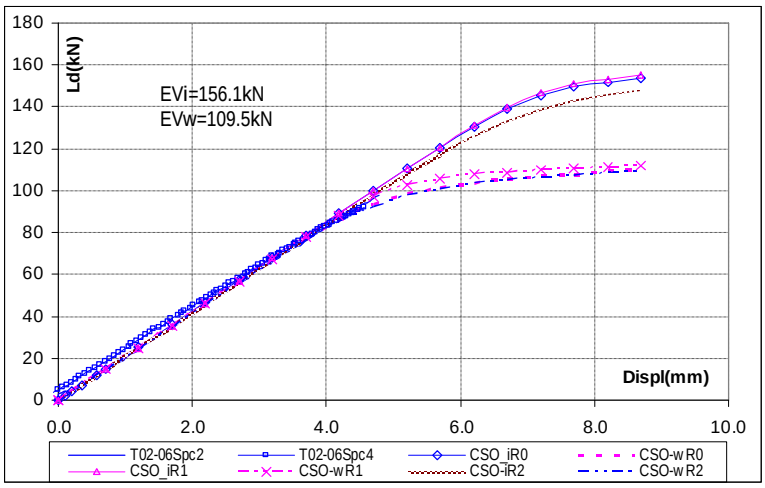

Figure 4.23 T02-06 - Load-Axial displacement

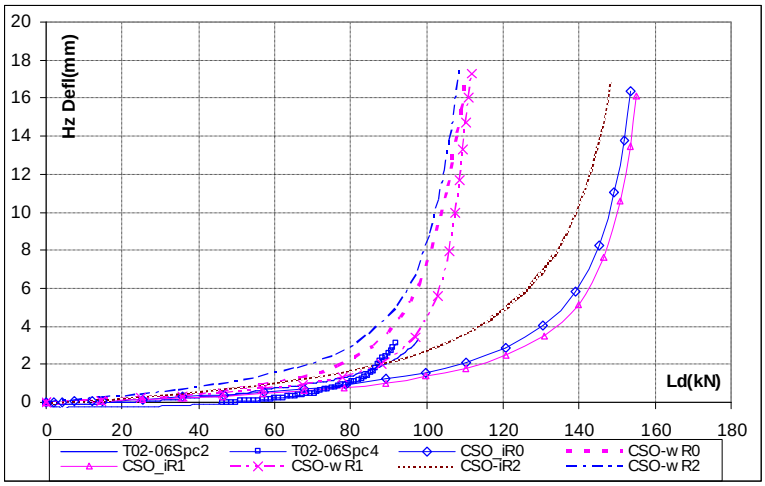

Figure 4.24 T02-06 – Horizontal displacement-Load

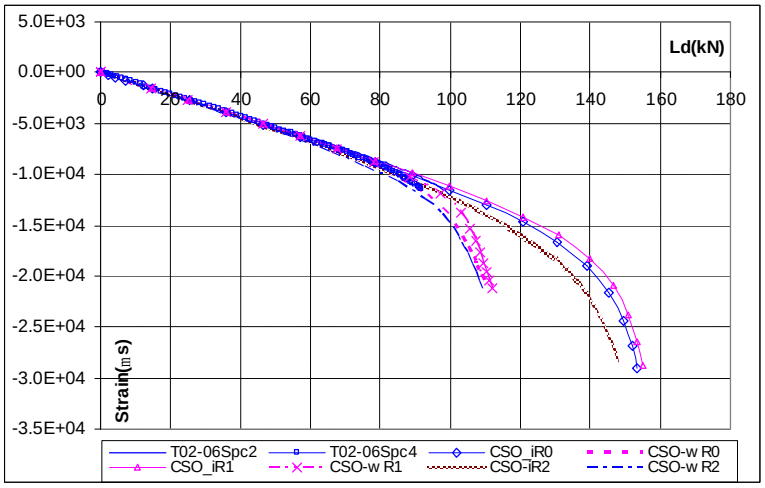

Figure 4.25 T02-06 – Maximum strain-Load

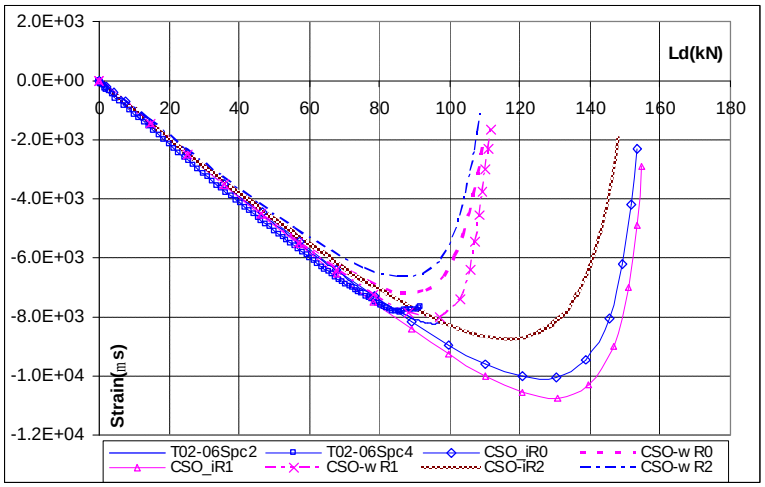

Figure 4.26 T02-06 - Minimum strain-Load

Table 4.6 T02-06 – FE analysis parameters

Analysis	Imperfection	Weak core[12]	Notes
CSO_iR0	1mm mid-height	No	Riks and NL analysis based on EV mode shape
CSO_iR1	1deg at movable support	No	NL analysis
CSO_iR2	2deg at movable support	No	NL analysis
CSO_wR0	1mm mid-height	G_c=35MPa	Riks and NL analysis based on EV mode shape
CSO_wR1	1deg at movable support	G_c=35MPa	NL analysis
CSO_wR2	2deg at movable support	G_c=35MPa	NL analysis

Table 4.7 T02-06 - Summary of predicted failure capacities

Failure	Parameters	e %	s (MPa)	Ld(kN)
Overall buckling (Eqn. 4-8)	Gc=158MPa	1.64%	373.0	147.7
Overall buckling (Eqn. 4-8)	Gc=35MPa	0.77%	176.6	69.9
Shear crimping (Eqn. 4-10)	Gc=158MPa	5.13%	1169.7	463.2
Shear crimping (Eqn. 4-10)	Gc=35MPa	1.14%	259.1	102.6
Micro buckling (Eqn. 4-11)		1.58%	360.0	142.6
Face wrinkling (Eqn. 4-14)	C=0.5, Gc=158MPa	5.18%	1181.7	467.9
Face wrinkling (Eqn. 4-14)	C=0.5, Gc=35MPa	1.51%	345.4	136.8
Experimental :T02-06Spc2		1.18%		98.9
T02-06Spc4		1.17%		92.4

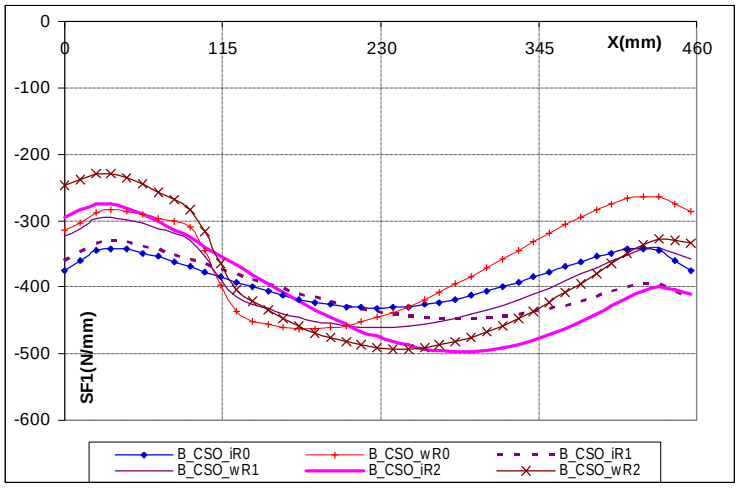

Figure 4.27 T02-06 – SF1 at bottom skin

[12] This value was based on the predicted column shear modulus by using ASTM C393 (2000).However, further verification is needed.

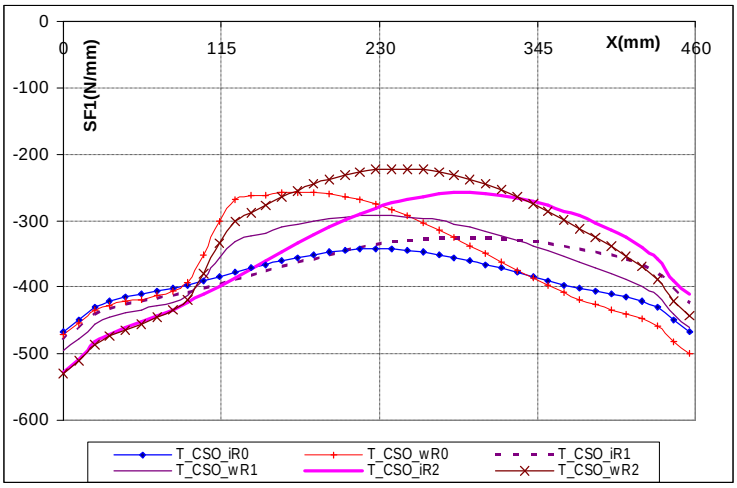

Figure 4.28 T02-06 – SF1 at top skin

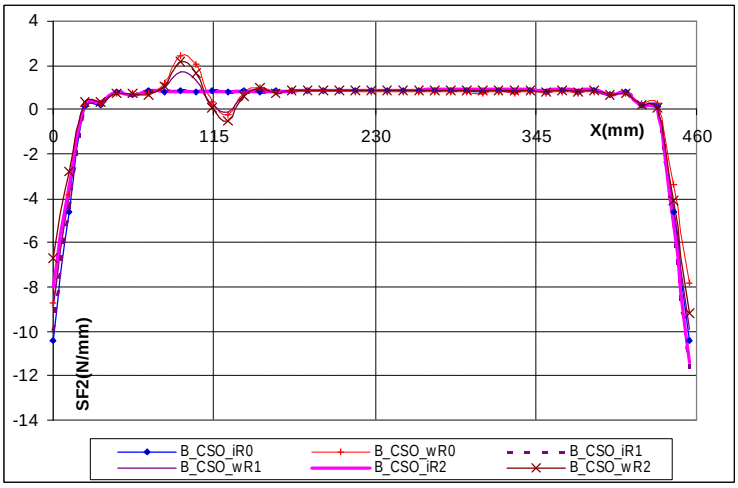

Figure 4.29 T02-06 – SF2 at bottom skin

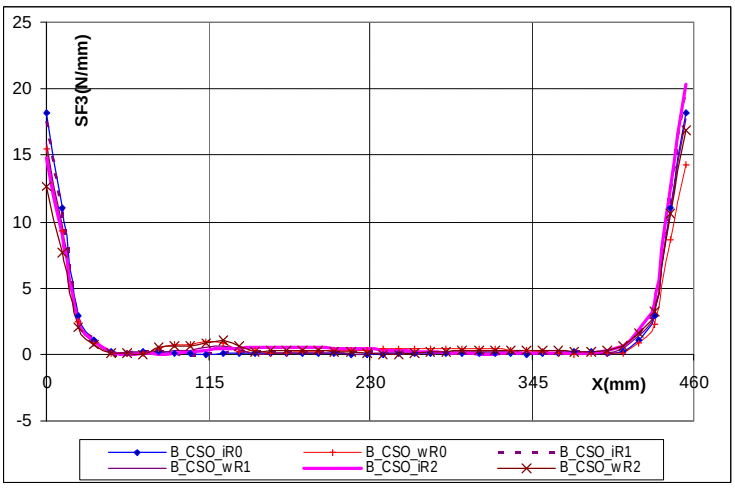

Figure 4.30 T02-06 – SF3 at bottom skin

The data presented in Figure 4.23 to Figure 4.30 and in Table 4.7 showed important information discussed below.

- The tested columns had nearly identical results with small difference in failure loads, in spite of failing in two different modes.
- The graphs show the effect of having a weak core zone and end rotational imperfection. The inclusion of a weak core zone significantly affected the model predictions including the Eigen values.
- End imperfections had limited effect on the column behaviour. The mid-height translational imperfection and the 1 degree rotational imperfection were the closest to the test records.
- The CSO_wR1 analysis results, with weak zone and 1 deg imperfection, was the closest to the test results.
- The shear-crimp failure of T02-06Spc2 was clearly due to having a weak core zone. The Equation 4-10 closely predicted the critical stress and accordingly the column capacity.
- It was difficult to explain the face micro-buckling of T02-06Spc4. in investigating Figure 4.27 to Figure 4.30, the axial forces (SF1) were the main force component in the column faces with transverse (SF2) and shear (SF3) forces developed at the column ends.
- Maximum compression forces (SF1) occurred at the column ends of the top skin and close to the mid-height of the bottom skin. Applying the Tsai-Wu failure criteria resulted in failure index factor (FIF) = 0.74 & 0.83 respectively. The smaller FIF for the top skin (despite having higher SF1) was attributed to the transverse compression forces (SF2) developed at the end due to the support availability.
- Failure load of T02-06Spc4 (92.4kN) was less than that predicted for micro-buckling (142.6kN, Table 4.7). There can be two explanations for that. The first is that the certainty level of predicting the miro-buckling capacity is low with the high scatter in their data[13], Some researchers stated that this

[13] The T02-06Spc6 was the second column to fail in face micro-buckling mode. It had a capacity of 104.4kN.

can be 25% or more (Fleck, 1997). The second explanation is that failure looked like a face micro-buckling, but it was a shear crimp failure instead. Shear crimp could have formed at the weakest core location. In having the weak core zone close to the support location, there was no room (due to the presence of the end blocks) for the crimp to form. This led to the development of a high strain demand on the column cross section leading to failure of the balsa core and debonding of the skins which resulted in the skins failing by micro-buckling.

The analysis results and discussions highlight the difficulties encountered in assessing the behaviour of the balsa columns. The balsa patterns affected the column capacities and failure modes. This suggests the need for further research in this field The FE modelling procedures predicted the behaviour of the columns well and accordingly, can be used as a credible tool in investigating the behaviour of sandwich columns.

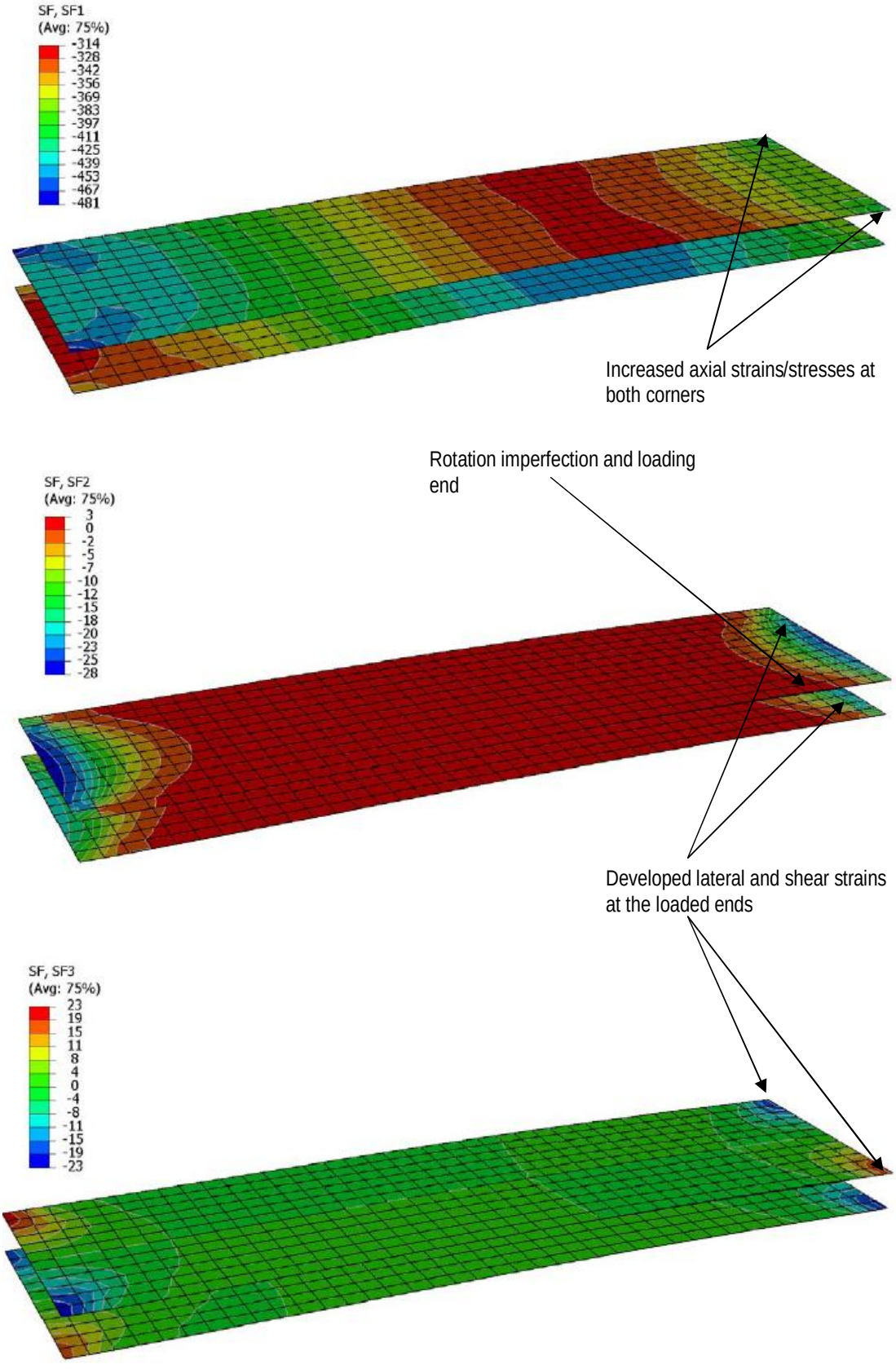

Figure 4.31 T02-06 - Typical section forces - CSO-R1

4.6. BEHAVIOUR OF DD-MPTS WITH DIAGONALS UNDER COMPRESSION (PANEL: P409)

To investigate the behaviour of DD-MPTS with diagonals under compression, a full-size test panel with a height of 1100mm was used.

4.6.1. P409 - PANEL MANUFACTURING

The DD-MPTS panel (P409) dimensions and test layout are shown in Figure 4.32. Similar to P309, SHS50x50x5 pultrusions (www.pacomp.com.au), MU4500 uni-glass and MX6000 db-glass (www.colan.com.au) were used to manufacture the panel. Hyrez 202[14] epoxy was used for the resin system. High-density closed-cell PVC foam, Airex C70.200 from ATL Composites (www.atlcomposites.com), was used for the core.

With the diagonals under compression, transverse tensile stresses were expected. Accordingly, the diagonal skins were laminated with a 90˚ glass layer to improve the skin resistance in the lateral direction (Figure 4.32). The packers were laminated using the same fibre architecture as the gussets [+45/-45/0/90/+45/-45].

Compared with P309, a few modifications were introduced to simplify manufacturing the panel. P409 was manufactured by assembling the first two frames with the first laminate layer in one step. Then after sanding and cleaning, the foam and the last frame, with the last laminate layer, were assembled in a single, second, step. After curing for 24 hours at room temperature, the hard points were glued to the inside of the pultrusions. The panel was post-cured at 80˚C for six hours with one hour ramp.

After cutting the laminates, it was observed that their dimensions were 5mm to 10mm short (Figure 4.33), due to inaccurate cutting measurements. Based on the FE predictions, the skin and glue stresses diminished quickly once getting between the pultrusions. So, it was decided to use the defected laminates and determine if the panel was sensitive to this type of manufacturing defect. This can be assessed if failure occurred in the adhesive layers at the gap locations.

[14] Similar formulation to Hyrez 201 with components sourced from a different company due to cost benefits.

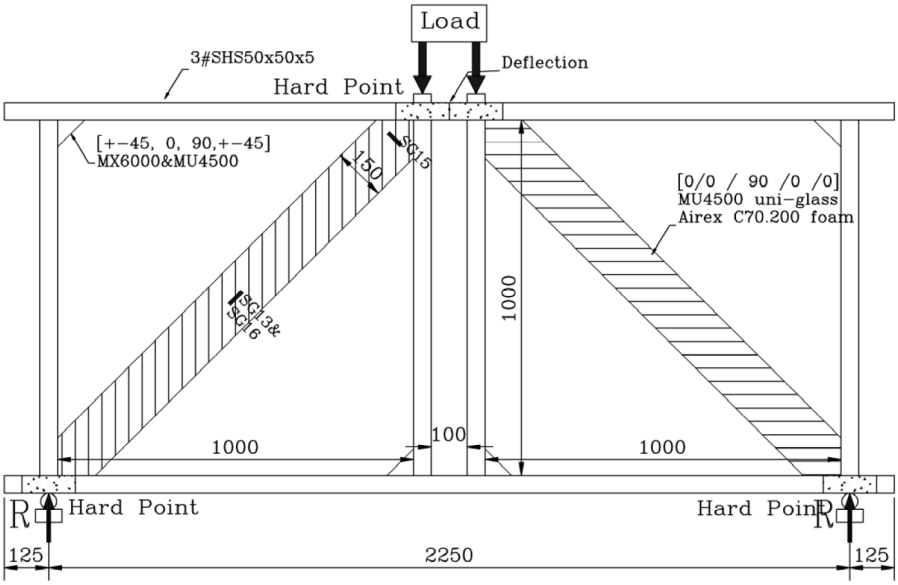

Figure 4.32 P409 - Test layout

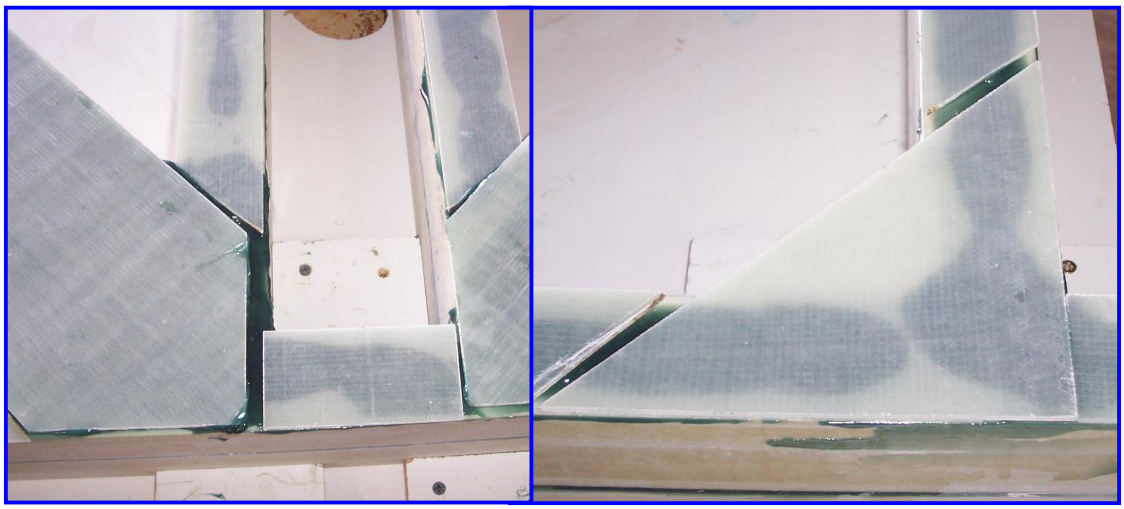

Figure 4.33 P409 – Manufacturing defects

4.6.2. P409 - FE MODELLING

FE modelling procedures were similar to those used in Chapter 3, with the necessary modifications to pick the buckling mode of the panel members. Similar to T02 columns, an initial imperfection was introduced to the model by conducting EV analysis as the first step, with unit load applied at the mid-span loading points. Based on the EV analysis, the Eigen-Vector was used as the new imperfect geometry of the structure with a maximum value of 1mm at the middle of the diagonal (Figure 4.34). Using the imperfect geometry, a Riks analysis was conducted. Analysis convergence criteria were set to the values specified in Sec.3.5.4 (p49).

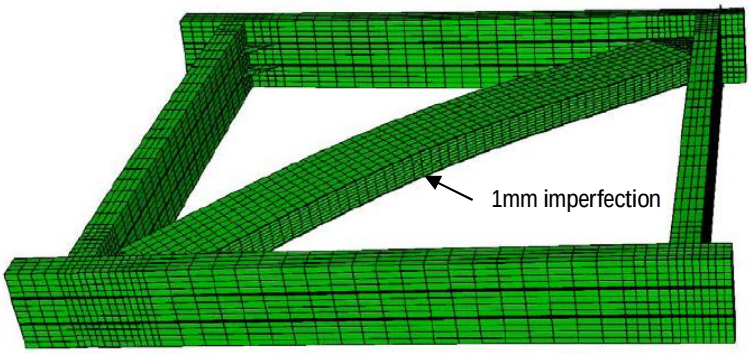

Figure 4.34 P409 – Eigen-Vector as initial imperfection

4.6.3. P409 - TEST OBSERVATIONS & FE RESULTS

P409 was tested in a four point beam mode (Figure 4.32). Loads were applied using an Instron loading ram (model A1340-1006ASP, capacity 600kN) at a displacement-controlled loading rate of 2mm/min. Mid-span load and deflection were recorded using the System 5000 data acquisition system with a recording rate of 0.10s. Failure was expected to occur in the diagonal skins. Accordingly, strain gauges were attached to the mid-length on both skins (SG13 & SG16) and across the diagonal (SG15 was on the same skin as SG13) at a distance of 100mm from the corner (Figure 4.32). As expected, the diagonal failed at the skins at 263.8kN load. Failure initiated at the four corners of the diagonal skins close to the pultrusions (Figure 4.35 and Figure 4.36). On reaching the ultimate capacity, the panel completely lost its strength and stiffness.

The FE model predictions and the test records are shown in Figure 4.37 and Figure 4.38. As shown, the FE model predicted the panel behaviour very well, with a slight over-estimation of the strain levels. Using simple statics (for pin-ended truss), the equivalent diagonal force for the ultimate load is 186.5kN. The predicted buckling capacity for the diagonal is 160.2kN, using Allen's Equation 4-8. The difference can be attributed to two factors. Firstly, Allen's equation has shown to be conservative when predicting the buckling capacity for high modulus cores compared to the FE model predictions (Figure 4.39 is developed for the column T02 layout for a range of core shear modulus, Sec.4.5 p94). Secondly, the diagonal length was based on the diagonal dimension of the panel corners, while it is partly restrained by the joints.

Figure 4.35 P409 - Failure at the lower corner

Figure 4.36 P409 - Failure at the upper corner

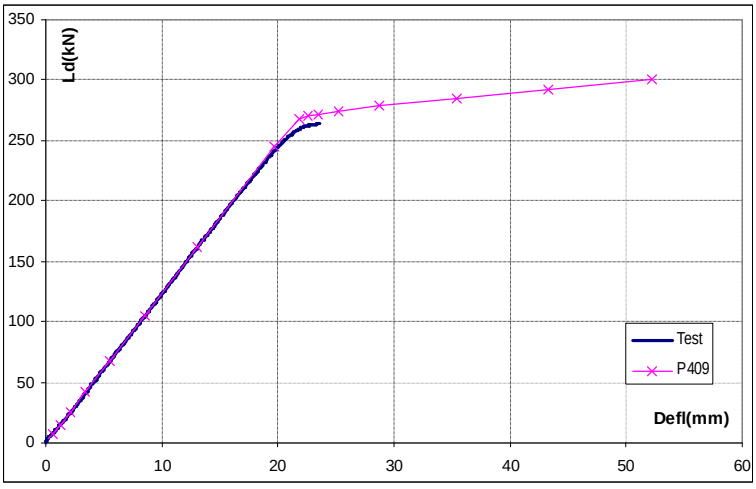

Figure 4.37 P409 - Load-deflection curves

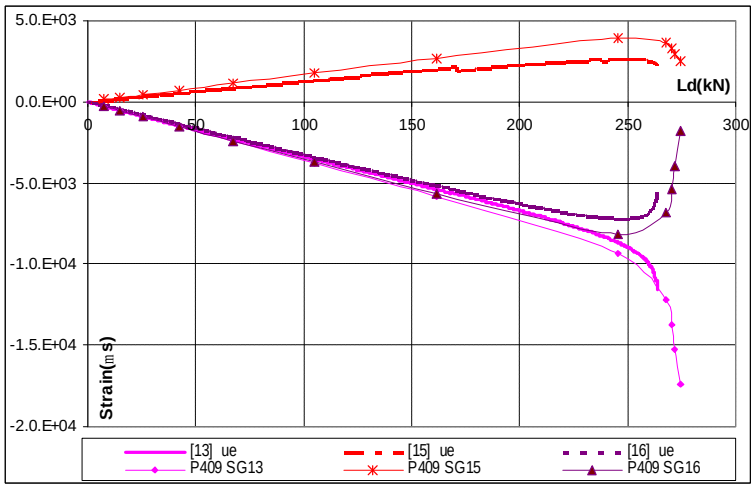

Figure 4.38 P409 - Load-strain curves

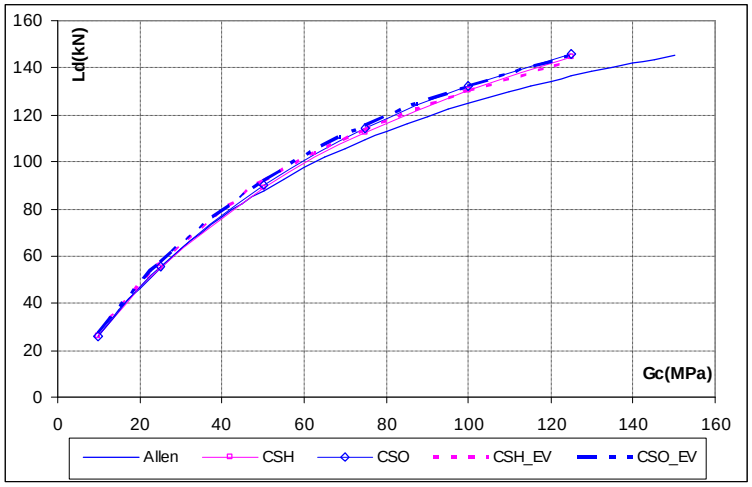

Figure 4.39 Predicting the buckling load of sandwich columns

The FE model predicted an increase in the axial forces (SF1, under compression) by 10% at the lower part of the diagonal at the bottom corner and the upper part of the diagonal at the top corner. This is due to the loading geometry of the panel that initiated an in-plane bending moment in the diagonal. This was accompanied by developing both lateral forces (SF2, under tension) and shear forces (SF3) at these locations, due to the confinement effect (Figure 4.40). This explains why failure occurred at these locations. As observed in the load-deflection and the strain-load curves, the diagonal seemed to buckle at 255kN load. Reaching this point, significant strain increase was observed, in the maximum compression side. Failure initiated at the bottom corner in the main reinforcement. This led to the reduction in the main reinforcement cross-section, and accordingly, increased the stresses on the remaining

part of the diagonal skins. The opposite corner became the most stressed zone, so its fibre ruptured causing further reduction in the cross-section. This collapse continued until reaching complete failure. Loosing one skin, led to shearing of the core material as shown in Figure 4.35. This process took about 70s to reach ultimate failure. This was clearly shown in the load-time graph where the relationship was almost linear, and then the load was sustained for this period of time prior to the final failure (Figure 4.41). This sequence also explains having failure occurring at the top corner (Figure 4.36). According to the FE predictions, the top corner was slightly less stressed, compared to the bottom corner. During the last 70s, the load increased from 255kN to 263kN. This led to the initiation of the failure process at the top corner skin. Reaching ultimate capacity with the release of the loading energy, the top corner failed in exactly the same way as the bottom corner.

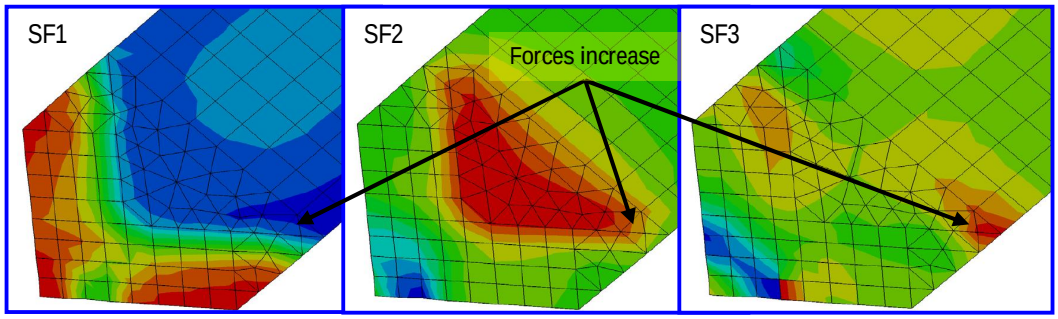

Figure 4.40 Section forces (SF1, SF2 & SF3) at the diagonal bottom corner

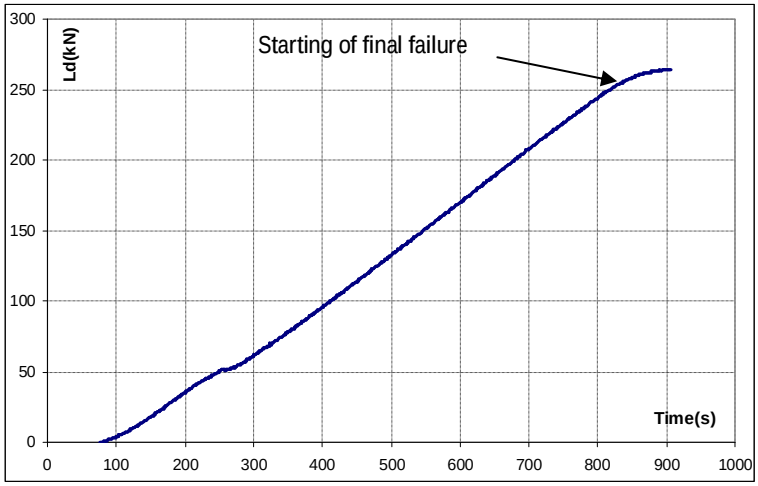

Figure 4.41 P409 - Load-time curve

As discussed in Sec.4.4.2.4 (p95), Tsai-Wu criterion is one of the best failure criteria in predicting failure of composite materials. Based on the FE model predictions, Tsai-Wu criterion was used to assess the failure index factor (FIF) for the element at the bottom corner (Figure 4.42). At the buckling load (255kN), the model predicted the FIF for the 0˚ and 90˚ direction layers to be 1.75 & 0.80

respectively. As observed, the model predicted higher strain levels compared to the test records (Figure 4.38). Correlating the test records to the test results, the approximate FIFs of the corner element were 1.20 and 0.72[15]. The 0˚ direction difference in FIF (between the FE model and the test) was mainly due to the lateral force component (SF2). The FIF factor was found sensitive to this force, as it is compared to the 2-2 tensile strength of the laminae (24MPa). Considering (i) the difficulties in assessing the compression strength of composites under compression, (ii) the approximations in the FE model, (iii) the imperfections in the manufacturing process, and (iv) the limitations of the failure criterion, the predictions of the FE model and the Tsai-Wu criterion can be considered to have predicted very well the final failure mode. They slightly over-estimated the failure index factor (conservatively). Therefore they can be used to conduct reliable analysis for the DD-MPTS. In reaching the final design stage, it is important to verify these predictions by testing.

The manufacturing process of P409 involved (i) cutting and sanding pultrusions, (ii) laminating and cutting skins, gussets and packers, and (iii) assembling by adhesively-bonded joining. In this process, the most probable manufacturing defect arose from cutting the laminates, due to the nature of cutting on angles. Based on P409, it seems that the panel performance was insensitive to this form of manufacturing defect. The continuation of the adhesive layers, along with the filling of these gaps with adhesives, worked well in avoiding failure in the joint. This panel characteristic is quite good in two aspects. The first is that its manufacturing defects are easily identified. The second is that, if the panel was used commercially, some tolerances can be accepted in this respect, which means lower manufacturing costs.

In correlating the load capacity of the panel to the strain level in the diagonal, as a measure of the level of stress at ultimate load, P409 in compression reached 27.6N/microstrain which is very close to that for P309 in tension (Sec. 3.6.2.5 p72).

[15] This was conducted by factoring the FE model section forces predictions by the ratio of the test strains to the FE strains at SG13 & SG15. These forces were then used to calculate the FIFs.

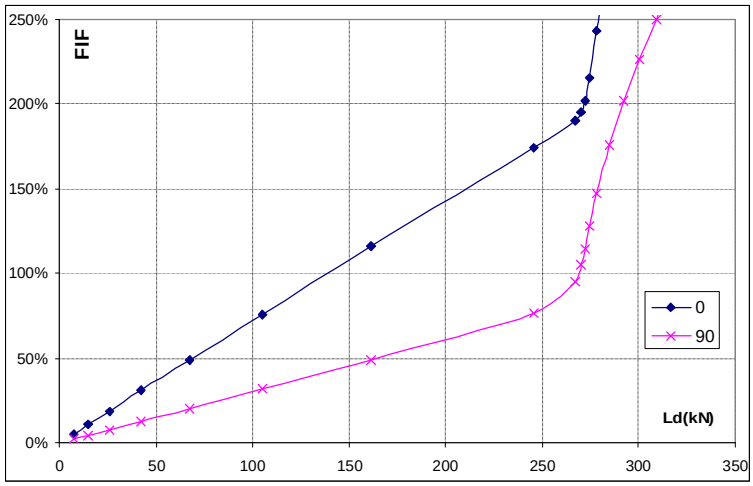

Figure 4.42 Tsai-Wu criterion - Failure index factor at lower corner

4.7. CONCLUSIONS

In this chapter, important behavioural aspects of sandwich columns were discussed. In sandwich columns, the core shear modulus has a major effect on the column capacity. For low-modulus cores (relative to the skin modulus), global failure is the predominant mode. For high-modulus cores, face wrinkling is the predominant mode. In columns, end rotations increase the stresses developed at the skins. However, for small rotations, this effect is not major. Balsa is a complex material to model and it is difficult to predict its properties accurately due to its variations as a natural material (with marginal properties) and the random patterns of its sheets. These variations may not be as important for large surfaces (like in boat industry). However, for small component they can affect the element behaviour.

The FE modelling procedures were successfully implemented to model both the sandwich columns and the panel with diagonals subject to compressive forces. It is important to include an initial imperfection to predict the buckling mode. Both the Solid-Shell and the Shell-Only models performed well in predicting the sandwich column behaviour.

The DD-MPTS panel with diagonals under compression showed good characteristics, carrying high load levels with failure initiated and propagated in the diagonal skins. No failure was observed in the joint area or in the adhesive layers. The panel was insensitive to manufacturing defects, and accordingly can tolerate some variation during manufacture. The only draw-back in this panel system was the

sudden failure that led to losing all the panel stiffness and strength on reaching the ultimate capacity. The panel behaviour was predicted very well by using the FE modelling procedures. The use of Tsia-Wu failure criterion predicted conservatively the final failure of the panel.

4.8. REFERENCES

Allen, H. G. (1969). *Analysis and design of structural sandwich panels*, Pergamon Press, Oxford.

Allen, H. G., and Feng, Z. (1997). Classification of structural sandwich panel behaviour. Mechanics of Sandwich Structures, Proceeding of the EUROMECH 360 Colloquium, A. Vautrin, ed., Kluwer Academic Publishers, Saint-Etienne, France, 1-12.

American Society for Testing and Materials. (2000). ASTM C393 : Standard Test Method for Core Shear Properties of Sandwich Constructions by Beam Flexure.

Anon. (1955). Materials, properties and design criteria Part II, sandwich construction for aircraft. *MIL-HDBK-23*, Department of the Air Force Research and Development, USA.

Argon, A. S. (1972). Fracture of composites. Treatise on Material Science and Technology, Academic Press, New York, 79-114.

ATL Composites Homepage. http://www.atlcomposites.com.au.

Bazant, Z. P. (1971). A correlation study of incremental deformations and stability of continuous bodies. *ASME Journal of Applied Mechanics*, 38, 919-928.

Bazant, Z. P. (2003). Shear buckling of sandwich, fiber composite and lattice columns, bearings, and helical springs: paradox resolved. *ASME Journal of Applied Mechanics*, 70, 75-83.

Bazant, Z. P., and Beghini, A. (2004). Sandwich buckling formulas and applicability of standard computational algorithm for finite strain. *Composites Pt B*, 35, 573-581.

Bazant, Z. P., and Cedolin, L. (1991). *Stability of structures*, Oxford University Press Inc, Oxford.

Bitzer, T. N. (1992). Recent honeycomb core developments. *Second International Conference on Sandwich Construction*, UK, 555-563.

Budiansky, B. (1983). Micromechanics. *Computers and Structures*, 16(1-4), 3-12.

Butalia, T. S., and Wolfe, W. E. (2002). A strain-energy based failure criterion for non-linear analysis of composite laminates subjected to bi-axial loading. *Composites Science and Technology*, 62, 1697-1710.

Colan Homepage. http://www.colan.com.au.

Davies, J. M. (1997). Design criteria for sandwich panels for building construction.

ASME Aerospace Division, Structures and Materials Committee, ASME-AD_Vol 55, New York, 273-284.

Davila, C. G., Camanho, P. P., and Rose, C. A. (2005). Failure criteria for FRP laminates. *Journal of Composite Materials*, 39(4), 323-345.

Diab Homepage. http://www.diabgroup.com.

Dreher, G. (1992). Stability failure of sandwich structures. *Sandwich Constructions 2 - Proceedings of the Second International Conference on Sandwich Construction*, Gainesville, Florida, USA.

Engesser, F. (1891). Die knickfestigkeit gerader stabe. *Zentralblatt des Bauverwaltung*, 11, 483-486.

Euler, L. (1744). De curvis elasticis. Burges, Lausanne, Switzerland.

Export911 Homepage. http://www.export911.com.

Fairbairn, W. (1849). *An account of the construction of the Britannia and Conway tubular bridges*, John Weale, London.

Fleck, N. A. (1997). Compressive failure of fibre composites. *Advances in Applied Mechanics*, 33, 43-117.

Fleck, N. A., and Sridhar, I. (2002). End compression of sandwich columns. *Composites Pt A*, 33, 353-359.

Gdoutos, E. E., Daniel, I. M., and Wang, K.-A. (2003). Compression facing wrinkling of composite sandwich structures. *Mechanics of Materials*, 35, 511-522.

Gere, J. M., and Timoshenko, S. P. (1990). *Mechanics of materials*, PWS-KENT Publishing Company, Boston.

Gotsis, P. K., Chamis, C. C., and Minnetyan, L. (1998). Prediction of composite laminate fracture: micromechanics and progressive fracture. *Composites Science and Technology*, 58, 1137-1149.

Gotsis, P. K., Chamis, C. C., and Minnetyan, L. (2002). Application of progressive fracture analysis for predicting failure envelopes and stress-strain behaviors of composite laminates: a comparison with experimental results. *Composites Science and Technology*, 62, 1545-1559.

Haringx, J. A. (1948). On highly compressible helical springs and rubber rods and their application for vibration-free mounting. *Philips Research Report Vol.3*, Eindhoven.

Hibbitt, Karlsson & Sorensen Inc. (2004a). *ABAQUS Analysis user's manual*.

Hibbitt, Karlsson & Sorensen Inc. (2004b). *ABAQUS Theory manual*.

Hinton, M. J., Kaddour, A. S., and Soden, P. D. (2002a). Evaluation of failure prediction in composite laminates: background to part 'B' of the exercise. *Composites Science and Technology*, 62, 1481-1488.

Hinton, M. J., Kaddour, A. S., and Soden, P. D. (2002b). A comparison of the predictive capabilities of current failure theories for composite laminates judged against experimental evidence. *Composites Science and Technology*, 62, 1725-1797.

Hinton, M. J., and Soden, P. D. (1998). Predicting failure in composite laminates: the background to the exercise. *Composites Science and Technology*, 58, 1001-1010.

Hoff, N. J., and Mautber, S. E. (1945). The buckling of sandwich type panels. *Journal of Aeronautical Sciences*, 12(3), 285-297.

Huang, H., and Kardomateas, G. A. (2002). Buckling and initial postbuckling behavior of sandwich beams including transverse shear. *AIAA Journal*, 40(11), 2331-2335.

Humphreys, M. F., Van Erp, G. M., and Tranberg, C. (1999). The structural behaviour of monocoque fibre composite truss joints. *Advanced Composite Letters*, 8(4), 173-180.

Huntsman home page. http://www.huntsman.ivt.com.au.

Karbhari , V. (1997). Application of composite materials to the renewal of twenty-first century infrastructure. *Eleventh International Conference on Composite Materials*, Gold Coast, Australia.

Kardomateas, G. A., and Simitses, G. J. (2004). Comparative studies on the buckling of isotropic, orthotropic and sandwich columns. *Mechanics of Advanced Materials and Structures*, 11, 309-327.

Kuraishi, A., Tsai, S. W., and Liu, K. K. S. (2002). A progressive quadratic failure criterion - part B. *Composites Science and Technology*, 62, 1683-1695.

Librescu, L., and Hause, T. (2000). Recent developments in the modeling and behavior of advanced sandwich constructions: a survey. *Composite Structures*, 48, 1-17.

Liu, K. S., and Tsai, S. W. (1998). A progressive quadratic failure criterion for a laminate. *Composites Science and Technology*, 58, 1023-1032.

Mamalis, A. G., Manolakos, D. E., Ioannidis, M. B., and Papapostolou, D. P. (2005). On the crushing response of composite sandwich panels subjected to edgewise compression: experimental. *Composite Structures*, 71, 246-257.

Marguerre, K. (1944). The optimum buckling load of a flexibly supported plate composed of two sheets joined by a light weight filler, when under longitudinal compression. *ZWB UM 1360/2*, Deutsche Vierteljahrsschrist für Literalurwissenschaft und Giests Geschichte, D V L.

Pacific Composites Homepage. http://http://www.pacomp.com.au/.

Piggott, M. R. (1981). A theoretical framework for the compressive failure of aligned fibre composites. *Journal of Material Science*, 16, 2837-2845.

Piggott, M. R., and Harris, B. (1980). Compression strength of carbon, glass and Kevlar-49 fibre reinforced polyester resins. *Journal of Material Science*, 15, 2523-2538.

Plantema, J. F. (1966). *Sandwich construction*, Wiley, New York.

Puck, A., and Schurmann, H. (1998). Failure analysis of FRP laminates by means of physically based phenomenological models. *Composites Science and Technology*, 58, 1045-1067.

Puck, A., and Schurmann, H. (2002). Failure analysis of FRP laminates by means of physically based phenomenological models. *Composites Science and Technology*, 62, 1633-1662.

Rheinfrank, G. B., and Norman, W. A. (1944). Molded glass fiber sandwich fuselage for BT-15 airplane. Army Air Corps Technical Report No 5159, USA.

Robert Scherer Homepage. http://www.bobscherer.com.

Soden, P. D., Hinton, M. J., and Kaddour, A. S. (1998). Comparison of the predictive capabilities of current failure theories for composite laminates. *Composites Science and Technology*, 58, 1225-1254.

Sun, C. T., and Tao, J. (1998). The prediction of failure envelopes and stress-strain behavior of composite laminates. *Composites Science and Technology*, 58, 1125-1136.

Sun, C. T., Tao, J., and Kaddour, A. S. (2002). The prediction of failure envelopes and stress-strain behavior of composite laminates: comparison with experimental results. *Composites Science and Technology*, 62, 1673-1682.

Vinson, J. R. (1999). *The behavior of sandwich structures of isotropic and composite materials*, Technomic Publishing Company, Lancaster, Pennsylvania.

Vonach, W. K., and Rammerstorfer, F. (2000). The effect of in-plane core stiffness on the wrinkling behaviour of thick sandwiches. *Acta Metallurgica*, 141, 1-10.

Wikipedia home page. http://en.wikipedia.org/wiki/Beechcraft_Starship.

Wolfe, W. E., and Butalia, T. S. (1998). A strain-energy based failure criterion for non-linear analysis of composite laminates subjected to bi-axial loading. *Composites Science and Technology*, 58, 1107-1124.

Zinoviev, P. A., Grigoriev, S. V., Lebedeva, O. V., and Tairova, L. P. (1998). The strength of multilayered composites under a plane stress state. *Composites Science and Technology*, 58, 1209-1223.

Zinoviev, P. A., Lebedeva, O. V., and Tairova, L. P. (2002). A coupled analysis of experimental and theoritical results of numerical predictions and experimental observations for symmetric composite laminates. *Composites Science and Technology*, 62, 1711-1723.

Chapter 5 Notations

SF1	Longitudinal section forces (in 1-1 direction, N/mm)
SF2	Transverse section forces (in 2-2 direction, N/mm)
U3	Out-of-plane displacement (mm)
Nt1	Integrated sectional axial forces (SF1) on the shell element (kN)
SM1	Section bending moments in 1-1 direction (Nmm/mm)
SM2	Section bending moments in 2-2 direction (Nmm/mm)
SF3	Shear section forces (in the 1-2 plane, N/mm)

5. Behaviour of Diaphragm, Multi-Pultrusion Truss Systems (DI-MPTS)

5.1. GENERAL

Traditionally trusses are formed from discrete members. Truss systems presented in Chapter 2 and the DD-MPTS panel presented in Chapters 3 and 4 followed this tradition. As presented, the DD-MPTS proved to be an efficient structural form where the truss carried high load-levels, the joints were protected, and the truss was easy to manufacture. When the truss diagonals were loaded under tension, the system offered load redundancy, with partial strength and stiffness reserved, after reaching the ultimate capacity, Chapter 3. However being under compression, the diagonal failed in the sudden brittle mode, leading to immediate loss of the member capacity, Chapter 4. The failure mode was predicted well using FE modelling procedures.

Composites provide opportunities that are difficult to find in other construction materials. This is attributed to their characteristics that include light weight and free formability. As the failure originated and propagated in the diagonal skins, it was thought that in changing the diagonal system, the capabilities of the MPTS could be increased; more specifically, increasing the load-carrying capacity and allowing redundancy, after reaching ultimate capacity. This led to the idea of changing the bracing system from the traditional discrete-diagonal (DD) to diaphragm-type (DI) system.

In this chapter, the behaviour of a diaphragm-type MPTS (DI-MPTS) is presented. Consistent with previous procedures, the concept was tested on a small-scale panel. When tested in the cantilever mode, the panel failed prematurely due to a localised clamping effect. The investigations continued by testing another prototype

panel in beam-mode. The panel performed well but suffered from excessive lateral buckling of the skins that was believed to affect the panel capacity. The concept was improved by using low-density foam to provide sandwich construction in the form of cross-bracing. The concept was then extended by using complete sandwich construction for the diaphragm, and the behaviour of each of these panel systems was investigated using FE modelling procedures. The chapter ends with a comparison of the attributes of each system investigated in Chapters 3, 4 and 5.

5.2. DEVELOPMENT OF THE DIAPHRAGM, MULTI-PULTRUSION TRUSS SYSTEM (PANEL: P509)

The concept of DI-MPTS was developed over a few stages. The first panel to be investigated with a diaphragm-type bracing system was P509. knowing that the verticals carried less load than the chords, the P509 was manufactured with single verticals and two skins inserted between the chord multi-pultrusions in an attempt to reduce the anticipated weight of the panel (Figure 5.1). To reduce the costs, P509 was tested as a single panel in cantilever mode. Prior to testing the panel, the following points were noted:

- The laminated webs act as a tension-only diaphragm. With the continuous diaphragm, stress concentrations in the skins and in the adhesive layers should be significantly reduced.
- The diaphragm webs are expected to provide significant redundancy in the case of tensile failure in the diaphragm fibres.
- As with the DD-MPTS, the joint area is protected and the panel is simple to manufacture.

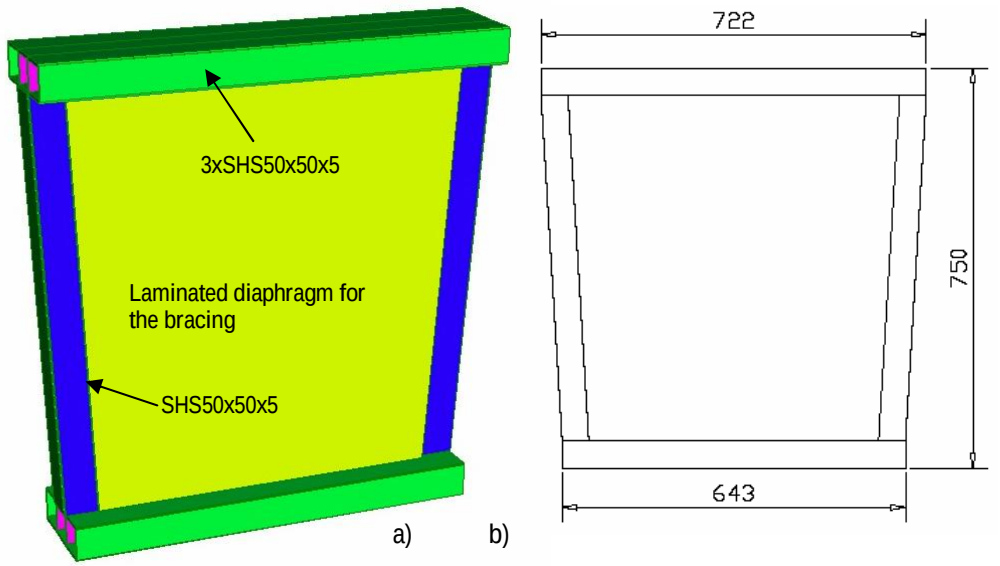

Figure 5.1 P509 – Panel (a) General concept and (b) dimensions

5.2.1. P509 - MATERIALS USED

P509 was manufactured with two main components, the pultrusions and the laminated web. Glass/polyester pultrusions, SHS50x50x5 from Pacific Composites (www.pacomp.com.au), were used to manufacture the panel frames. The panel web was laminated by using hand lay-up of two plies of glass double bias (db) MX6000 (600gsm) $[+45/-45]_s$, from Colan (www.colan.com.au), and Hyrez 201 epoxy (Rogers, 2004). Frames and web laminates were assembled using adhesive bonding at the interface. ATL Composites (www.atlcomposites.com), HPR26 thixotropic toughened epoxy adhesive with HPR26 hardener was used with 100:50 mixing ratio, by weight, of adhesive to hardener.

5.2.2. P509 – PANEL MANUFACTURING

The manufacturing of P509 commenced with cutting the pultrusions to length followed by sanding and cleaning. Hand lay-up was used to laminate the skins with peel plies on both faces. After curing the laminates for 24 hours, they were cut to dimensions. Assembly started from the middle frame, where the verticals were glued to the chords on a special jig. After curing for 24 hours at ambient temperature, the excess glue was sanded and cleaned. The peel plies were peeled off the laminate faces. Frames were glued and clamped on the central one from one side to another on a special jig, with the skin laminates in-between (Figure 5.2). The assembly was left to cure for 24 hours at ambient temperature. Excess glue was sanded using an air sander. The panel was post-cured at 60ºC and 100ºC for four hours with one-hour ramp.

Figure 5.2 P509 – Panel during assembly

5.2.3. P509 - TEST RESULTS AND EVALUATION

P509 was tested in a cantilever mode. It was placed between two brackets attached to a steel loading frame (Figure 5.3). Loads were applied using a manually-operated hydraulic jack of 300kN capacity. Due to the horizontal component of the load, the panel was laterally clamped to the testing frame. Both the load and deflections were recorded at the cantilever end of the panel.

Figure 5.3 P509 - Test layout

The load-deflection curve (Figure 5.4) suggested that at load level of 16.6kN, significant reduction in stiffness occurred. This was attributed to the buckling of the web (Figure 5.5). With further load application, the panel continuously lost stiffness, yet to a lesser extent, when compared with pre-buckling/post-buckling change. This is shown by the slopes of the straight line segments of the fitted curve (Figure 5.4).

In reaching the ultimate load (62kN), the panel failed in a sudden brittle mode with complete loss of its strength. This was not consistent with the expectation of having load redundancy. Two failure zones were noticed at the location of the bottom clamp (Figure 5.6). One was interlaminar shear in the web laminate and the other was in the adhesive layer. The location and nature of the failures indicated that they were due to the localised effect of the clamping technique. The geometry of the failure (Figure 5.6) suggested that all horizontal force components (equal to the applied forces) were applied at the bottom clamp location. Clamping was applied to the outer frames causing the clamping forces to be transferred to the loading frame through the outer two adhesive layers, which were the first parts to fail. With the failure in the outer adhesive layers, the middle pultrusion and the laminate started to move relative to the clamped outer pultrusions. This generated high shear stresses in the laminate and accordingly led to complete failure of the web by inter-laminar shear.

During the test, it was observed that the web buckled un-symmetrically relative to the diagonal centreline (Figure 5.5), and that the buckle had shifted towards the vertical member. As there was only one vertical pultrusion at each vertical member, peel stresses between the web laminate and the vertical pultrusion could be another potential problem affecting the behaviour of DI-MPTS. Consequently, the panel design was modified to include three pultrusions per vertical thereby reducing the possibility of failure due to premature peel of the web skins from the vertical. The consequential increase in panel weight was noted for future consideration. The modified panel (P609) was tested in a beam mode with no clamps (similar to P309) to overcome the problems experienced while testing P509.

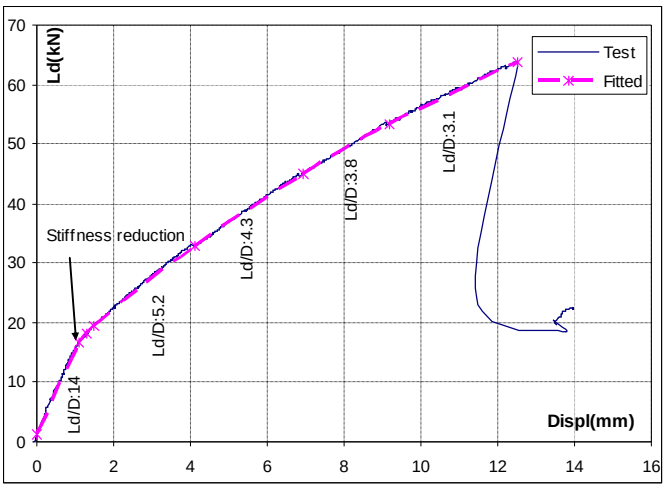

Figure 5.4 P509 – Load-displacement curves

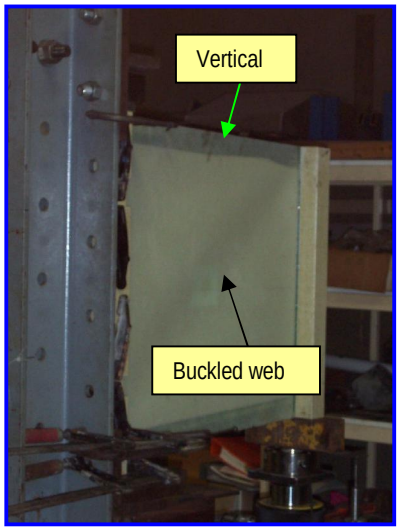

Figure 5.5 P509 - Web buckling during test

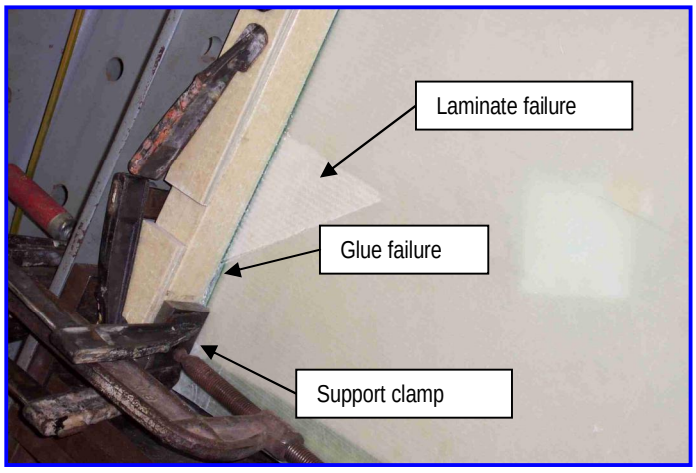

Figure 5.6 P509 - Failure modes

5.3. DEVELOPMENT OF AN UPDATED DIAPHRAGM, MULTI-PULTRUSION TRUSS SYSTEM (PANEL: P609)

The P609 panel was an updated version of P509, modified to include three pultrusions at each vertical. In this section, the behaviour and test results of P609 are presented and discussed.

5.3.1. P609 - TEST SET-UP

The dimesnions of the P609 panel and test set-up are shown in Figure 5.7. The manufacturing procedures were similar to that of the discrete-diagonal panel (P309), Sec.3.4 (p41). The panel skins were laminated using a similar architecture as the diaphragm panel (P509). P609 was tested in a beam-mode with loads applied at mid-span. A servo-controlled testing machine with Instron loading ram of 600kN capacity (type: A1340-1006ASP) was used with the displacement-controlled loads applied at

a rate of 0.75mm/min. Loads were recorded by 444kN loading cell. Mid-span deflections were recorded by LVDT. Standard 120Ohm strain gauges (Kyowa) were distributed around the panel as shown in Figure 5.11. The loading cell, the LVDT and the strain gauges were connected to two MTS System-5000 data acquisition systems which were connected to a standard PC. Data were collected at 0.10s intervals.

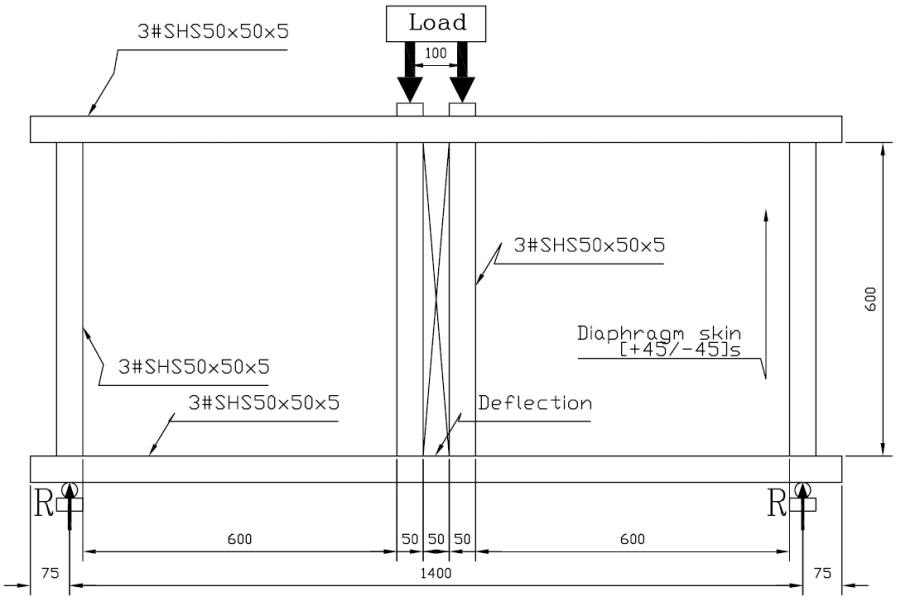

Figure 5.7 P609 – Dimensions and test layout

5.3.2. P609 FE MODELLING

Based on the experience of modelling the discrete-diagonal panel (P309), Sec.3.5 (p44), S4 shell elements were used to model P609 pultrusions and laminates. A similar approach was used to model the interactions within each frame and between the frames and the adjacent adhesive layers. As it had two separate skins with no core one quarter of the panel was modelled assuming symmetry about the 1 and 3 axis (Figure 5.8). Material properties for the different components are presented in Table 3.2 to Table 3.5 (Sec.3.3.2, p37-38).

Three analysis models were used for P609 with different in analysis procedures. In the first model (13-01), displacement loads were directly applied in a single loading step, using the geometrical non-linear option.

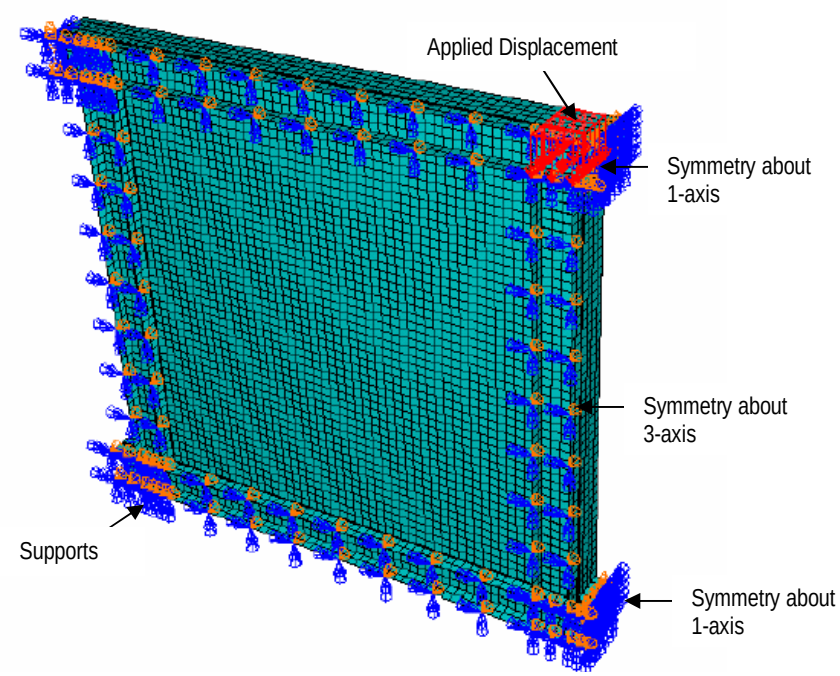

Figure 5.8 P609 - FE Model layout

In the second model (13-03), analysis was conducted in two stages. In the first stage (run) an Eigen-Value (EV) analysis was conducted to obtain the shape of the buckling mode (Figure 5.9). The nodal configuration of the first EV mode shape was then used as an initial imperfection in the second stage analysis, Riks (arc-length) non-linear analysis. An initial imperfection factor of 0.10 was applied to the imperfect nodal coordinates, assuming an initial arc length of 5%.

The third model (13-04) was a non-linear analysis with displacement loads applied in two loading steps. In the first step, an initial horizontal displacement, 0.10mm, was applied to the central point of the web (Figure 5.10), to initiate the imperfect geometry. This displacement was then disabled in the second loading step, where the loading displacement was introduced.

In all models, a fine mesh was found necessary to determine the right buckling mode. Accordingly, an element size of 12.5mm was used for all parts of the model with an aspect ratio equalled one. Convergence criteria similar to P309, Sec.3.5.4 (p49), were applied to the FE models.

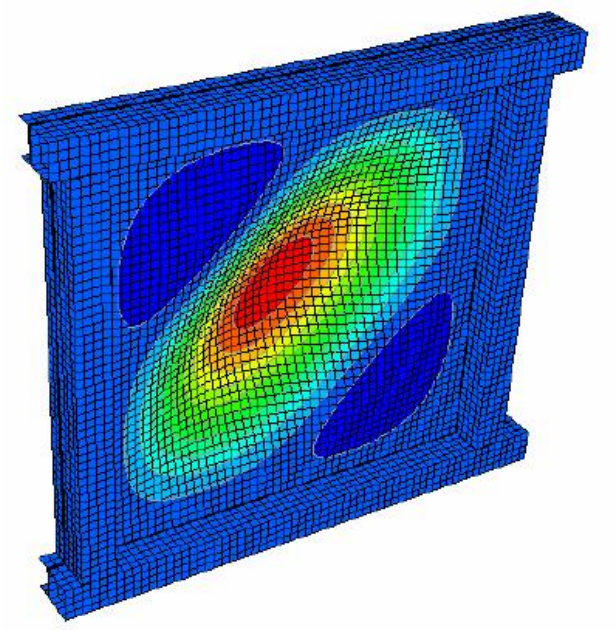

Figure 5.9 First mode shape using EV analysis for 13-03 run

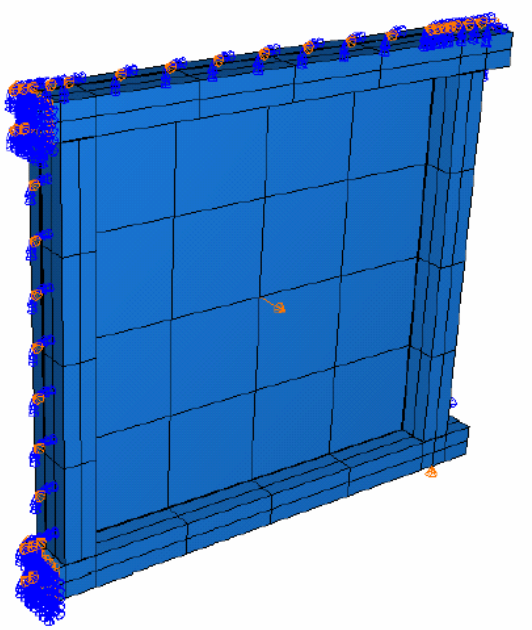

Figure 5.10 Imperfection displacement for 13-04 run

5.3.3. P609 TEST AND FE RESULTS

Both the test records and the FE model results are presented in this section. Based on this data, the main behavioural issues of P609 and recommendations in modelling it are discussed in Sec.5.3.4.2. Mid-span load-displacement (Ld-Displ) curves are shown in Figure 5.12. Strain-deflection curves are shown in Figure 5.13 to Figure 5.15. Strain gauge (SG) locations are shown in Figure 5.11. Graph legends show the FE model number. The CPU analysis time and parameters are shown in Table 5.1.

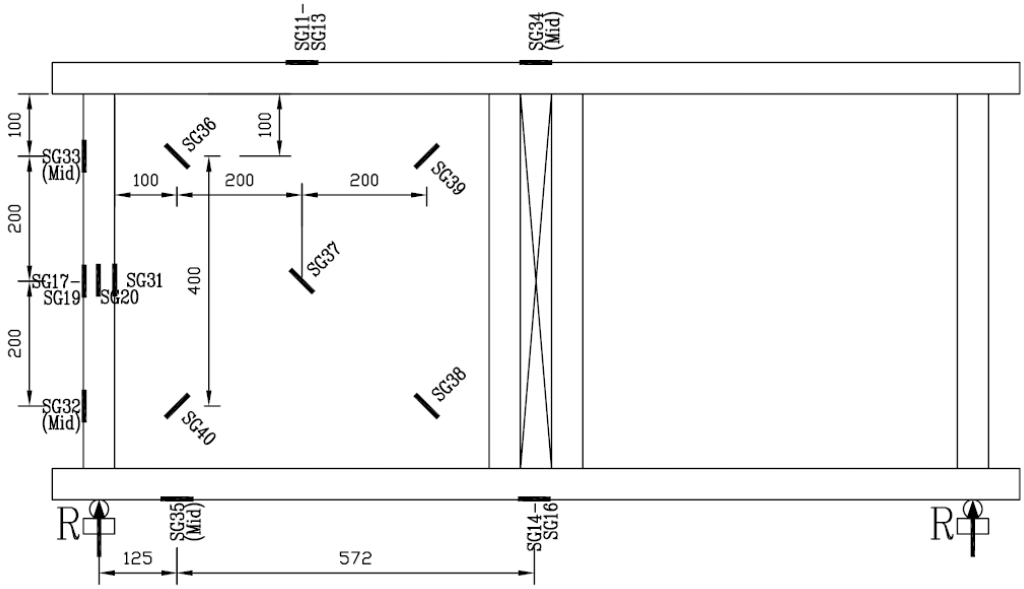

Figure 5.11 P609 - Strain gauge locations

Note: SG14-SG16: strain gauges 14, 15 & 16 at the same elevation on pultrusion 1, 2 & 3 respectively

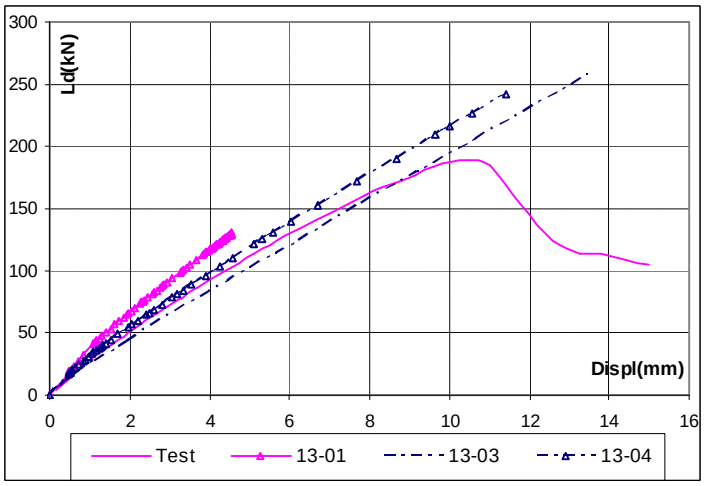

Figure 5.12 P609 - Load-displacement curves

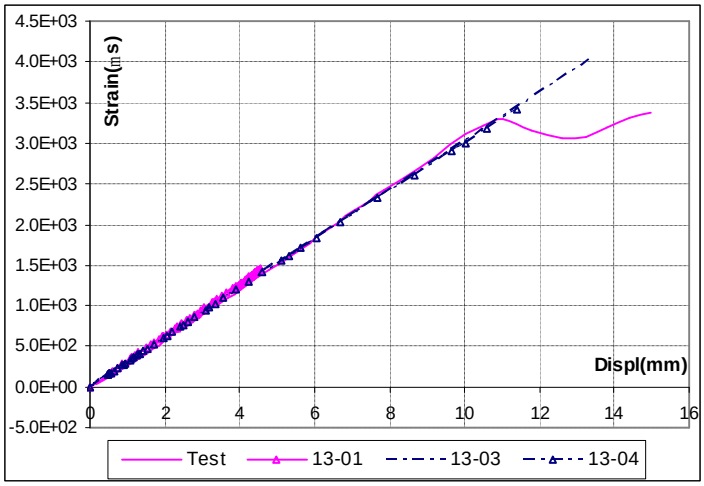

Figure 5.13 P609 - SG15 Strain-displacement curves

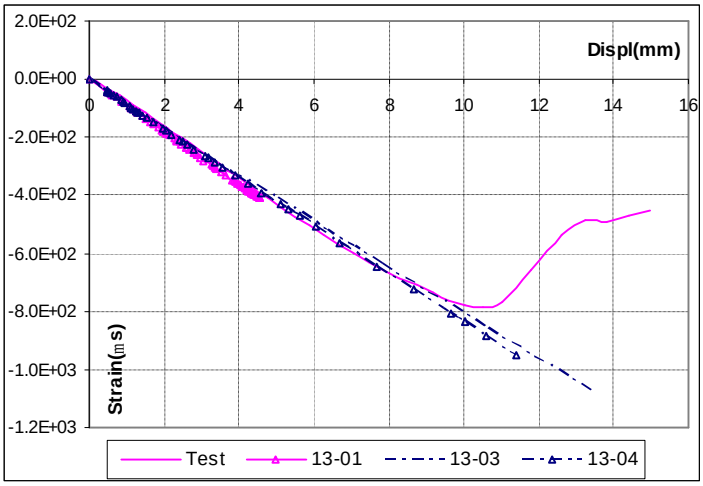

Figure 5.14 P609 - SG20 Strain-displacement curves

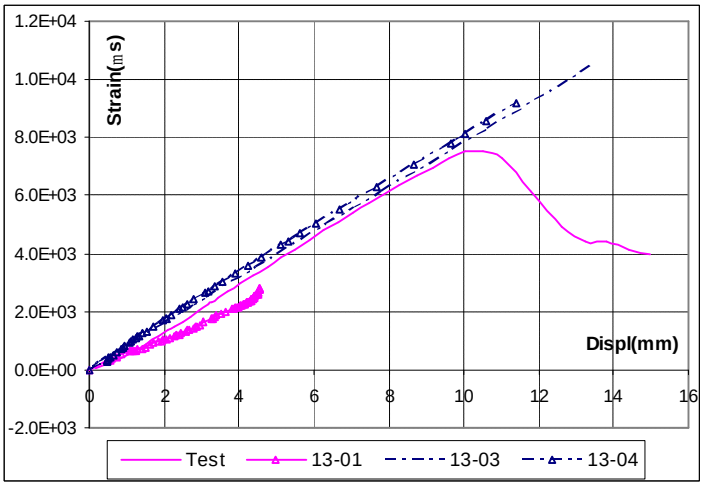

Figure 5.15 P609 - SG37 Strain-displacement curves

Table 5.1 P609 - FE analyses parameters

Analysis Type	Analysis Run	Imperfection (mm)	Imperfection/Thk ratio	Analysis Time(s)
NL	13-04	0.1	6%	6639
	13-04a	2.0	125%	1198
	13-04b	1.5	94%	1545
	13-04c	1.0	63%	1816
	13-04d	0.5	31%	5164
Riks	13-03		10%	5882
	13-03a		100%	2882

5.3.4. P609 - EXPERIMENTAL OBSERVATIONS AND FE MODEL VERIFICATIONS

In this section, the test observations and the FE models performance are presented. The best representative FE model and test observations are used to explain the panel behaviour in the next section.

5.3.4.1. Test Observations

Unlike P509, the panel stiffness did not significantly reduce due to web buckling (Figure 5.16). The buckling amplitudes continued to increase with the increase of applied displacement. Like the other tested MPTS, failure initiated and propagated in the diaphragm laminates. No failure was observed in the adhesive layers. The ultimate capacity of P609 was 189kN, at 10.4mm displacement. This compared to 303kN for P309 (with diagonal under tension) and 263kN for P409 (with diagonal under compression). However, after reaching the ultimate capacity, failure[1] started to propagate parallel to the vertical and the top chord (Figure 5.17) and the panel reduced in stiffness and load-carrying capacity.

The important aspect of the panel was it did not fail suddenly. Reaching the ultimate capacity, the panel retained this level of forces for 42s (at 11.1mm displacement) where strength gradually decreased to 112kN in 84s (at 13.0mm displacement). With continued applied load, it followed this stepped-pattern failure until the test was terminated at 22.9mm displacement (Span/62). The test was terminated due to excessive damage in the panel and the high displacement it reached. There was no final failure load, until reaching this displacement, as the panel still carried a load of 55.4kN. In releasing the applied loads, the panel recovered most of its displacement, in spite of the extensive damage.

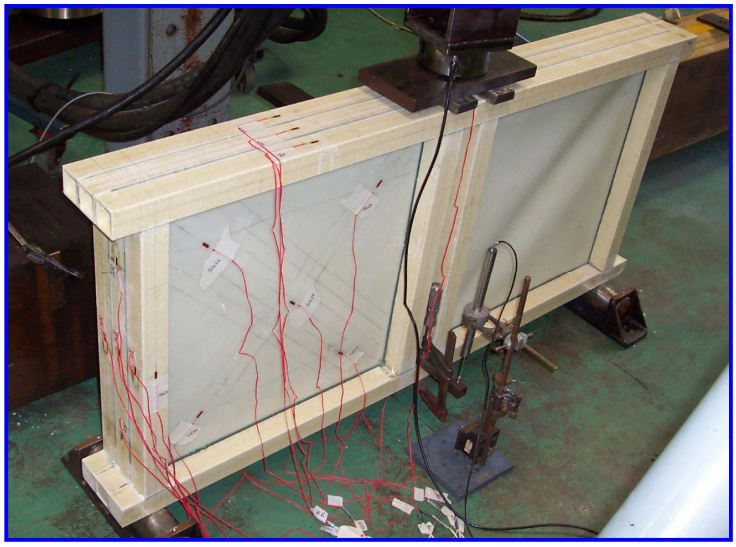

Figure 5.16 P609 – Web bucling mode

[1] Originated at the top corner of the panel.

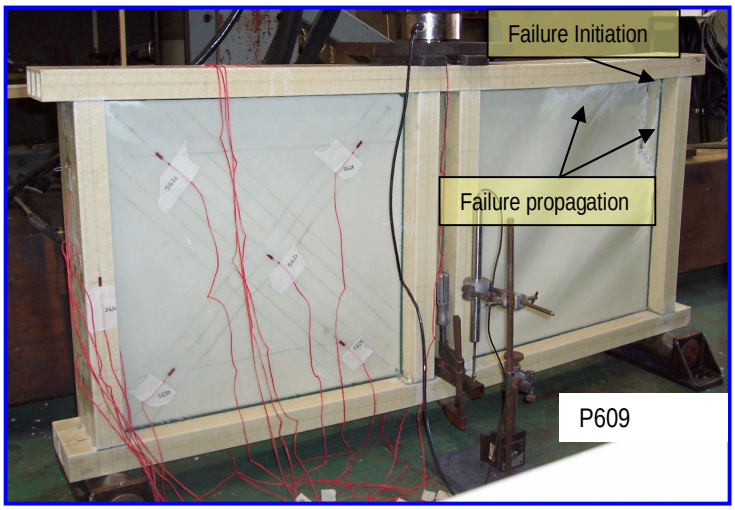

Figure 5.17 P609 – Failure mode

5.3.4.2. Performance of the FE Models

The FE models were verified with the test records by comparing the load (Ld), the displacement (Displ) and the strain gauge readings. The 13-01 analysis model was the only one that had numerical difficulty, and accordingly was terminated prior to reaching the applied displacement (Figure 5.18). Other model solutions finished well, with a warning message of negative Eigen-Values. This was because the web had equal probability to buckle on either side. In studying the different figures (Figure 5.12 to Figure 5.15), the following can be noted:

- Models with initial imperfections matched the tested panel results quite well with the best representation by the Riks analysis model (13-03).
- The 13-04 model showed similar strain results to the Riks model (13-03), however, with slightly higher stiffness (Figure 5.12). It reached higher loads for the same displacement. In comparing the slope of the load-displacement curves (Figure 5.19), it was noticed that the difference between the two models became small in reaching 4mm deflection. This indicated that the 13-04 model was stiffer than 13-03 model until establishing its buckling mode, where both models behaved similarly.
- In conducting further analysis, by changing the degree of imperfection, it was found that Riks analysis predictions were very similar; however, increasing the imperfection reduced the analysis costs significantly (Table 5.1).

- Increasing the level of initial imperfection benefited the two-stage non-linear models in two aspects. Firstly, it improved the accuracy of the non-linear analysis. Secondly, there was a reduction in the analysis time (Table 5.1).
- The non-linear models, with initial imperfections (ip) exceeded half the web thickness (t) showed very similar predictions to the Riks analysis (Figure 5.20), at lesser analysis costs, (Table 5.1).

In conclusion, the two-stage geometrical non-linear analysis provided an accurate representation of the buckling behaviour of the panel, with less computational time than the Riks analysis. As a rule of thumb, initial imperfection should, at least, equal the web thickness.

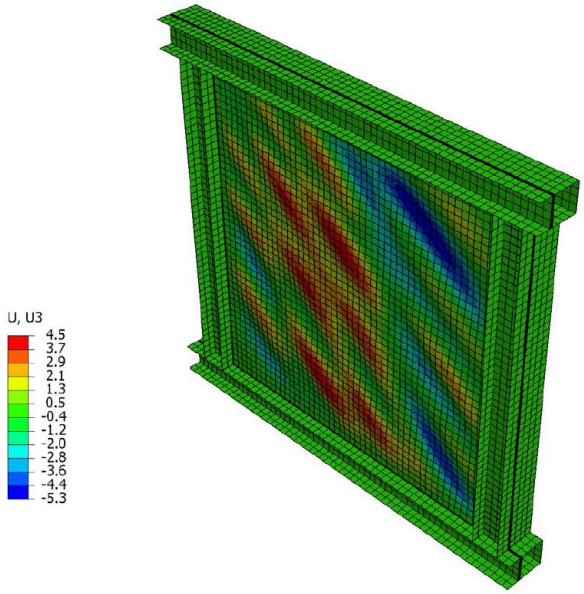

Figure 5.18 P609 - Analysis 13-01 lateral displacement

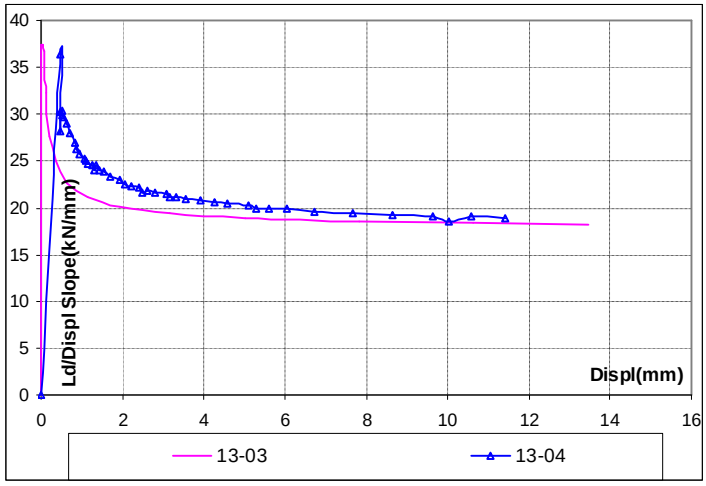

Figure 5.19 P609 - Slope of load-displacement curves for FE Analyses

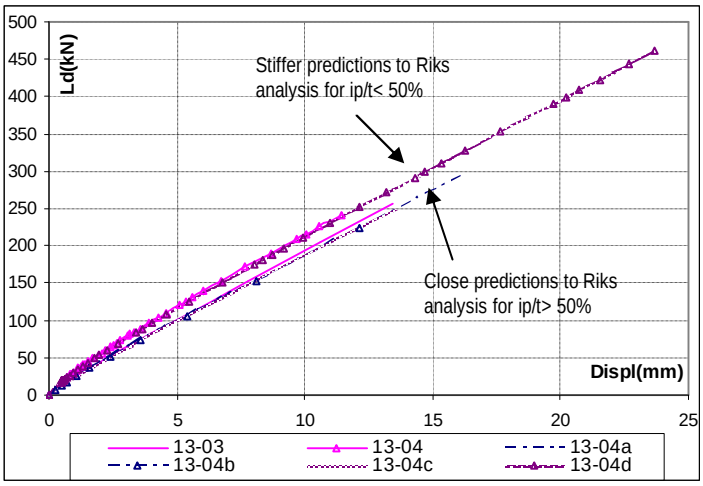

Figure 5.20 P609 – Initial imperfection effect on load-displacement curves

5.3.5. P609 - BEHAVIOUR

Panels P609 and P309 were based on the concept of multi-pultruded members with a different bracing systems. Accordingly, it was expected that both panels would have common behavioural issues except for the bracing system. In this section the main behavioural differences between P609 and P309 are discussed. The (13-03) Riks model was used as a representative model of P609. The data graphs were for the analysis increment closest to the ultimate load[2]. The behaviour of each of the panel components is discussed in a separate sub-section. This section concludes with details of the general behaviour of P609.

5.3.5.1. P609 – Behaviour of the Diaphragms

To aid the behavioural investigations, two section paths (L_Dia and X_Dia, Figure 5.21) were aligned with the principal axes of the diaphragm-laminate. Out-of-plan deflections (U3) and section forces, for the L_Dia, are shown in Figure 5.22, and Figure 5.24 to Figure 5.25. For X_Dia, out-of-plan deflections and section forces are shown in Figure 5.23, and Figure 5.26 to Figure 5.28. The X-axis of the graphs is the percentage of the distance along-the-path (from the origin of the diaphragm to the element location) to the total path length.

The main behavioural issues of the diaphragm can be summarised as follows:

[2] Inc 83 in 13-01 = 130kN, Inc 20 in 13-03 = 205.8kN, Inc 42 in 13-04 = 209.24kN and Inc 8 in 13-04a = 201.17kN.

- The diaphragm webs were subjected to double curvature with values increased at corners (Figure 5.22).
- The buckled shape of the web was symmetric about the web origin (Figure 5.23).
- Unlike the discrete-diagonal panel (Sec. 3.6.2.1, p57), SF1 increased gradually reaching the ends of the diaphragm (Figure 5.24). This increase can be attributed to the continuous web. The L_Dia fibres, under tension, terminated at different lengths. Fibres that terminated at the vertical and chord members transfer their forces to the connected members and, through the web, to adjacent longer fibres that have not terminated yet. This led to the development of shear forces towards the corners (Figure 5.29).
- Longitudinal forces (SF1) increase at corners was accompanied by sharp increase in the transverse forces (SF2, Figure 5.25). Maximum forces were found in the upper corner where cracks initiated during the test.
- Along the X_Dia path, longitudinal forces (SF1) increased in a linear form, from the corners of the web towards its origin (Figure 5.26).
- Integrating SF1 forces, by assuming that they were accumulated from the origin towards corners, Figure 5.28 showed that 80% of the diagonal forces were transferred within the middle 42% of the web dimension.
- The diaphragm acted in a tension-only mode with very small transverse compressive forces (~5N/mm, Figure 5.27).

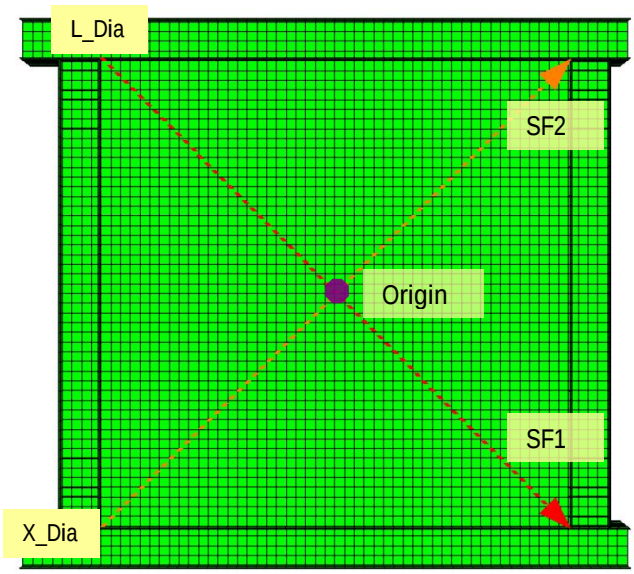

Figure 5.21 P609 - Skin paths and local axes

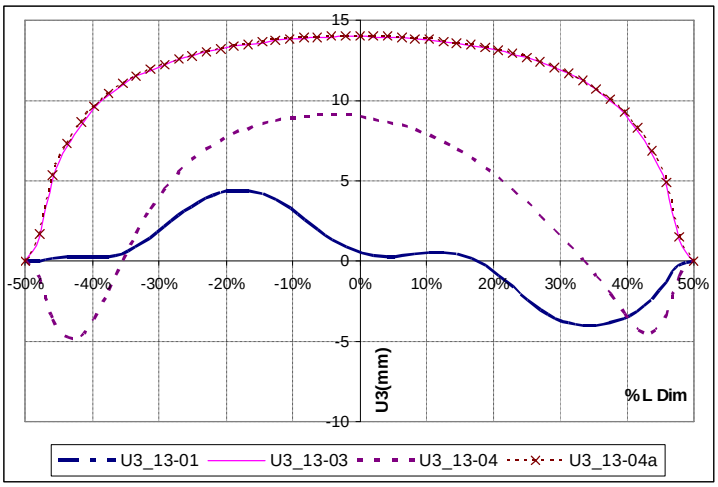

Figure 5.22 P609 - L_Dia out-of-plane displacement

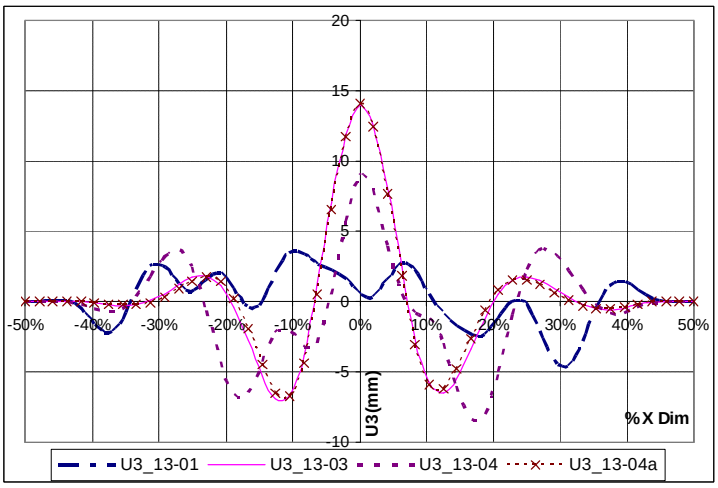

Figure 5.23 P609 - X_Dia out-of-plane displacement

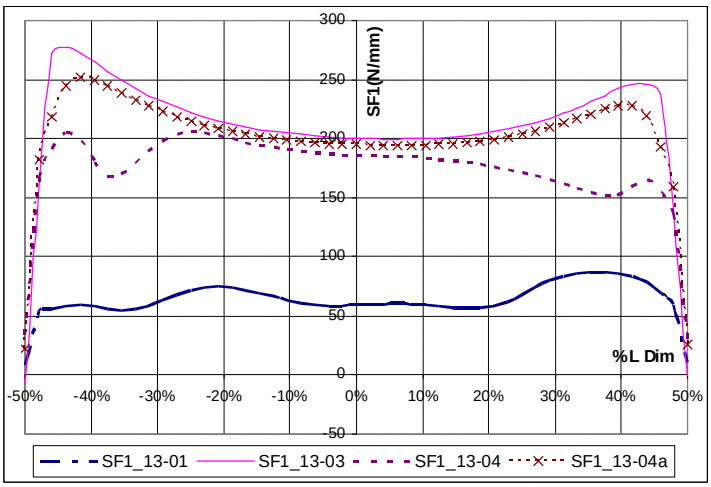

Figure 5.24 P609 - L_Dia longitudinal section forces (SF1)

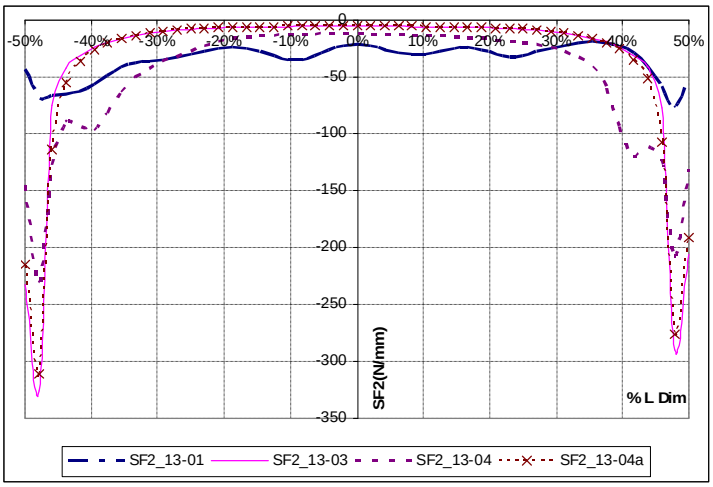

Figure 5.25 P609 - L_Dia transverse section forces (SF2)

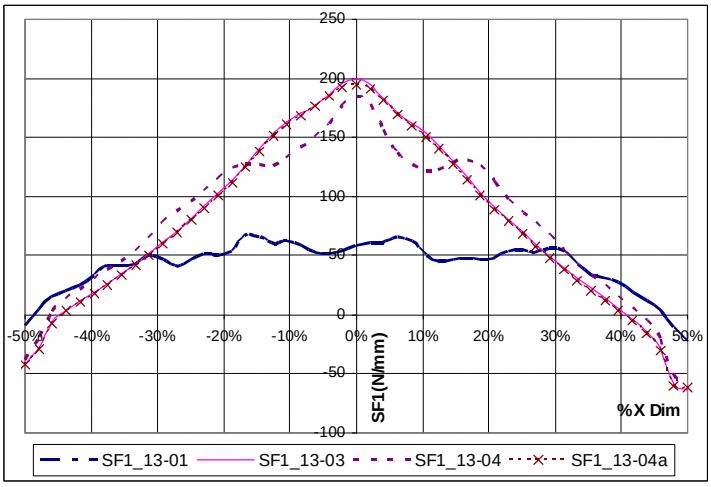

Figure 5.26 P609 - X_Dia longitudinal section forces (SF1)

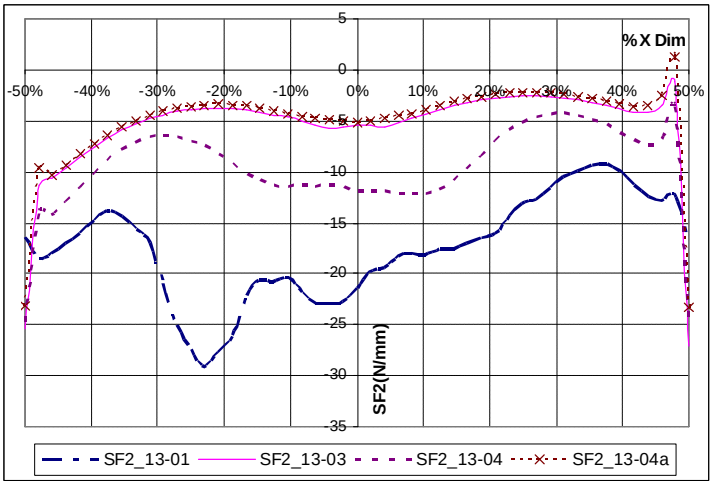

Figure 5.27 P609 - X_Dia transverse section forces (SF2)

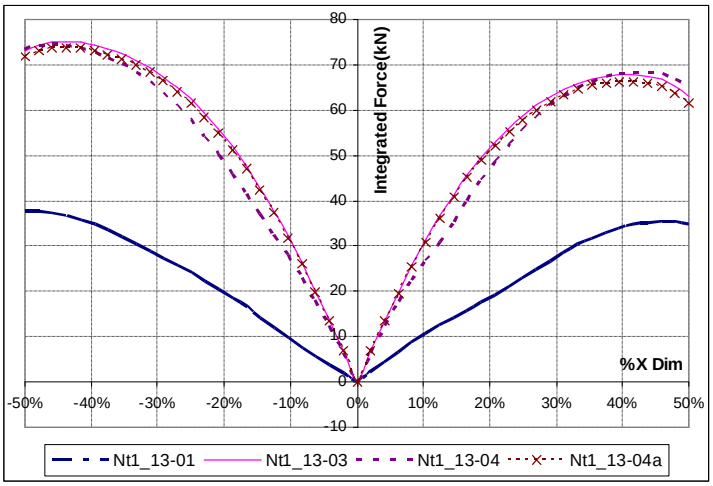

Figure 5.28 P609 - X_Dia integrated section forces (Nt1)

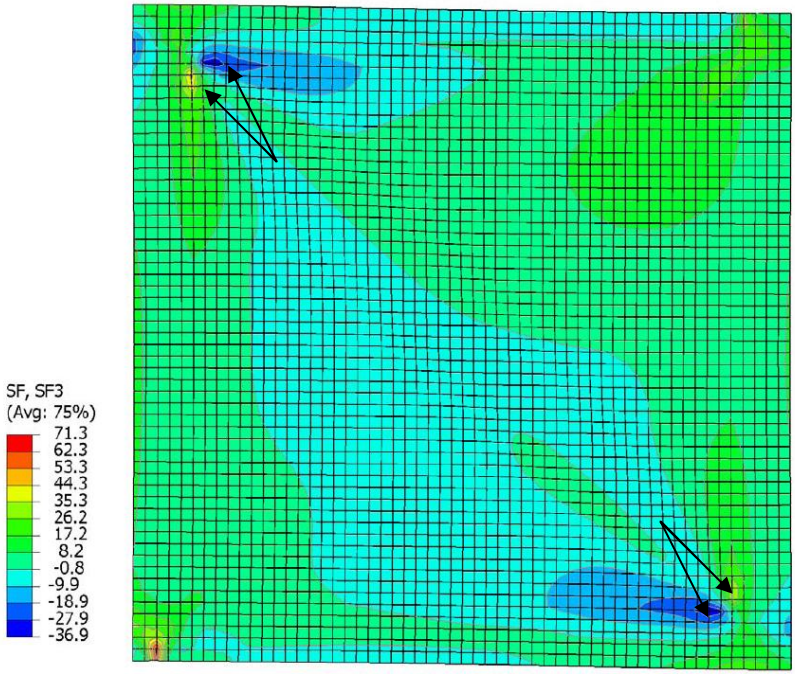

Figure 5.29 P609 - Developed shear forces (SF3) at corners

5.3.5.2. P609 – Behaviour of the Pultrusions

In general, the behaviour of the pultrusions (vertical and chord members) was similar to that of the discrete-diagonal panel (P309), Sec.3.6.2.2 (p61). However, the complicated buckling shape resulted in highly non-linear stress distributions along the pultrusions. This can be attributed to the continuous transfer of forces from the diaphragm skins along its length (Figure 5.30).

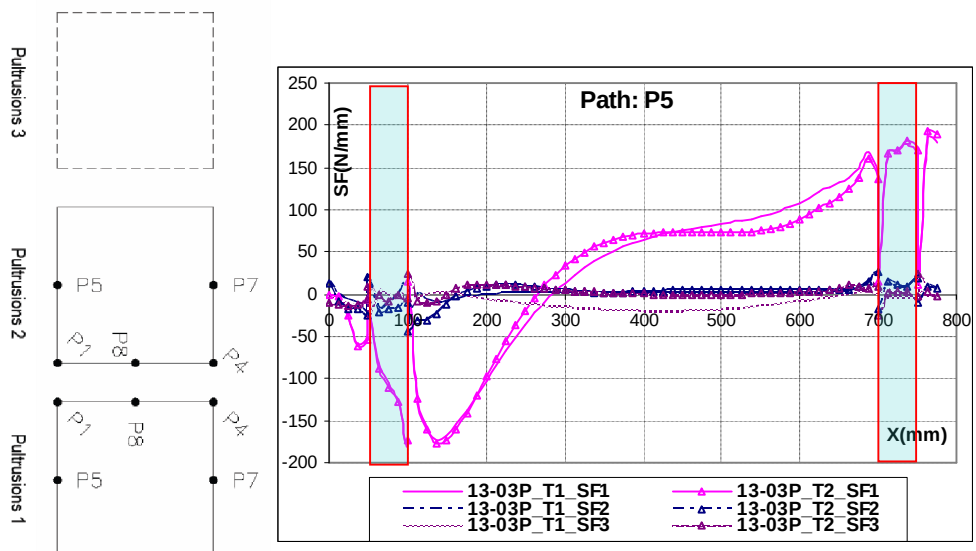

Figure 5.30 P609 - Section forces along top chord – P5

5.3.5.3. P609 – Behaviour of the Adhesive Layers

The adhesive shear stresses reached its maximum value of 31MPa at the face of the vertical member. Along the path, continuous transfer of forces was observed (Figure 5.31). This provided better distribution of stresses when compared with dicrete diagonal panel (P309), where all the adhesive stresses were concentrated at the diagonal corner with maximum value of 80MPa[3] (Sec.3.6.2.3, p67).

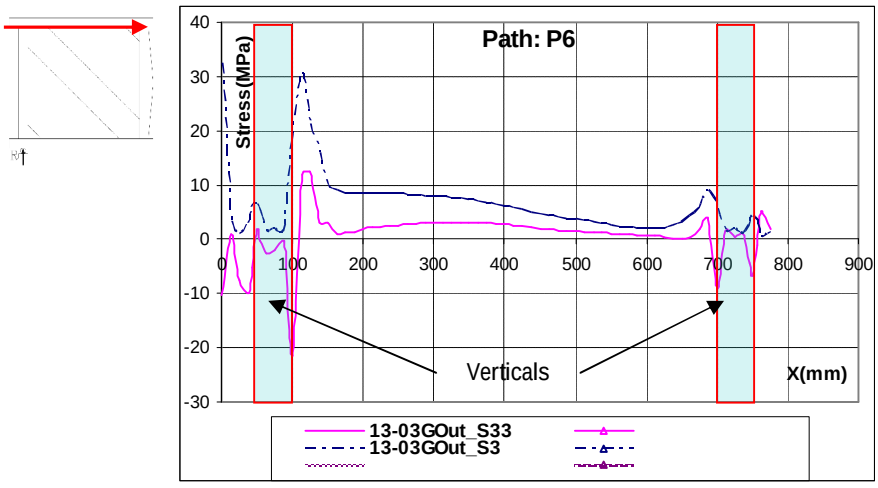

Figure 5.31 P609 - Glue stresses along path P6

5.3.5.4. P609 – General Behaviour

The FE models provided an excellent representation of the P609 test. They explained the main characteristic of the bracing system well. Buckling was a predominant behaviour of this panel which significantly increased the strain demand on the web laminates at the corner positions.

[3] This is at load of 333kN compared to load of 189kN for P609

It was difficult to assess the exact level of load where failure (at the laminate scale) was initiated until reaching the ultimate capacity. The crack development process is shown in Figure 5.32. The FE model[4] was used to predict the shell section forces and moments at 17.7mm (node: 1156, Figure 5.33) and 35.4mm (node: 1166, Figure 5.33) from the top right corner, where failure was initiated. The relationship between load and section forces/moments was linear with the confinement forces (SF2) component higher than the SF1 component, node 1156. For node 1166, SF2 significantly reduced (compared to 1156); however, the bending moments increased in a non-linear form (Figure 5.33). The Tsai-Wu failure criterion was found conservative in predicting the initial failure of the laminate (at 150kN, Failure Index Factor, FIF, ranged from 100% to 290% for the different plies).

In correlating the load capacity of the panel to the strain level in the diagonal, P609 in reached 25.1N/microstrain which is slightly less than P309 in tension (Sec. 3.6.2.5 p74)

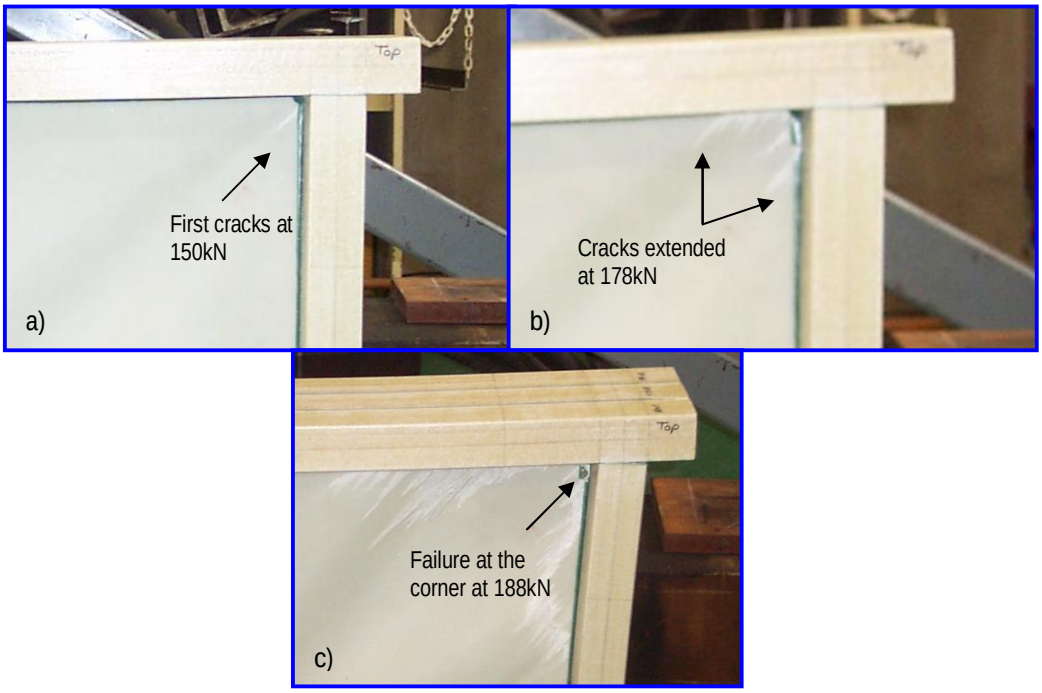

Figure 5.32 P609 – Development of the cracks and failure at the diaphragm

[4] 13-04a model was used because of the ability to control the load increment.

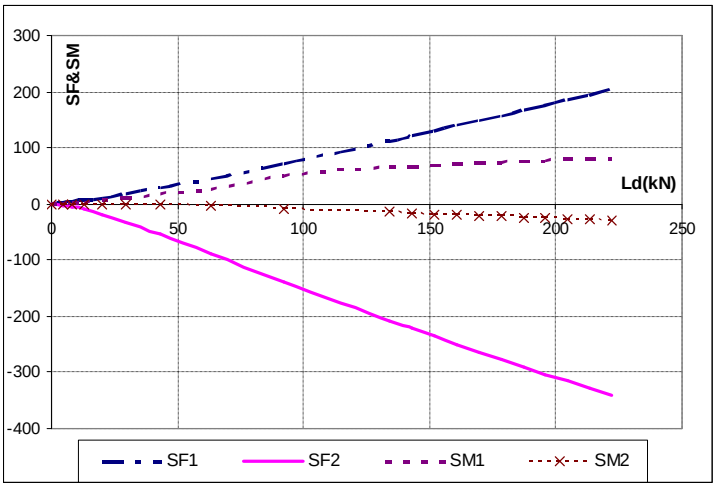

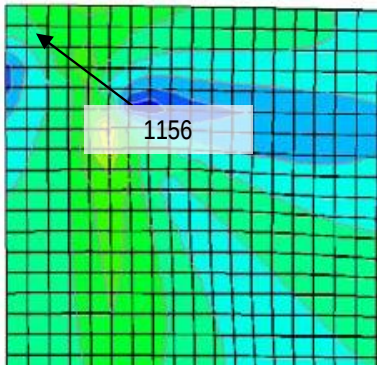

Figure 5.33 Shell forces and moments at node: 1156

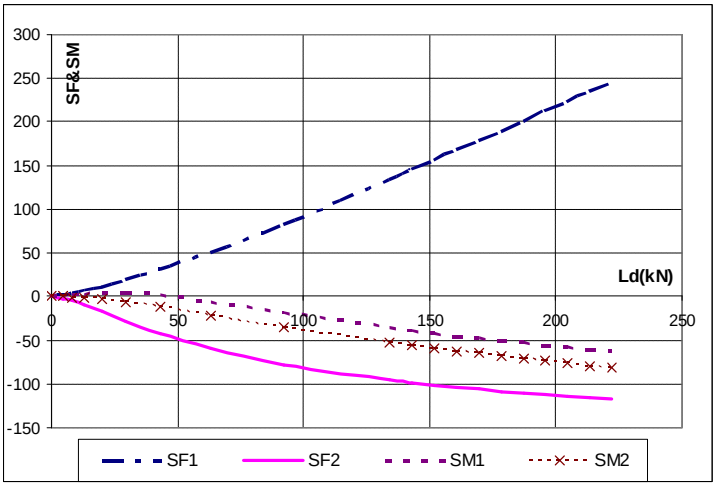

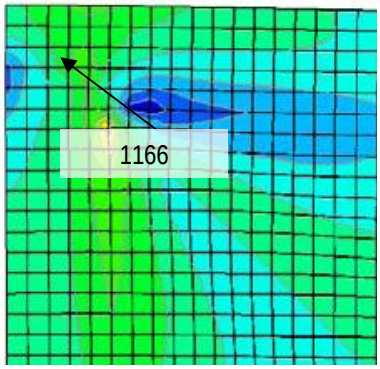

Figure 5.34 Shell forces and moments at node: 1166

5.4. SANDWICH-DIAPHRAGM, MULTI-PULTRUSION TRUSS SYSTEMS (PANEL: P709 AND P809)

Investigations of the behaviour of P609 panel showed that the diaphragm system provided some advantages over the discrete diagonal system with associated drawbacks. Structurally, the disadvantages were associated with the web buckling. In order to improve on this behaviour, it was decided to use sandwich construction to reduce adverse effect of the web buckling. In order not to increase the weight significantly, a low-density closed-cell PVC foam was used for the web core.

Two forms of sandwich panels were considered at this stage of investigations. One used X core layout (P709) while the other used complete core fill (P809). In this section, the manufacturing process and related difficulties are briefly presented

followed by the modelling options, tests results and FE results that are then used to discuss the main behavioural issues of both of these panel systems.

5.4.1. P709 AND P809 – PANEL MANUFACTURING

Full-height DD-MPTS panels P709 and P809 were manufactured and tested, with similar dimensions to that of P409 (Chapter 4). P709 was the first attempt to reduce the web buckling effect at corners by using a cross-bracing foam of 150mm wide (Figure 5.35). The second system used complete foam within the panel, P809 (Figure 5.36).

Similar procedures were followed for the manufacturing of both panels. After initial preparations of the laminates and pultrusions, the first two frames with laminates were assembled by adhesive bonding. Then after sanding and cleaning, the foam and the last frame with laminates were assembled (Figure 5.37 & Figure 5.38).

Similar to panel P609, SHS50x50x5 pultrusions (www.pacomp.com.au), MX6000 glass double bias (www.colan.com.au), and Hyrez 202 epoxy were used to manufacture the panel components. A non-symmetric laminate architecture [-45/+45/-45/+45] was used for the diaphragm skins in a mid-plane symmetric sandwich construction.

Low-density closed-cell PVC foam, Airex C70.55 (55kg/m^3) from ATL Composites (www.atlcomposites.com), was used for the core. After curing for 24 hours at ambient temperature, hard points were glued to the inside of the pultrusions at the load and support locations. The panel was post-cured at 80˚C for six hours with a one-hour ramp. Standard (120Ohm) strain gauges were placed at the diaphragm origin on both skins in the compression direction (SG13 and SG16), and on one skin in the tension direction (SG12), with gauges placed normal to these directions (100mm from the corners) to measure the confinement strains (Figure 5.35 and Figure 5.36).

Some difficulties were encountered. In spite of the precautions taken to ensure contact between the core and the skins, for example (i) applying glue to both the foam and the laminate surfaces, (ii) preparing an elevated table to support the bottom laminate and (iii) applying additional loads on the top laminate, large sections of the

diaphragm were observed to entrap air causing separation between the core and the skins. This necessitated repairing these sections (Figure 5.39), by drilling 3mm holes and injecting Hyrez 202 epoxy resin[5]. The epoxy resin was used to allow good flow through the formed voids. However, it took a long time to gel consequently this slowed the rate of repair. In addition, the repair work was not easy as the panels had to be flipped to guide the flow of the resin under gravity.

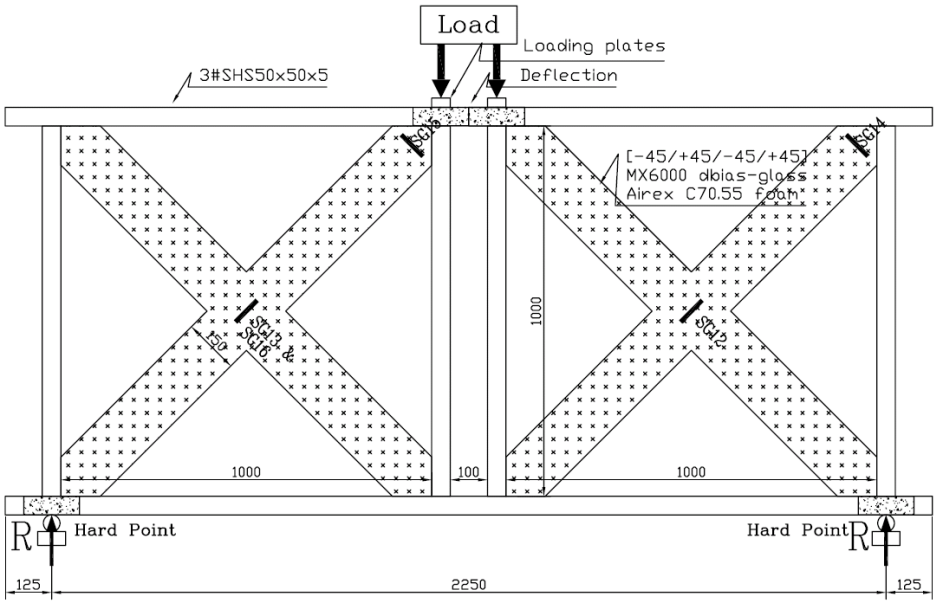

Figure 5.35 P709 - Dimensions and test layout

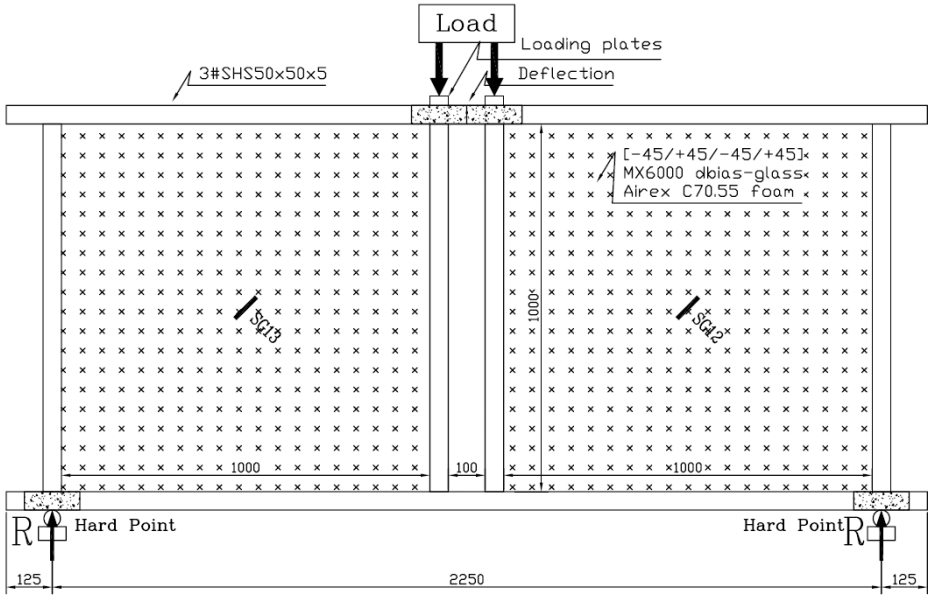

Figure 5.36 P809 – Dimensions and test layout

[5] Without thixotropic additives used.

Figure 5.37 P709 - Panel during manufacturing

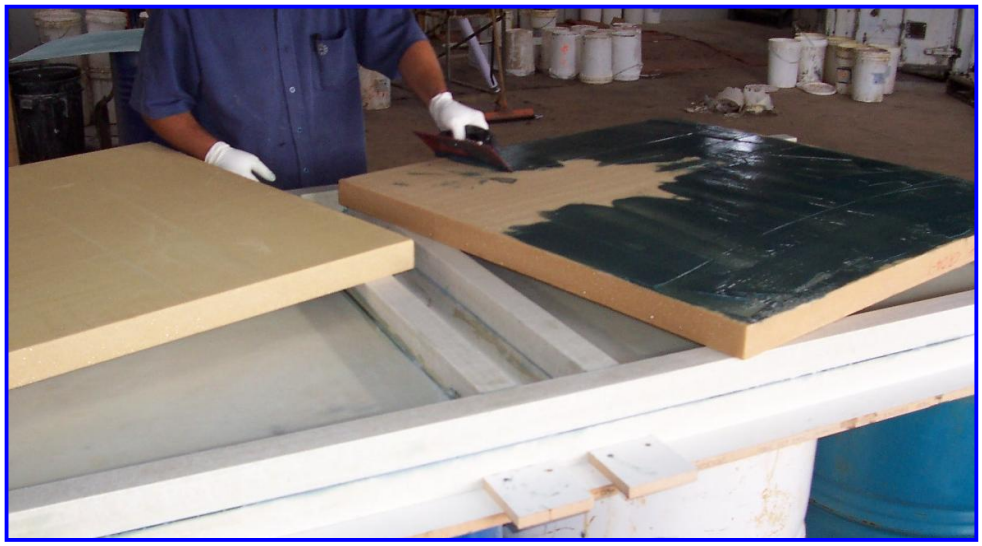

Figure 5.38 P809 - Panel during manufacturing

Figure 5.39 P709 - Panel during repair

5.4.2. MODELLING OPTIONS

P709 followed similar modelling procedures to that of other MPTS panels, non-linear analysis predicted the buckling mode of this type of structure by applying an initial imperfection to the frame geometry[6]. For P709 an initial imperfection of 1.50mm was introduced to the model in the first loading step. Loads were then applied, commencing from the second loading step displacement-controlled loads were applied.

Linear analysis was used to model P809, with incremental applied displacement in each loading step. As no buckling behaviour was observed, it was assumed that the imperfection/diaphragm-depth ratio was too small and accordingly, the imperfection effect was ignored in this model. After verifying the analysis results, Sec.5.4.4, this assumption was found reasonable.

5.4.3. P709 - TEST AND FE RESULTS

The servo-controlled testing machine with Instron loading ram of 600kN capacity (type: A1340-1006ASP) was used with the displacement-controlled loads applied at a rate of 0.75mm/min with data collected to a standard PC through System-5000 data acquisition system. The test records and the FE model results are shown in the same figures. The load-deflection curves are shown in Figure 5.40. The strain-load curves are shown in Figure 5.41 and Figure 5.42. For strain gauge locations, reference should be made to Figure 5.35.

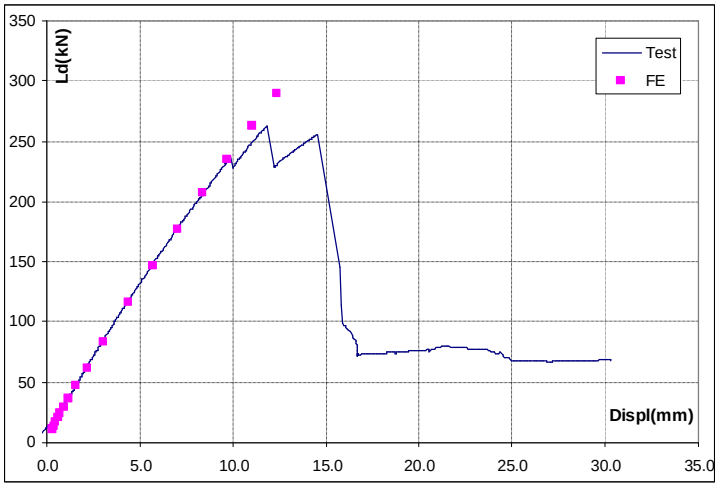

Figure 5.40 P709 – Load-deflection curves

[6] with a value that equals the web shell element thickness.

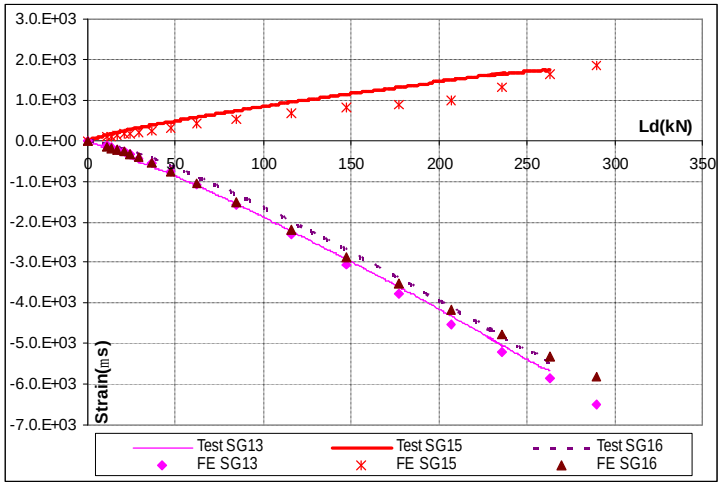

Figure 5.41 P709 – Left side strain-load curves

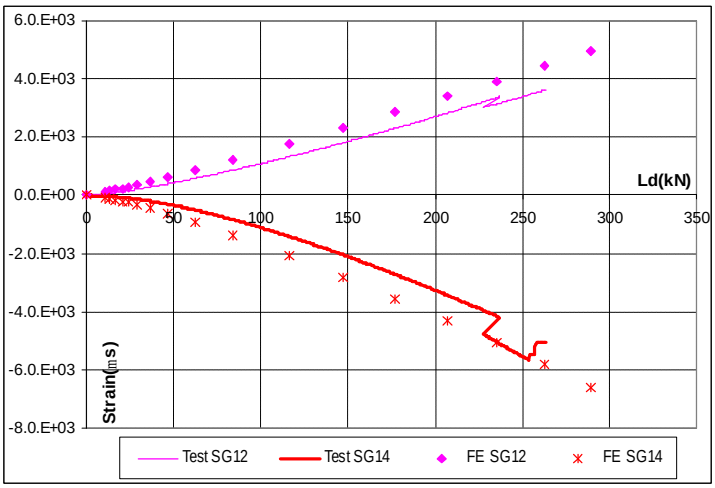

Figure 5.42 P709 – Right side strain-load curves

5.4.4. P709 - EXPERIMENTAL OBSERVATIONS AND FE MODEL VERIFICATIONS

5.4.4.1. Test Observations.

Similar to the other MPTS panels tested, failure was originated and propagated in the diaphragm laminates. No failure was observed in the adhesive layers. P709 reached an ultimate load capacity of 263kN. This was a significant increase compared to P609 (187kN). The P709 behaviour was different from that of P609. The unsupported skins (triangular portions of the web with no core) started to buckle, under compression. At 235kN load, a noise was heard. This was associated with a slight reduction of the load-carrying capacity of the panel, which shows as first kink in the panel load-deflection curve (Figure 5.40). It was observed that the skins on panel P709 had debonded from the core at two locations, where the web buckling extended across the diagonal cores under compression (Figure 5.43). With the continual application of loads, the panel reached its ultimate capacity, of 263kN,

where failure originated in the un-supported portion of the web (Figure 5.44). This shows as the second kink, in the load-deflection curve (Figure 5.40). At this stage, the load-carrying capacity was reduced to 232kN. With further application of loads, the panel reached its second maximum load of 255kN which was followed by extensive damage in its web (Figure 5.45), and indicated as third kink in the load-deflection curve (Figure 5.40). At this point, the panel continuously carried a constant load of 76kN with the continual increase of the applied displacement. At a deflection of 30.3mm (Span/75), the test was terminated. When the applied loads were released, the panel recovered most of its deflection in spite of the extensive damage in the diaphragm skins. No failure was observed at any of the diaphragm corners.

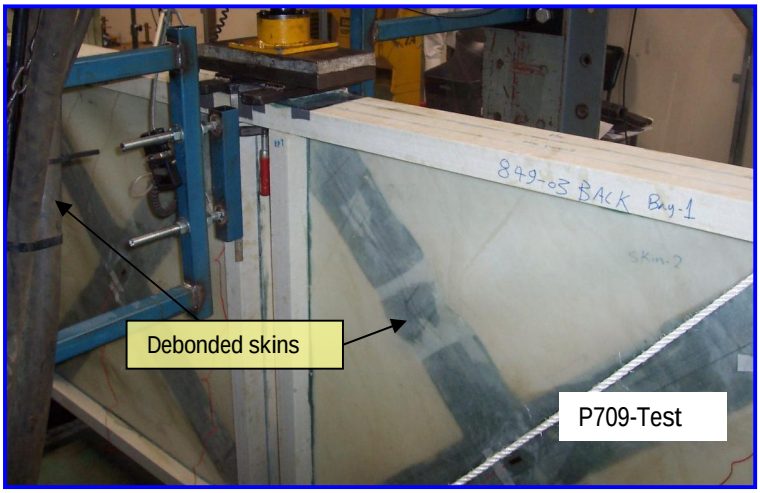

Figure 5.43 P709 with skins buckled and debonded

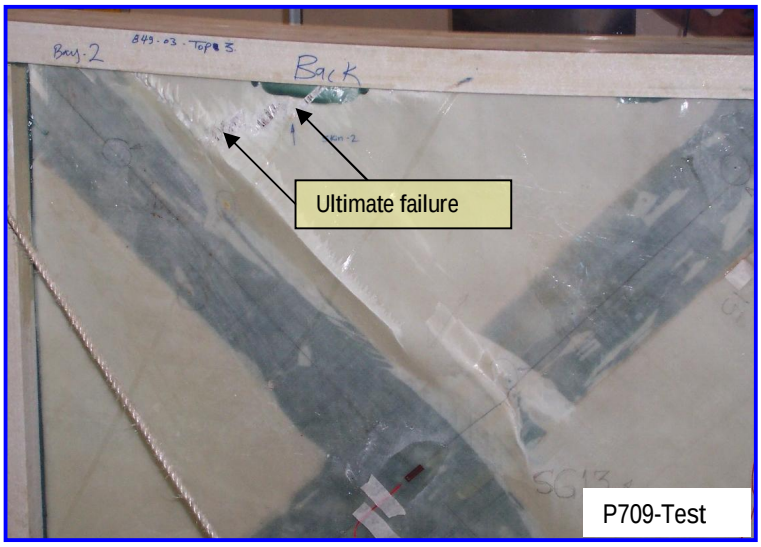

Figure 5.44 P709 - Failure at ultimate load

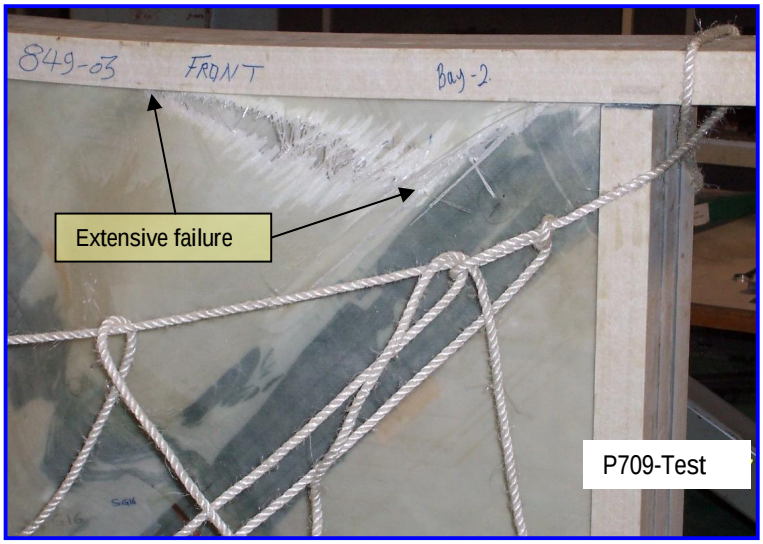

Figure 5.45 P709 – Extensive damage

5.4.4.2. Performance of the FE Model

The FE model showed quite good correlation with the test data (Figure 5.40 to Figure 5.42). With the experience gained in modelling the different panels, the modelling procedures became well-established and provided an excellent representation of the different panel systems.

5.4.5. P809 TEST AND FE RESULTS

Similar to P709, the test records and the FE model results for P809 are shown in Figure 5.46 and Figure 5.47.

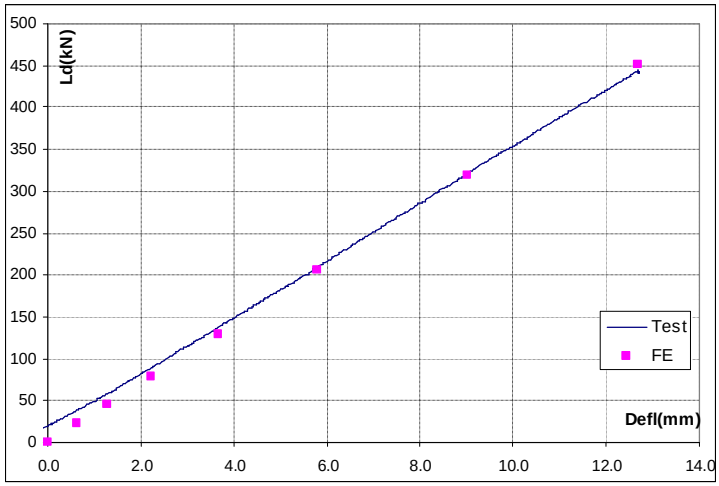

Figure 5.46 P809 – Load-deflection curves

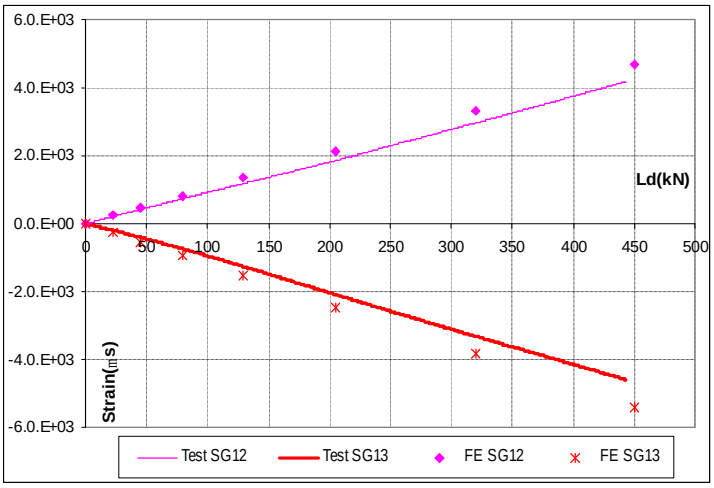

Figure 5.47 P809 – Strain-load curves

5.4.6. P809 EXPERIMENTAL OBSERVATIONS AND FE MODEL VERIFICATIONS

5.4.6.1. Test Observations.

The performance of P809 was quite good as the panel behaved linearly with no failure observed in any of its components until reaching the maximum test load of 440.3kN. At this high load level, the test was terminated due to safety issues. The panel completely resumed its original shape when the load was released. P809 was much stiffer, load-displacement ratio 34.1kN/mm compared to 23kN/mm for P709. During the test, there were no signs of any buckling in the diaphragm.

5.4.6.2. Performance of the FE Model

The FE modelling for panel P809 was the simplest with no buckling complications. The model predicted accurately both the load-deflection (Figure 5.46) and the strain-load (Figure 5.47).

5.4.7. P709 AND P809 BEHAVIOUR

In this section, the behaviour of both P709 and P809 is discussed. Reference is made to P609 to show how the introduction of sandwich construction for the diaphragm and the change in the core layout affected the panel behaviour.

5.4.7.1. P709 and P809 – Behaviour of the Diaphragms

Investigations were based on the loading increment, with applied load of 262.9kN and 450.5kN, for P709 and P809 respectively. Two section paths were used

to report the section forces in the web laminates, defined in Figure 5.21 (p138). The L_Dia section forces and moments are shown in Figure 5.48 and Figure 5.50. The X_Dia section forces are shown in Figure 5.49. These figures can be compared with Figure 5.24 to Figure 5.28 for P609. The main behavioural issues of P709 and P809 are summarised as follows:

- The introduction of core material reduced the section moments, along L_Dia and X_Dia, in both panels. This eliminated the secondary effects of having double curvature at the corners, and accordingly increased their load-carrying capacity compared with P609.
- P809 behaviour was linear. The panel carried loads in both 1-1 and 2-2 directions. Forces were uniformly distributed along the section paths in both directions.
- P809 did not show concentration of stresses at corners. This can be attributed to its rigid structure, which in turn, led to it acting as a complete diaphragm with little distortion.
- With the difference in load levels between P709 and P809 close maximum section forces were observed along the section paths. In both panels these forces were less (about half) than those of P609 (Figure 5.24).
- P709 showed quite interesting behaviour. Except at three locations, SF2 (compressive) was very low (~10N/mm). They increased to ~110N/mm, at the origin and the corner zones, which indicated that diaphragm fibres under compression were effective at these three locations only (Figure 5.51).
- For P709, the availability of the core at corners restricted the skin buckling and accordingly increased the diaphragm stiffness. This led to carrying higher loads at corners when compared to P609 (Figure 5.53).
- With the above mentioned performance, P709 can be considered as an intermediary between P609 and P809. The availability of the cross core, prevented buckling of the skins at corners. However buckling occurred at the no-core triangular zones. The buckled portions were able to carry tensile forces, which had little compressive resistance. SF2 in the L_Dia (Figure 5.48) was under compression; accordingly, other than at the corners and the

central zones (where core material was available), there was very little force transfer. In the X_Dia (Figure 5.49), similar to P609 (Figure 5.26), tensile forces were developing from the corners towards the web origin. This means that most of the tensile forces were bundled within the central zone.

- In calculating the resisting diaphragm forces, from Figure 5.53, the P709 force components were 141.8kN under compression and 131.4kN under tension. This totals 273.2kN.
- For P809, the force components were 247.2kN under compression and 220.5kN under tension. This totals 467.7kN.
- For P609, The force components were (52.9kN) under compression and (136.2kN) under tension. This totals 189.1kN.
- For P709 and P809, the diaphragms forces were shared between compressive and tensile forces (Figure 5.51 & Figure 5.52) while almost all forces were carried by the diaphragm under tension in P609.
- P809 showed equal force distributions across the diaphragm while P709 had localised tensile forces around the diaphragm origin and compression forces at the origin and the corners.
- For P709, ultimate strains in the diaphragm were 0.55% under compression (SG13 and SG16) and 0.36% under tension (SG12), Figure 5.54. Reaching the ultimate failure, compressive strains dropped to 0.28% (due to failure in their fibre directions and accordingly releasing the compressive force components), while the tensile strains were proportional to the applied loads.
- This indicated that P709 still had significant reserve. Failure would continue to propagate across the fibres under compression (due to the extended buckling effect) but the fibres (in the core zone) under tension will keep carrying the loads until reaching their failure strains.
- As failure occurred in compression fibres due to the extension of the buckling of the un-supported zones, the panel capacity and post-failure behaviour can be improved by preventing this extension. This can be

achieved by securing adhesion between the core material and the skins, for example, by using stitching techniques.

- The web buckling in P709 led to higher tensile stresses in the core at the wave-forming locations (Figure 5.55). This resulted in initiating the debonding at these locations (Figure 5.43). This effect was magnified by the imperfect contact between the skins and the core, in spite of the attempts to inject the formed voids, Sec5.4.1 (p145).
- For P809, at the maximum load, maximum strains were 0.46% under compression and 0.42% under tension. This means that the diaphragm system had quite substantial reserve until failure. This can shift the failure to other parts of the panel. Further discussion about the stresses in the adhesive layers and the pultrusions are discussed in the next sections.
- In both P709 & P809, much higher load per unit strain was achieved. P709 reached 47.8N/microstrain which is nearly double that of P309 in tension (Sec. 3.6.2.5 p74) and P609 (Sec. 5.3.5.4, p147) while, at the termination load, P809 reached 96.58N/microstrain. These figures clearly show the structural superiority of both of these panels.

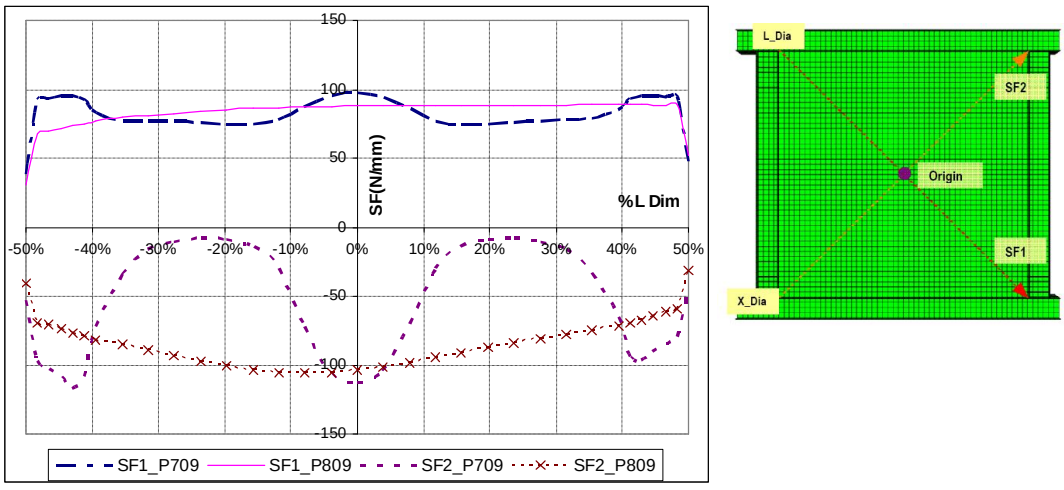

Figure 5.48 P709 and P809 – L_Dia SF1 and SF2

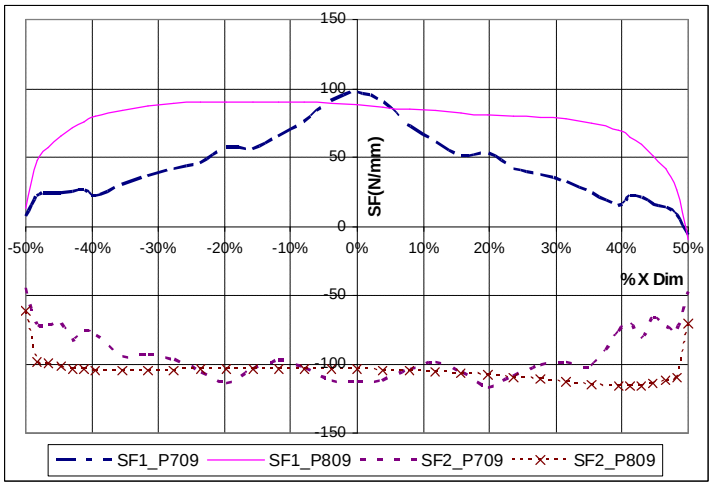

Figure 5.49 P709 and P809 – X_Dia SF1 and SF2

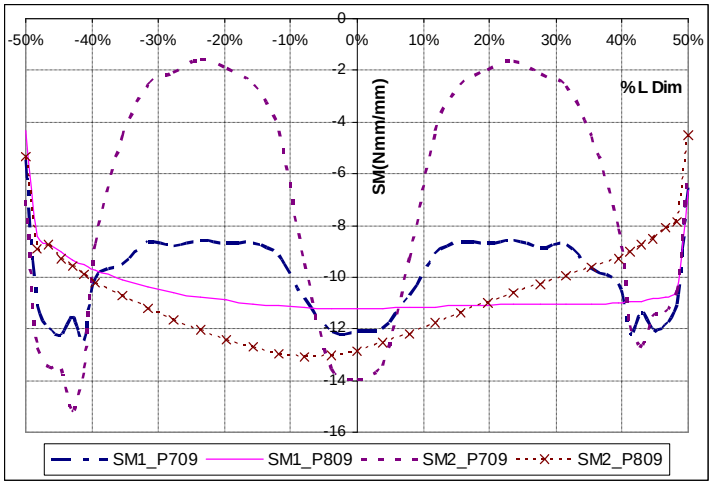

Figure 5.50 P709 and P809 – L_Dia SM1 and SM2

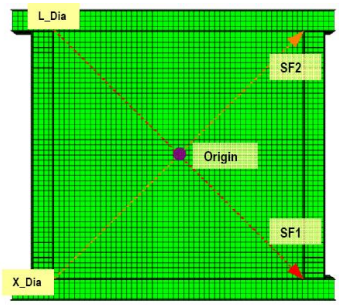

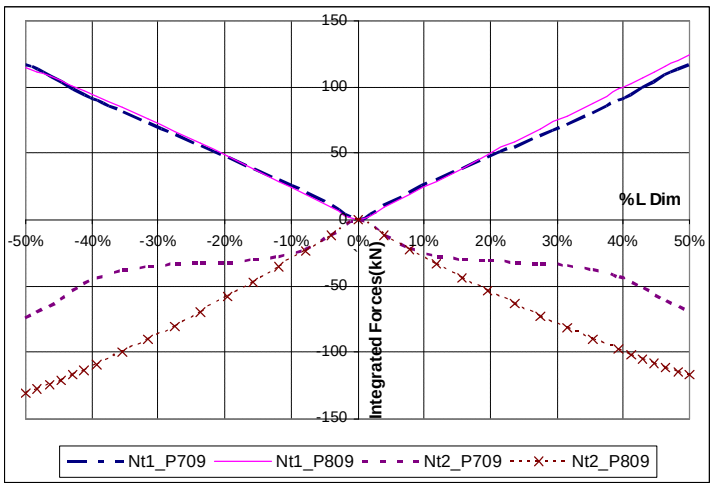

Figure 5.51 P709 and P809 – L_Dia Nt

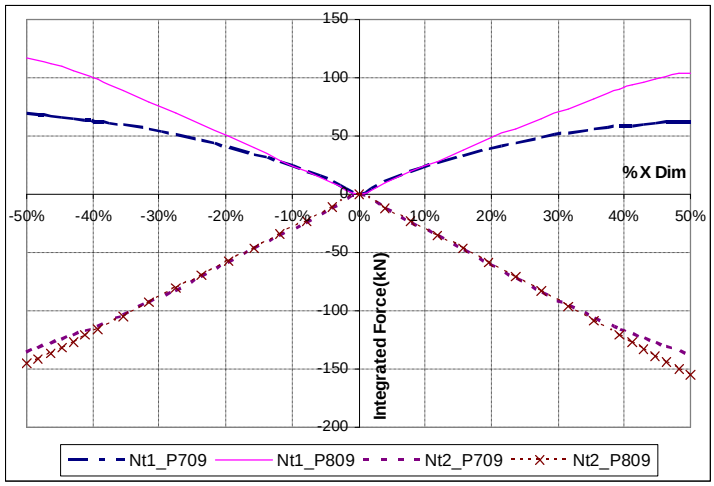

Figure 5.52 P709 and P809 – X_Dia Nt

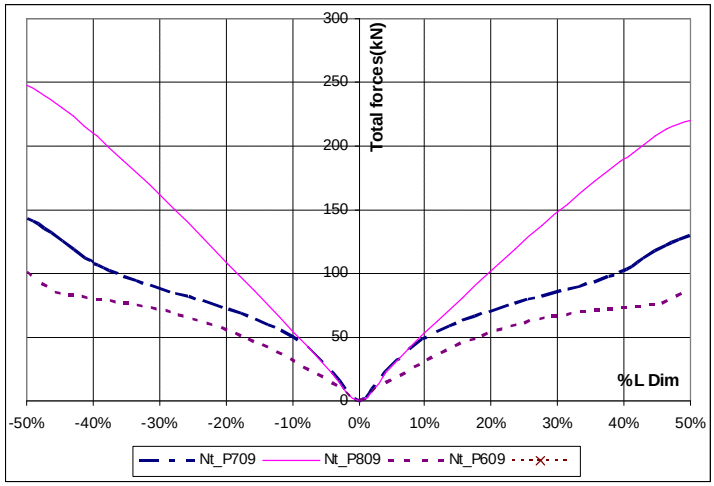

Figure 5.53 P709, P809 and P609- Total diaphragm forces

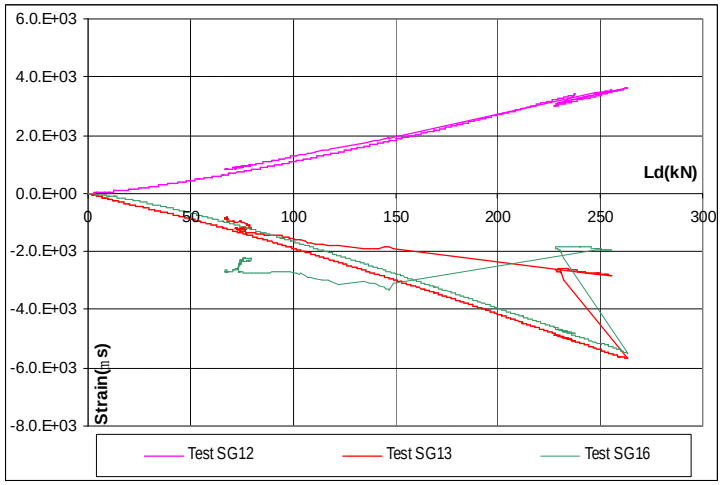

Figure 5.54 P709 - Strain-load curves

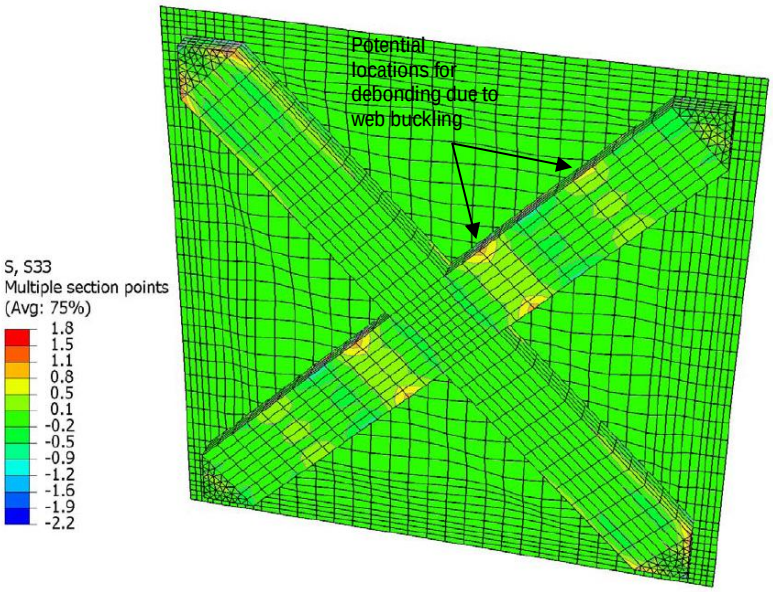

Figure 5.55 P709 – Potential locations for debonding

5.4.7.2. P709 and P809 – Behaviour of the Pultrusions

The introduction of core materials in P709 and P809 led to redistribution of stresses between the fibres under tension and compression, Sec.5.4.7.1. Accordingly, it was expected that other parts of the panels would have better stress distributions. The behaviour of the pultrusions of P709 and P809 were investigated by checking the force distributions at different paths. Based on the data presented in Figure 5.56 to Figure 5.60, the behaviour of pultrusions is detailed as below:

- Compared with P309 (Figure 3.37 to Figure 3.39, p62-63), P709 & P809 showed fundamental difference in force distributions. For P809, axial forces (SF1) increased towards the centre of the panel at all section paths (P5, P7 & P8). This indicated that stresses are distributed between parts due to their location to the centre of the panel.
- P709 behaviour was more complicated with stresses continue to develop towards the centre of the panel (P8, Figure 5.58). However, there was change in stresses in paths (P5 & P7). This complication is attributed to the complexity of the buckling mode of the unsupported skin zones.
- For P809, continuous transfer of shear forces (SF3) was observed along the diaphragm length. SF3 were recorded at the P8PT1 (Figure 5.58). This

indicated the continuous transfer of forces along the diaphragm. SF3 values were small and therefore not critical for the member design.

- P709 showed high non-linear behaviour. However its forces followed the same trend as that of P809.
- Longitudinal section forces (SF1) increased within the panel half with diagonals stressed under tension (Figure 5.58).
- Transverse axial forces (SF2) were negligible.
- Forces developed in the verticals (Figure 5.60) are similar to that developed in the top chord (Figure 5.58).

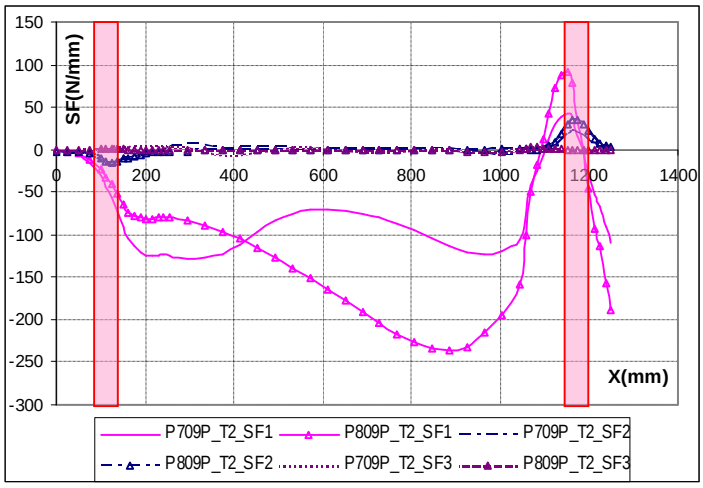

Figure 5.56 P709 and P809 – Section forces in top pultrusion 2-P5 path

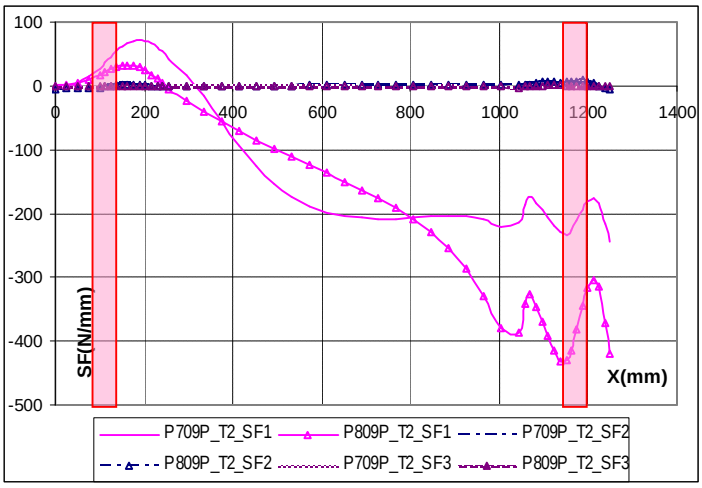

Figure 5.57 P709 and P809 – Section forces in top pultrusion 2-P7 path

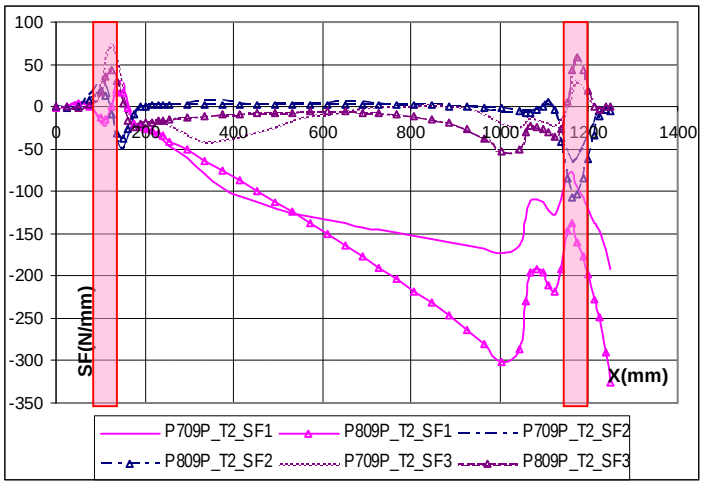

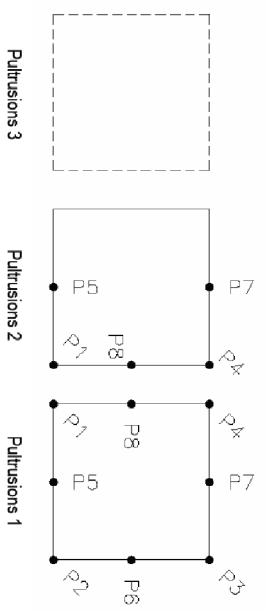

Figure 5.58 P709 and P809 – Section forces in top pultrusion 2-P8 path

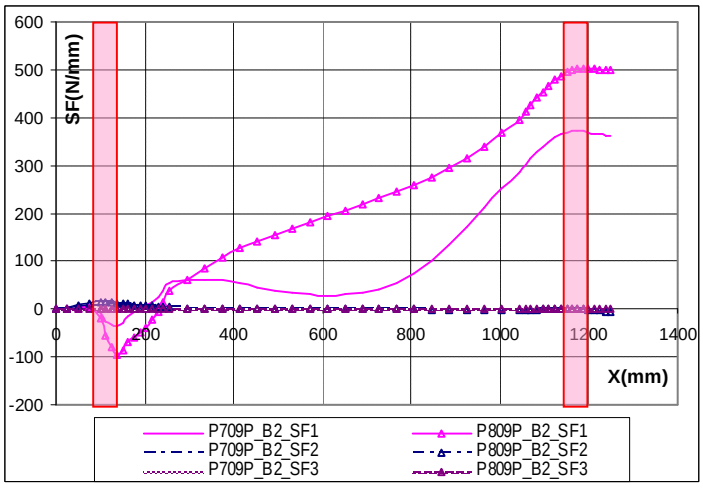

Figure 5.59 P709 and P809 – Section forces in bottom pultrusion 2-P7 path

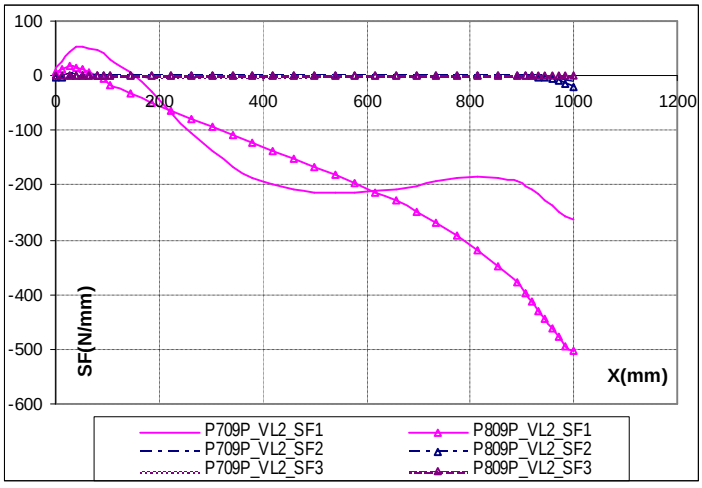

Figure 5.60 P709 and P809 – Section forces in edge vertical pultrusion 2-P7 path

5.4.7.3. P709 and P809 – Behaviour of the Adhesive Layers

The inner adhesive layers had different structures in P709 and P809. For P709, they were available at the cross-core and the pultrusion, while complete layers were available for P809 (due to having a completely-filled diaphragm). Section path P6 axial and shear stresses are shown in Figure 5.61 and Figure 5.62.

As shown, both the tensile and shear stresses in the adhesive layers were quite small compared to other MPTS panels. For P709, the maximum stresses were found at the core with fibres under tension. As discussed in Sec.5.4.7.1, diaphragm tensile forces increase from the corners towards the origin.

For P809, glue lines between the middle pultrusions and skins of the diaphragm (inner glue) were subjected to very small stresses (less than 2MPa) stresses. Glue lines between the outer pultrusions and the diaphragm skins (outer glue lines) were subjected to uniform shear stress of ~9MPa.

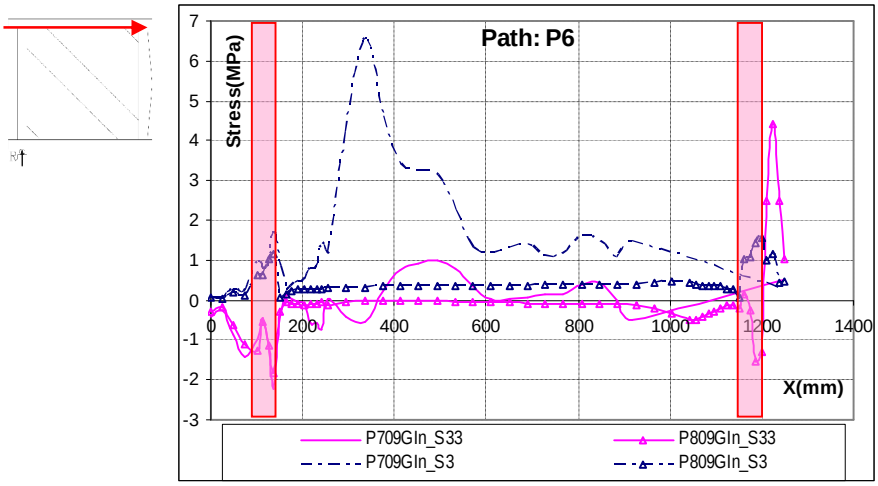

Figure 5.61 P709 and P809 - Inner glue stresses

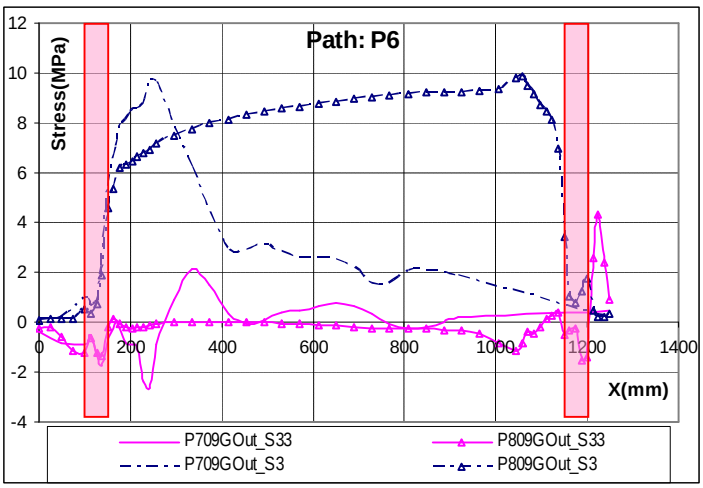

Figure 5.62 P709 and P809 - Outer glue stresses

5.4.7.4. P709 and P809 – General Behaviour

It was found that the introduction of the core significantly improved the panel performance. The core eliminated the buckling of the skins and thus reduced the associated secondary effects of having excessive curvatures. P709 was the only panel to fail. After reaching its ultimate capacity, the panel continued to carry partial loads with significant reserve in the panel system. P809 had the higher carrying capacity with the highest stiffness. Sandwich construction distributed the resisting forces well within both panels avoiding a concentration of stresses in the connecting parts with significant reserve in the adhesive layers.

Clearly, P709 showed redundancy by loosing its capacity in steps (not in a sudden brittle failure) without complete loss of its strength despite reaching excessive displacement. Testing P809 did not reach its ultimate capacity and accordingly the characteristics of its failure could not be judged. However, in comparing the level of stresses in the different panel components of P809 & P309 (Sec 3.6.2.3, p67) the FE analysis results suggests that diaphragm skins is stressed to 45% of P309 (where failure occurred in P309), the adhesive layers 13% and the pultrusions 72% (did not fail in both panels). With the stresses in pultusions reaching 90MPa, compared to its uni-directional capacity of 450MPa, Table 3.2 p37, failure is not expected to occur in the pultrusions. Accordingly, failure of P809 is expected to occur in the diaphragm skins.

5.5. MULTI-PULTRUSION TRUSS SYSTEMS - COMPARING THE DISCRETE-DIAGONAL AND DIAPHRAGM SYSTEMS

The development of the concept of MPTS detailed from Chapter 3 to Chapter 5 involved the investigation of two categories of panels; Discrete-Diagonal (DD) and Diaphragm (DI). Both categories showed high load-carrying capacity, with the allowance of load redundancy in reaching their ultimate capacity, except for DD with diagonals under compression. In this section, the two systems are compared from the perspective of structural performance, cost, weight, and future potential. Each of these factors is discussed in a separate sub-section.

5.5.1. STRUCTURAL PERFORMANCE

The main difference between the two panel systems was the bracing system; with confinement effects at corners as an important characteristic. However, its effect was more apparent in DD and DI with no core material. The behaviour of the DD-MPTS was simpler to predict and explain. The use of high-shear-modulus core material was essential to the success of DD-MPTS. The diagonal compressive capacity, and therefore the panel capacity, was highly affected by the core properties. The diagonal confinement resulted in lateral forces of opposite sign to that in the diagonal direction. Accordingly, the most critical load condition is with diagonals under compression. This loading condition generated tensile stresses in the lateral direction (with the least reinforcements) and accordingly reduced the laminate efficiency in carrying loads in the diagonal direction. The overall buckling of the diagonal is another characteristic of DD-MPTS. These characteristics can be managed as structural behaviour of this panel behaviour can be accurately predicted.

In DI-MPTS the diaphragm forces were carried by the skins. The distribution of these forces, and accordingly the panel capacity, were dependent on the level of control of the buckling of the skins. With no core, the diaphragm acts as a tension-only diaphragm, with most of the diaphragm forces carried by fibres under tension. Buckling resulted in high secondary bending stresses, which significantly reduced the axial load-carrying capacity of the laminate. With the introduction of a core to form a sandwich diaphragm, the panel performance was significantly increased. The use of a fully-filled diaphragm maximised the load-carrying capacity of the DI panel. It was found that the panel performance was not very sensitive to the core material used, permitting the use of low-shear-modulus (density) cores. The second important feature of this system was the availability of alternative load paths through the diaphragm which prevented complete loss of strength when the panel reached ultimate capacity. However, this could not be judged for the fully filled diaphragm panels as the tested panel capacity could not be reached during testing.

5.5.2. PANEL COSTS

There are many factors that can affect the manufacturing costs of the panels. Material costs and labour costs need to be optimised. The manufacturing procedures for both types of panels were traditional with no high technology or automated

procedures. DD-MPTS used less material than DI-MPTS and consequently had a of lighter weight. The diaphragm availability made the clamping process difficult. In addition, controlling the quality of the gluing process, between the skins and the core, was very difficult to achieve. The DD-MPTS laminates involved cutting more pieces than the DI-MPTS.

As the DI-MPTS has fewer and larger components than the DD-MPTS, it would seem the easier of the two systems to be adopted for automated manufacturing. In addition, it may be possible to laminate the skins directly on the core material, thereby eliminating the use of adhesives.

5.5.3. PANEL WEIGHTS

Based on a panel size of 1250mmLx1100mmH, the weights of the components in each of the panels are shown in Table 5.2.

The vertical members are the heaviest components but as they are subject to less stress than the chords, pultrusions with thinner walls could be used to reduce the weight of the panels. Weight differences in the adhesives required in the different bracing could be reduced by using a direct laminating process for the P809panel. As this panel has a specific strength (per unit weight) that is marginally higher than that of the other panel systems, it was concluded that P809 is the most attractive panel alternative as it provides higher capacity with a comparable weight.

Table 5.2 Comparison of panels weights

Part	P409	P709	P809
Top chord	6.19	6.19	6.19
Bottom chord	6.19	6.19	6.19
Verticals	9.90	9.90	9.90
Diagonal	4.23	6.99	9.02
Adhesive	1.26	1.62	2.84
Packers	1.57	0.00	0.00
Gussets	0.27	0.00	0.00
Total Wt (kg)	**29.61**	**30.88**	**34.13**
Load/Unit Wt (kN/kg)	**8.95**	**8.52**	**>12.89**

5.6. CONCLUSIONS

The concept of Diaphragm MPTS was developed and investigated in this chapter. The DI-MPTS concept was based on using double skins, replacing the discrete diagonal sandwich member. Using diaphragms with no core material led to excessive buckling which reduced the load-carrying capacity of the panel.

In introducing the core material to form a sandwich web, the diaphragm forces were shared between fibres in both directions (under compression and tension). Increasing the percentage of core material distributed the forces evenly and accordingly led to having panels with very high load-carrying capacity. The diaphragm eliminated the concentration of stresses in other components. This was due to the continuous transfer of forces at the diaphragm interface. The other main advantage of this system was providing significant redundancy in the system that prevented the occurrence of complete loss of strength in reaching the ultimate capacity. This panel system was more difficult to manufacture, using the current procedures. However, it has more potential for developing an automated process that can reduce its weight as well.

The finite element models used to predict the panel behaviour were efficient tools to investigate their behaviour. For the different panel systems, the FE closely predicted both the load-deflection and strain-load behaviour. Accordingly, these models can be used to verify the efficiency of the macro-level models which can be used to conduct complete-frame analysis.

In Chapter 6, simplified modelling procedures are proposed to allow the prediction of the panel behaviour within the overall frame analysis. These procedures will be verified with the FE modelling procedures presented in Chapter 3 to Chapter 5 to ensure their suitability.

5.7. REFERENCES

ATL Composites Homepage. http://www.atlcomposites.com.au.

Colan Homepage. http://www.colan.com.au.

Pacific Composites Homepage. http://www.pacomp.com.au/.

Rogers, D. (2004). Characterisation of Hyrez 201 laminating resin. Polymer Testing Laboratory, University of Southern Queensland, Toowoomba, Queensland.

Chapter 6 Notations

$\mathbf{A}$	Equivalent beam section cross sectional area
$\mathbf{A_s}$	Equivalent beam section shear area
$\mathbf{E_1}$	Tensile modulus in the 1-1 (fibre) direction
$\mathbf{G}$	Equivalent beam section shear modulus
$\mathbf{G_{12}}$	Shear modulus in the 1-2 plane
$\mathbf{I}$	Equivalent beam section second moment of area

6. Simplified Analysis Models for the Multi-Pultrusion Truss Systems (MPTS)

6.1. INTRODUCTION

In this thesis, the concept of a multi-pultrusion truss system (MPTS) has been developed using either the discrete-diagonal (DD) or the diaphragm (DI) bracing system. FE modelling procedures were used to predict the behaviour of both panel types at micro level. The FE models simulated the behaviour of the tested panels well. This led to developing a basic understanding of these behaviours, Chapter 3 to Chapter 5.

Due to their detailed nature, the micro FE models are time-consuming, both in preparing the models and in analysing them. In addition, reasonably high computational power is required. This necessitates the development of simplified modelling procedures at macro level. A macro model can be a valuable tool in two ways. The first is optimising the panel layout then conducting micro-model analysis on the optimum configuration. The second is conducting overall frame analysis which is important for practising engineers who are interested in using the MPTS. Thus, the macro models should be, practically, easy-to-model and provide good prediction of the panel behaviour.

This chapter focuses on the simplification of modelling procedures. After addressing the important behavioural aspects to be considered, the simplified modelling concepts of DD-MPTS and DI-MPTS are presented. To validate these simplification procedures, the macro models analysis results were correlated to their micro-models counterparts, for DD-MPTS (P409, Chapter 4) and DI-MPTS (P809, Chapter 5). The chapter concludes with general recommendations for the simplified modelling procedures.

6.2. IMPORTANT SIMPLIFIED MODEL COMPONENTS

The adhesive layers, the pultrusions, the laminates, and the sandwich bracing system were the main components of the DD-MPTS and the DI-MPTS. In all of the investigated panels, Chapter 3 to Chapter 5, no failure was observed in the adhesive layers at the ultimate capacity. In addition, these layers made only limited contribution to the panel capacity, due to their low modulus, compared to the reinforced pultrusions and the bracing laminates. Therefore, the first simplification to consider was ignoring the adhesive layers.

During investigations of the stress distributions in the pultrusions, it was observed that the member forces were well-distributed between the multi-pultrusion sections, with limited local effects at the diagonal joint locations (Sec. 3.6.2.2, p.61). Accordingly, the second simplification was to assume that the multi-pultrusion section acted as a fully-integrated section with an equivalent cross-section. The equivalent section properties were derived from the superposition of the pultrusions and the laminates properties (Figure 6.1).

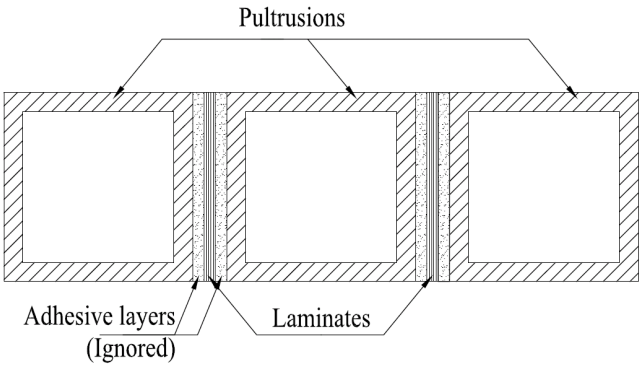

Figure 6.1 Pultrusion cross-section

One of the main characteristics of the MPTS was the confinement effect on the bracing systems, due to their finite dimension. The important location where effects of this confinement occurred was at the face of the pultrusions. This necessitated defining these corners in the simplified modelling.

6.3. P409 - MACRO MODEL CONCEPTS, ANALYSIS RESULTS AND DISCUSSIONS

The P409 macro model was based on the general simplifications of Sec. 6.2. In this section, the modelling procedures and the macro analysis results are presented and discussed.

6.3.1. P409 - MACRO MODEL

The main parts of the P409 model are presented in this section. It covers the materials, the modelling elements, the interaction between parts and the analysis procedures. The model layout is shown in Figure 6.2. The simplified analysis was conducted using the Abaqus FE package (Hibbitt et al, 2004a). However, similar modelling procedures can be conducted using other FE packages.

B31 beam elements were used to model the chord and the vertical members (Hibbitt et al, 2004a). The beam elements were defined by the nodes located at the centreline of the pultrusions (Figure 6.2). The connections between the verticals and the chords were assumed rigid. This assumption was considered reasonable for two reasons. In verifying the analysis results of the rigid connection, this assumption provided good panel representation (Sec. 6.3.2 below). The second reason was the simplicity associated with this assumption. Assessing the joint stiffness can be a complex process due to the availability of the gusset and the diagonal skins outside the joint zone.

For the chord and the vertical members, the laminates theory was used to calculate the properties of the laminates between the pultrusions. The principle of superposition was used to calculate the equivalent section properties of the beam elements, based on the pultrusion and the laminates properties. The section area and inertias were calculated assuming the along-the-member section properties, while the section shear areas were calculated based on the web area in both directions. The adhesive layers were ignored; however, their thicknesses were included as spaces in the calculation of the section modulus. The equivalent EA, EI and GA_s were divided by the E_1 and G_{12} of the pultrusion (which was used as the beam material properties) to obtain the equivalent section areas and inertias.

As discussed in Chapter 4, Shell-Only (CSH) modelling procedures predicted the behaviour of the sandwich columns very well. This indicated that CSH can be used as a simplification for the sandwich bracing system. S4R shell elements were used to model the diagonal and the gussets (Hibbitt et al, 2004a). The boundaries of the diagonal and gussets ended at the faces of the pultrusions (Figure 6.2). The sandwich diagonal was modelled as a composite shell with plies representing the structure of the skins with the core material as the middle ply. A similar modelling approach was used for the gussets. The interactions between the pultrusion beams and the diagonal and gusset shells were modelled by using node-to-surface tie constraints (Hibbitt et al, 2004a).

Similarly to the micro model of P409 (Sec. 3.5.4, p.49), symmetry about the panel centreline was assumed. Load application was assumed on the 50mm zone centred with the middle diagonal with corners restraint in the 3-axis.

Analysis was conducted in three stages. The first stage was an EV analysis to obtain the mode shape that was used as an imperfection for the Riks analysis. Riks analysis (the second stage) was terminated prior to reaching the buckling load of the panel. Displacement-controlled non-linear analysis (the third stage) was restarted after the Riks analysis with displacement reaching 30mm.

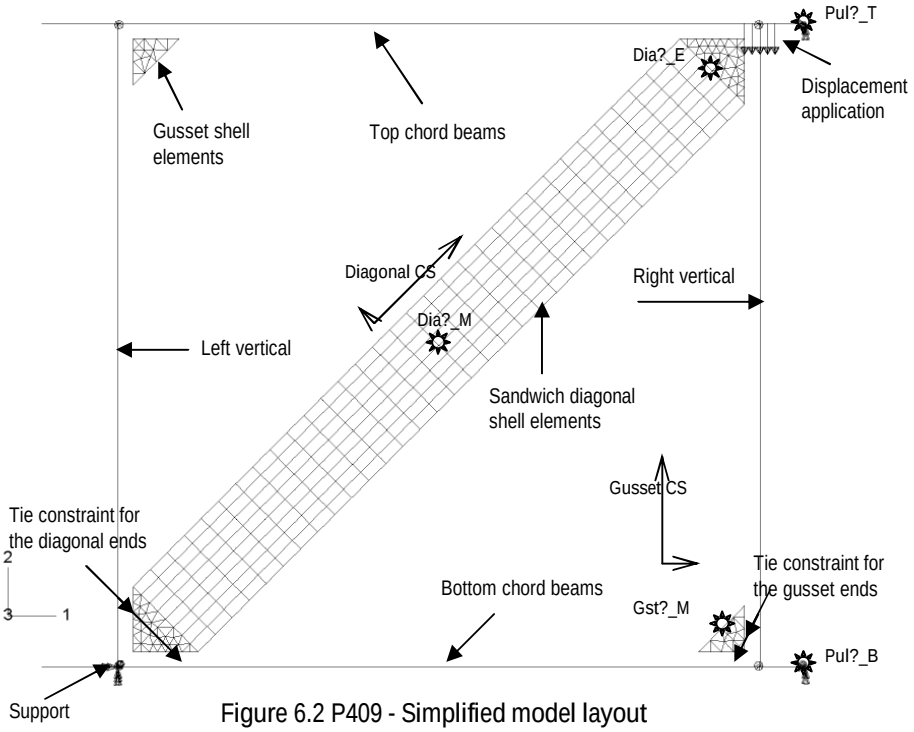

Figure 6.2 P409 - Simplified model layout
?: Diagonal skin, gust, or pultrusion number

6.3.2. P409 - MACRO MODEL RESULTS

The macro-model results (mac) of P409 were verified with the micro-model results (mic). To conduct this verification, load-vertical displacement curves are shown in Figure 6.3. In addition, the stresses in each component of the model (shown as ✲ in Figure 6.2) were plotted against the applied loads. Stresses of the diagonal skins and gussets are presented in the 11-direction (long arrow) and the 22-direction (short arrow) coordinate system (CS), Figure 6.4 to Figure 6.7. Stresses in the pultrusions were calculated from the beam actions at the symmetric plane. Stresses at the pultrusions top (Pul_T) and bottom (Pul_B) chords are presented in the upper (u) and lower (l) flanges, Figure 6.8 and Figure 6.9.

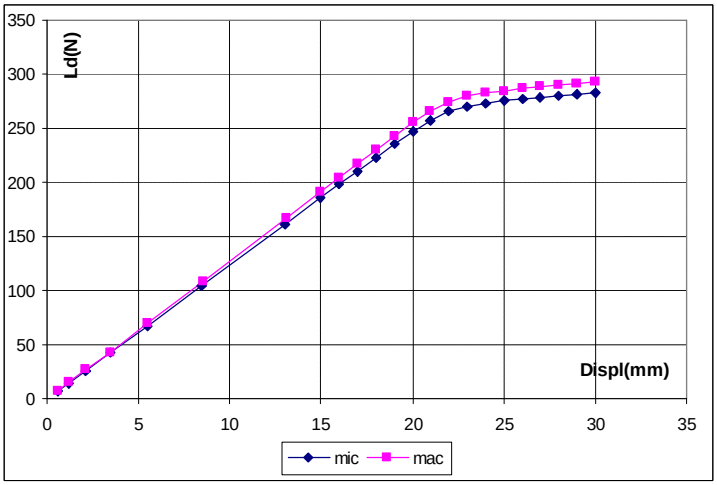

Figure 6.3 P409 - Micro and macro models – load-displacement

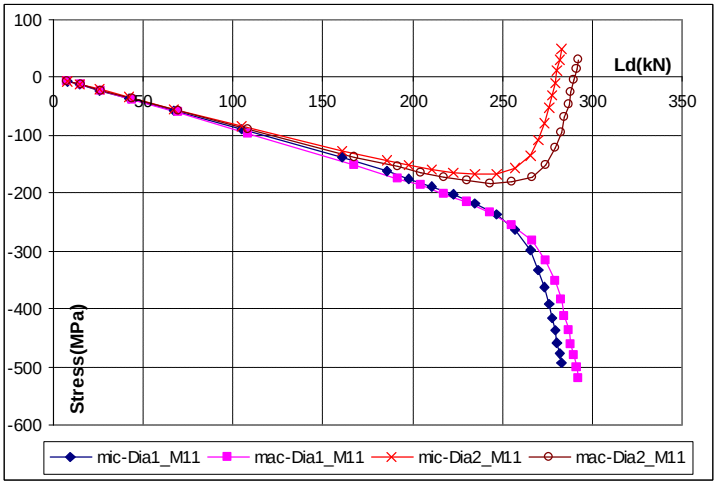

Figure 6.4 P409 - Micro and macro models – Dia_M11 stresses

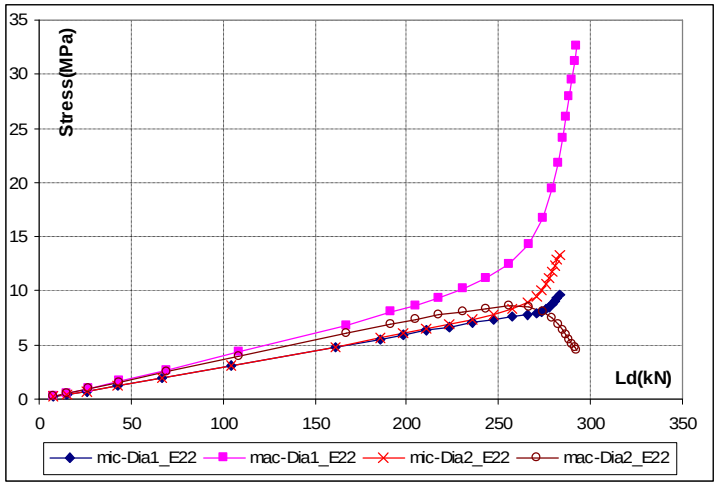

Figure 6.5 P409 - Micro and macro models – Dia_E22 stresses

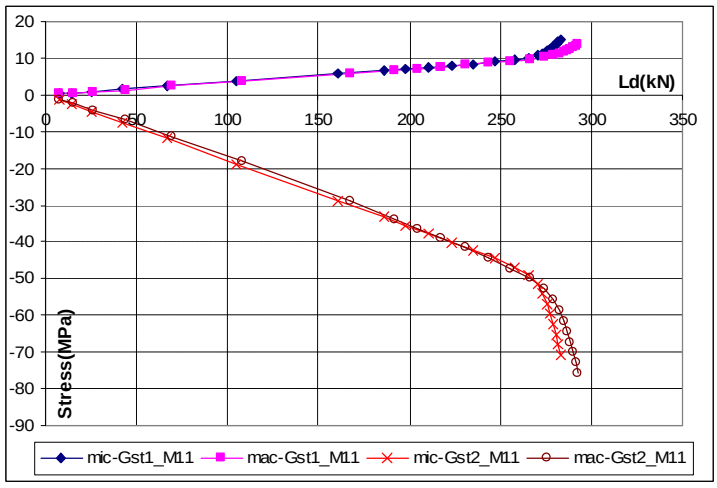

Figure 6.6 P409 - Micro and macro models – Gst_M11 stresses

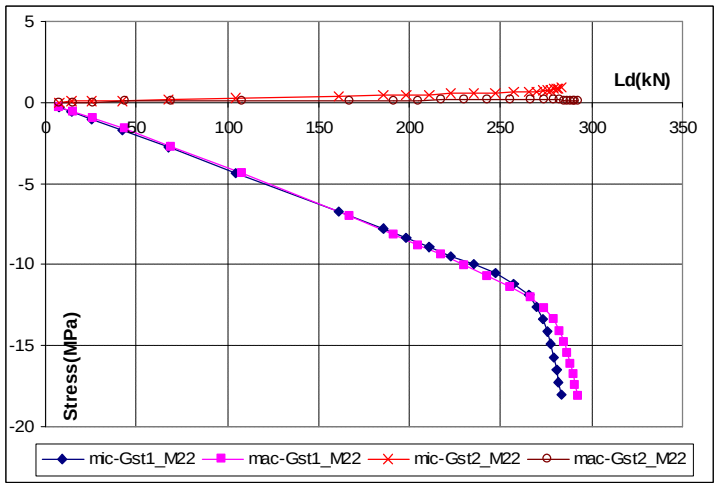

Figure 6.7 P409 - Micro and macro models – Gst_M22 stresses

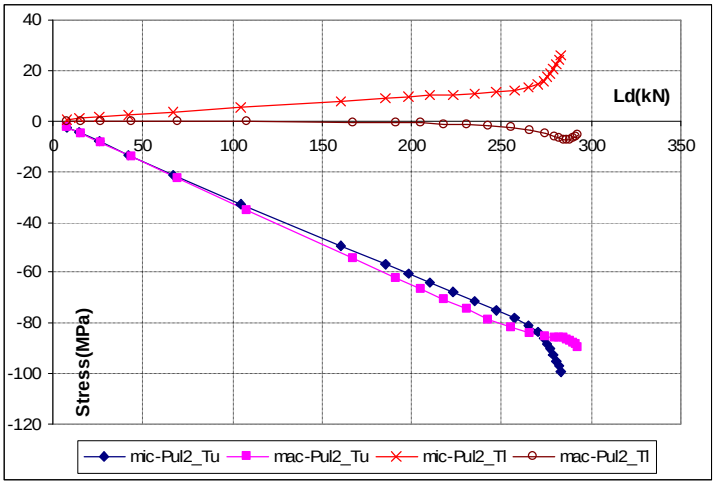

Figure 6.8 P409 - Micro and macro models – Pul2_T stresses

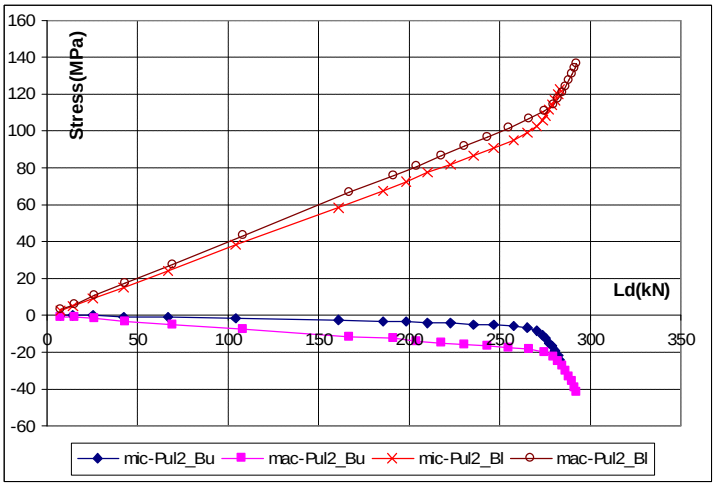

Figure 6.9 P409 - Micro and macro models – Pul2_B stresses

6.3.3. P409 - MACRO MODEL DISCUSSIONS

The analysis time of the macro model was less than 1% of the time required to conduct the micro model analysis (Table 6.1). In comparing the graphs of the two analysis results (Figure 6.3 to Figure 6.9), the following can be concluded:

- The macro model analysis results correlated well with the micro model analysis results for the different components of the panel.
- The macro model predicted the panel capacity 3% higher than that of the micro model. This effect was shown in all the stress-load graphs.
- The confinement effect of the diagonal skins was well predicted by the macro model (Figure 6.5). This was for both of the diagonal skins. The

stresses in the 11 direction of the diagonal skins were also well predicted (Figure 6.4).

- The main difference between the micro and macro model predictions (however still small) were found in the top chord lower flange (Pul2_Tl, Figure 6.8) and the bottom chord upper flange (Pul2_Bu, Figure 6.9).

Table 6.1 P409 - Micro and macro models analysis time (s)

Model\Analysis	EV	Riks	NL	Total
micro	1110	2912	10128	14150
macro	2	15	36	53

From the above, it was clear that the macro model performed well in predicting the stress levels in the different directions of the panel components. The differences observed in Pul2_Tl (Figure 6.8) and Pul2_Bu (Figure 6.9) can be attributed to using beam elements in short spans. The Beam theory is the one-dimensional approximation of a three-dimensional continuum (Hibbitt et al, 2004b). The reduction in dimensionality is a direct result of the slenderness assumptions; of having cross-section dimensions smaller than the dimension along the axis of the beam. This assumption was not well satisfied at the selected chord node locations where the distance between the edge of the right vertical face to the symmetry plane (support) was 50mm.

Thus, it can be said that the differences between the macro and micro model predictions were associated with the test set-up and its loading conditions. The effect of these differences was found to be insignificant on the overall predictions of the panel behaviour. Consequently, the above simplified modelling procedures can be considered sufficiently accurate to predict the panel behaviour.

6.4. P809 - MACRO MODEL CONCEPTS, ANALYSIS RESULTS AND DISCUSSIONS

The P809 macro model was based similarly on the general simplifications discussed in Sec. 6.2. Due to its simplicity, the model is presented briefly in this section, highlighting the differences between it and the P409 macro model (Sec. 6.3). After presenting the analysis results, the model performance is discussed.

6.4.1. P809 - MACRO MODEL

Beam elements (B31, Hibbitt et al (2004a)) were used for the chord and the vertical members (Figure 6.11). Shell elements (S4R, Hibbitt et al (2004a)) were used for the diaphragm. The panel symmetry was considered by modelling one half of the panel with the symmetry plan in the horizontal direction. Due to its simple behaviour, as the panel did not experience buckling behaviour, linear analysis procedures were conducted with loads applied in a single loading step of 12.7mm.

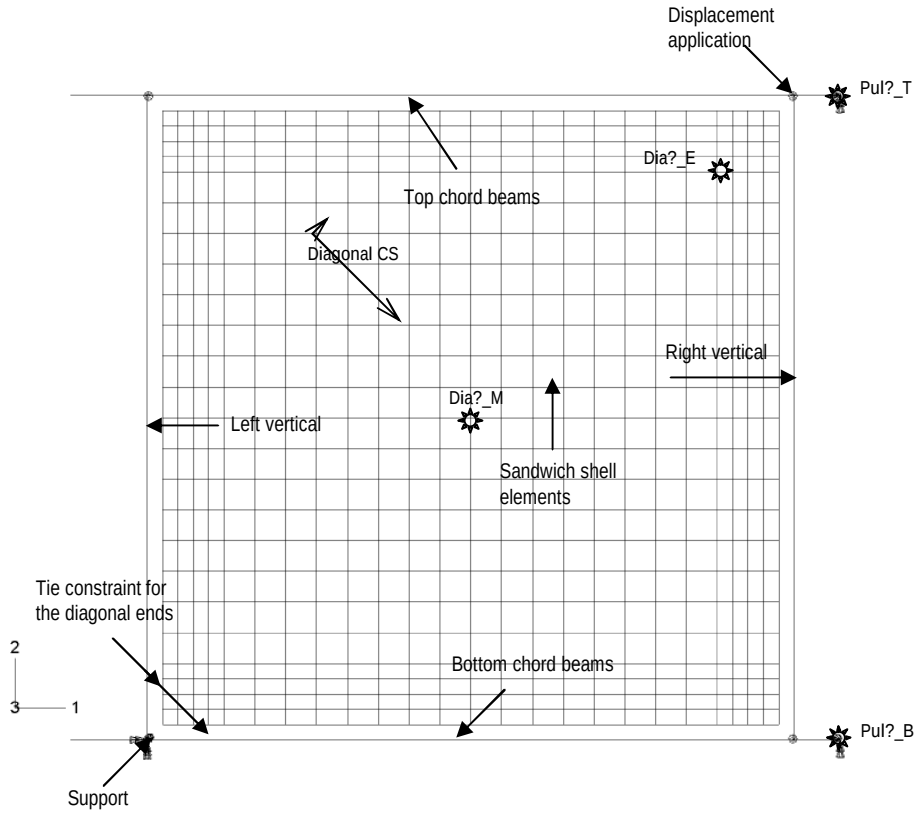

Figure 6.10 P809 - Simplified model layout

?: Diagonal skin or pultrusion number

6.4.2. P809 - MACRO MODEL RESULTS

The macro-model analysis results were verified with the micro-model analysis results. The load-vertical displacement curves are shown in Figure 6.11, the stress-load curves of the diagonal skin are shown in Figure 6.12 , and the stress-load curves of the chords are shown in Figure 6.13 and Figure 6.14.

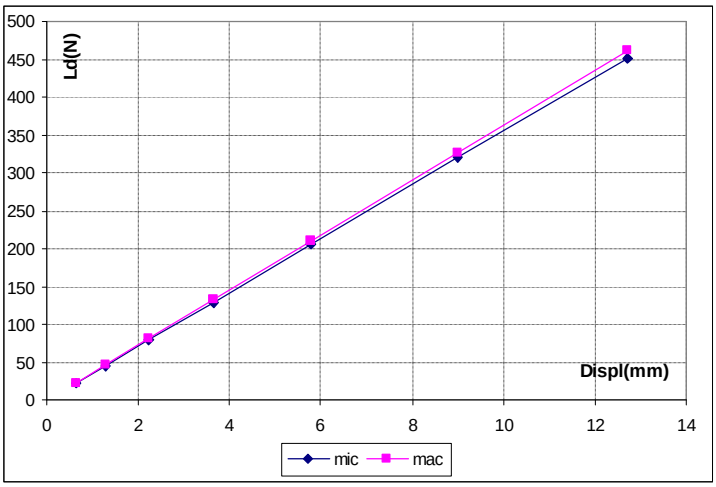

Figure 6.11 P809 - Micro and macro models – load-displacement

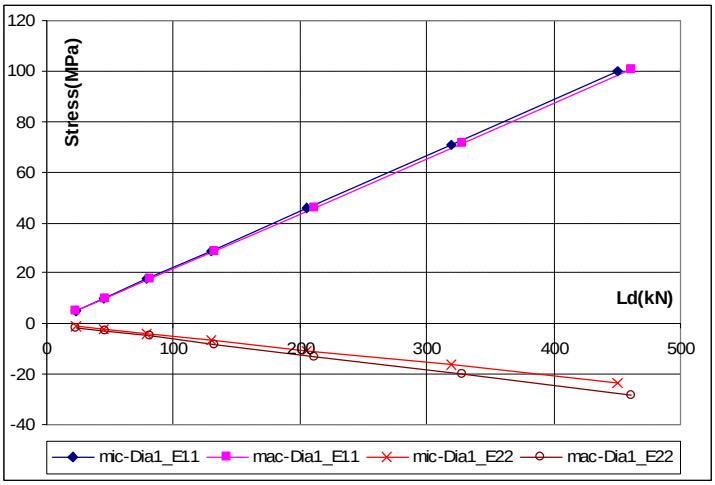

Figure 6.12 P809 - Micro and macro models – Dia_E stresses

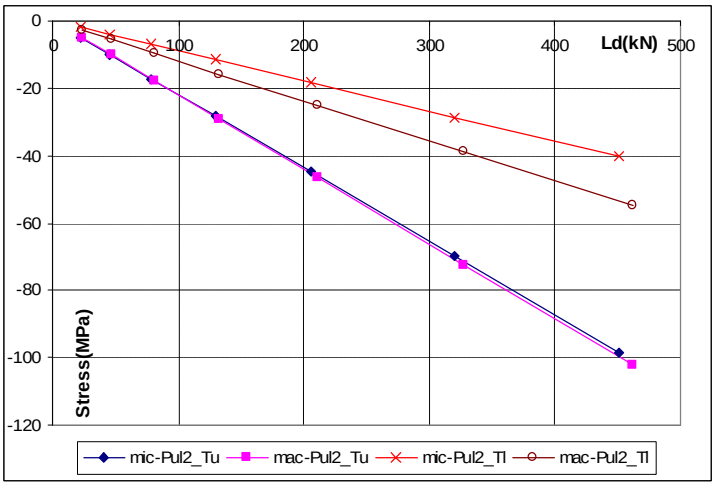

Figure 6.13 P809 - Micro and macro models – Pul2_T stresses

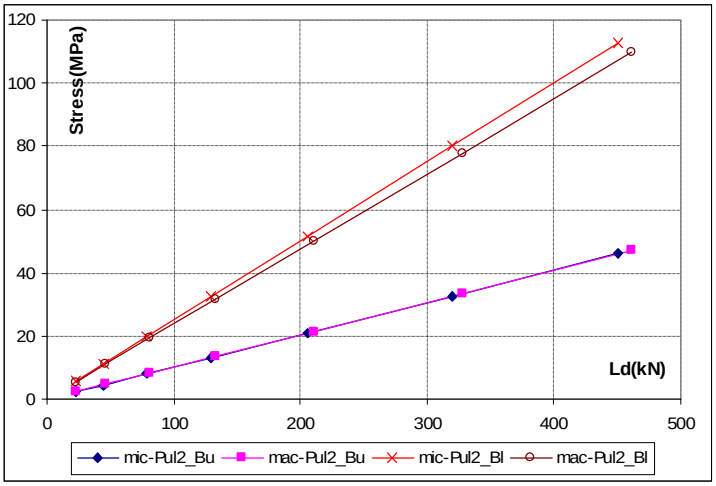

Figure 6.14 P809 - Micro and macro models – Pul2_B stresses

6.4.3. P809 - MACRO MODEL DISCUSSIONS

The analysis time for the macro-model was 4s while that of the micro-model was 1920s. The macro-model predicted the panel behaviour very well at much less computational cost. The effect of the test set-up and the slenderness assumption in using beam elements showed some effect on predicting the stresses at the lower flange of the top chord (Pul2_Tl, Figure 6.13). However this effect can be considered insignificant and the simplified modelling procedures can be considered sufficiently accurate to predict the panel behaviour.

6.5. CONCLUSIONS

The discrete-diagonal (DD) and the diaphragm (DI) multi-pultrusion panels showed excellent structural performance that included high load-carrying capacity. The FE modelling procedures were successfully implemented, at micro level, to predict their response to loads and to develop a basic understanding of their behaviour. However, the micro-analysis was time-consuming and could only be used practically on limited-size panels. This necessitated conducting FE modelling at the macro-level. This was to allow the conduct of quick parametric studies prior to the conduct of more expensive micro-analysis. In addition, it provided a model with a sufficient level of accuracy for the design of the panels that can be used for overall frame analysis.

The macro-models were based on using beam elements for the chord and vertical members and shell elements for the gussets, diagonals and diaphragms. The shell elements boundaries were formed by the faces of the connected members, while the beam elements were located at the centreline of the related members. The beam elements constrained the adjacent shell elements by using node-to-surface tie constraints. Similar to the micro-model, analyses were conducted in three stages for the DD panel. To predict the buckling behaviour of the panel (i) Eigen-Value analysis was conducted to obtain the panel mode shape. The mode shape was used as an imperfection in (ii) Riks analysis, reaching a load level lower than the buckling capacity of the panel. Then (iii) non-linear displacement-controlled analysis was used until reaching the required displacement. DI panel analysis was a single-step linear analysis.

The macro-model predicted very well the behaviour of the different panel components. The only difference in predictions was found in the lower flange of the top chord. This was attributed to not fully satisfying the slenderness assumption for using beam elements. However, this difference can be considered insignificant as it was related to the test set-up.

6.6. REFERENCES

Hibbitt, Karlsson & Sorensen Inc. (2004a). *ABAQUS Analysis user's manual*.

Hibbitt, Karlsson & Sorensen Inc. (2004b). *ABAQUS Theory manual*.

7. Conclusions and Suggestions for Further Research Work

7.1. INTRODUCTION

Deployable shelters are an important sub-set of deployable structures that can be used for military and/or civil applications. The M^2S^2 deployable shelter system is a further development of the stressed-arch concept implemented by Strarch in their steel frames. The M^2S^2 research programme aims to extend the existing Strarch concept into a system with dramatically improved deployment characteristics. This study was not a research project that had pre-defined research outcomes. It was the first to investigate the concept of M^2S^2, a fibre composite re-deployable curved shelter system, and a number of important aspects had to be addressed prior to conducting detailed investigations. These include reviewing available deployable shelter systems, investigating the deployability requirements, assessing the loading criteria and the member forces, exploring the structural systems for composite trusses, investigating different modular panel alternatives that suit the concept of M^2S^2 and then developing an understanding of the main behavioural issues of these alternatives.

Conclusions presented in this chapter are divided into three parts. The first part relates to the different structural systems of the composite trusses, concluding with the main behavioural aspects of the multi-pultrusion truss system (MPTS). The second part relates to the FE modelling of the MPTS, both at the micro-level and the macro-level. The third part relates to general conclusions observed from the course of this study. The chapter closes with suggestions for further research work.

7.2. STRUCTURAL SYSTEMS FOR COMPOSITE TRUSSES

Fibre composites are relatively new materials for use in civil engineering applications. Their unique nature and flexibility add complexity to their application as a construction material when compared to traditionally-used timber, steel and concrete. Based on the literature review and the investigations conducted during this study, the main conclusions regarding the fibre composite truss systems can be summarised as:

- In conventional truss systems, the use of pultruded sections with bolted and/or adhesive joints limits the full mobilisation of the fibre composite materials used. The use of these systems can be justified, as the serviceability limit state of deflection and/or durability can be the governing limit states, and accordingly, the pultrusions used are not usually stressed to their limit.
- Due to the arch-shaped geometry of M^2S^2 frames, the deflection of the frames is not a governing limit state. In addition, the frame members carry high forces. Thus following the conventional truss system will provide inefficient uneconomical solution.
- In a bonded joint, the properties of the adhesive, the adherent and the joint geometry significantly affect the joint capacity and mode of failure. In general, using higher inter-laminar shear resins along with stiffer and thinner adherents and symmetric joint lay-up, improve the joint capacity. However, the use of gussets in the truss joints limits the improvement in its capacity due to the concentration of stresses associated with transferring all the bracing member forces through the gusset.
- In this study, this limitation was overcome by introducing the concept of Multi-Pultrusion Truss System (MPTS). In this system, the chord members (which usually carry more forces compared with other members) and the vertical members were formed from a number of pultrusions in a plane-truss construction, with two alternatives for the sandwich bracing system.
- In the MPTS, the use of gussets was eliminated by extending the skins of the sandwich bracing between the pultrusion members in adhesively bonded joints. This modification had many advantages: (i) direct force transfer

between the truss members, (ii) the skins functioned as the gusset plate to join the vertical members to the chord members, (iii) provided continuous media of adhesive layers which reduced the stress concentrations in the adhesion significantly, and (iv) the joint layout was favourable in having a double-lap joint between each two-pultrusions with rigid box-section adherents.

- In all of the tested MPTS, the ultimate capacity failure occurred in the bracing system. This means that the composites were utilised to their limit with the advantage of achieving controlled failure mode.
- Both of the MPTS alternatives had a high load-carrying capacity with a very well predictable behaviour. The tested panels had structural redundancy, as alternative load paths were formed once reaching the ultimate capacity.
- The main characteristic of the MPTS was the confinement effect of the bracing system between the adjacent vertical and chord members. This generated bi-axial forces, of opposite sign, which led to failure initiation and propagation in the skins of the bracing system.
- The Discrete-Diagonal Multi-Pultrusions Truss System (DD-MPTS) was the first system to be investigated. When the panel diagonals were under tension, lateral compression stresses were generated at the corners, due to the confinement effect. In this loading condition, the system had redundancy. After reaching the ultimate capacity, the skins of one of the diagonals failed partially, by rupturing of its fibres under the bi-axial stress condition. This led to losing part of its strength. Increasing the applied loads utilised the strength of the undamaged side of the skins until reaching the point of final failure.
- When the diagonals were under compression, the core material of the diagonal was identified as the critical factor in defining the panel capacity as failure occurred by global shear buckling. This was the only loading condition where sudden failure occurred. However, this failure mode was predicted accurately by using the FE modelling and/or the analytical equations (for sandwich columns assuming clamped-end conditions).
- The Diaphragm Multi-Pultrusions Truss System (DI-MPTS) was the second alternative to be investigated. Using diaphragms with no core material led to excessive buckling, which generated secondary bending stresses. This

reduced the load-carrying capacity of the panel, with forces concentrated within the central half of the diaphragm. In this set-up, the diaphragm behaved as a tension-only membrane with confined compressive stresses which initiated failure at the diaphragm corners.

- When the core material was introduced to form a sandwich bracing system, the diaphragm forces were evenly shared between compression and tensile directions. This resulted in panels with a very high load-carrying capacity. The concentration of stresses in the other components were eliminated due to the continuous transfer of forces at the diaphragm interface.
- The continuous nature of the diaphragm provided significant redundancy in the panel system that prevented the occurrence of complete loss of strength in reaching the ultimate capacity.
- The structural performance of the MPTS can be attributed to loading each of their components in its strength direction. This system maximised the advantages of using fibre composites in a new truss system.

7.3. MODELLING CONSIDERATIONS OF THE MPTS

Two levels of FE analyses were conducted during this study. The micro-model analysis enabled the development of a basic understanding of the behaviour of the DD-MPTS and the DI-MPTS. The macro-model analysis established simplified modelling procedures that can be used as a preliminary to the more expensive micro-analysis (to set the different panel parameters) and for the overall analysis of frames of these panel types. The main modelling recommendations at these two levels are detailed in Sec 7.3.1 and Sec. 7.3.2.

7.3.1. FE MICRO MODEL

- Three-dimensional thick shell elements provided good representation for the pultrusions, the diagonal skins, the gussets and the packers between the pultrusions.
- Reduced-integration shell element models delivered solutions at slightly less cost compared to full-integration shell models with the same accuracy level.

- Due to the closed shape of the pultrusions, it was necessary to compensate for the overlapping effect of the shells at corners by using an equivalent shell thickness.
- Core material and adhesive layers were modelled using reduced-integration second-order solid continuum elements.
- Surface-to-surface and node-to-surface tie constraints were found to be a convenient modelling practice to join each of the model parts.
- For the DD-MPTS with diagonals under compression, analysis needed to be conducted in three steps. The imperfection was introduced to the model by retrieving the nodal modal shape from Eigen-Value analysis. Then arc-length (Riks) analysis was conducted on this imperfect geometry. Due to having both the load and displacement as unknowns, Riks analysis was terminated prior to reaching the buckling capacity of the panel, when geometrically nonlinear analysis was then used with controlled displacement.
- The no-core DI-MPTS was found to be a highly nonlinear problem. However, three steps analysis procedures provided good representation of the panel behaviour.
- An alternative analysis approach was established by introducing imperfection by applying a disturbing displacement to the centre of the diaphragm in the first step. Then this displacement was released in the second step where the main loads were applied. This alternative was found more efficient to analyse, compared to Riks analysis. However, the accuracy of the analysis was found to be dependent on the level of applied imperfection. In general, an imperfection that at least equalled the thickness of the shell elements provided reasonably accurate results.
- Due to its nature, as a shear wall, the DI-MPTS panel with complete core filling was accurately modelled using linear analysis procedures.

7.3.2. FE MACRO MODEL

- Three-dimensional beam elements were used for the chord and the vertical members.

- The assumption of a rigid connection between the vertical member ends and the chord members was found to be satisfactory. In addition, it simplified the modelling procedures.
- Three-dimensional thick shell elements were used for the gussets, the diagonals and the diaphragms.
- The shell elements boundaries were formed by the faces of the connected members, while the beam elements were defined at the centreline of the related members.
- The beam elements constrained the adjacent shell elements by using node-to-surface tie constraints.
- Similar to the micro-model, analyses were conducted in three stages for the DD-MPTS while single-step linear analysis was conducted for the DI-MPTS panel.
- The macro-model predicted very well the behaviour of the different panel components. The only difference with the micro-model predictions was found in the lower flange of the top chord. This was attributed to not fully satisfying the slenderness assumption for using beam elements. This difference can be considered insignificant as it was related to the test set-up.

7.4. GENERAL CONCLUSIONS

The general conclusions related to the current investigations are summarised as follows:

- Frame-supported shelter systems are the most commonly-used systems for deployable shelters with reasonably free spans. The concept of prestressed arch technology was found to be unique. None of the identified systems used fibre composite materials for the main frames.
- Good practice in the development and implementation of fibre composite systems is to use as many standard components as possible, simplify the concept with the least force transfers, avoid concentration of stresses, and to exploit the unique properties of composite materials. Simulating technologies

used with other construction materials can result in expensive, inefficient, structural composite systems.

- The MPTS was simple to manufacture, with few system components, and easy to analyse, once establishing the analysis procedures. It utilised the characteristics of fibre composites and achieved good structural performance. In addition, the system behaviour was insensitive to minor manufacturing defects, tolerating some variance in production and further reduction in the associated manufacturing costs.
- The intentions to model the failure process of the DD-MPTS were replaced by further development of the concept of the DI-MPTS. This was mainly due to the limitations in predicting the failure and post-failure behaviour of fibre composites using the available analysis tools and theories. This decision facilitated research into further structural systems and their behaviours.
- Using elastic material models in linear (for cored DI-MPTS) and nonlinear (for non-cored DI-MPTS and DD-MPTS) analyses was found to be suitable for predicting the behaviour of both truss systems. In addition, using Tsai-Wu failure criteria, based on the model predictions, provided reasonable predictions of the laminate failure.
- The macro-analysis models provided quick and efficient ways to predict the behaviour of the MPTS. For the DD-MPTS, the diagonal capacity can be predicted by using Allen's buckling equation (Allen and Feng, 1997).
- In reaching the first suggestion for the diagonal fibre architecture, macro-analysis can be conducted to assess the effect of confinement and the overall panel behaviour. In conducting a few iterations of this type, the suggested panel layout can be obtained for further micro-analysis.

7.5. SUGGESTIONS FOR FURTHER RESEARCH WORK

During the course of this study, ideas that need to be explored in future research were identified. Areas for further research are suggested below.

- As seen in the literature, each deployable shelter system was based on different design criteria. An international system is needed to assess the design loads on these structures. This system should acknowledge regional differences and practices. The proposed loading scenarios, Appendix A, can be considered as a preliminary effort that addressed and tried to rationalise this issue.
- Fire-resistance is another area that needs to be addressed. More clear and realistic fire resistance requirements should be specified for these types of structures. In addition, a testing technique should be established to verify these requirements.
- Using fibre composite materials for the main structural framing system may necessitate further material research regarding fire resistance. This could lead to further development of resin systems (either incorporated into the structural composites or provide protective coatings). The cost factor is another challenge for application in civil engineering.
- Macro-analysis modelling concepts should be combined with the proposed frame analysis technique (Appendix B) to conduct overall frame analysis that covers overall stability. The output of this analysis should be used to assess the suitability of the used properties. In reaching satisfactory model behaviour, full-scale or scaled frames testing should be conducted.
- The long-term effects on the structural components, especially chord members that are continuously under compressive forces, need to be addressed and investigated. The MPTS joining system has the advantage of having joints concealed between the multi-pultrusions. However, temporal effects should be investigated on this system as well. So that, the most appropriate resin systems can be selected for the pultrusions and adhesives.
- The M^2S^2 can be considered as a hybrid system with a combination of composite panels and steel prestressing cables. The effect of temperature, friction and time on the system as a structure should be investigated.
- The investigations for the MPTS were conducted on panels with square bays. However, panels with different geometries (aspect ratios) need to be

investigated to develop a more general approach for these systems and to ensure the accuracy of predicting their behaviour.

- The joining system is an integral part of any truss system. The M^2S^2 joining system needs more attention due to the changing nature of the structure. Innovative joint systems need to be explored by investigating the different parameters that affect their capacity and behaviour.
- With the new system of M^2S^2 and using the MPTS for the main frames, suitable roof sheeting and end walls are other challenges that need to be considered. The change in the geometry of the structure and potential stability requirements for the main frames need to be investigated within the framework of the roof sheeting and end-wall systems.
- The concept of using mixed-core sandwich construction needs further investigation. This concept can provide some redundancy, by controlling the failure mode, to avoid the sudden failure mode observed in sandwich columns.

Bibliography

Adams, R. D. (1997). *Structural adhesive joints in engineering*, Chapman and Hall, London.

Ahmed, S., Irons, S., and Zienkiewicz, O. C. (1970). Analysis of thick and thin shell structures by finite elements. *International Journal of Numerical Meth Engineering*, 2, 419-451.

Aiello, M. A., and Ombres, L. (1997). Local buckling loads of sandwich panels made with laminated faces. *Composite Structures*, 38(1-4), 191-201.

Akfert, A. (1994). Finite element analysis of composite sandwich beams and plates, MSc, University of Manchester, Manchester.

Allen, H. G. (1969). *Analysis and design of structural sandwich panels*, Pergamon Press, Oxford.

Allen, H. G., and Feng, Z. (1997). Classification of structural sandwich panel behaviour. Mechanics of Sandwich Structures, Proceeding of the EUROMECH 360 Colloquium, A. Vautrin, ed., Kluwer Academic Publishers, Saint-Etienne, France, 1-12.

Anon. (1955). Materials, properties and design criteria Part II, sandwich construction for aircraft. *MIL-HDBK-23*, Department of the Air Force Research and Development, USA.

Ayers, S. R. (2001). Material foundations for the application of fibre composite materials in civil and structural engineering, PhD, University of Southern Queensland, Toowoomba.

Bakis, C. E., Brown, V. L., Cosenza, E., Davalos, J. F., Lesko, J. J., Machida, A., Rizkalla, S. H., and Triantafillou, T. C. (2002). Fibre-reinforced polymer composites for construction, State-of-the-art review. *J for Composites for Construction*, 6(2), 73-87.

Batts, M. E., Cordes, M. R., Russell, L. R., Shaver, J. R., and Simiu, E. (1980). Hurricane wind speeds in the United States. Washington, D.C.

Bazant, Z. P. (1971). A correlation study of incremental deformations and stability of continuous bodies. *ASME Journal of Applied Mechanics*, 38, 919-928.

Bazant, Z. P. (2003). Shear buckling of sandwich, fiber composite and lattice columns, bearings, and helical springs: paradox resolved. *ASME Journal of Applied Mechanics*, 70, 75-83.

Bazant, Z. P., and Beghini, A. (2004). Sandwich buckling formulas and applicability of standard computational algorithm for finite strain. *Composites Pt B*, 35,

573-581.

Bazant, Z. P., and Cedolin, L. (1991). *Stability of structures*, Oxford University Press Inc, Oxford.

Bitzer, T. N. Recent honeycomb core developments. (1992). *Second International Conference on Sandwich Construction*, UK, 555-563.

Bradford, N., Sen, R., and Mosallam, A. (2001). Development of a new modular composite panel system. *46th International SAMPE Symposium and Exhibition 2001 a Materials and Processes Odyssey*, Long Beach, CA, USA, 931-942.

Brown, J. R., and St John, N. A. (1996). Fire retardant low temperature cured phenolic resins and composites. *TRIP*, 4(12), 416-420.

Brown, R. T., and Zureick, A. (2001). Lightweight composite truss section decking. *Marine Structures*, 14, 115-132.

Budiansky, B., and Sanders, J. L. (1963). On the `Best' first-order linear shell theory. *Progress in Applied Mechanics*, The Prager Anniversary Volume(Macmillan), 129-140.

Butalia, T. S., and Wolfe, W. E. (2002). A strain-energy based failure criterion for nonlinear analysis of composite laminates subjected to bi-axial loading. *Composites Science and Technology*, 62, 1697-1710.

Carradine, D. M., and Plaut, R. H. (1998). Arch supported membrane shelters under wind and snow loading. *International journal of space structures*, 13(4), 197-202.

Challa, G. (1993). Polymer chemistry: An introduction. Ellis Horwood Ltd, Chichester.

Clarke, J. L. (1996). Structural design of polymer composites - Eurocomp. E & FN Spon, London.

Clarke, M. J., and Hancock, G. J. (1994). Behaviour and design of stressed-arch (Strarch) frames. *IASS-ASCE International Symposium 1994 on spatial, lattice and tension structures*, Atlanta, USA, 200-209.

Clarke, M. J., and Hancock, G. J. (1995). Tests and nonlinear analysis of small scale stressed-arch frames. *Journal of Structural Engineering*, 121(2), 187-200.

Clarke, R. C. The kinematics of novel deployable space structure system. *3rd International Conference on Space Structures*, Guildford, United Kingdom.

Conner, A. H., Lorenz, L. F., and Hirth, K. C. (2002). Accelerated cure of phenol-formaldehyde resins: studies with model compounds. *Journal of Applied Polymer Science*, 86, 3256-3263.

Davies, J. M. Design criteria for sandwich panels for building construction. (1997). *ASME Aerospace Division, Structures and Materials Committee, ASME-AD_Vol 55*, New York, 273-284.

Davila, C. G., Camanho, P. P., and Rose, C. A. (2005). Failure criteria for FRP laminates. *Journal of Composite Materials*, 39(4), 323-345.

Dreher, G. (1992). Stability failure of sandwich structures. *Sandwich Constructions 2*

- *Proceedings of the Second International Conference on Sandwich Construction*, Gainesville, Florida, USA.

Engesser, F. (1891). Die knickfestigkeit gerader stabe. *Zentralblatt des Bauverwaltung*, 11, 483-486.

Euler, L. (1744). De curvis elasticis. Burges, Lausanne, Switzerland.

Fairbairn, W. (1849). *An account of the construction of the Britannia and Conway tubular bridges*, John Weale, London.

Ferreira, A. J. M., Maques, A. T., and de Sa, J. C. (1998). Comparison of three shear-deformation theories in the nonlinear analysis of sandwich shell elements. Mechanics of sandwich structures, A. Vautrin, ed., Kluwer Academic Publishers, Saint-Etienne, 79-88.

Fitzer , E., and Manocha, L. M. (1998). *Carbon reinforcements and carbon/carbon composites*, Springer-Verlag, Karlsruhe.

Fleck, N. A. (1997). Compressive failure of fibre composites. *Advances in Applied Mechanics*, 33, 43-117.

Fleck, N. A., and Sridhar, I. (2002). End compression of sandwich columns. *Composites Pt A*, 33, 353-359.

Fowler, W., and Sinofsky, M. (1986). Development of an improved air-supported battalion aid station. *TR-88/029L*, US Army Natick Soldier Centre, Buffalo, New York.

Gere, J. M., and Timoshenko, S. P. (1990). *Mechanics of materials*, PWS-KENT Publishing Company, Boston.

Gibson, L. J., and Ashby, M. F. (1997). *Cellular solids: structure & properties*, Cambridge University Press, Cambridge.

Gilby, J. (1998). Pultrusion provides roof solution. *Reinforces Plastics*, 42(6), 48-52.

Globalsecurities. Homepage, http://www.globalsecurity.org/military/systems/aircraft/systems/xldahs-pics.htm.

Goldsworthy, W. B., and Hiel, C. (1998). Composite structures. *SAMPE Journal*, 34, 24-30.

Goodman, S. H. (1998). Handbook of thermoset plastics. Noyes Publications, New Jersey.

Gotsis, P. K., Chamis, C. C., and Minnetyan, L. (1998). Prediction of composite laminate fracture: micromechanics and progressive fracture. *Composites Science and Technology*, 58, 1137-1149.

Gotsis, P. K., Chamis, C. C., and Minnetyan, L. (2002). Application of progressive fracture analysis for predicting failure envelopes and stress-strain behaviors of composite laminates: a comparison with experimental results. *Composites Science and Technology*, 62, 1545-1559.

Han, S., Kim, W. G., and Yoon, H. G. (1998). Curing reaction of biphenyl epoxy resin with different phenolic functional hardners. *Journal of Polymer Science - Part A*, 36, 773-783.

Han, S., Kim, W. G., and Yoon, H. G. (1998). Kinetic study of the effect of catalysts on the curing of biphenyl epoxy resin. *Journal of Applied Polymer Science*, 68, 1125-1137.

Haringx, J. A. (1948). On highly compressible helical springs and rubber rods and their application for vibration-free mounting. *Philips Research Report Vol.3*, Eindhoven.

Hashin, Z. (1980). Failure criteria for unidirectional fibre composites. *Journal of Applied Mechanics*, 47, 329-334.

Haug, A., and Jamjian, M. (1996). Numerical simulation of the impact resistance of composite structures. Numerical analysis and modelling of composite materials, J. W. Bull, ed., Blackie Academic, London, 185-244.

He, G., Riedl, B., and Ait-Kadi, A. (2002). Curing process of powdered phenol-formaldehyde resol resins and the role of water in the curing systems. *Journal of Applied Polymer Science*, 89, 1371-1378.

Heap, P. Advanced composites in civil engineering - a critical overview at this high interest, low use stage of development. (1996). *Advanced Composite Materials in Bridge Structures ACMBS II*, Montreal, Canada, 3-15.

Hiltz, J. A., Kuzak, S. G., and Waitus, P. A. (2001). Effect of thermal exposure on the properties of phenolic composites: dynamic mechanical analysis. *Journal of Applied Polymer Science*, 79, 385-395.

Hinton, M. J., Kaddour, A. S., and Soden, P. D. (2002a). Evaluation of failure prediction in composite laminates: background to part 'B' of the exercise. *Composites Science and Technology*, 62, 1481-1488.

Hinton, M. J., Kaddour, A. S., and Soden, P. D. (2002b). A comparison of the predictive capabilities of current failure theories for composite laminates judged against experimental evidence. *Composites Science and Technology*, 62, 1725-1797.

Hinton, M. J., and Soden, P. D. (1998). Predicting failure in composite laminates: the background to the exercise. *Composites Science and Technology*, 58, 1001-1010.

Hoff, N. J. (1986). *Monocoque, sandwich and composite aerospace structures*, Technomic Publishing Company, Lancaster, PA.

Hoff, N. J., and Mautber, S. E. (1945). The buckling of sandwich type panels. *Journal of Aeronautical Sciences*, 12(3), 285-297.

Hollaway, L. (1994). *Handbook of polymer composites for engineers*, Woodhead Publishing, Cambridge.

Holmes, J. D. (2001). *Wind loading on structures*, Spon Press, London.

Huang, H., and Kardomateas, G. A. (2002). Buckling and initial postbuckling behavior of sandwich beams including transverse shear. *AIAA Journal*, 40(11), 2331-2335.

Humphreys, M. F. (2003). Development and structural investigation of monocoque fibre composite trusses, Queensland University of Technology, Brisbane.

Humphreys, M. F., Van Erp, G. M., and Tranberg, C. (1999). The structural

behaviour of monocoque fibre composite truss joints. *Advanced Composite Letters*, 8(4), 173-180.

Jeandrau, J. P. (1991). Analysis and design data for adhesively bonded joints. *International Journal of Adhesion and Adhesives*, 11(2), 71-79.

Kabhari, V. Application of composite materials to the renewal of twenty-first century infrastructure. (1997). *Eleventh International Conference on Composite Materials*, Gold Coast, Australia.

Kardomateas, G. A., and Simitses, G. J. (2004). Comparative studies on the buckling of isotropic, orthotropic and sandwich columns. *Mechanics of Advanced Materials and Structures*, 11, 309-327.

Keller, T. (2001). Recent all-composite and hybrid fibre-reinforced polymer bridges and buildings. *Prog. Structural Engineering Materials*, 3, 132-140.

Key, P. W. (2004). The Starch modular military shelter system - Load specification. Strarch, Sydney.

Ko, T., and Ma, T. (1998). Effect of post curing on the mechanical properties of carbonized phenolic resins. *Polymer composites*, 19(4), 456-462.

Krayer, W. R., and Marshall, W. R. (1992). Gust factors applied to hurricane winds. *Bulletin of the American Meteorological Society*, 73, 613-617.

Kumar, S. (1989). Structure and properties of high performance polymeric and carbon fibers - an overview. *SAMPE Quarterly*, 20(2), 3-8.

Kuraishi, A., Tsai, S. W., and Liu, K. K. S. (2002). A progressive quadratic failure criterion - part B. *Composites Science and Technology*, 62, 1683-1695.

Lee, J. D. (1982). Three dimensional analysis of damage accumulation in composite laminates. *Composite Structures*, 15(3), 335-350.

Li, Q. M., Mines, R., and Birch, R. S. (2000). The crush behaviour of Rohacell-51WF structural foam. *International Journal of Solids and Structures*, 37, 6321-6341.

Librescu, L., and Hause, T. (2000). Recent developments in the modeling and behavior of advanced sandwich constructions: a survey. *Composite Structures*, 48, 1-17.

Liu, K. S., and Tsai, S. W. (1998). A progressive quadratic failure criterion for a laminate. *Composites Science and Technology*, 58, 1023-1032.

Lubin, G. (1982). Handbook of composites. Van Nostrand Reinhold, New York, 272-317.

Maiti, S. K., Gibson, L. J., and Ashby, M. F. (1984). Deformation and energy absorption diagrams for cellular solids. *Acta Metallurgica*, 32(11), 1963–1975.

Mamalis, A. G., Manolakos, D. E., Ioannidis, M. B., and Papapostolou, D. P. (2005). On the crushing response of composite sandwich panels subjected to edgewise compression: experimental. *Composite Structures*, 71, 246-257.

Manet, V., Han, W. S., and Vautrin, A. (1998). Static analysis of sandwich plates by finite elements. Mechanics of sandwich structures, A. Vautrin, ed., Kluwer

Academic Publishers, Saint-Etienne, 53-60.

March, H. W. (1955). Effects of shear deformation in the core of a flat rectangular sandwich panel. Report 1583.

Marguerre, K. (1944). The optimum buckling load of a flexibly supported plate composed of two sheets joined by a light weight filler, when under longitudinal compression. *ZWB UM 1360/2,* Deutsche Vierteljahrsschrist für Literalurwissenschaft und Giests Geschichte, D V L.

Medeiros, E. S. d., Agnelli, J. A. M., Joseph, K., de Carvalho, L. H., and Mattoso, L. H. C. (2003). Curing behaviour of a novolac-type phenolic resin analysed by differential scanning calorimetry. *Journal of Applied Polymer Science,* 90, 1678-1682.

Mines, R., and Alias, A. (2002). Numerical simulation of the progressive collapse of polymer composite sandwich beams under static loading. *Composites Pt A,* 33, 11-26.

Mines, R., and Jones, N. (1995). Approximate elastic-plastic analysis of the static and impact behaviour of polymer composite sandwich beams. *Composites,* 26(12), 803-814.

Mines, R., Worrall, C. M., and Gibson, L. J. (1994). The static and impact behaviour of polymer composite sandwich beams. *Composites*, 25(2), 95-110.

Mirawate, A. (1999). 3-D textile reinforcements in composite materials. 4.

Mouritz, A. P. (2002). Post-fire flexure properties of fibre reinforced polyester, epoxy and phenolic composites. *Journal of Materials Science,* 37, 1377-1386.

Mouritz, A. P., and Mathys, Z. (1999). Post-fire mechanical properties of marine polymer composites. *Composite Structures*, 47, 643-653.

Mouritz, A. P., and Mathys, Z. (2000). Mechanical properties of fire-damaged glass-reinforced phenolic composites. *Fire and Materials*, 24, 67-75.

Muc, A., and Zuchara, P. (2000). Buckling and failure analysis of FRP faced sandwich plates. *Composite Structures,* 48, 145-150.

Omar, T., Heldt, T., Key, P., and Van Erp, G. M. (2006). M2S2 modular deployable composite shelters - comcept and loading criteria. *Australian Journal of Structural Engineering*, 6(3), 217-226.

Osswald, T. A. (1995). *Materials science of polymers for engineers*, Hanser/Gardner, Munich.

Pagano, N. J. (1970). Exact solutions for rectangular bidirectional composites and sandwich plates. *Journal of Composite Materials,* 4, 20-34.

Park, B., Reidl, B., Kim, Y. S., and So, W. T. (2002). Effect of synthesis parameters on thermal behaviour of phenol-formaldehyde resol resin. *Journal of applied polymer science,* 83, 1415-1424.

Peterka, J. A., and Shahid, S. (1998). Design gust wind speeds in the United States. *Journal of Structural Engineering,* 124(2), 207-214.

Peters, S. T. (1998). Handbook of composites. Chapman & Hall, London.

Potluri, P., Kusak, E., and Reddy, T. Y. (2003). Novel stitch-bond sandwich

composite structures. *Composite Structures*, 59, 251-259.

Puck, A., and Schurmann, H. (1998). Failure analysis of FRP laminates by means of physically based phenomenological models. *Composites Science and Technology*, 58, 1045-1067.

Puck, A., and Schurmann, H. (2002). Failure analysis of FRP laminates by means of physically based phenomenological models. *Composites Science and Technology*, 62, 1633-1662.

Quinn, J. A. (1999). *Composites design manual*, First Technomic Publishing.

Raskin, I. (1998). Stiffness and stability of deployable pantographic columns, PhD, University of Waterloo, Waterloo, Ontario.

Raskin, I., and Roorda, J. (1996). Buckling force for deployable pantographic columns. *Proceedings of MARAS'96, the second International Conference on Mobile and Rapidly Assembled Structures*, Seville, Spain, 305-314.

Redjel, B. (1995). Mechanical properties and fracture toughness of phenolic resin. *Plastics, Rubber and Composites Processing and Applications*, 24(4), 221-228.

Rheinfrank, G. B., and Norman, W. A. (1944). Molded glass fiber sandwich fuselage for BT-15 airplane. Army Air Corps Technical Report No 5159, USA.

Shariatmadari, A. A., Parry, T. V., and Parton, G. M. (1996). Fracture strength and toughness of some phenolic concretes. *Journal of materials science*, 31, 413-422.

Shen, H., Lavoie, A. J., and Nutt, S. R. (2003). Enhanced peel resistance of fiber reinforced phenolic foams. *Composites A*, 34, 941-948.

Soden, P. D., Hinton, M. J., and Kaddour, A. S. (1998). Comparison of the predictive capabilities of current failure theories for composite laminates. *Composites Science and Technology*, 58, 1225-1254.

Sun, C. T., and Tao, J. (1998). The prediction of failure envelopes and stress-strain behavior of composite laminates. *Composites Science and Technology*, 58, 1125-1136.

Sun, C. T., Tao, J., and Kaddour, A. S. (2002). The prediction of failure envelopes and stress-strain behavior of composite laminates: comparison with experimental results. *Composites Science and Technology*, 62, 1673-1682.

Tsai, S. W. (1991). *Composite Design*, Think Composites, Dayton, Ohio.

Turvey, G. J. (2000). Bolted connections in PFRP structures. *Prog. Structural Engineering Materials*, 2, 146-156.

Tyberg, C. S. (2000). Void-free flame retardant phenolic networks: properties and processability, PhD, Virginia Polytechnic Institute and State University.

Tyberg, C. S., Sankarapandian, M., and Bears, K. (1999). Tough, void free, flame retardant phenolic matrix materials. *Construction and Building Materials*, 13, 343-353.

Vaidya, U. K., V, H. M., Kumar, P., Mahfuz H, Haque, A., and Jeelani, S. (1999). Impact damage resistance of innovative functional sandwich composite.

Symposium on Recent Developments in the Study of Impacts on Composite Materials with ASME 1999 Mechanics and Materials Conference, VA.

Vannucci, P., Aivazzadeh, S., and Verchery, G. (1998). A comparative analysis of some theories and finite elements for sandwich plates and shells. Mechanics of sandwich structures, A. Vautrin, ed., Kluwer Academic Publishers, Saint-Etienne, 45-52.

Vickery, P. J., and Twisdale, L. A. (1995a). Windfield and filling models for hurricane wind speed predictions. *Journal of Structural Division*, 121(11), 1700-1709.

Vickery, P. J., and Twisdale, L. A. (1995b). Prediction of hurricane wind speed in the United States. *Journal of Structural Division*, 121(11), 1691-1699.

Wang, Z.-W. (1997). The geometrically nonlinear theory of anisotropic sandwich shells faced with laminated composites. *Journal of Mech Appl Math*, 50(3), 1393-1403.

Wolfe, W. E., and Butalia, T. S. (1998). A strain-energy based failure criterion for nonlinear analysis of composite laminates subjected to bi-axial loading. *Composites Science and Technology*, 58, 1107-1124.

Wolfrum, J., and Ehrenstein, G. W. (1999). Interdependence between the curing, structure, and the mechanical properties of phenolic resins. *Journal of Applied Polymer Science*, 74, 3173-3185.

Yu, Y. Y. (1962). Nonlinear flexural vibrations of sandwich plates. *Journal of Acoustic Society of America*, 34, 1176.

Zinoviev, P. A., Grigoriev, S. V., Lebedeva, O. V., and Tairova, L. P. (1998). The strength of multilayered composites under a plane stress state. *Composites Science and Technology*, 58, 1209-1223.

Zinoviev, P. A., Lebedeva, O. V., and Tairova, L. P. (2002). A coupled analysis of experimental and theoritical results of numerical predictions and experimental observations for symmetric composite laminates. *Composites Science and Technology*, 62, 1711-1723.

Appendix A Notations

$\mathbf{M_d}$	Wind direction multiplier
$\mathbf{M_s}$	Shielding multiplier
$\mathbf{M_t}$	Topographic multiplier
$\mathbf{M_{z,cat}}$	Terrain/height multiplier
$\mathbf{V_{25}}$	3s gust wind speed based on 25 years return period
$\mathbf{V_{50}}$	3s gust wind speed based on 50 years return period

Appendix A: Assessing Loads on Deployable Shelters

A.1. INTRODUCTION

While various forms of deployable shelters are still under development (Chapter 2), the performance and design criteria for such structures are not clearly defined. The major structural loads to be considered can be categorised as dead loads, live loads, wind loads and snow loads. Depending on the cladding system, the dead loads are expected to be 0.08kPa over the whole area of the roof, in addition to the frame's own weight. Live loads are assessed as per the requirements of the related loading codes for curved roofs. They are usually associated with the tributary area of structural elements under consideration. Assuming frames of 35m span and spaced 6m apart, live load is 0.25kPa (AS/NZS 1170.1, 2002) and 0.36kPa (ASCE 7-95, 1996). Snow loads can be considered of a nominal value of 1.0kPa. All of the above mentioned loads can be assessed with little difficulty.

Assessing the wind loading criteria for deployable structures is a challenging process that requires engineering judgement. Loading codes are mainly developed for buildings (of fixed nature) and, whilst more recent codes included some recommendations for deployable structures, none has specific recommendations for deployable shelters. For the different building systems presented in Chapter 2, no justification was found for the specified wind loading criteria. This might be related to the fact that they are used for military applications only. However, the M^2S^2 shelter system can be used for both military and civil applications. Accordingly, there was an early recognition of the need to establish a generic system to determine the design loads for the shelter system. This system should be flexible enough to be used with different international loading codes and a range of different loading scenarios. An important factor that should be considered during this exercise is cost effectiveness. Designing a deployable structure for the worst loading scenario that can happen anywhere around the world would be very expensive and result in a structure that is over-designed for most other locations.

Due to the lightness of the M^2S^2 structure, wind loads are the most critical loading type that determines the design. In addition, it is the most disputable loading type. In this appendix, a wind loading assessment approach is proposed for further consideration. The differences between the loading codes, as located in the literature, are presented, along with an approach to correlate them. For deployable shelters, a wind loading scenario is presented, followed by an example of assessing the wind pressures on frames of 35m span and spaced 6m apart, by applying these scenarios with two different loading codes (AS/NZS 1170.1, 2002 and ASCE 7-95, 1996).

A.2. WIND DATA IN LOADING CODES

Clearly with the international move towards limit states design, this philosophy should form the basis for describing the loading criteria. Holmes (2001) stated that advanced wind loading standards contain the following:

- a specification of a basic (reference) wind speed;
- modification factors for the effect of height and terrain type and sometimes for change of terrain, wind direction, topography and shelter;
- shape factors for the different structural shapes;
- some account of possible resonant dynamic effects of wind on flexible structures.

Basic wind speeds are specified differently in the loading codes. The European pre-standard ENV 1991-2-4 (1997), ISO 4354 (1997) and the Japanese AIJ (1996) based wind load calculation on 10minutes mean wind speed, British code BS6399-Part 2 (1997) used mean hourly wind speed, American codes (ASCE 7-95, 1996) and ASCE 7-98, 1998) along with the Australian/New Zealand code (AS/NZS 1170.2, 2002) used 3s gust wind speed while the American code (ASCE 7-93, 1993) used fastest-mile-of-wind. The first step to consider was to correlate between the different reference wind speeds.

Durst (1960) suggested a relationship between mean hourly, non-cyclonic, wind speed and wind speeds averaged over different times (which was incorporated in the ASCE 7-93 (1993) commentary Table C5). This data was then used by Batts et al (1980) to obtain the fastest-mile-of-wind. Comparing 50 years peak gust wind speeds

from analysis and ASCE 7-93 (1993) based fastest-mile-of–wind, Peterka and Shahid (1998) suggested an average factor of 1.20.

Based on updated information by Krayer and Marshall (1992) gust factors for cyclonic winds are higher than that of non-cyclonic wind by about 10%. Peterka and Shahid (1998) suggested using data published by Batts et al (1980) to obtain peak gusts for cyclonic winds (from fastest-mile-of-wind data) by dividing them by appropriate gust factors in Durst (1960) to obtain the effective hourly mean, then multiplying by the Krayer-Marshall gust factor of 1.69 for cyclones.

Some codes provide guidance on directional wind speed for non-cyclonic wind. This is not applicable in cyclone-prone regions as the maximum wind speed is likely to occur in any direction (AS/NZS 1170.2-Supplementary 1, 2002). Loading standards that deal with cyclonic winds introduced region speed factor to allow for the uncertainties in the predicted design wind speeds. AS/NZS 1170.2 (2002) specifies a factor of 1.05 and 1.10 for tropical cyclone regions C and D respectively. In ASCE 7-93 (1993), a cyclone coast factor of 1.05 was implemented in the importance factor. Peterka and Shahid (1998) noticed that non-cyclonic wind speeds on the cyclonic coast are not significantly different from speeds at interior stations with a typical range of 38m/s to 42.5m/s, for 50 years case, with decreasing speeds on the western coast of the United States.

Tropical cyclones occur over tropical oceans. They rapidly degenerate when they move over land or into cooler water and are usually at full strength between latitude 20 and 30 with the possibility of reaching latitude 10 (Holmes, 2001). Decay of cyclones inland have been predicted by Batts et al (1980) (well beyond 200km) and Vickery and Twisdale (1995a,b) (100km) for 50 years winds. In developing the wind map for ASCE 7-95 (1996), Peterka and Shahid (1998) used a distance of 160km, as specified in ASCE 7-93 (1993). AS/NZS 1170.2-AMDT No 1 (2005) specified 50km in each change from cyclonic regions D to C to B (Figure 3.1-AS/NZS 1170.2, 2002).

A.3. WIND LOADING ON DEPLOYABLE SHELTERS

A typical characteristic of shelter structures is that they generally have large doors. Internal wind pressures can change significantly, in magnitude and in direction, depending on the size and status of the door opening. Accordingly, the decision to design for open-door or closed-door buildings will have a major effect on the overall design. Little information was found in the literature to assist in this decision making. In the case of M^2S^2 the situation is further complicated by the fact that the structure might have no doors at all (i.e open at both sides).

The two major wind categories that are found in the international loading codes are cyclonic wind and non-cyclonic wind. Designing the M^2S^2 structure to withstand cyclonic wind and then using it in non-cyclonic regions has significant cost consequences. Accordingly, the concept used in assessing the wind loads should recognise the necessity of having a cost effective alternative that allows using the structure in both cyclonic and non-cyclonic regions without major cost penalties.

In spite of not specifically being developed for deployable shelters, the Unified Facilities Criteria (UFC) documents specify a few important parameters for designing shelter systems. The UFC 4-211-01N (2004) specifies the borderline between open-door and close-door load cases to be 27m/s. In cyclonic zones, the UFC 3-310-01 (2005) specifies an importance factor for temporary structures of 0.77.

The shelter system is not flexible enough for dynamic wind effects to have a major influence. In assessing shape factors, some differences were found in the different international loading codes (Holmes, 2001). This can be attributed to the fluctuation in the instantaneous wind pressures due to the nature of turbulent flow over large roofs. However, for arched roofs, the maximum negative pressure coefficients in the central part of the roof are quite similar in most international loading codes (Holmes, 2001).

Most deployable shelters are expected to be placed in open terrain. Accordingly, a standard category (water surfaces, open terrain, grassland with few well scattered obstructions) seems reasonable for the shelter ultimate limit state (ULS) design. In assessing wind loads in this project, non-directional wind speed was considered. This

is a conservative approach but, it provides consistency with the different loading codes. Other special factors, such as topography and shelter factors, are not considered due to their local nature.

As shown in Sec. A.2, loading codes have different approaches in assessing the basic wind speed. However, all codes assess the basic wind speed/pressure based on the estimated design life of the structure and its intended use.

The ROC (MCCDC, 1990) specified a minimum design life of 15 years for deployable shelters (Chapter 2). AS/NZS 1170.2 (2002) states that the minimum design working life[1] for ultimate limit state (ULS) considerations of any structure shall be 25 years[2] (Sec 3.3 AS/NZS 1170.2-2002). The expected design life for composite materials is about 25 years. It is a reasonable assumption to set the design life of the M^2S^2 shelter system to 25 years.

M^2S^2 shelters can be used as shelters for military forces, civilian humanitarian aid, natural disaster scenarios and as exhibition halls. When used without doors, the shelter will be of temporary nature (eg exhibition halls). When doors are open, the shelter will be in a temporary stage, until the doors are closed. In using the loading codes, the shelter can be considered as a temporary structure in these two cases (scenario 1). With doors closed, the shelter should be able to carry the maximum site wind loads as a normal structure (scenario 2). This approach was also applied to non-cyclonic regions.

In placing the shelter in a cyclonic region, the related wind loads should be considered. Peterka and Shahid (1998) found that non-cyclonic wind speeds on the cyclonic coasts of the United States are not significantly different from wind speeds at interior stations. Accordingly, it was decided to design the M^2S^2 shelter for the maximum wind speed of the non-cyclonic region directly adjacent to the cyclonic region for scenarios 1 and 2. Cyclonic wind speeds/factors are applied to the structure with doors assumed closed (scenario 3 with cyclone kit installed).

More recent loading codes (like AS/NZS 1170.2 - 2002) combine the design life of the structure and the importance level to assess the annual probability of

[1] The time where the structure is extended and subject to wind, AS/NZS1170-2 2002.
[2] For New Zealand

exceedance, used to calculate the basic wind speed. Other codes have used wind speed factors to accommodate the change in design life of the structure (usually set to 50 years). The importance factor is then used in the calculation of wind pressure (like ASCE 7-95 1996). In the next section the discussed approach is used to assess the wind pressure on the M^2S^2 shelter system using these two types of loading codes.

A.4. WIND PRESSURES ON M^2S^2 USING AS/NZS 1170.2 (2002) & ASCE 7-95 (1996)

Based on the approach presented in Sec. A.3, it is required to assess the wind pressure on a shelter roof placed in a cyclonic zone. The shelter is assumed to be 35mWx13.5mH (average height of 6.75m) with frames spaced 6m apart. Two loading codes (Australian code AS/NZS 1170.2 2002 and American code ASCE 7-95 1996) are used to assess the wind pressure for the different loading scenarios.

A.4.1. USING AS/NZS 1170.2 (2002)

It is required to place a shelter in the cyclonic region on the eastern coast of Queensland, Australia (Zone 'C' Figure 3.1 AS/NZS 1170.2). The three scenarios of assessing the wind pressures on the shelter roof, in using AS/NZS 1170.2 (2002), are summarised in Table A.1. Other factors used in assessing the site wind speed are summarised below:

- M_d = 0.95, for zone B, C & D (AS/NZS 1170.2 2002 – Sec. 3.3.2);
- $M_{z,cat}$ = 0.941 for zone B (AS/NZS 1170.2 2002 – Table 4.1A);
- $M_{z,cat}$ = 0.967 for zone C (AS/NZS 1170.2 2002 – Table 4.1B);
- M_s = 1.0 (AS/NZS 1170.2 2002 – Sec. 4.3);
- M_t = 1.0 (AS/NZS 1170.2 2002 – Sec. 4.4).

Table A.1 Wind Pressures Calculations – AS/NZS 1170.2 (2002)

Case Scenario	Wind Type	Wind Region	Importance Level	ULS Prop of Exceed.	V_r (m/s)	V_{des} (m/s)	Wind Pr (kPa)	Notes
1	**Non-Cyclonic**	**B**	1	1/50	44	39	0.91	Doors open
2	**Non-Cyclonic**	**B**	2	1/250	53	47	1.33	Doors closed
3	**Cyclonic**	**C**	2	1/250	65	60	2.16	Doors closed with storm kit
AS/NZS 1170.2-2002 Reference		**Sec. 3**	**Table F1 AMDT No 2-2003**	**Table F2 AMDT No 2-2003**	**Table 3.1**	**Sec. 2.3**	**Sec. 2.4**	

A.4.2. USING ASCE 7-95 (1996)

It is required to place a shelter in the cyclonic region on the eastern coast of North Carolina (V_{50} = 58m/s, Fig 6-1, ASCE 7-95 1996). The basic wind speed map (Fig 6-1) in ASCE 7-95 (1996) is based on 0.02 annual probability of exceedance (50 years design life). Peterka and Shahid (1998) presented conversion factors for cyclonic (hurricane) regions and non-cyclonic regions (with speed reaching 45m/s) for other design lives. The three scenarios of assessing the wind pressures on the shelter roof, using ASCE 7-95 (1996), are summarised in Table A.2. Other factors used in assessing the wind velocity pressure are summarised below:

- K_z = 0.92 for Cat C (ASCE 7-95 (1996) – Table 6-3)
- K_{zt} = 1.0 (ASCE 7-95 (1996) – Sec. 6.5.5)

Table A.2 Wind Pressures Calculations – ASCE 7-95 (1996)

Case Scenario	**Wind Type**	**Design Life Conv Fact**	**Importance Level**	**V_{50} (m/s)**	**V_{25} (m/s)**	**Wind Pr* (kPa)**	**Notes**
1	**Non-Cyclonic**	0.93	0.87	45	42	1.21	Doors open
2	**Non-Cyclonic**	0.93	1.00	45	42	1.39	Doors closed
3	**Cyclonic**	0.90	1.00	58	52	2.17	Doors closed with storm kit
ASCE 7-95 (1996) Reference		**Peterka (1998) – Fig 5**	**Table 6-2**	**Fig 6-1**	**V_{50}*Conv Fact**	**Sec. 6.5.1**	

* Factored by 1.30 for ULS, Sec 2.3 ASCE 7-95 (1996)

A.4.3. GENERAL COMMENTS

Table A.1 and Table A.2 show good correlation in predicting the wind pressures for the closed-door scenarios 2 & 3 (considering the load factor 1.30 used in ASCE 7-95 (1996) for ULS compared to unit factor in AS/NZS 1170.2 2002). The American code predicted scenario 1 wind pressures 33% higher than that predicted by the Australian code. The assumption of having a structure of temporary nature (scenario 1) led to design the open-door case to 68% of the maximum site wind pressure (scenario 2), using AS/NZS 1170.2 (2002). This is compared to 87% in using the ASCE 7-95(1996).

A.5. REFERENCES

American Society of Civil Engineers. (1993). Minimum design loads for buildings and other structures. *ANSI/ASCE 7-93*, ASCE, Reston, Va.

American Society of Civil Engineers. (1996). Minimum design loads for buildings and other structures. *ANSI/ASCE 7-95*, ASCE, New York.

American Society of Civil Engineers. (1998). Minimum design loads for buildings and other structures. *ANSI/ASCE 7-98*, ASCE, New York.

Architectural Institute of Japan. (1996). AIJ recommendations for loads on buildings. AIJ, Tokyo.

Batts, M. E., Cordes, M. R., Russell, L. R., Shaver, J. R., and Simiu, E. (1980). Hurricane wind speeds in the United States. Washington, D.C.

British Standards Institute. (1997). Basis of design and actions on structures - wind loads. *DD ENV 1991-2-4*, BSI, London.

British Standards Institute. (1997). Loading for buildings - Part 2. Code of practice for wind loads. *BS6399: Part 2: 1997*.

Carradine, D. M., and Plaut, R. H. (1998). Arch supported membrane shelters under wind and snow loading. *International Journal of Space Structures*, 13(4), 197-202.

Department of Defence. (1996). Loads. *Military Handbook 1002/2A*. USA.

Department of Defence. (2004). Design: aircraft maintenance hangers: type I and type II. *UFC 4-211-01N*. USA.

Department of Defence. (2005). Structural load data. *UFC 3-310-01*. USA.

Durst, C. S. (1960). Wind speeds over short periods of time. *Meteorological Magazine*, 89, 181-186.

Holmes, J. D. (2001). *Wind loading on structures*, Spon Press, London.

International Standards Organisation. (1997). Wind actions on structures. *ISO 4354*.

Krayer, W. R., and Marshall, W. R. (1992). Gust factors applied to hurricane winds. *Bulletin of the American Meteorological Society*, 73, 613-617.

MCCDC. (1990). Required operational capability (ROC) for a marine corps expeditionary aircraft maintenance shelter. *LOG 33.1A*, Virginia.

Peterka, J. A., and Shahid, S. (1998). Design gust wind speeds in the United States. *Journal of Structural Engineering*, 124(2), 207-214.

Standards Australia. (2002a). AS/NZS 1170.0:2002 Structural design actions - General principles. Sydney.

Standards Australia. (2002b). AS/NZS 1170.1:2002 Structural design actions - Part 1: Permanent, imposed and other actions. Sydney.

Standards Australia. (2002c). AS/NZS 1170.2:2002 Structural design actions - Wind actions. Sydney.

Strarch. (1991). Analysis of US military requirements for large deployable shelters. Sydney.

Strarch. (2004). The Starch modular military shelter system - Load specification. Sydney.

Vickery, P. J., and Twisdale, L. A. (1995a). Prediction of hurricane wind speed in the United States. *Journal of Structural Division*, 121(11), 1691-1699.

Vickery, P. J., and Twisdale, L. A. (1995b). Windfield and filling models for hurricane wind speed predictions. *Journal of Structural Division*, 121(11), 1700-1709.

Appendix B: M^2S^2 Analysis Procedures

B.1. INTRODUCTION

The Military Modular Shelter System (M^2S^2) initiative is a research project that aims to develop a fibre composite re-deployable arched shelter system with rigid PVC or fabric cladding. The main frames are formed from modular fibre composite panels that are connected and stressed in position by prestressing cables. Using prestressing as a deploying mechanism, applying loads at the erection and assembly stages and changing of the support boundary conditions necessitates the inclusion of the erection process in the frame analysis. This appendix presents a brief description of the three analysis procedures, two linear and one non-linear, used to predict the frame member. The analyses comparison shows that modelling the erection process along with applying loads relevant to each deploying stage, by nonlinear analysis, is essential for this type of structure.

B.2. STRUCTURAL ANALYSIS OF M^2S^2 SHELTER FRAMES

B.2.1. MODEL DEVELOPMENT

Prior to conducting detailed investigations of the M^2S^2 shelter system, it was important to establish modelling procedures to assess the stress levels in the different components. As presented in Chapter 1, both the boundary conditions and the applied loads change from the erection stage to the deployed stage. The support (boundary) conditions change from sliding during the erection stage to hinge in the deployed stage. The structure's own weight, roofing and services dead loads are carried by the frames while on the ground, prior to carrying any prestressing. Reaching the final deployed position, the prestressing cables are blocked and the moving supports are fixed. Other loads are then applied on the deployed (stressed) structure.

Structural analyses were conducted for 35m frames, nominal span, with standard panel dimension of 1452mm at top chord, 1150mm at the bottom chord and centreline height of 1400mm and 200mm packer size. Commercial finite element (FE) software 'Strand7' (Strand7, 2005) was used for the frame analyses.

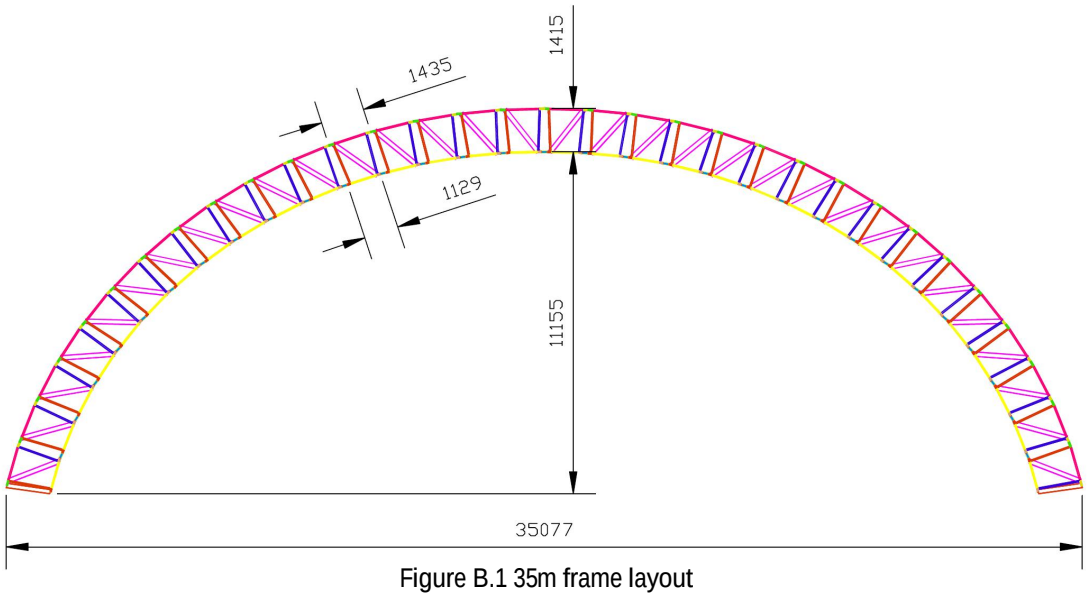

Figure B.1 35m frame layout

Three modelling procedures were implemented. The first procedure was a one stage linear analysis (LinA 1) where both supports were fixed in position. Dead loads, prestressing forces and other loads were applied as separate load cases.

The second model was a two-stage linear analysis (LinA 2). The first stage assumed free-to-slide-right support with dead loads and prestressing forces applied on non-stressed arch-shaped structure. In the second stage, other load cases (live loads, wind loads, etc) were applied on stress-free arch-shaped structure with supports on both sides fixed. Results of the different load cases were then combined by using 'Combine File Results' feature in Strand7 (Strand7, 2005). In both linear analyses, loads were applied while the structure was in its deployed stress-free geometry. Hinged joints were assumed between adjacent panels at the top chord and at the ends of the bottom chord packers.

The third analysis is a more complicated nonlinear analysis (NLinA). The frame was modelled while on the ground until reaching the deployed stage followed by the application of service loads. The analysis simulated the prestressing process by

increasing the prestressing force in the cable until closing all the bottom chord gaps and achieving the level of prestressing that prevents any possibility of gap opening during the serviceability limit states. Material properties for the different parts of the model, are shown in Table B.1.

Table B.1 Material properties used in frame analysis

Property	Members	Cables
E_{11} (MPa)	30,000	200,000
E_{22} (MPa)	6,900	
G_{12} (MPa)	29,000	
n_{12}	0.30	0.30
Density(T/m3)	1.7	7.8

Panel members were modelled as beam elements assuming rigid end connections (within the panel). Composite box section of 150x50x5mm was used to model the panel members. Steel prestressing cable of 16mm diameter was modelled as truss elements that are string-grouped and post-tensioned to the required prestressing force (Strand7, 2005). In linear analyses, the cable elements were connected to the support nodes at both ends. In addition, they were connected to the ends of the bottom chord member in each panel. The packers were modelled as beam elements with both end restraints released (Figure B.2).

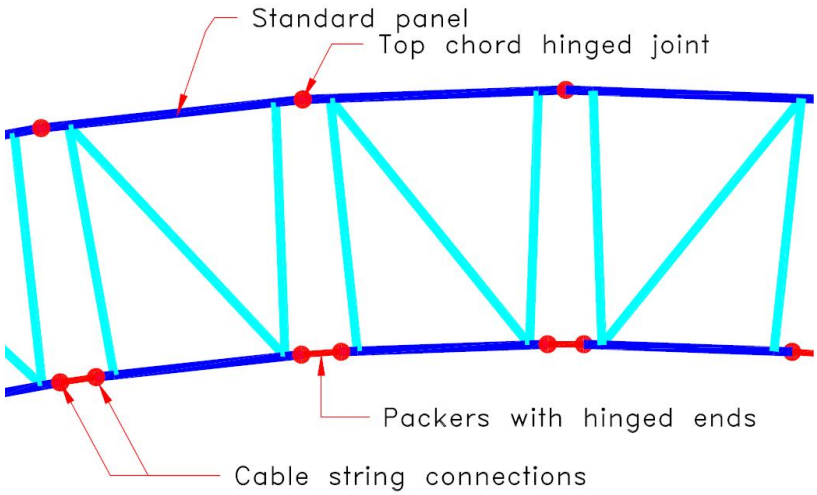

Figure B.2 Linear FE models - cable connectivity

In nonlinear analysis, a few components were added to the model to allow modelling the structure and transforming it from one stage to another. The main characteristics of the model can be summarized as follows, with reference to Figure B.2:

- Virtual end offsets of 20mm were assumed at the bottom chord ends of each panel.
- On the ground and prior to applying any prestressing, dead loads from the roof decking and services were applied to the top chord. This necessitated using gap lockers to avoid widening of the gaps between panels under the applied dead loads. Materials nonlinear cut off bars (Strand7, 2005) were used to model the gap lockers. They acted as tension-only-members.
- Packers were modelled as beam elements with RHS150x50x5 cross section. It was found necessary to provide nominal rotational restraint at the end that connects the packer to the adjacent panel (Figure B.3). This was to stabilize the joint. A joint stiffness of 0.10kNm/rad was used. After analysis, the packer end moment was checked to ensure that it had zero value (approximately).
- Prestressing cables were modelled as catenary cable elements with geometrical nonlinear analysis option.
- The cables needed to have similar connections as the packers to guide them to be in contact with the adjacent panel ends.
- Zero-gap contacts were used between the free end of the packer and the end of the next panel bottom chord. Once the gaps were closed, the connections carried compression forces. A nominal compression stiffness of 5x105kN/m was used (the analysis results were not sensitive to this value).
- With the gap closed, cable elements going through the gap would diminish in length leading to solution divergence. Virtual offsets, where the cable elements going through the gaps were joined with the packer from one end and the virtual end offset from the other end, were found necessary.

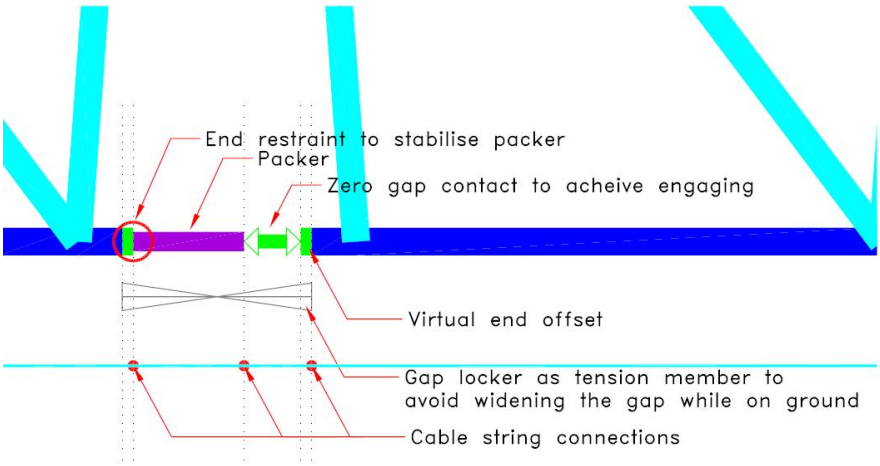

Figure B.3 Nonlinear FE model components at the bottom chord

B.2.2. APPLYING LOADS

In this exercise, loads were assessed according to AS/NZS1170.2 (Standards Australia, 2002). An equivalent dead load of 0.10kPa and wind loads due to wind on 0deg (across the frame) with doors open in Region B (non-cyclonic) were used. For linear analyses, loads were applied as individual load cases that were then combined to obtain the member forces and nodal deflections. For nonlinear analysis, loads were applied in the following sequence:

- Dead loads were applied as uniform distributed loads on the top chord members.
- The prestressing process was modelled by applying the necessary force on the cable to accommodate the change in geometry and finally achieve the 175kN prestressing force at the end of the prestressing process (erection stage).
- After finishing the prestressing, the right support was then locked in position by applying a fixed inward horizontal displacement that equalled that obtained from the prestressing.
- The analysis results of the erection stage were then used as initial conditions for applying wind or live loads.
- Two wind load situations were used with internal pressure fluctuating from inwards to outwards (Standards Australia, 2002).

The analysis results of the three models are shown in Table B.2.

Table B.2 Analysis results

Item		DL+PT			DL+PT+WL ext -WL int			DL+PT+WL ext+WL int		
		LinA 1	LinA 2	NLinA	LinA 1	LinA 2	NLinA	LinA 1	LinA 2	NLinA
Pre-stressing force (kN)		174.4	176.3	175.6	155.1	157.0	165.1	209.0	210.9	210.9
Displacement at (mm)										
Middle span	X	0.0	-93.3	-607.3	8.0	-85.3	-585.9	71.6	-21.8	-485.4
Middle span	Y	-94.1	-2.7	267.9	-111.8	-20.4	192.7	-17.0	74.4	404.6
Support	X	0.0	-186.7	-1260						
Reaction at support (kN)										
Left	X	-2.9	0.0	0.0	17.5	20.4	12.4	-70.3	-67.4	-55.6
	Y	18.2	18.2	17.6	80.4	80.4	77.7	-62.2	-62.2	-61.7
Right	X	2.9	0.0	0.0	-20.9	-23.8	-16.0	39.3	36.3	23.4
	Y	18.2	18.2	17.9	78.9	78.9	76.8	-75.8	-75.8	-72.7
Member forces (kN)										
Top chord		-108.7	-85.7	-61.0	-133.7	-110.7	-108.8	-41.5	-18.5	35.6
Bottom chord		-63.7	-91.3	-115.0	-82.2	-109.8	-113.0	-63.1	-90.7	-166.0

Where,

DL: Dead loads, PT: Prestressing force, WL: Wind loads in the 0-degrees direction (the most critical)
int: Internal pressure, ext: External pressure
LinA 1: One-stage linear analysis, LinA 2: Two-stages linear analysis, NLinA: Non-linear analysis
X: Horizontal, Y: Vertical

B.3. DISCUSSIONS OF THE ANALYSIS RESULTS

The three analyses were compared by presenting the top and bottom chord forces at mid-span, deflections at mid-span and at the movable support, and the support reactions. Based on the analysis results (Table B.2), the following can be noted:

- Under prestressing loads, the predicted deformed shapes of the frames were different in the three analyses. This is clear from the horizontal displacement at the movable support. In non-linear analysis the support displaced by 1260mm, prior to its locking. This was compared to 186mm for the 2-stage linear analysis. Linear analyses LinA 1 & LinA 2 predicted mid-span sag of 94.1mm and 2.7mm respectively while the nonlinear analysis (NLinA) predicted camber of 268mm (Figure B.4 to Figure B.6);
- In applying loads, the nonlinear model predicted higher deflections compared to the other models. This can be attributed to the change in geometry from the stress-free arch shape, due to prestressing;
- Maximum vertical deflection of 136mm (span/248) was still acceptable within the commonly used limit for normal structures (span/250). However, there were no guidelines for this allowance in any of the located references;

- All models predicted similar vertical reactions. However, the non-linear model predicted smaller horizontal reactions. This was attributed to the increase in subtended angle (during the stressing process) with less horizontal force component;
- Member force predictions were quite different in all analyses. One of the serviceability limit state (SLS) criteria in designing this type of structures is to have the bottom chord in compression under all load combinations. It is apparent that the distribution of forces between the chords and the level of these forces will influence this limit state. For example, in DL+PT+WL ext+WL int, the reported chord forces in single stage linear analysis are (-41kN top & -63kN bottom) while for 2-stage linear analysis are (-18kN top & -90kN bottom). In non-linear analysis the chord forces are (+35kN top & -166kN bottom). This implication has significant effect on assessing the level of prestressing and accordingly the different frame behaviours that are affected by the prestressing level.

Based on the comparison conducted above, it is clear that the analysis technique does affect the prediction of force distributions in the frame, support reactions and frame deflections. Linear analyses are not suitable for this type of structure. Nonlinear analysis is required, where both the assembly stage and the erection stage are included. However, it is important to verify the analysis results by testing frames under applied loads. Friction effects could be another factor to be included in the model.

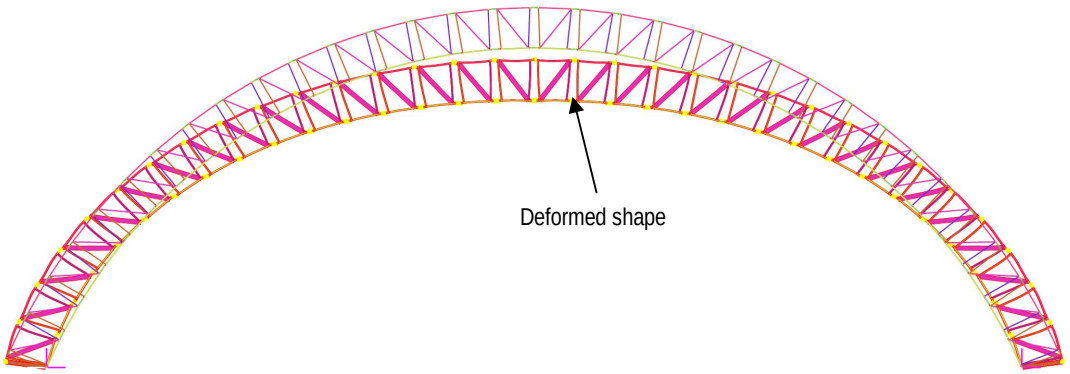

Figure B.4 Deflected shape of the frame predicted by LinA 1

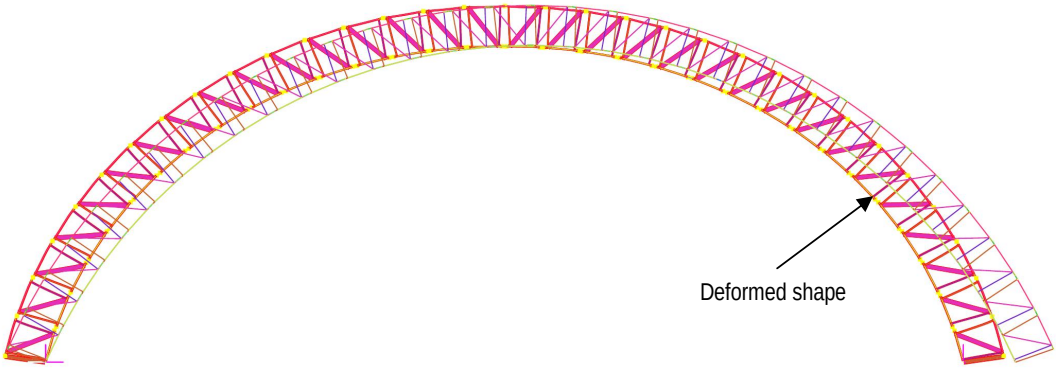

Figure B.5 Deflected shape of the frame predicted by LinA 2

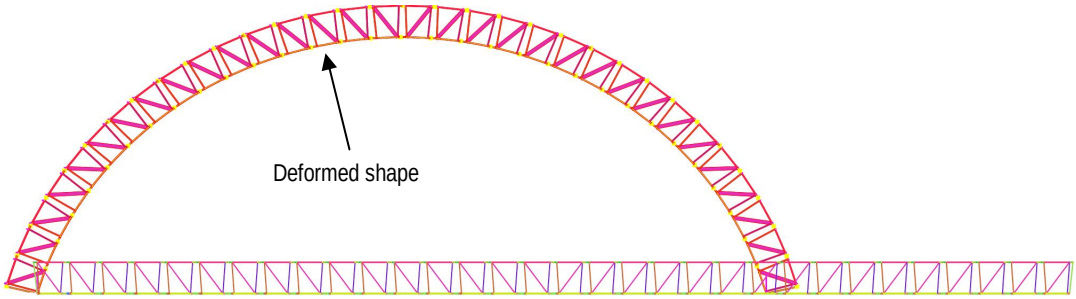

Figure B.6 Deflected shape of the frame predicted by NLinA

B.4. REFERENCES

Standards Australia. (2002). AS/NZS 1170.2:2002 Structural design actions - Wind actions. Sydney.

Strand7. (2005). Strand7 User Manual. Sydney, Australia

Appendix C: Sandwich Columns with Mixed-Cores – Test Results

C.1. INTRODUCTION

As discussed in Chapter 4, single core columns are commonly used to manufacture sandwich columns. No reference was located that addressed the behaviour of columns with mixed material cores. This appendix presents test results and failure modes for sandwich columns with mixed-core, providing data for further investigations.

Material availability, weight optimisation, cost, and failure and post-failure structural behaviour were among the reasons for testing the mixed-core columns. Two concepts of mixed-core columns were tested. The first used a symmetric layout of two core materials, middle end-grain balsa (SB100 from ATL composites, www.atlcomposites.com) and outer low density PVC foam (Klegecell-R45 from Diab, www.diabgroups.com), Figure C.1. The second used R45 core material with laminated end caps at the edges of the column, to improve its overall shear stiffness and accordingly its capacity (Figure C.2). The core material dimensions for the different columns are shown in Table C.1.

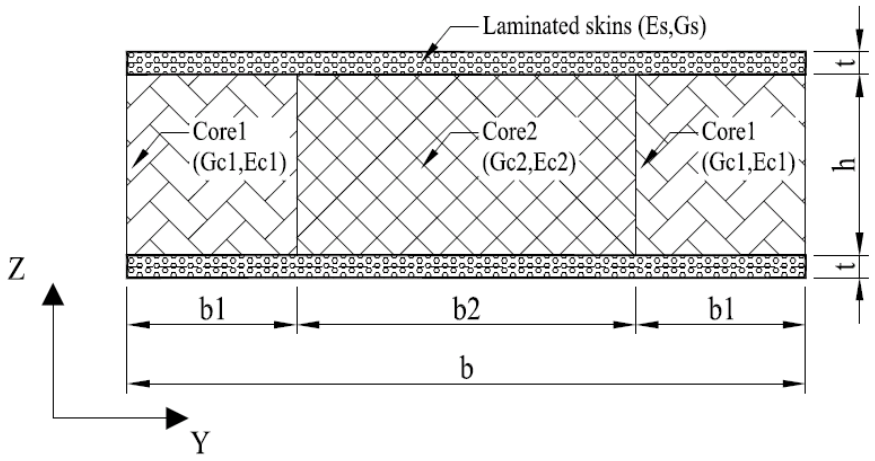

Figure C.1 Mixed-core column by using two types of core

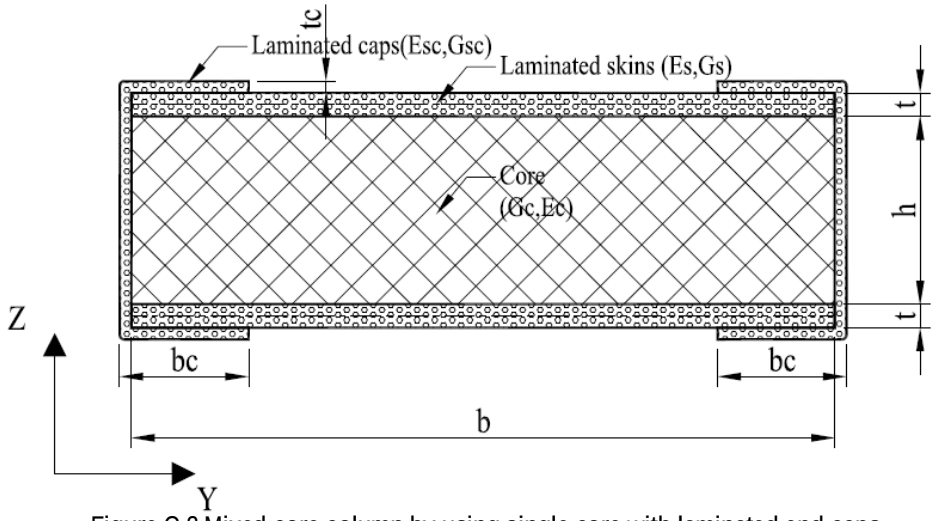

Figure C.2 Mixed-core column by using single core with laminated end-caps

Table C.1 Mixed-core column geometries

	Core width (mm)		
Column	**Core1(Balsa)**	**R45 foam**	**Core2 (Balsa)**
T02-02 (with end caps)	0.00	120.00	0.00
T02-03	15.00	90.00	15.00
T02-04	20.00	80.00	20.00
T02-05	30.00	60.00	30.00

Due to the differences in the manufacturing sequence, the procedures used in producing both column types are presented and followed by the testing procedures. The test records for the different column sets are presented along with the test observations. The appendix ends with a brief discussion of the different columns' behaviour.

C.2. COLUMN SPECIMEN PREPARATIONS AND TESTING PROCEDURES

Prototype columns of 550mmL[1]x120mmWx24mmThk were manufactured. The manufacturing procedures for the two types were slightly different. The skins of the columns were laminated from 3 plies of uni-glass 450gsm from Huntsman (www.huntsman.ivt.com.au) using Hyrez 202 epoxy-resin (Rogers, 2004) with peel plies at each face. After curing for 24 hours at room temperature, the laminated sheets were cut to 140mm wide by 600mm length using a bench saw with a diamond-coated cutting wheel. The column specimens with end caps (T02-02) were

[1] 460mm clear height.

manufactured similarly to the single-core columns presented in Sec. 4.5.1, p97. Then end caps were adhesively bonded to both edges with bc=25mm and tc=1.25mm (Figure C.2). The fibre architecture of the end caps was [+45/-45/0/90] using MX6000 (600gsm) glass double bias (DB) and 300gsm bi-axial glass tapes from Colan (www.colan.com.au). The end caps were laminated by hand-lay-up with Hyrez 202 epoxy-resin. After laminating on a flat surface, a male-female mould was used to form the cap where the male part was clamped in position for 24 hours to allow curing of the laminates (Figure C.3). The caps were cut to dimension, the HPR26 thixotropic-toughened epoxy glue system from ATL Composites (www.atlcomposites.com.au) was applied to both of the adherents' surfaces. Then the column was clamped to allow curing of the adhesive.

Figure C.3 Manufacturing of the end caps for T02-02

For columns T02-03 to T02-05, the manufacturing procedures conducted after the preparations of the skins are as follows:

- The width of the R45 foam was cut to dimensions with length of 600mm and thickness of 20mm, using a band saw.
- The balsa was cut to a width of (b1+10mm) with length and thickness equalled to the R45 foam.
- Cores were vacuumed, using a normal vacuum cleaner, to remove dust.
- Cores were primed by spraying Hyrez 202 epoxy. This process needed three coats to achieve a permanent glossy surface. This was to control the amount

of adhesives absorbed through the core gaps as well as to achieve good bonding between the core and the skins.

- The core of each column was weighed before and after spraying to assess the amount of resin utilised.
- The primed core was allowed to cure for 24 hours at room temperature. Skins were glued to the core material using the HPR26 thixotropic-toughened epoxy glue system from ATL Composites (www.atlcomposites.com.au).
- The columns were clamped in bundles of three to squeeze out excess glue and left to cure for 24 hours at room temperature.
- Columns were cut to dimension (120mmWx550mmL) on a bench saw with diamond-coated blade.

The remaining manufacturing procedures were similar to that for single-core columns (Sec. 4.5.1, p97).

As with the single-core column tests, mixed-core columns tests were conducted on the Shimadzu CSP-300. Clamped-end restraints were implemented using a special fixture attached to the machine ram (Figure 4.14, p100). Applied loads were recorded with a 222kN loading cell. Vertical displacement was recorded using a string pot and horizontal displacement was recorded using LVDT while strain gauges were attached at the mid-height of the column at both faces. All data were collected by the System 5000 data-acquisition system and recorded on a standard PC at time increments of 0.10s.

C.3. TEST RECORDS AND OBSERVATIONS

The average capacities and weights for all columns, including the single-core for comparison, are shown in Table C.2 while their stiffness (the slope of the load-displacement curves) are shown in Table C.3. A representative specimen from each column group (the specimen number was shown after the column name) was selected to be compared with other column specimens. The load, displacement, horizontal displacement and mid-face strains are shown in Figure C.4 to Figure C.7. In Figure C.8, the percentage of using balsa is plotted against the average column capacity. The failure modes of the columns are shown in Figure C.9 to Figure C.11.

Table C.2 Mixed-core columns capacities and specific strength

Column	Ultimate strength (kN)			Weight (gr)	Sp Strength (kN/gr)
	Avg	Std Dev	Var		
T02-01 (all foam)	36.15	2.21	4.90	493	0.073
T02-02 (all foam with end caps)	77.69	2.90	8.41	645	0.120
T02-03 (25% balsa)	59.82	4.90	23.99	518	0.115
T02-04 (33% balsa)	64.15	4.09	16.71	510	0.126
T02-05 (50% balsa)	75.84	2.51	6.28	539	0.141
T02-06 (all balsa)	99.47	4.47	20.00	595	0.167

Table C.3 Mixed-core columns stiffness

Column	Stiffness (kN/mm)		
	Avg	Std Dev	Var
T02-01	16.20	1.52	2.30
T02-02	23.81	0.52	0.27
T02-03	20.08	1.38	1.91
T02-04	18.10	0.74	0.55
T02-05	20.11	2.71	7.33
T02-06	20.00	1.40	1.95

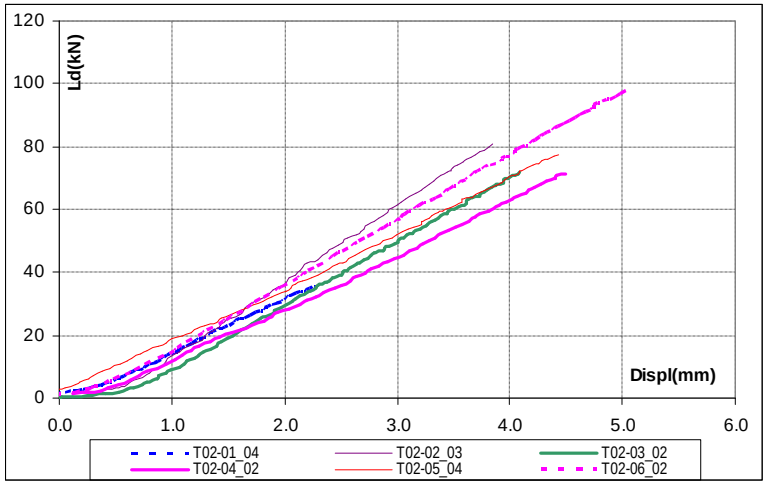

Figure C.4 Mixed-core columns load-displacement

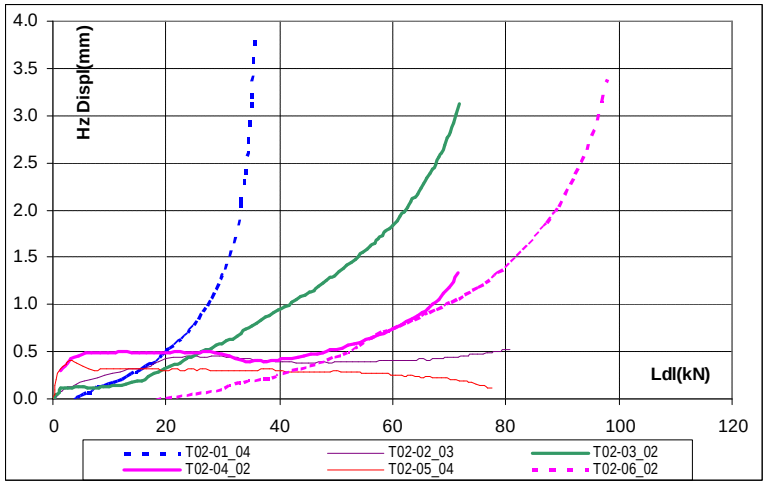

Figure C.5 Mixed-core columns horizontal displacement-load

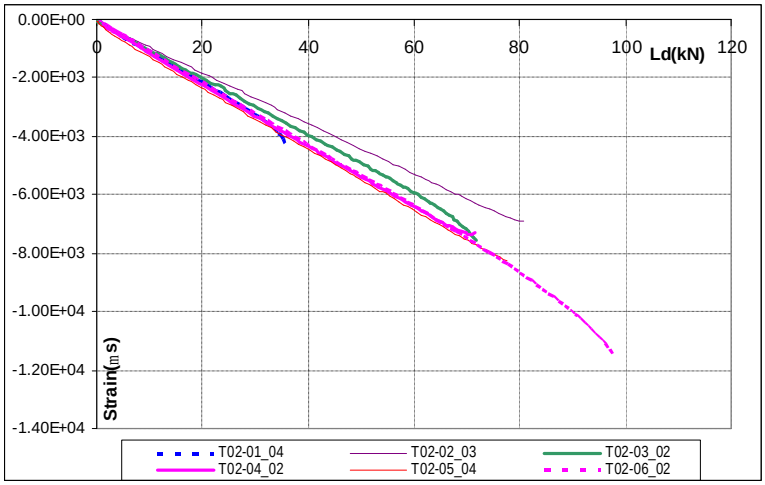

Figure C.6 Mixed-core columns maximum strain-load

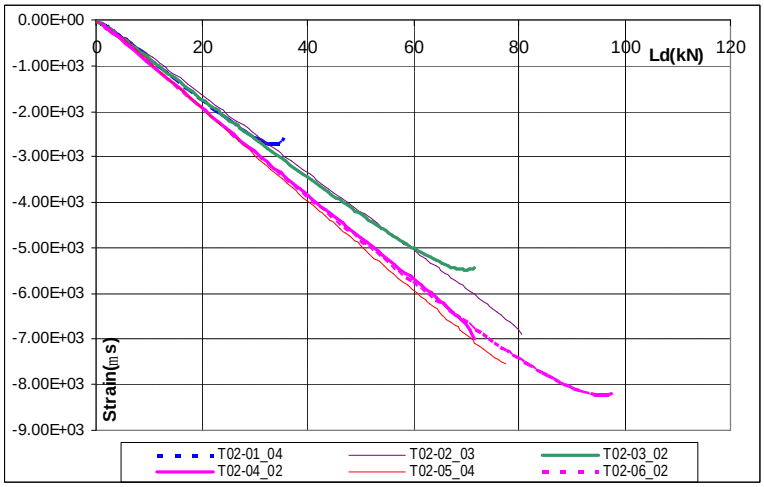

Figure C.7 Mixed-core columns minimum strain-load

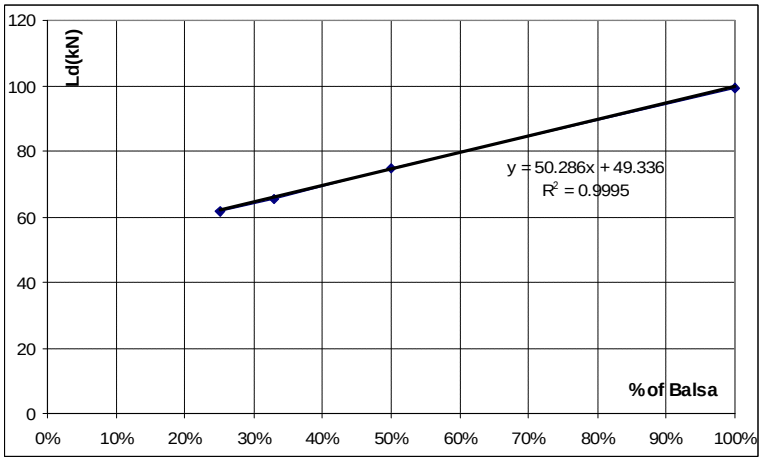

Figure C.8 Effect of using Balsa on column capacity

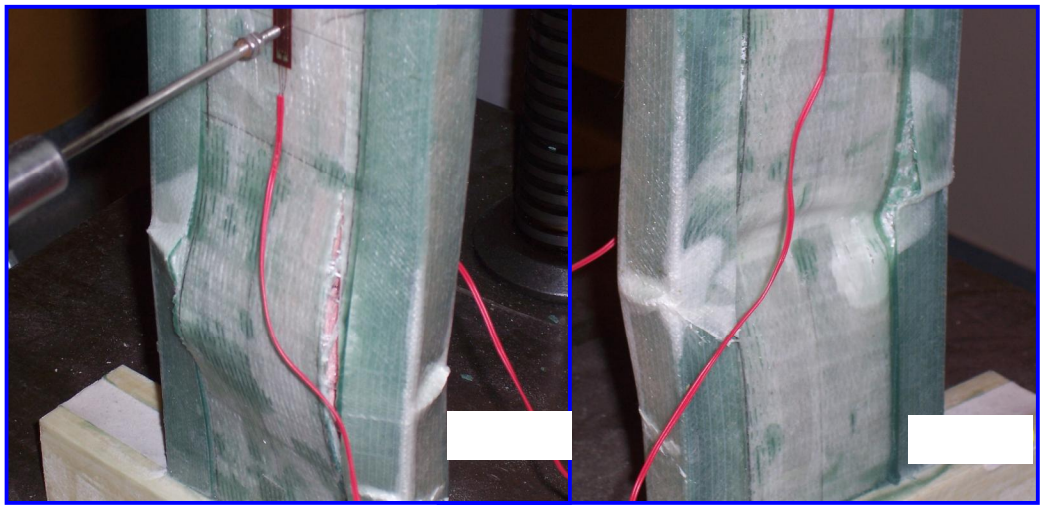

Figure C.9 Column T02-02 failure

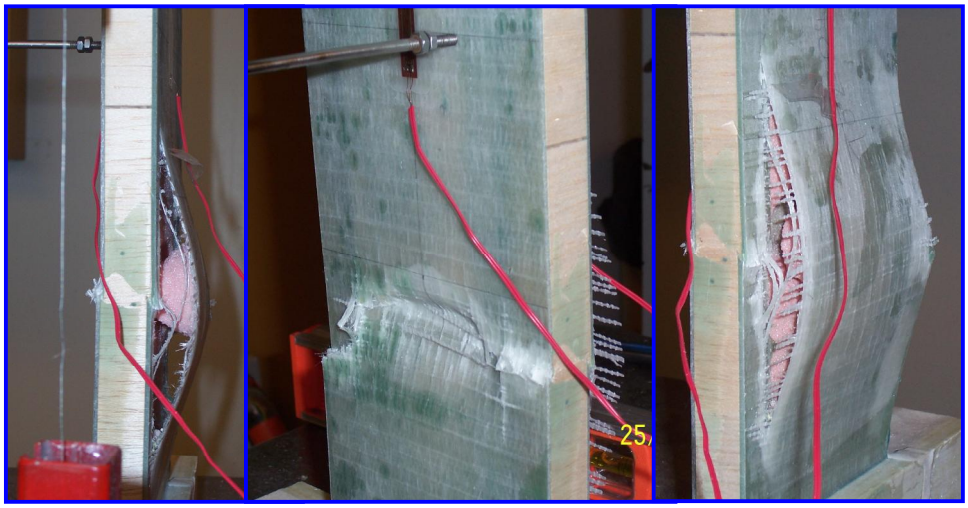

Figure C.10 Failure type-1 for two-type mixed-core columns

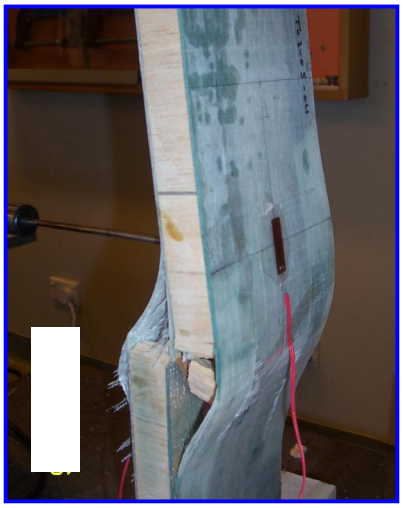

Figure C.11 Failure type-2 for two-type mixed-core columns

From the above tables and figures, the following observations were noted:

- The trend of the column capacity was clear. Increasing the core shear modulus increased the column capacity. However, there was significant scatter in the data of the columns that contain balsa cores. The highest scatter was observed in column T02-03 with the least percentage of balsa.
- Two-core columns exhibited close stiffness values.
- Using end caps was effective in increasing the column capacity. In addition, it increased the column stiffness compared to all other columns tested.
- An approximate linear relationship between the applied loads and axial displacement was observed in all columns.
- Increasing the balsa content in the core increased the column ultimate capacity in a linear relationship (Figure C.8).
- For T02-02 (end caps) column, failure occurred due to shear buckling at the middle portion of the column. The face under minimum compression, the laminated skin split vertically adjacent to the cap edges (Figure C.9).
- The face under maximum compression buckled inwards separating the skins from the end caps.
- At this instance the caps seemed to buckle after debonding from the column face in (maximum compression side).
- Two failure modes were observed in two-core columns (T02-03 to T02-05).
- The first failure mode (Figure C.10) was observed for columns T02-03, T02-04, and some of the T02-05 specimens, while second failure mode (Figure C.11) was observed in some of the T02-05 specimens.
- The first failure mode (type 1) was identified to that of the end caps column T02-02.
- The second failure mode was similar to the shear mode failure of T02-06 column (Sec.4.5.2, p98).
- In all columns failure was of a sudden brittle nature.

C.4. DISCUSSION OF THE BEHAVIOUR OF THE MIXED-CORE COLUMNS

The discussion in this section raises points about the behaviour of mixed-core columns and identifies considerations for future investigations.

- The weak core material was at the centre while the strong core material (either balsa or end caps) were at the outside of the columns. Reversing the the core layout, can it allow failure of the outer column edges (with weak cores) and accordingly, provide a system to release energy in reaching the ultimate capacity?
- The end caps increased the strength and stiffness of the column although they contributed to heavier columns.
- The structure of the skins was uni-directional. For both types of mixed-core columns, failure in the skins was observed along the line of the strong core. Does this indicate that in modifying the fibre architecture we can have any secondary behaviour that allows sustaining some of the column capacity after reaching its ultimate capacity?
- The effect of the natural variation in the balsa became more pronounced in columns with the least balsa content leading to more scatter in the column behaviour.
- The linear relationship between the balsa content and the ultimate capacity (Figure C.8) needs further investigation, because of the change of the failure mode in the low-balsa and high-balsa content columns.
- The mixed-core concept requires further investigations using a more consistent material (like PVC foam) to highlight this relationship.
- The skin strains at specified load level were smaller in T02-02 column compared to other columns. This can be attributed to the contribution of the end caps to the column carrying capacity.
- A FE model that can capture the behaviour of the mixed-core columns is needed to achieve better understanding of the mechanism of their behaviour.

C.5. REFERENCES

ATL Composites Homepage. www.atlcomposites.com.au.

Colan Homepage. www.colan.com.au.

Diab Homepage. www.diabgroup.com.

Huntsman home page. www.huntsman.ivt.com.au.

Rogers, D. (2004). Characterisation of Hyrez 201 laminating resin. Polymer Testing Laboratory, University of Southern Queensland, Toowoomba, Queensland.

Appendix D: Double-Bay DD-MPTS – Test Results

D.1. INTRODUCTION

After the successful testing of the DD-MPTS (P309, Chapter 3 and P409, Chapter 4), another DD-MPTS layout was tested. The double-bay panel (P819) had symmetric layout with two diagonals meeting at the central vertical member (Figure D.1). This layout had a few advantages that can be summarised as follows:

- The panel was symmetric, which provides easier manufacturing with fewer different components produced.
- Using panels with a rectangular shape, reduced the number of panels, and thus the number of inter-panel joints, required to cover the same area. This layout can provide a lighter weight and more economical alternative.
- Testing the panel in this configuration provides the toughest test for its jointing system, where forces are changed in direction from one diagonal to the other. In addition, the diagonals meeting at the central vertical skins were connected to half the vertical width.

The P819 was manufactured with low-density core foam for the diagonals (Klegecell R45, www.diagroup.com). With the concept of M^2S^2 in mind, the panel was prestressed to load level of 140kN prior to applying any loading. The panel was tested under dynamic loads for 500,000 cycles with load magnitudes ranging from 5kN-50kN (about 50% of its capacity) with loading frequency of 1.10Hz. Then the panel was loaded until failure by static testing. Passing the dynamic test without any stiffness degradation adds to the good structural characteristics of this type of construction. Mid-span load and displacements were recorded along with the strain at the different locations as shown in Figure D.2. Data were collected by a System 5000 data acquisition system connected to a standard PC at a rate of 0.1s. In this appendix the test records are presented in graph form followed by a brief discussion of the test results.

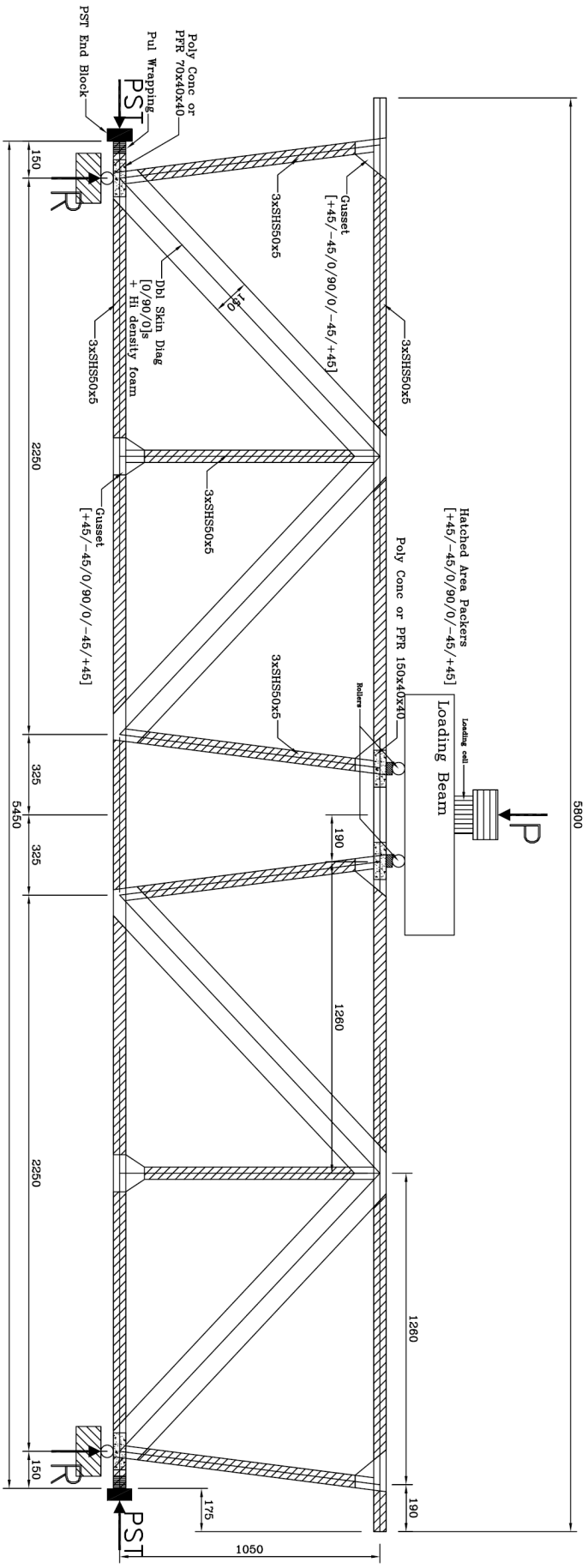

Figure D.1 P819 Layout

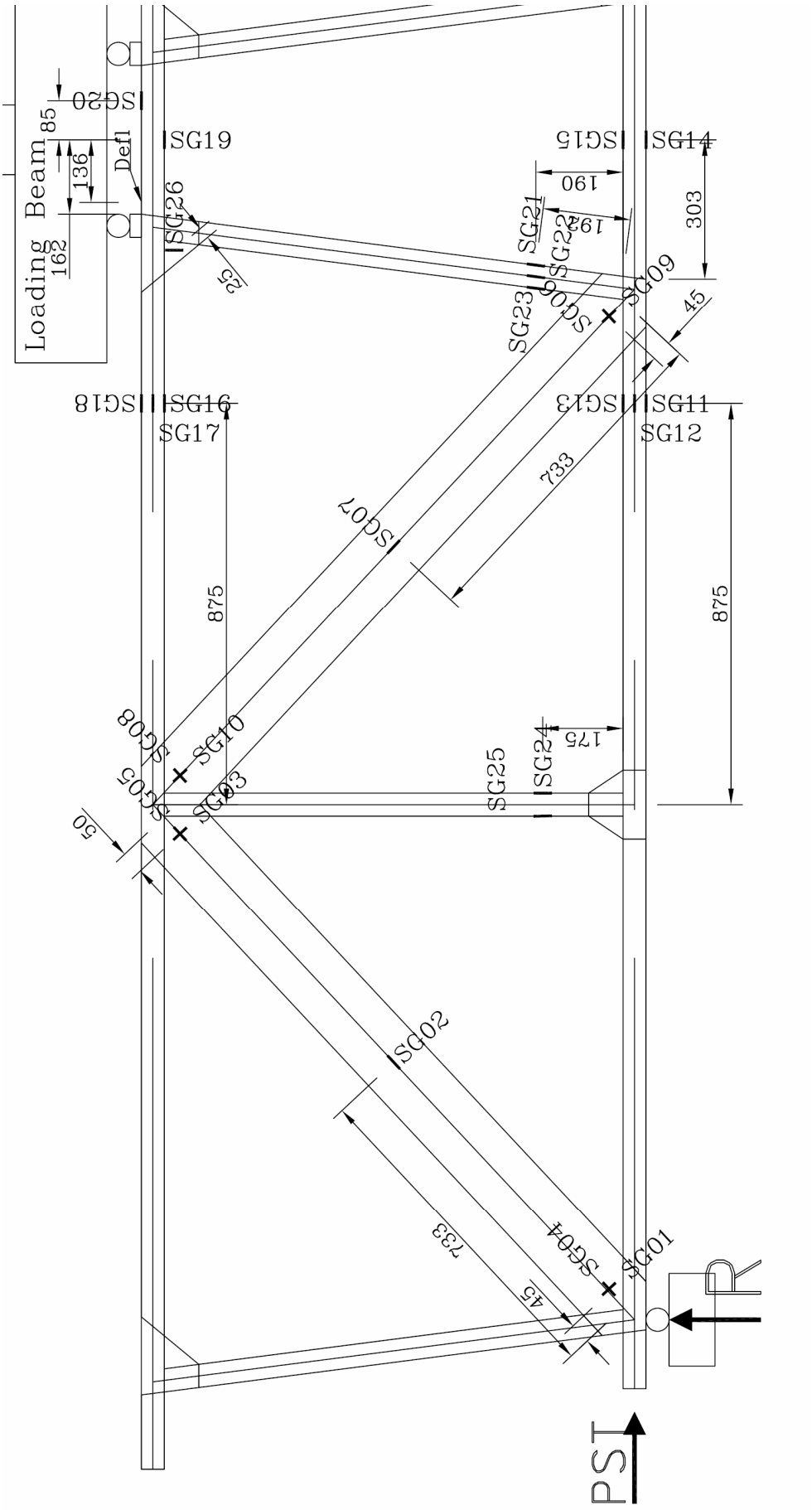

Figure D.2 P819 strain gauge locations

D.2. TEST RECORDS

D.2.1. PRESTRESSING PROCESS

The load, displacement and strains were recorded during the prestressing process. The prestressing process was conducted with a manually-operated hydraulic pump with a prestressing jack of 300kN capacity (Figure D.3). The panel was prestressed to a load level of 161kN then reduced to 138kN where the prestressing force was kept for the rest of the tests. In this section the main strains are presented along with the prestressing load (PST) and displacement (Figure D.4 and Figure D.5). In conducting further testing, the displacement and strains were re-zeroed. So, to combine the effect of the PST, these values should be added.

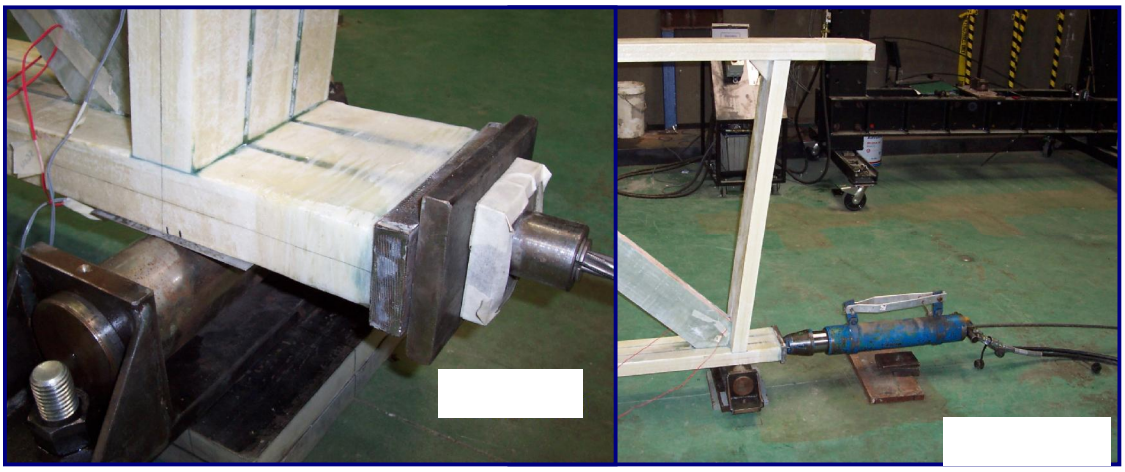

Figure D.3 Prestressed panel with end grips

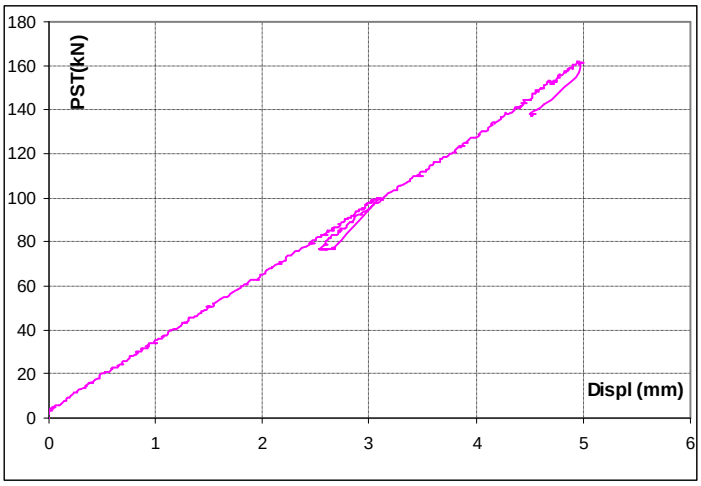

Figure D.4 Prestressing load-displacement

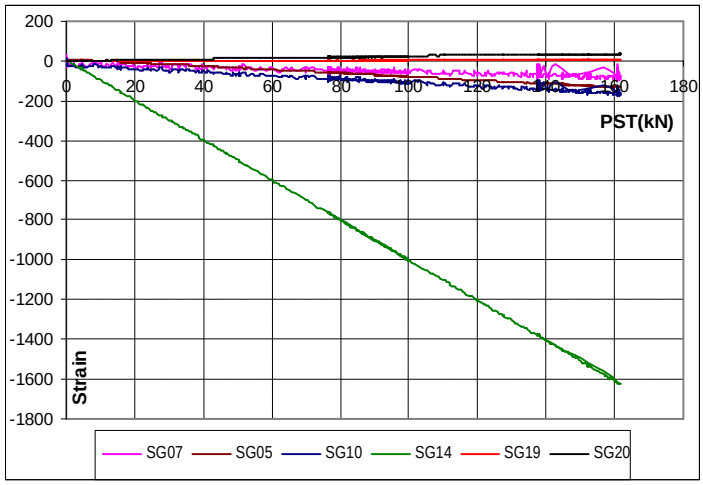

Figure D.5 Effect of PST on different strain levels

D.2.2. DYNAMIC TEST

As mentioned, the main objective of the dynamic test was to observe any stiffness degradation under repeated loads. The data records presented in this section were located at the beginning of the test and towards the end, with the graph legends showing the number of cycles (in thousands), Figure D.6. Each of these records lasted for nine seco

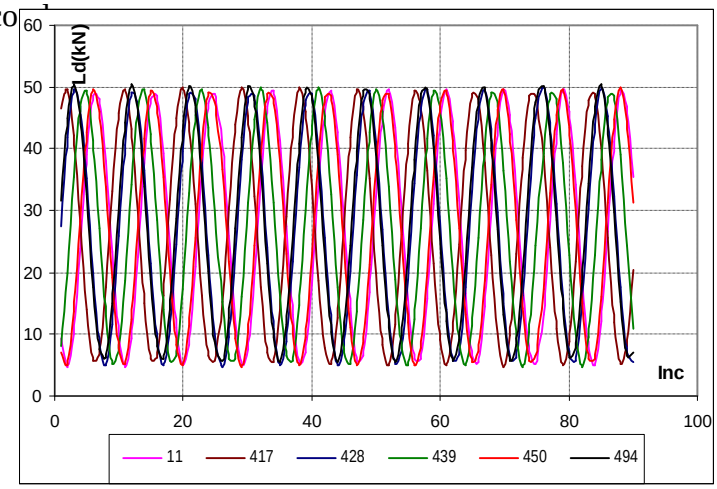

Figure D.6 Dynamic loading patterns

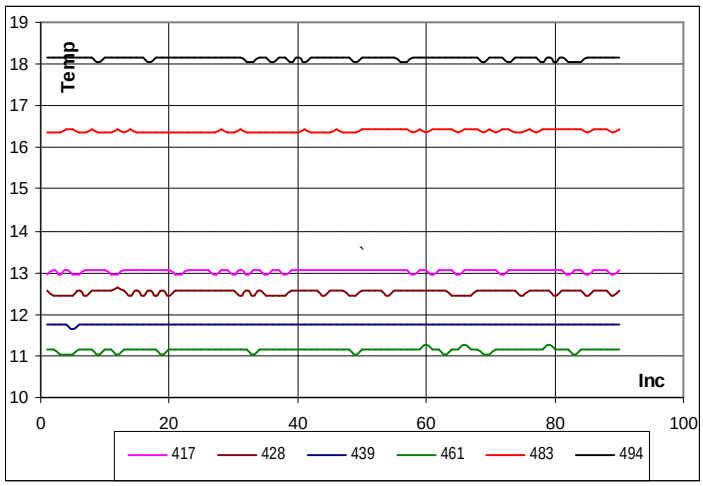

Figure D.7 Temperature change during the last day

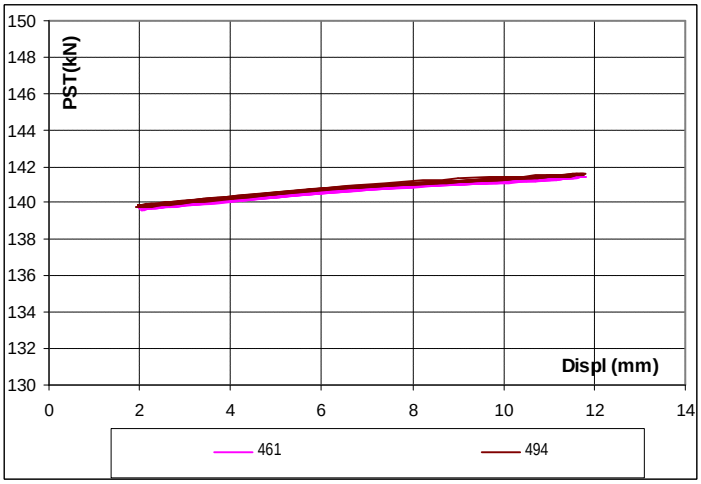

Figure D.8 Effect of temperature change on the PST force

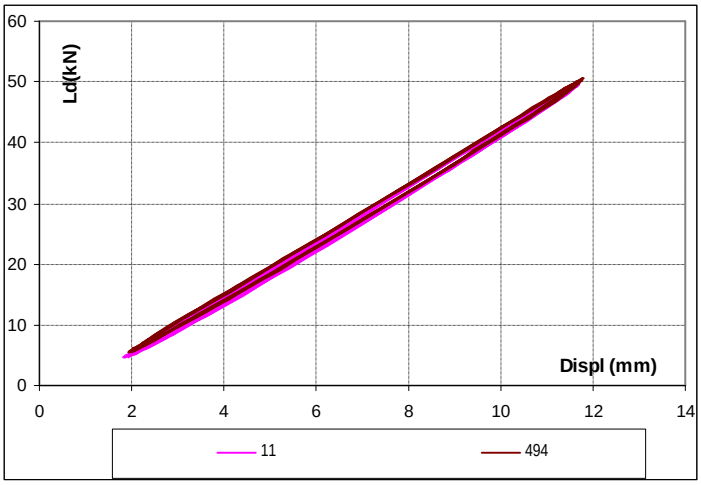

Figure D.9 Load-displacement* for the beginning and end records

* from the stressed position

D.2.3. STATIC TEST TO FAILURE

The static test records are shown in Figure D.10 to Figure D.15.

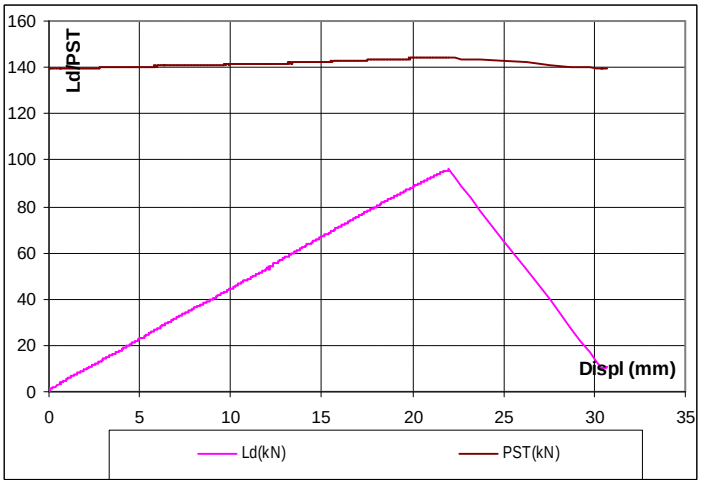

Figure D.10 Prestressing and load-displacement curves

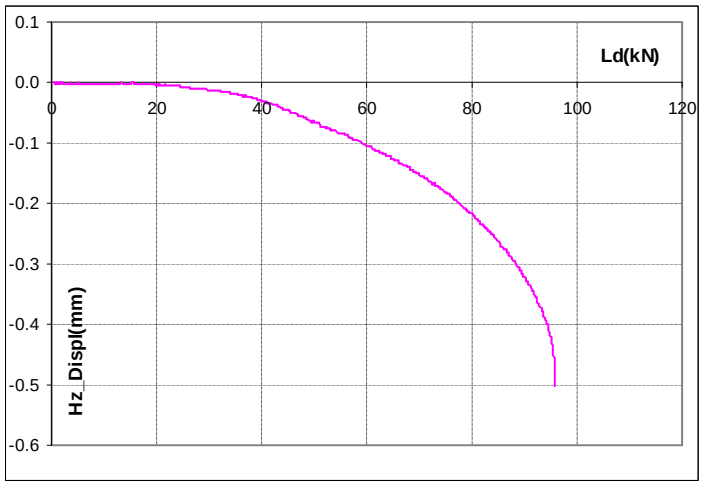

Figure D.11 Load-Hz displacement at middle of the left diagonal

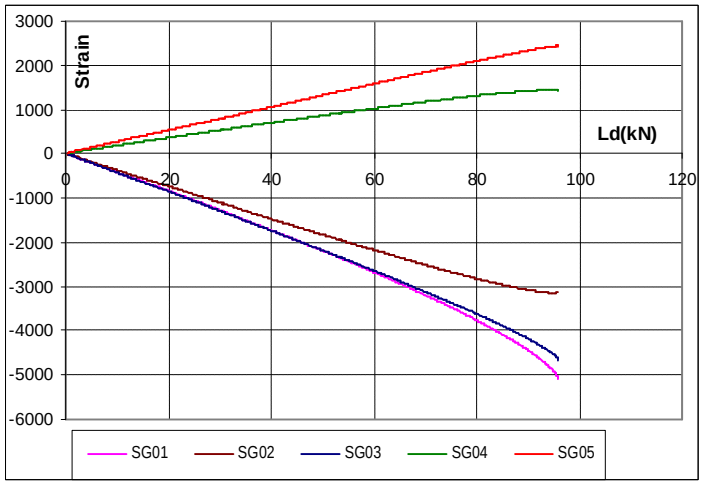

Figure D.12 Left diagonal strain-load curves

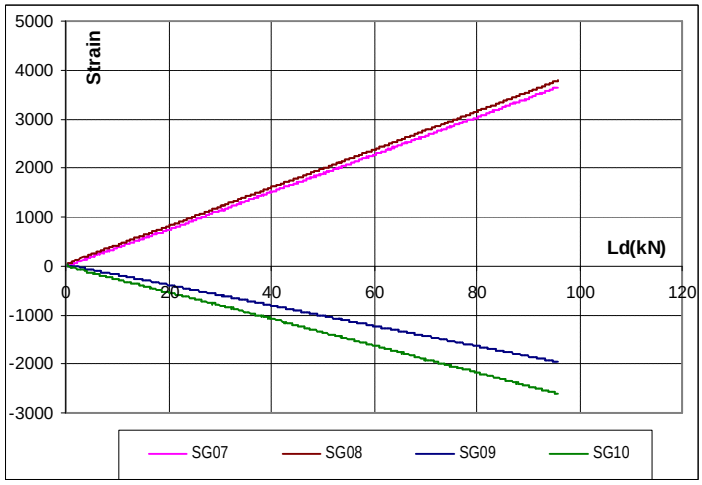

Figure D.13 Middle-left diagonal strain-load curves

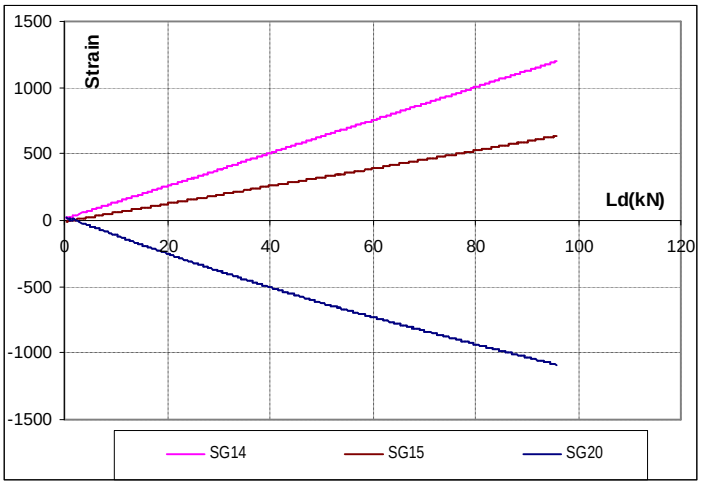

Figure D.14 Chord strain-load curves

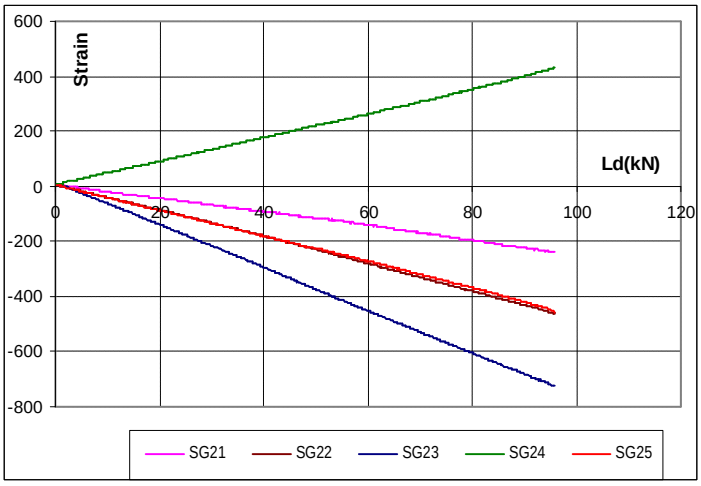

Figure D.15 Verticals strain-load curves

D.3. TEST OBSERVATIONS AND COMMENTS

The main observations during the three testing stages can be summarised as follows:

- In conducting the prestressing process, there was a camber occurred. The relationship between the prestressing force and the mid-span displacement was linear, reaching 4.52mm for PST=140kN (Figure D.4).
- The PST generated nominal strains in the panel components other than the bottom chord which was strained to 0.14% (Figure D.5).
- After conducting the prestressing process, it was noticed that the edge diagonals had out-of-plane displacement (Figure D.16). The largest was in the left diagonal with value of 5mm. It seems that this was due to an

imperfect edge of the bottom chord pultrusions that led to lateral rotation of the base plates when subjected to the prestressing forces.

- During the dynamic test, the temperature was recorded to compensate for the effect of temperature on the strain gauge and PST loading readings. The data shown in Figure D.7 represented the temperature range along the last testing day. As can be observed, the temperature changed from 11˚C to 18˚C.
- The effect of temperature change on the PST forces was not significant (Figure D.8).
- In comparing the load-displacement curves of the 11k and 494k cycles (Figure D.9), it became clear that the panel stiffness has not degraded, as both curves were identical.
- In conducting the static test with loading rate of 1mm/min, the panel failed at load of 95.4kN due to shear buckling of the left diagonal in compression (Figure D.17).
- The equivalent diagonal failure load was estimated to be 84kN (based on the SG02 strain gauge readings), while the predicted capacity using Allen's Equation 4.8 (p91) was 83kN. This indicated that the out-of-plane displacement had little effect on the load-carrying capacity of low-density core sandwich column capacity.
- The strain-load curves were linear except for the diagonal in compression where the effect of buckling started to show close to the failure loads (Figure D.12).
- There was nominal effect of the load on the verticals, where loads were mainly transferred through the diagonals. Accordingly, lighter sections can be used for the verticals.
- The behaviour of this type can be well-predicted by using the FE modelling procedures presented in Chapter 4 and Chapter 6. Accordingly, it can be optimised numerically prior to conducting further testing.

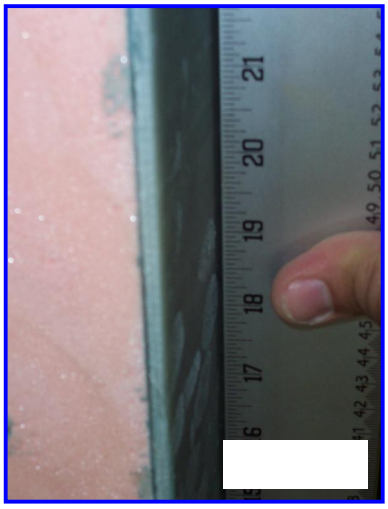

Figure D.16 Out-of-plane displacement due to prestressing

Figure D.17 P819 - Failure due to shear buckling

D.4. REFERENCES

Diab Homepage. http://www.diabgroup.com.